Heating and Evaporation of Automotive Fuel Droplets

Mansour Al Qubeissi

A thesis submitted in partial fulfilment of the requirements by the
University of Brighton for the degree of
Doctor of Philosophy

April 2015

Sir Harry Ricardo Laboratories, Centre for Automotive Engineering,
School of Computing, Engineering and Mathematics
University of Brighton, United Kingdom

ABSTRACT

The previously introduced fuel droplet heating and evaporation models, taking into account temperature gradients, recirculations, and species diffusion within droplets, are further developed and generalised for the application to a broad range of automotive fuel droplets. The research has been conducted in three directions: modelling of biodiesel fuel droplets, modelling of Diesel fuel droplets, and modelling of gasoline fuel droplets.

Firstly, the analysis is focused on several (up to 19) types of biodiesel fuels. It is shown that the model based on the assumption that the diffusivity of species in droplets is infinitely fast and the liquid thermal conductivity is infinitely large under-predicts the droplet evaporation time compared with the model taking into account the effects of finite diffusivity and conductivity, by up to about 15%. A similar under-prediction of the single-component model, in which the transient diffusion of species is ignored and the liquid thermal conductivity is assumed to be infinitely large, is shown to be about 26%.

Secondly, the components of Diesel fuel with close thermodynamic and transport properties are grouped to form quasi-components, using the newly introduced Multi-Dimensional Quasi-Discrete (MDQD) model. In contrast to the original quasi-discrete model, this model takes into account the contribution of all groups of hydrocarbons in Diesel fuels (in addition to alkanes). Also, in contrast to the original quasi-discrete model, the contributions of individual components are not approximated by the distribution function of carbon numbers, but they are considered individually. It is shown that the approximation of Diesel fuel by 15 quasi-components/components leads to errors in estimated temperatures and evaporation times in typical Diesel engine conditions not exceeding about 3.7% and 2.5%, respectively, which is acceptable for most engineering applications. This approximation has also reduced CPU time 85% compared with the case when all 98 components are taken into account.

Thirdly, the MDQD model is applied to gasoline fuel droplets in realistic engine conditions. In contrast to the original MDQD model, where n-alkanes and iso-alkanes are merged into one group of alkanes, in this approach separate contributions of these two groups are taken into account. The results are compared with the predictions of a single-component model and the approximation of gasoline fuel by iso-octane. It is shown that the application of these models leads to under-predictions of the droplet evaporation times by approximately 67% and 47% respectively. Also, the approximation of the actual composition of gasoline fuel by 6 quasi-components/components, using the MDQD model, leads to errors in estimated droplet surface temperatures and evaporation times of about 0.9% and 6.6% respectively; which can be tolerated in many engineering applications. This approximation has also reduced CPU time about 70% compared to that for the model taking into account all 20 components.

PREFACE

The work presented in this thesis was conducted at the Sir Harry Ricardo Laboratories (SHRL), Centre for Automotive Engineering (CAE), School of Computing, Engineering and Mathematics (CEM), University of Brighton (UoB), United Kingdom. The research project was sponsored by the UoB and the European regional development fund Franco-British INTERREG IVa (Project E3C3, Reference 4274).

The author joined SHRL – UoB in October 2012 as a PhD candidate in Engineering, with the following degrees in Mechanical Engineering related disciplines: BSc, MSc, and MPhil; a designated reviewer on the following IEEE proceedings: ICEED2012, PECON2012, ISBEIA2012, CHUSER2012, BEIAC2013, SHUSER2013, ISBEIA2013, CoAST2013, CEAT2013, InCIEC2013, a Conference chairing member at UoB doctoral research conference (July 2013, July 2014), and currently serving as a Scientific and Technical Committee Member of the World Academy of Science, Engineering and Technology (WASET); Editorial Board Member of Laboratoire de Recherche en Hydraulique Souterraine et de Surface (LARHYSS), and International Journal of Mechanical Engineering and Automation (IJMEA).

The research project was supervised by:

Sergei S. Sazhin (Professor of Thermal Physics, Fellow of the Institute of Physics, Chartered Physicist, Member of the editorial board of the International Journal of Engineering Systems Modelling and Simulation (2007-present), and Journal of Irrigation and Drainage Systems Engineering (2012-present), Member of the scientific committee of the French programme Méthodes d'analyses expérimentales et de simulations de brouillard multi-composant);

Morgan R. Heikal (Ricardo Professor of Automotive Engineering, Member of the national Research Excellence Framework (REF) assessment panel (B12) – UK, Head of the CAE, Leader and Director of SHRL, Visiting Senior Professor – UTP – Malaysia, Chair of the Universities' Internal Combustion Engines Group (UnICEG), Fellow of the Institution of Mechanical Engineers (IMechE), Member of Society of Automotive Engineers (SAE) Transactions Selection Committee, Member of EPSRC Peer Review College (2002–2009), Member of Scientific Council of the International Centre for Heat and Mass Transfer, Member of Combustion Engines and Fuels Group IMechE (since 1999), Chairman of the Combustion Engines and Fuels Group IMechE (2001–2003), Member and chair of organising committees of a number of national and international conferences, Member of the Heat Exchanger Advisory Group – Europe (1990–present), Reviewer of many international journals); and

Paul J. Harris (Reader in Applied Mathematics, leader of the Computational Mathematics Group – UoB, Author and Editor of many papers and books in internationally refereed journals in Applied Mathematics related disciplines).

Mansour Al Qubeissi

March 2015

ACKNOWLEDGEMENT

DECLARATION

I declare that the research contained in this thesis, unless otherwise formally indicated within the text, is the original work of the author. The thesis has not been previously submitted to this or any other university for a degree, and does not incorporate any material already submitted for a degree.

1st April 2015

CONTENTS

LIST OF TABLES

LIST OF FIGURES

XIII

NOMENCLATURE

A Constants, or alkylbenzene in Figures 4.13 and 4.15

B_M Spalding mass transfer number defined by Equation (2.23)

B_T Spalding heat transfer number defined by Equation (2.25)

C_m Constant, introduced in Equation (2.54)

c_l Specific heat of liquid [$W\,kg^{-1}K^{-1}$]

c_p Specific heat (of vapour or air) at constant pressure [$W\,kg^{-1}K^{-1}$]

D Diameter [m] or liquid/vapour mass diffusivity [$m^2\,s^{-1}$]

D_v Binary diffusion coefficient [$m^2\,s^{-1}$]

E Activation energy [$J\,mol^{-1}$]

f_m Distribution function of components (Equation 2.53)

$F(B_M)$ Mass film thickness correction factor, defined after Equation (2.24)

$F(B_T)$ Heat film thickness correction factor, defined after Equation (2.10)

H Heat transfer coefficient [$W\,m^{-2}K^{-1}$]

h_{0T} $\left(\frac{hR_d}{k_{eff}}\right) - 1$, parameter introduced in Equation (2.8)

h_{0Y} $-\left(1 + \frac{\alpha R_d}{D_{eff}}\right)$, parameter introduced in Equation (2.19)

h_m Mass transfer coefficient [$m\,s^{-1}$]

j Mass flux [$kg\,s^{-1}m^{-2}$], introduced in Section 2.10.

k Thermal conductivity [$W\,m^{-1}K^{-1}$]

k_B Boltzmann constant   [$J\,K^{-1}$]

k_R Parameter, defined after Equation (2.8)

L	Latent heat of evaporation [J kg^{-1}]
L_d	Diffusion length [m]
Le	Lewis number
M	Molar mass [g mol^{-1}]
$\dot{m}_d$	Droplet evaporation rate [kg s^{-1}]
N	Number of moles or number of terms
Nu	Nusselt number
Nu*	Nusselt number for non-evaporating droplets (Equation 2.28)
Nu$_n$	Nu/Nu$_{iso}$
p	Pressure [Pa]
p_{vis}^*	Partial vapour pressure of the ith species in the case when X$_{lis}$ = 1 (Equation 2.32)
Pe	Péclet number
Pr	Prandtl number
Q_L	Power spent on the droplet heating [J s^{-1}]
q_n	Parameter introduced in Equation (2.8)
R	Distance from the centre of a spherical droplet [m]
$\dot{R}_d$	Rate of change of radius defined by Equation (2.29) [m s^{-1}]
$\dot{R}_{dE}$	Rate of change of radius due to evaporation defined by Equation (2.31) [m s^{-1}]
$\dot{R}_{dT}$	Rate of change in radius due to thermal expansion, defined by Equation (2.30) [m s^{-1}]
Re	Reynolds number
R_u	Universal gas constant = 8.314472 [J K^{-1} mol^{-1}]

Sc   Schmidt number

Sh   Sherwood number

Sh_n $= Sh/Sh_{iso}$

Sh^* Sherwood number for non-evaporating droplets (Equation 2.27)

T Temperature [K], or tricycloalkane in Figures 4.13 and 4.15

t Time [s]

t_0 Time at the beginning of time step [s]

t_1 Time at the end of time step [s]

T_{eff} Effective temperature [K]

T^* Normalized temperature [K], defined after Equation (2.42)

U Velocity [m s^{-1}]

v_n Parameter introduced at Equation (2.8)

V Volume [m^3]

X Molar fraction

Y Mass fraction

Greek symbols

α Parameter defined by Equation (2.17)

β Collision integral between molecules used in Equations (2.67) and (2.68).

β_i Constant parameter defined in Expression (2.69); $\beta_i = 1$ in most cases.

γ Activity coefficient defined by Equation (2.32)

Δt Time step [s]

ε Molecular energy (Lennard-Jones potential) [J], defined after Equation (2.42)

κ Liquid thermal diffusivity [m² s⁻¹]

$\lambda_{0,n}$ Eigenvalues (see Equation (2.9), for temperature, and Equation (2.19), for species diffusion)

ϵ_i Evaporation rate of individual species i, defined by Equation (2.18)

μ Dynamic viscosity [Pa s]

$\mu_0(t)$ Parameter introduced at Equation (2.8)

ν Kinematic viscosity [m² s⁻¹]

ρ Density [kg m⁻³]

σ Minimal length of molecules (Leonard-Jones distance parameter) [Å]

τ Time instant in transient states

φ Parameter introduced in Equation (2.26)

χ Recirculations parameter, used in Equations (2.4) and (2.15)

Ω_D Collision integral defined by Equation (2.43)

Superscripts

$^{-}$ Average property for a mixture of components (Section 2.8)

$^{\sim}$ Corrected values, or converted to SI unit formats (Chapter 5)

Subscripts

0 Initial, or beginning of a numerical step

1 End of a numerical step

A Air

av   Average

b   Boiling

C   Droplet centre

c/cr   Critical

d   Droplet

eff   Effective property (taking into account droplet movement)

f   Fuel

g   Gas or region of influence

iso   Isolated droplet

l   Liquid

lis   Liquid property at the surface of the droplet

M   Species diffusion, or mass property

r/ref   Reference value

s   Droplet surface

T   Temperature, or thermal, property

v   Vapour

vis   Vapour property at the surface of the droplet

∞ Far from the droplet surface

Abbreviations

BME   Butter Methyl Ester

CAN   Canola seed Methyl Ester

CFD   Computational Fluid Dynamics

CME   Coconut Methyl Ester

CNE   Corn Methyl Ester

CPU   Central Processing Unit

C/QC   Components/Quasi-Components

CSE   Cottonseed Methyl Ester

CT   Continuous Thermodynamics

DC   Discrete Components

DCM   Discrete Component Models

DI   Direct Injection

DNS   Direct Numerical Simulation

ED   Effective Diffusivity

ETC   Effective Thermal Conductivity

FACE   Fuel used in Advanced Combustion Engines

HME1   Hemp seed Methyl Ester (produced in the Ukraine)

HME2   Hemp seed Methyl Ester (produced in the EU)

IC   Internal Combustion

ID   Infinite Diffusivity

IO   Iso-Octane

ITC   Infinite Thermal Conductivity

LME   Lard Methyl Ester

LNE   Linseed Methyl Ester

MDQC	Multi-Dimensional Quasi-Discrete
ME	Multi-component and Effective thermal conductivity-Effective diffusivity
MI	Multi-component with Infinitely fast diffusion of species
PME	Palm seed Methyl Ester
PMK	Palm Kernel Methyl Ester
PTE	Peanut Methyl Ester
QD	Quasi-Discrete
RME	Rapeseed Methyl Ester
SI	Single-component with Infinitely large thermal conductivity and Infinitely fast deffusivity
SMD	Sauter Mean Diameter
SME	Soybean Methyl Ester
SNE	Sunflower Methyl Ester
TME	Tallow Methyl Ester
TGE	Tung Methyl Ester
WME	Waste cooking-oil Methyl Ester

1   INTRODUCTION

1.1   Background

Estimation of the delay in combustion processes due to the heating and evaporation of automotive fuel droplets is crucial for the design and performance of internal combustion engines [1]–[3]. Furthermore, the amount of engine emission is proportional to the delay in ignition in the Direct Injection (DI) Internal Combustion (IC) Engines [4]. Hence, an understanding of liquid fuel heating and evaporation processes in DI-IC engines is important for modelling and optimising these engines [5]–[8]. In most cases, measurements related to these processes are very complex, expensive, time consuming, and not always available. Modelling can be an alternative for understanding automotive fuel droplet heating and evaporation processes preceding the onset of combustion in IC engines. These processes are illustrated in Figure 1.1.
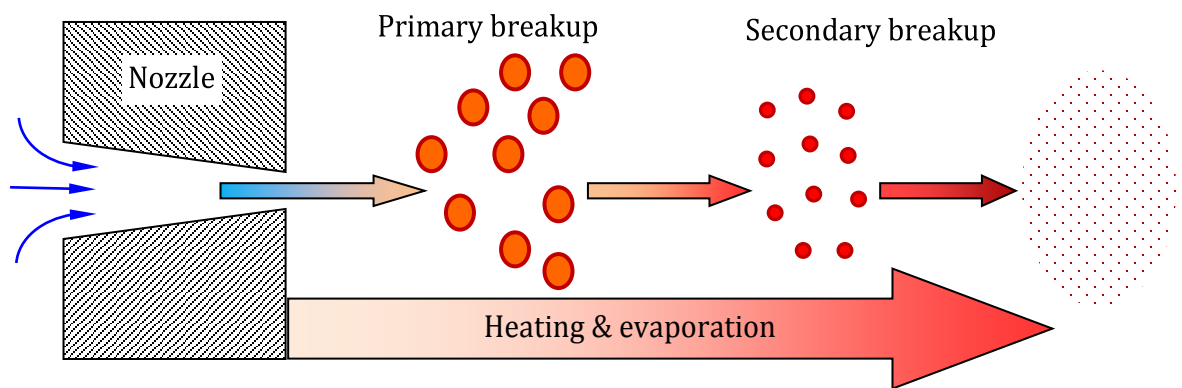
Figure 1.1 Schematic of the injection, breakup and evaporation processes, preceding the onset of combustion in IC engines.

There have been extensive studies of the heating and evaporation processes of micro-sized droplets [5], [9]–[12]. In most previous studies, multi-component fuel droplets have been represented with mono-component fuel droplets [13]–[22]. These approaches rely upon the assumptions that the effects of species diffusions within droplets during the evaporation processes can be ignored. Also, in most previous studies, many effects such as finite thermal conductivity

inside the droplets are ignored to reduce complexity of the models [23], [24]. These rather crude approximations are not always applicable for realistic industrial applications [7], [9], [25], [26].

The previous studies mainly focused on two approaches to modelling multi-component droplet heating and evaporation: firstly, those based on the analysis of individual components, known as Discrete Component Models (DCM) [26]–[33], applicable in the cases when a small number of components needs to be taken into account; and secondly, those based on the probabilistic analysis of a large number of components, such as the Continuous Thermodynamics (CT) approach [12], [34]–[40] and the Distillation Curve Model [10], [41], [42]. In the second family of models, a number of additional simplifying assumptions were used, including the assumptions that species inside droplets mix infinitely quickly or do not mix at all. These assumptions were shown to be very crude for modelling realistic automotive fuel droplets [25], [43]–[47]. Compromised approaches, to combine the benefits of the abovementioned models with further simplifications, were suggested in [39], [48]–[50].

The current study focuses on the application of the previously developed models to automotive fuel droplets, containing limited number of components (biodiesel fuels) [46], [51]–[53], and the generalisation of the recently developed multi-component models [5], [45], [54], [55]. These models take into account the effects of the realistic number of components, finite thermal conductivity, species diffusivity and recirculation inside droplets (Effective Thermal Conductivity (ETC) and Effective Diffusivity (ED) models). In both cases, the models used in the analysis, are based on the previously obtained analytical solutions to the heat transfer and species diffusion equations within droplets.

The recently developed 'quasi-discrete' model [43], [47] is an alternative approach to the DCM for modelling droplets containing large number of components. This model is based on grouping of components with close thermodynamic and transport properties and the introduction of hypothetical components with non-integer numbers of carbon atoms. These hypothetical components are called 'quasi-components' (QC). There are some similarities

2

between the QC introduced in [47] and the pseudo-components used in [48], but the pseudo-component model ignores the diffusion of species within the droplet.

In contrast to the previously suggested models, designed for large numbers of components, the model suggested in [47] took into account the diffusion of liquid species and thermal diffusion alongside recirculation inside droplets, without losing the features of the original DCM. In [43], this model was generalised to take into account the differences in liquid density, viscosity, specific heat capacity, and thermal conductivity for liquid components in Diesel and gasoline fuels.

Although the usefulness and efficiency of the quasi-discrete model has been clearly demonstrated, this model still has a number of serious limitations; the most important of which is that it is based on the assumption that Diesel and gasoline fuels consist only of n-alkanes [43], [45], [47]. At the same time, the total molar fraction of alkanes (n-alkanes and iso-alkanes) is only about 40% of the overall composition of Diesel fuels, as shown in Figure 1.2, (a similar conclusion could be drawn for gasoline fuel [56]). Hence, the contribution of other components apart from alkanes cannot be ignored. In the approach described in this thesis, the model originally suggested in [47] is generalised to take into account the realistic composition of Diesel fuels. The new model is called the 'multi-dimensional quasi-discrete' model [57].
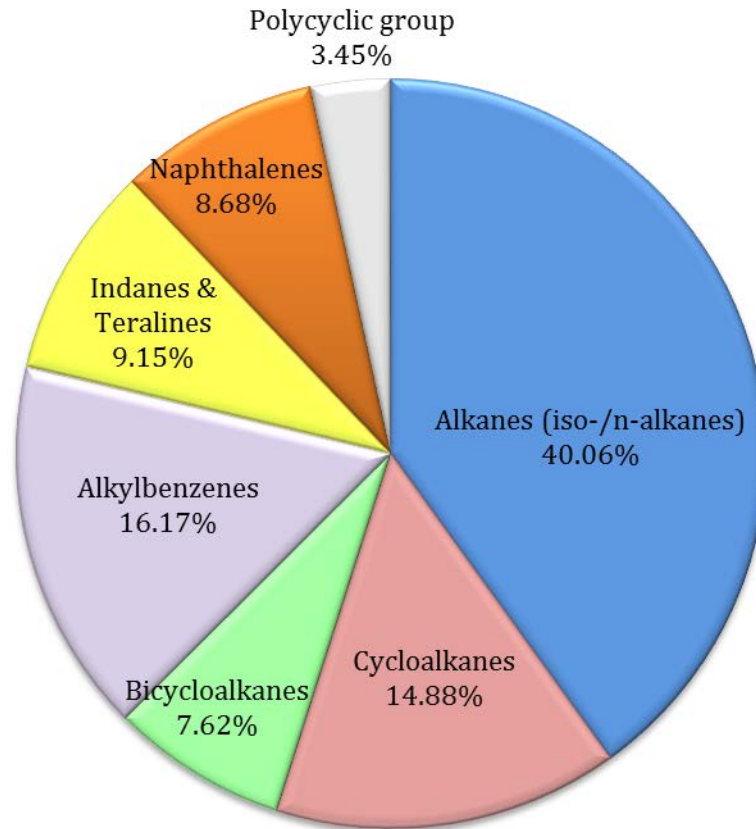
Figure 1.2 The contributions of the most important groups of species in a typical Diesel fuel.

1.2   Objectives

The objectives of this study are as follows.

1.   To understand the underlying physics in automotive fuel droplet heating and evaporation processes.

2.   To apply the previously developed Discrete Component Models to the analysis of industrial multi-component biodiesel fuel droplet heating and evaporation.

3.   To generalise the previously developed quasi-discrete model to take into account realistic composition of Diesel fuel, leading to the introduction of the Multi-Dimensional Quasi-Discrete (MDQD) model.

4.   To apply the MDQD model to the analysis of realistic gasoline fuel droplet heating and evaporation.

5.   To investigate feasibility of implementing the developed (FORTRAN based) models into a commercial CFD code (ANSYS-Fluent software) for a wider range of applications.

1.3   The structure of the thesis

In Chapter 2, the basic models used in the analysis are presented and discussed. In Chapter 3, the Discrete Component Model is applied to the analysis of heating and evaporation of biodiesel fuel droplets. Chapter 4 focuses on the description of the new 'Multi-Dimensional Quasi-Discrete' model and its application to realistic commercial Diesel fuel droplets. Chapter 5 presents the application of the 'Multi-Dimensional Quasi-Discrete' model to typical FACE (Fuel used in Advanced Combustion Engines) gasoline fuel droplets. The main results of the thesis are summarised in Chapter 6. SI units are used for all variables presented in this thesis.

1.4   Dissemination of the results

The original results presented in the thesis have been reported in the following papers published in international refereed journals: [46], [57]–[62]; and international refereed conference proceedings: [25], [51], [63]–[68]. These and related publications are summarised below.

Refereed journal articles

1. **Al Qubeissi M.**, Sazhin S.S., Turner J., Begg S., Crua C., Heikal M.R., 2015. Modelling of gasoline fuel droplets heating and evaporation. *Fuel* 159, 373-384.

2. Sazhin, S.S., Shishkova I.N., **Al Qubeissi M.,** 2015. A self-consistent kinetic model for droplet heating and evaporation. Submitted to *Int J Heat and Mass Trans*.

3. **Al Qubeissi M.**, Sazhin S.S., Crua C., Turner J., Heikal M.R., 2015. Modelling of biodiesel fuel droplet heating and evaporation: effects of fuel composition. *Fuel* 154, 308-318.

4. Sazhin S.S., Shishkova I.N., **Al Qubeissi M.,** 2014. Heating and evaporation of a two-component droplet: hydrodynamic and kinetic models. *Int J Heat and Mass Trans* 79, 704-712.

5. Sazhin S.S., **Al Qubeissi M.**, Xie J.-F., 2014. Two approaches to modelling the heating of evaporated droplets. *Int Comm Heat Mass Trans* 57, 353-356.

6. Sazhin S.S., **Al Qubeissi M.**, Nasiri R., Gunko V.M., Elwardany A.E., Lemoine F., Grisch F., Heikal M.R., 2014. A multi-dimensional quasi-discrete model for the analysis of Diesel fuel droplet heating and evaporation. *Fuel* 129, 238-266.

7. Sazhin S.S., **Al Qubeissi M.**, Kolodnytska R., Elwardany A.E., Nasiri R., Heikal M.R., 2014. Modelling of biodiesel fuel droplet heating and evaporation. *Fuel* 115, 559–572.

Invited papers

8. **Al Qubeissi M.**, Sazhin S.S., 2015. Modelling of droplet heating and evaporation: an application to biodiesel, gasoline and Diesel fuels. Invited through: *ICTEA-8: 8th International Conference on Thermal Engineering: Theory and Applications*, Amman, Jordan; submitted to *Int J Eng Sys Model Simu*.

9. **Al Qubeissi M.**, Sazhin S.S., Crua C., Heikal M.R., 2015. Modelling of Heating and Evaporation of Biodiesel Fuel Droplets. Invited through: WASET- index 97; published by *Int J Mech Aero Indus Mechat Eng*, 9 (1), 46 – 49.

10. Sazhin S.S., **Al Qubeissi M.**, 2014. Modelling of automotive fuel droplet heating and evaporation: mathematical tools and approximations. Invited through: *MURPHYS-HSFS-2014; J Physics: Conf series* (in press).

Refereed conference papers

11. Sazhin S.S., **Al Qubeissi M.**, Heikal M.R., 2015. Modelling of heating and evaporation of automotive fuel droplets: recent results and unsolved problems. *BHTC'2015: 7th Baltic Heat Transfer Conference*, Tallinn, Estonia, 24-26 August 2015, pp. 181-186.

12. **Al Qubeissi M.**, Sazhin S.S., de Sercey G., Crua C., 2014. Multi-dimensional quasi-discrete model for the investigation of heating and evaporation of Diesel fuel droplets. *ILASS-2014: 26th European Conference on Liquid Atomization and Spray Systems*, Bremen, Germany, 1-4 September 2014, paper ABS-135.

13. Duret B., **Al Qubeissi M.**, Sazhin S.S., Crua C., 2014. Evaporating droplets: comparisons between DNS and modelling. *ILASS-2014: 26th European Conference on Liquid Atomization and Spray Systems*, Bremen, Germany, 1-4 September 2014, paper ABS-187.

14. Sazhin S.S., Shishkova I., **Al Qubeissi M.**, 2014. Kinetic modelling of Diesel fuel droplet heating and evaporation: effects of the approximation of fuel composition. *ILASS-2014: 26th European Conference on Liquid Atomization and Spray Systems*, Bremen, Germany, 1-4 September 2014, paper ABS -148.

15. Sazhin S.S., **Al Qubeissi M.**, Heikal M.R., 2014. Modelling of biodiesel and diesel fuel droplet heating and evaporation. *IHTC-15: 15th International Heat Transfer Conference*, Kyoto 10-15 August 2014, paper IHTC15-8936. ISBN: 978-1-56700-421-2.

16. Sazhin S.S., **Al Qubeissi M.**, 2014. Modelling of automotive fuel droplet heating and evaporation: mathematical tools and approximations. Proceedings of *7th Multi-Rate Processes and Hysteresis (MURPHYS-HSFS-2014),* Berlin, Germany, 7th-11th April 2014.

17. Kolodnytska R., **Al Qubeissi M.**, Sazhin S.S., 2013. Biodiesel fuel droplets: transport and thermodynamic properties. *Proceedings of the ILASS – Europe 2013, 25th European Conference on Liquid Atomization and Spray Systems*, Chania, Greece, 1-4 September, Paper No. 7 (CD).

18. **Al Qubeissi M.**, Kolodnytska R., Sazhin S.S., 2013. Biodiesel fuel droplet: modelling of heating and evaporation processes. *Proceedings of the ILASS – Europe 2013, 25th European Conference on Liquid Atomization and Spray Systems*, Chania, Greece, 1-4 September, Paper No. 4 (CD).

Abstracts/ research communications

19. **Al Qubeissi M.**, Sazhin S.S., 2015. Modelling of droplet heating and evaporation: an application to biodiesel, gasoline and Diesel fuels. *ICTEA-8: 8th International Conference on Thermal Engineering: Theory and Applications*, Amman, Jordan, 18-21 May 2015.

20. **Al Qubeissi M.**, Sazhin S.S., 2015. Modelling of automotive fuel droplet heating and evaporation. *INTERREG E3C3 project steering committee* meeting, CNRS, Caen, France, 26th March.

21. **Al Qubeissi M.**, Sazhin S.S., Crua C., and Heikal M.R., 2015. Modelling of Heating and Evaporation of Biodiesel Fuel Droplets. *ICHTA-2015: XIII International Conference on Heat Transfer and Applications*, World Academy of Science, Engineering and Technology (WASET) , London, UK, 19-20 January 2015, 2 (9), paper 672.

22. **Al Qubeissi M.**, Sazhin S.S., 2014. Progress in modelling of automotive fuel droplet heating and evaporation. Centre for Automotive Engineering (CAE) Research Workshop, UoB: *Optical diagnostics and numerical modelling for diesel spray combustion,* UoB, UK, 17th October 2014.

23. **Al Qubeissi M.**, Sazhin S.S., 2014. Modelling of automotive fuel droplet heating and evaporation. *INTERREG E3C3 project steering committee meeting*, University of Cambridge, UK, 29th September 2014.

24. **Al Qubeissi M.**, Sazhin S.S., 2014. A multi-dimensional quasi-discrete model for the heating and evaporation of Diesel fuel droplets. *ILASS-2014: 26th*

European Conference on Liquid Atomization and Spray Systems, Bremen, Germany. Book of Abstracts, edited by Lydia Achelis and Udo Fritsching, published by the University of Bremen, pp. 171-172.

25. Duret B., **Al Qubeissi M.**, Sazhin S.S., Cyril C., 2014. Evaporating droplets: comparisons between DNS and modelling. *ILASS-2014: 26th European Conference on Liquid Atomization and Spray Systems*, Bremen, Germany. Book of Abstracts, edited by Lydia Achelis and Udo Fritsching, published by the University of Bremen, pp. 127-128.

26. Sazhin S.S., Shishkova I.N., **Al Qubeissi M.**, 2014. Kinetic modelling of Diesel fuel droplet heating and evaporation: effects of the approximation of fuel composition. *ILASS-2014: 26th European Conference on Liquid Atomization and Spray Systems*, Bremen, Germany. Book of Abstracts, edited by Lydia Achelis and Udo Fritsching, published by the University of Bremen, pp. 109-110.

27. **Al Qubeissi M.**, Sazhin S.S., 2014. Heating and evaporation of automotive fuel droplets. CAE Research Workshop, UoB: *New approaches to spray modelling*, UoB, 19th August 2014.

28. **Al Qubeissi M.**, Sazhin S.S., 2014. Development of new models for the heating and evaporation of automotive fuel droplets. *The Faculty of Science and Engineering Doctoral Research Student Conference,* UoB, 22th-23rd July 2014.

29. **Al Qubeissi M.**, Sazhin S.S., 2014. Modelling of automotive fuel droplet heating and evaporation. *INTERREG E3C3 project steering committee meeting*, Brighton, UK, 25th March 2014.

30. **Al Qubeissi M.**, Sazhin S.S., 2013. Modelling of multi-component fuel droplet heating and evaporation. *Ricardo meeting: a possible fund to the University of Brighton*, Ricardo plc, Shoreham, UK, 6th December 2013.

31. **Al Qubeissi M.**, Sazhin S.S., Cyril C., Heikal M. R., 2013. Modelling of fuel-droplet heating and evaporation processes. *INTERREG E3C3 project steering committee meeting*, Rouen, France, 16th September 2013.

32. Kolodnytska R., **Al Qubeissi M.**, Sazhin S.S., 2013. Biodiesel fuel droplets: transport and thermodynamic properties. *ILASS-2013: 25th European Conference on Liquid Atomization & Spray Systems*, Crete, Greece, 1st-4th September 2013.

33. **Al Qubeissi M.**, Kolodnytska R., Sazhin S.S., 2013. Biodiesel fuel droplet: modelling of heating and evaporation processes. *25th European Conference on Liquid Atomization & Spray Systems,* Crete, Greece, 1st-4th September 2013.

34. **Al Qubeissi M.**, 2013. Biodiesel fuel droplets: modelling of heating and evaporation processes. CAE Research Workshop, UoB: *Modelling of droplet and spray dynamics, heating and evaporation*, UoB, 16th August 2013.

35. **Al Qubeissi M.**, Sazhin S.S., 2013. Modelling of biodiesel droplet heating and evaporation. *The Faculty of Science and Engineering Doctoral Research Student Conference,* UoB, 8th-9th July 2013.

36. **Al Qubeissi M.**, 2013. Modelling of biodiesel and Diesel fuel droplet heating and evaporation: hydrodynamics analysis. CAE Research Workshop, UoB: *Droplet and sprays: new approaches to modelling*, UoB, 5th June 2013.

37. Sazhin S.S., **Al Qubeissi M.**, Heikal M.R, 2013. Modelling of automotive fuel droplets heating and evaporation. *Droplet Impact Phenomena & Spray Investigations Workshop*, Bergamo, Italy, 31st May 2013.

38. **Al Qubeissi M.**, Kolodnytska R., Sazhin S.S., 2013. Modelling of biodiesel droplets. *UoB Research poster competition*, Brighton, 22nd March 2013.

39. **Al Qubeissi M.**, 2012. A quasi-discrete model for multi-component fuels. CAE Research Workshop, UoB: *New approaches to modelling of droplet heating and evaporation*, UoB, 17th October 2012.

2 BASIC EQUATIONS

2.1 Introductory comments

As in [9], [12], [23], [24], [55], the processes in the droplets are assumed to be spherically symmetric. The models used in our analysis take into account the following processes inside the droplet: 1) diffusion of species; 2) finite thermal conductivity; and 3) internal recirculation (vortices) due to relative velocity between ambient gas and the droplet. Only the effects of ambient gas on droplets are taken into account, the effects of coupling between gas and droplets are ignored (see [69] for a possible approach to take into account this coupling).

The models presented in the thesis are built on the previously developed and validated analytical solutions to the heat transfer and species diffusion equations inside droplets [16], [44], [70], [71]. The quasi-discrete (QD) model, described in [43], [47], is further modified to include several groups in a commercial Diesel fuel [57]. This generalised version of the QD model is described as Multi-Dimensional Quasi Discrete (MDQD) model [57], [63], [64].

The models described in this chapter are based on the equations describing heating, evaporation and species diffusion in the liquid phase. The equations describing these processes and their approximations are presented and discussed in Sections 2.2-2.7. The analysis of these equations is followed by the presentation of the methods of averaging the thermodynamic and transport properties, in Section 2.8. In Section 2.9, the predictions of the conventional model, in which the heat rate supplied to the droplet is inferred from balance equations for heat and mass transfer in the gas phase [9], are compared with the prediction of the model for mono-component droplet presented in Sections 2.2-2.8. The applications of some newly developed models to kinetic modelling of droplet heating and evaporation are discussed in Section 2.10. The details of the numerical algorithm used for the hydrodynamic calculations of droplet

heating and evaporation are presented and discussed in Section 2.11. The main results of the chapter are summarised in Section 2.12.

2.2 Droplet heating

The process of heating of mono- and multi-component droplets is described by the following transient heat conduction equation for the temperature $T = T(t, R)$ in the liquid phase [72], [73]:

$$\frac{\partial T}{\partial t} = \kappa \left(\frac{\partial^2 T}{\partial R^2} + \frac{2}{R} \frac{\partial T}{\partial R} \right),$$ (2.1)

where t is time, R is the distance from the centre of the droplet (assumed spherical), T is the temperature and κ is the effective thermal diffusivity defined as [7], [9], [44]:

$$\kappa = k_{\text{eff}}/c_l \rho_l,$$ (2.2)

c_l is the specific heat capacity of liquid, ρ_l is the density of liquid, and k_{eff} is the Effective Thermal Conductivity (ETC), defined by the following expression:

$$k_{\text{eff}} = \chi k_l,$$ (2.3)

χ takes into account the effect of recirculation inside droplets as [7], [74], [75]:

$$\chi = 1.86 + 0.86 \tanh\left[2.225 \log_{10}\left(\text{Pe}_{d(l)}/30\right)\right],$$ (2.4)

χ varies between 1 (when Peclet number $\text{Pe}_l = \text{Re}_{d(l)}\text{Pr}_l < 10$) and 2.72 (for $\text{Pe}_{d(l)} > 500$), $\text{Re}_{d(l)} = \frac{2\rho_l u_s R_d}{\mu_l}$ is the Reynolds number, $U_s = \frac{1}{32}\Delta U \left(\frac{\mu_g}{\mu_l}\right) \text{Re}_d C_F$ is the maximum surface velocity inside droplet, $\Delta U = |U_g - U_d|$ and $C_F = \frac{12.69}{\text{Re}_d^{2/3}(1+B_M)}$ is the friction drag coefficient, $\text{Pr}_l = \frac{c_l \mu_l}{k_l}$ is the Prandtl number, u_g is the gas velocity, U_d is the droplet velocity, μ_l and k_l are liquid dynamic viscosity and thermal conductivity, respectively. This approach is known as the Effective Thermal Conductivity (ETC) model. A typical distribution of temperature inside a moving droplet using DNS is shown in Figure 2.1 [67].

(a)

(b)

(c)
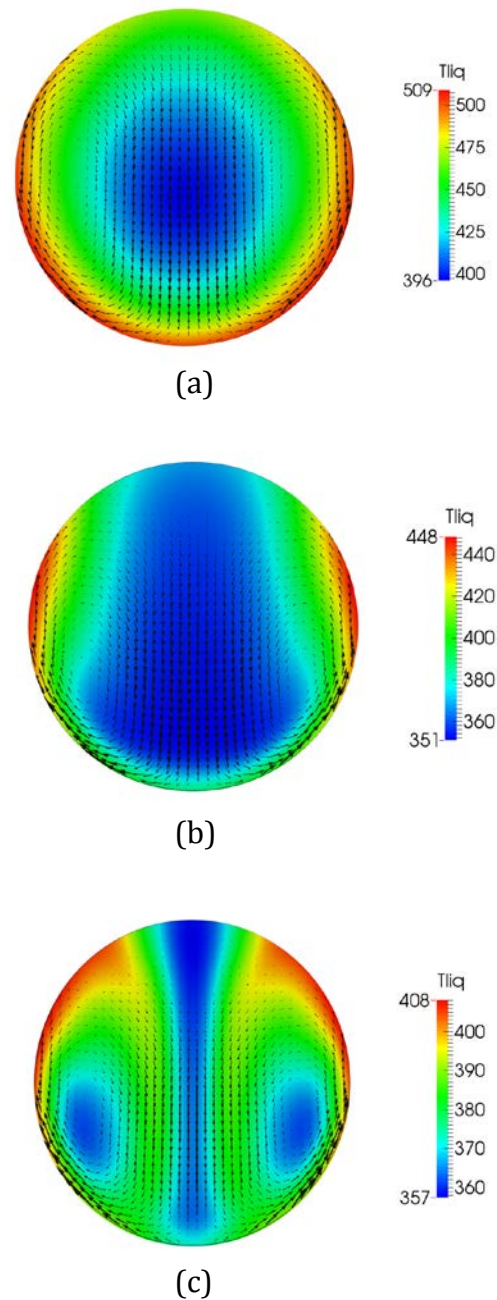
Figure 2.1 The effect of internal recirculation on temperature distribution inside droplets moving with relative velocities (a) 0.2 m s^{-1}, (b) 1 m s^{-1} and (c) 3 m s^{-1}. Reproduced from [67] with permission.

In contrast to Figure 2.1, the ETC model alone cannot describe adequately the distribution of temperature inside a moving droplet, but can predict the the average temperature at the surface of the droplet which is most important for practical engineering applications, including modelling of the evaporation process.

The initial and boundary conditions for Eq. (2.1) are introduced as:

$$
\left.
\begin{aligned}
T(t = 0) &= T_{d0}(R) \\
h(T_g - T_s) &= k_{\text{eff}} \left.\frac{\partial T}{\partial R}\right|_{R = R_d - 0}
\end{aligned}
\right\},
\tag{2.5}
$$

where $T_s = T_s(t)$ is the droplet surface temperature, R_d is the droplet radius, $T_g = T_g(t)$ is the ambient gas temperature, $h = h(t)$ is the convective heat transfer coefficient, linked with the Nusselt number Nu by the following expression:

$$
Nu = 2R_d \, h/k_g,
\tag{2.6}
$$

k_g is the gas thermal conductivity. To take into account the effect of evaporation, the gas temperature T_g is replaced with the effective temperature T_{eff} [76]:

$$
T_{\text{eff}} = T_g + \frac{\rho_l L \dot{R}_{dE}}{h},
\tag{2.7}
$$

where L is the latent heat of evaporation and $\dot{R}_{dE}$ is the rate of change of droplet radius due to evaporation only, which is taken from previous time step and estimated using Equation (2.31). At any given time step, R_d is assumed constant in the analytical solutions and is updated at the end of the time step Δt: $R_{d(new)} = R_{d(old)} + \dot{R}_d \Delta t$, where the value of $\dot{R}_d$ is controlled by the droplet evaporation and swelling (see Equations (2.29)-(2.31) in Section 2.4). Remembering the physical background to the problem, this work is only interested in a solution which is continuously twice differentiable in the whole domain. This implies that T should be bounded for $0 \leq R \leq R_d$.

Assuming that $h =$ constant, the analytical solution to Equation (2.1), applied for the time step $\Delta t = t_1 - t_0 \equiv t_1 - 0$, gives the following expression for the temperature at the end of each time step, when $t = t_1$ [71]:

$$
T(R,t) = \frac{R_d}{R} \sum_{n=1}^{\infty} \left\{
\begin{aligned}
& q_n \exp[-\kappa_R \lambda_n^2 t] - \frac{\sin \lambda_n}{\|v_n\|^2 \lambda_n^2} \mu_0(0) \exp[-\kappa_R \lambda_n^2 t] \\
& - \frac{\sin \lambda_n}{\|v_n\|^2 \lambda_n^2} \int_0^t \frac{d\mu_0(\tau)}{d\tau} \exp[-\kappa_R \lambda_n^2 (t - \tau)] d\tau
\end{aligned}
\right\} \sin\left(\lambda_n \frac{R}{R_d}\right) +
$$

$$
T_{\text{eff}}(t),
\tag{2.8}
$$

where

$$\|v_n\|^2 = \frac{1}{2}\left(1 - \frac{sin\,2\lambda_n}{2\lambda_n}\right) = \frac{1}{2}\left(1 + \frac{h_{0T}}{h_{0T}^2 + \lambda_n^2}\right); \quad q_n = \frac{1}{R_d\,\|v_n\|^2}\int_0^{R_d}\tilde{T}_0(R)\sin\left(\lambda_n\frac{R}{R_d}\right)dR;$$

$$k_R = \frac{k_{\text{eff}}}{c_l\rho_l R_d^2}; \quad \mu_0(t) = \frac{hT_g(t)R_d}{k_{\text{eff}}}; \quad h_{0T} = \left(\frac{hR_d}{k_{\text{eff}}}\right) - 1; \quad \mu_0' \equiv \frac{d\,\mu_0(t)}{dt}; \quad \text{and} \quad \tilde{T}_0(R) = R\,T_{d0}(R)/R_d.$$

A set of positive eigenvalues λ_n, $n > 0$ (the trivial solution $\lambda = 0$ is not considered), is found from the solution to the following equation:

$$\lambda \cos \lambda + h_{0T}\sin \lambda = 0. \tag{2.9}$$

In the limit $k_{\text{eff}} \to \infty$ the prediction of Expression (2.8) reduces to the one which follows from the model based on the assumption that $k_{\text{eff}} = \infty$ [20] (Infinite Thermal Conductivity (ITC) model). The value of Nu for an isolated moving droplet is estimated using the following equation [9]:

$$\text{Nu}_{\text{iso}} = 2\frac{\ln(1+B_T)}{B_T}\left[1 + \frac{(1+\text{Re}_d\text{Pr}_d)^{1/3}\max\{1,\,\text{Re}_d^{0.077}\}-1}{2\,F(B_T)}\right], \tag{2.10}$$

where $F(B_T) = (1 + B_T)^{0.7}\frac{\ln(1+B_T)}{B_T}$, B_T is the Spalding heat transfer number:

$$B_T = \frac{c_{pv}(T_g - T_s)}{L_{\text{eff}}}, \tag{2.11}$$

c_{pv} is the specific heat capacity at constant pressure of the fuel vapour and,

$$L_{\text{eff}} = L + \frac{Q_L}{\dot{m}_d} = \sum_i \epsilon_i L_i + \frac{Q_L}{\sum_i \dot{m}_i}, \tag{2.12}$$

Q_L is the power spent on the droplet heating, $\epsilon_i = \epsilon_i(t)$ are the evaporation rates of species i, and $\dot{m}_i = \epsilon_i\dot{m}_d$, $(\dot{m}_d = \sum_i \dot{m}_i)$. The effects of the interaction between droplets are ignored (simplified models for these effects are discussed in [16], [44], [69]). The analysis of $\dot{m}_i = \epsilon_i\dot{m}_d$ $(\dot{m}_d = \sum_i \dot{m}_i)$ in this chapter is based on the assumption that a mixture of vapour species can be treated as a separate gas i.e. $Y_{vs} = \sum_i Y_{vis}$ (see Equation (2.22) in Section 2.4).

2.3   Species diffusion in the liquid phase

Assuming that the processes inside droplets are spherically-symmetric, equations for mass fractions of liquid species $Y_{li} \equiv Y_{li}(t, R)$ can be presented as [5], [75], [77]:

$$\frac{\partial Y_{li}}{\partial t} = D_{\text{eff}} \left(\frac{\partial^2 Y_{li}}{\partial R^2} + \frac{2}{R} \frac{\partial Y_{li}}{\partial R} \right), \tag{2.13}$$

where i = 1,2,3,… (refers to species), D_{eff} is the effective liquid species mass diffusivity, linked with the liquid diffusivity D_l via the following equation:

$$D_{\text{eff}} = \chi_Y D_l, \tag{2.14}$$

D_l is calculated as described in Section 2.6 and the coefficient χ_Y is approximated as:

$$\chi_Y = 1.86 + 0.86 \tanh\left[2.225 \log_{10}\left(\text{Re}_{d(l)} \text{Sc}_l / 30\right)\right], \tag{2.15}$$

similar to Equation 2.4, χ_Y varies from 1 (at droplet mass diffusion Peclet number $\text{Pe}_l = \text{Re}_{d(l)} \text{Sc}_l < 10$) to 2.72 (at $\text{Pe}_l > 500$), $\text{Sc}_{d(l)} = \frac{\nu_l}{D_l}$ is the liquid Schmidt number, ν_l is the liquid kinematic viscosity and $\text{Re}_{d(l)}$ is the same as described in Section 2.2 (Equation 2.4). As in the case of the ETC model, the liquid fuel and transport properties and liquid velocity just below the surface of the droplet were used for calculating Re_l. The model based on Equations (2.13)-(2.15) is known as the Effective Diffusivity (ED) model [7], [9]. As in the case of the ETC model, this model cannot describe the details of underlining physics inside the droplet, such as vortex structure, but such details are not necessary in most engineering applications.

The analytical solution to Equation (2.13) was obtained subject to the following boundary condition [5]:

$$\alpha(\epsilon_i - Y_{lis}) = -D_{\text{eff}} \frac{\partial Y_{li}}{\partial R}\bigg|_{R=R_d-0}, \tag{2.16}$$

and the initial condition $Y_{li}(t = 0) = Y_{li0}(R)$, where $Y_{lis} = Y_{lis}(t)$ are liquid components' mass fractions at the droplet's surface,

$$\alpha = \frac{|\dot{m}_d|}{4\pi\rho_l R_d^2} = |\dot{R}_{dE}|, \tag{2.17}$$

$\dot{m}_d$ is the droplet evaporation rate, the calculation of which is discussed in the next section (see Equation (2.22)). As in the case of Equation (2.1), we are only interested in a solution which is continuously twice differentiable in the whole domain. This implies that Y_{li} should be bounded for $0 \le R \le R_d$. Moreover, the physical meaning of Y_{li}, as the mass fraction, implies that $0 \le Y_{li} \le 1$.

Assuming that species concentrations in the ambient gas are equal to zero (this assumption can be critical when applied to confined spaces), the values of ϵ_i can be found from the following relation [29], [55], [78]:

$$\epsilon_i = \frac{Y_{vis}}{\sum_i Y_{vis}}, \tag{2.18}$$

where the subscript v indicates the vapour phase and Y_{vis} is the mass fraction of species i. The conditions ϵ_i = const. and α = const. can always be guaranteed for sufficiently small time steps.

The analytical solution to Equation (2.13) can be presented as [55]:

$$Y_{li} = \epsilon_i + \frac{1}{R} \left\{ \begin{array}{l} \left[\exp\left[D_{\text{eff}}\left(\frac{\lambda_0}{R_d}\right)^2 t\right][q_{i0} - \epsilon_i Q_0] \sinh\left(\lambda_0 \frac{R}{R_d}\right) + \right. \\ \left. \sum_{n=1}^{\infty} \left[\exp\left[-D_{\text{eff}}\left(\frac{\lambda_n}{R_d}\right)^2 t\right][q_{in} - \epsilon_i Q_n]\sin\left(\lambda_n \frac{R}{R_d}\right)\right) \end{array} \right\}, \tag{2.19}$$

where, λ_0 and λ_n are determined from the solutions to equations $\tanh \lambda_0 = -\lambda_0/h_{0Y}$ and $\tanh \lambda_n = -\lambda_n/h_{0Y}$ (for n $\ge$ 1), respectively, $h_{0Y} = -\left(1 + \frac{\alpha R_d}{D_{\text{eff}}}\right)$,

$$Q_n = \left\{ \begin{array}{ll} -\frac{1}{\|v_0\|^2}\left(\frac{R_d}{\lambda_0}\right)^2 (1 + h_{0Y}) \sinh \lambda_0 & \text{when } n = 0 \\ \frac{1}{\|v_n\|^2}\left(\frac{R_d}{\lambda_n}\right)^2 (1 + h_{0Y}) \sin \lambda_n & \text{when } n \ge 1 \end{array} \right\}, \tag{2.20}$$

$\|v_n\|^2$ is obtained from Equation (2.8), replacing h_{0T} with h_{0Y}, and:

$$q_{in} = \left\{ \begin{array}{ll} \frac{1}{\|v_0\|^2}\int_0^{R_d} R\, Y_{li0}(R) \sinh\left(\lambda_0 \frac{R}{R_d}\right) dR & \text{when } n = 0 \\ \frac{1}{\|v_n\|^2}\int_0^{R_d} R\, Y_{li0}(R) \sin\left(\lambda_n \frac{R}{R_d}\right) dR & \text{when } n \ge 1 \end{array} \right\}, \tag{2.21}$$

When considering the diffusion of several species it is assumed that D_{eff} is the same for all species and that it can be estimated based on the average characteristics of the liquid fuel (see Section 2.6 for details). The model, based on Equation (2.13) is known as the Discrete Component Model (DCM).

2.4   Droplet evaporation

In the case of multi-component droplets the problem of modelling droplet evaporation is complicated by the fact that different species diffuse at different rates; and the evaporation rate of one of the species is affected by the evaporation rate of other species [16], [55]. As in [5], [14], the relative diffusion of components in the gas phase will be ignored and the analysis of evaporation of multi-component droplets will be based on the following expression for $\dot{m}_d$ (as in the case on mono-component droplets):

$$\dot{m}_d = -2\pi R_d D_v \rho_{\text{total}} B_M \, \text{Sh}_{\text{iso}}, \tag{2.22}$$

where D_v is the binary diffusion coefficient of vapour in gas (air), $\rho_{total} = \rho_g + \rho_v$ is the total density of the mixture of vapour and gas, ρ_g is the density of the ambient gas, B_M is the Spalding mass transfer number defined as [79]:

$$B_M = \frac{\rho_{vs} - \rho_{v\infty}}{1 - \rho_{vs}} = \frac{Y_{vs} - Y_{v\infty}}{1 - Y_{vs}}, \tag{2.23}$$

Y_v is the vapour mass fraction, ρ_{vs} and $\rho_{v\infty}$ are densities of vapour in the vicinity of droplets surfaces and at a large distance from them, Sh_{iso} is the Sherwood number approximated for isolated droplets by the following expression [9]:

$$\text{Sh}_{\text{iso}} = 2 \frac{\ln(1+B_M)}{B_M} \left[1 + \frac{(1 + Re_d Sc_d)^{1/3} \max\{1, Re_d^{0.077}\} - 1}{2 \, F(B_M)} \right], \tag{2.24}$$

The parameters in Equation (2.24) are the same of those used in Equation (2.10), except that Pr was replaced with Sc and B_T was replaced with B_M. B_T and B_M are linked by the following equation [9]:

$$B_T = (1 + B_M)^{\varphi} - 1, \tag{2.25}$$

where

$$\varphi = \left(\frac{c_{pv}}{c_{pa}}\right)\left(\frac{\text{Sh}^*}{\text{Nu}^*}\right)\frac{1}{\text{Le}}, \tag{2.26}$$

$\text{Le} = k_g/\left(c_{pa}\,\rho_g\,D_v\right)$ is the Lewis number, and

$$\text{Sh}^* = 2\left[1 + \frac{(1+\text{Re}_d\text{Sc}_d)^{1/3}\max\{1,\text{Re}_d^{0.077}\}-1}{2F(B_M)}\right], \tag{2.27}$$

$$\text{Nu}^* = 2\left[1 + \frac{(1+\text{Re}_d\text{Pr}_d)^{1/3}\max\{1,\text{Re}_d^{0.077}\}-1}{2F(B_T)}\right], \tag{2.28}$$

are Sherwood and Nusselt Numbers for non-evaporating droplets, respectively. The ratio $\frac{\text{Sh}^*}{\text{Nu}^*}$ has been assumed to be equal to 1 in [5], [55]. However, this assumption turned out to be too crude in some cases described in the thesis. Hence, Expressions (2.27) and (2.28) were used for the estimate of φ based on Equation (2.26). Note that $\dot{m}_d \leq 0$.

When calculating the value of $\dot{R}_d$, both droplets evaporation during the time step and the change in their density during this time step were taken into account, as [70]:

$$\dot{R}_d = \dot{R}_{dT} + \dot{R}_{dE}, \tag{2.29}$$

where $\dot{R}_{dT}$ is the change of droplet radius due to thermal expansion/contraction calculated based on the following equation [70]:

$$\dot{R}_{dT} = \frac{R_d(T_{av,0})}{\Delta t}\left[\left(\frac{\rho_l(T_{av,0})}{\rho_l(T_{av,1})}\right)^{1/3} - 1\right], \tag{2.30}$$

$T_{av,0}$ and $T_{av,1}$ are average droplet temperatures at the beginning $t = t_0$ and the end $t = t_1$ of the time-step. The value of $\dot{R}_{dE}$ is controlled by droplet evaporation[5]:

$$\dot{R}_{dE} = \frac{\dot{m}_d}{4\pi R_d^2 \rho_l}, \tag{2.31}$$

where $\dot{m}_d$ is given by Equation (2.22).

2.5   Species mass fractions at the surface of the droplet

To calculate the species evaporation rate $\dot{m}_i$ and the values of the evaporation rate of species ϵ_i based on Equation (2.18), the values of Y_{vsi} need to be calculated. The latter depend on the partial pressures of species i in the vapour state in the immediate vicinity of the droplet surface [80]:

$$p_{vis} = X_{lis}\gamma_i p_{vis}^*, \tag{2.32}$$

where X_{lis} is the molar fraction of the ith species in the liquid near the droplet surface, p_{vis}^* is the partial vapour pressure of the ith species in the case when $X_{lis} = 1$ (i.e. $p_{vis}^* = p_v(R_d)$ for the ith species), and γ_i is the activity coefficient.

In the limit when $\gamma_i = 1$, Equation (2.32) describes the Raoult's law (see [81]). This approximation will be used in the analysis. Some approximations for p_{vis}^* are given in Appendices B-C. All liquid properties are calculated for the average temperature inside droplets. All gas properties are calculated for the reference temperature $T_r = (2/3)T_s + (1/3)T_g$, where T_s and T_g are droplet surface and ambient gas temperatures respectively. The enthalpy of evaporation and saturated vapour pressure are estimated at T_s.

2.6   Liquid diffusion coefficient

In the original analysis [43], [44], [47], the diffusion coefficient of component j relative to all other components was estimated based on the simplified version of the Sanchez and Clifton formula [82]–[84]:

$$D_{jm} = X_j D_{mj}^0 + X_m D_{jm}^0, \tag{2.33}$$

where m refers to the mixture of all other components, D_{jm}^0 and D_{mj}^0 are diffusivities of dilute solute j in solvent m and dilute solute m in solvent j respectively. Note that there are typos in the corresponding expressions for D_{jm} given in [55], [69]. At the same time it was shown in [85], [86] that a more accurate approximation for D_{jm} is given by the formula:

$$D_{jm} = (D_{mj}^0)^{X_j} (D_{jm}^0)^{X_m}. \tag{2.34}$$

In this work, the difference between these approximations is not important as the simplified model, based on the assumption that $D_{jm}^0 = D_{mj}^0$, is used. Among various approximations for D_{jm}^0 and D_{mj}^0 the Wilke-Chang approximation is chosen. Assuming that D_{jm} is the same for all species, the liquid diffusion coefficient can be estimated as [87], [88]:

$$D_{jm} \equiv D_l = \frac{7.4 \times 10^{-15} \sqrt{\bar{M}_v T}}{\mu_l V_v^{0.6}}, \tag{2.35}$$

where T is temperature (in K), μ_l is the liquid dynamic viscosity (in kg m^{-1}s^{-1}), $\bar{M}_v$ is the average molar mass (in kg kmol^{-1}):

$$\bar{M}_v = \left[\sum_{i=1}^{i=N} \left(Y_i / M_i \right) \right]^{-1}. \tag{2.36}$$

Mass fractions Y_{im} are linked with the molar fractions X_i by the following Formula:

$$Y_i = \frac{X_i M_i}{\sum_i M_i X_i}, \tag{2.37}$$

N is the total number of components, V_v is the vapour molar volume at boiling temperature (in m^{3}mol^{-1}), defined as:

$$V_v = \left(\sigma_v / 1.18 \right)^3, \tag{2.38}$$

and σ_v is the Lennard-Jones length (in Angstrom (Å)). For individual components, this length can be estimated based on the following formula [89]:

$$\sigma_v{}^3 = 0.17791 + 11.779 \left(\frac{T_c}{p_c} \right) - 0.049029 \left(\frac{T_c}{p_c} \right)^2, \tag{2.39}$$

where T_c and p_c are critical temperature and pressure, in K and bar, respectively. Since the analysis is based on averaging the properties of multiple components, the following correlation for calculating σ_v is used instead of (2.39) [90]:

$$\sigma_v = 1.468 \, \bar{M}_v{}^{0.297}. \tag{2.40}$$

The values of σ_v calculated using Expression (2.40) appeared to be in good agreement with the experimentally observed values reported in [91] and other data reported in [92]–[94].

It should be emphasised that all parameters were updated at the end of each time step.

2.7   Vapour diffusion coefficient

Following [43], [47], [55], fuel vapour is assumed to diffuse from the droplet surface to ambient gas (air) without a change in its compositions. Hence, the average diffusion coefficient was estimated from the Wilke-Lee formula [82], [95]:

$$D_{va} = \frac{\left[3.03 - \left(0.98/M_{va}^{1/2}\right)\right]10^{-7}T^{3/2}}{p\, M_{va}^{1/2}\, \sigma_{va}^2\, \Omega_D\,(T^*)},$$ (2.41)

where D_v is in m^2s^{-1}, T is in K,

$$M_{va} = 2\left(\frac{1}{M_v} + \frac{1}{M_a}\right)^{-1},$$ (2.42)

M_a is molar masses of air, p is ambient pressure (in bar), $\sigma_{va} = (\sigma_v + \sigma_a)/2$ is the minimal distance between the molecules for vapour and air (measured in Å, as in Equation (2.38)), Ω_D is the collision integral, which depends on the normalised temperature $T^* = k_B T/\varepsilon_{va}$, k_B is the Boltzmann constant, $\varepsilon_{va} = \sqrt{\varepsilon_v \varepsilon_a}$, ε_v and ε_a are characteristic Leonard-Jones energies for vapour and air respectively. The collision integral Ω_D can be obtained from Table E.2 of [87] based on known values of T^*. An alternative approach can be based on the following approximation [82], [87]:

$$\Omega_D = \frac{1.06036}{(T^*)^{0.15610}} + \frac{0.19300}{\exp(0.47635T^*)} + \frac{1.03587}{\exp(1.52996T^*)} + \frac{1.76474}{\exp(3.89411T^*)}.$$ (2.43)

In the case of Diesel fuel, T^* can be determined based on the assumption that ε_v is equal to that of n-dodecane and $\frac{\varepsilon_{va}}{k_B} = 245\ K$ [76], [96]. This assumption is justified by the fact that Ω_D is a weak function of ε_v and the values of ε_v for most components of Diesel fuel are not known from the literature.

The approach based on Expression (2.41) could potentially take into account changes in D_{va} due to the change in composition of the multi-component fuel during the evaporation process. At this stage, however, the analysis is based on the assumption that D_{va} remains equal to the n-dodecane/air diffusion coefficient and the following approximation is used [74]:

$$D_v = 5.27 \times 10^{-6} \left(\frac{T}{300}\right)^{1.583} \frac{1}{p}. \tag{2.44}$$

2.8   Average values of thermodynamic and transport properties

The average values of liquid density, specific heat capacity, latent heat of evaporation and saturated vapour pressure were estimated using the following formulae [46], [82]:

$$\bar{\rho}_l = \left(\sum_{i=1}^{N} \frac{Y_i}{\rho_{li}}\right)^{-1}, \tag{2.46}$$

$$\bar{c}_l = \sum_{i=1}^{N} Y_i c_{li}, \tag{2.47}$$

$$\bar{L} = \sum_{i=1}^{N} \epsilon_i L_i, \tag{2.48}$$

$$\bar{p}_v = \sum_{i=1}^{N} X_i p_{vi}, \tag{2.49}$$

where the subscripts i refer to the components, N is the total number of components, Y_i are the values of the corresponding mass fractions averaged over the whole volume occupied by the droplets. These average values are recalculated at each time step.

Various approximations for liquid mixture viscosity are discussed in Sections 9-13 of [82]. Most of these approximations can be considered as further developments of the method originally suggested by Grunberg and Nissan [97]. According to this method the dynamic viscosity of the liquid mixture can be estimated from the following formula:

$$\ln \bar{\mu}_l = \sum_{i=1}^{N} X_i \ln \bar{\mu}_{li} + \frac{1}{2}\sum_{i=1}^{N} \sum_{j=1}^{N} X_i X_j G_{ij}, \tag{2.50}$$

where G_{ij} is an interaction parameter which is the function of components, temperature and sometimes composition. The estimate of G_{ij} is not a trivial task (see [82] for details) especially in the case of complex liquids, such as commercial Diesel fuel. The approximation for viscosity, however, can be simplified due to the fact that our results are very weak functions of viscosity. Hence, in our analysis this term is ignored altogether and Expression (2.50) is simplified to [46], [57]:

$$\ln \bar{\mu}_l = \sum_{i=1}^{N} X_i \ln \bar{\mu}_{li}. \tag{2.51}$$

When the ratios of thermal conductivity of components do not exceed two, as in the case of biodiesel fuel, the mixture conductivity can be estimated based upon the power law method as [82]:

$$\bar{k}_l = \left(\sum_{i=1}^{N} Y_i k_{li}^{-2} \right)^{-1/2}. \tag{2.52}$$

Formula (2.52) was successfully used in the case of biodiesel fuel [46]. For these droplets the ratios of thermal conductivities of components indeed do not exceed 2. In the case of Diesel fuel droplets, however, this ratio can be well above two, and the application of Formula (2.52) for them cannot be justified.

For the case of Diesel fuel, the values of average thermal conductivity for typical Diesel fuels as inferred from published data [57], [98] will be used. These are assumed to be reasonably close to the values of thermal conductivity of the commercial Diesel fuel described in Chapter 4. The details of the analysis of Diesel fuel thermal conductivity are presented in Appendix C.

Attention needs to be brought to a typo in Equation (49) of [46] (minus was omitted before '2'). The correct formula is presented in this thesis as Expression (2.52) and Equasion (46) of [57]. It should be emphasised that the values obtained from Equations (2.46)-(2.52) were verified and validated using the available experimental data and calculations reported by other authors, as shown in Appendix B.

2.9 Heating of evaporating droplets

Since the pioneering publications by Spalding (see [79]), the evaporation rate of stationary droplets $\dot{m}_d$ has been estimated using Expression (2.22). The derivation of Expression (2.22) is based on a number of assumptions, perhaps one of the most important of which is the assumption that ρ_{total} = const and does not depend on the distance from the droplet surface. This assumption can be justified when the temperature of the droplet is low and the difference between gas and droplet surface temperature is small (slow evaporation). In practical engineering applications, however, theis restriction on the range of applicability of Expression (2.22) has been commonly ignored (e.g. [46]). Note that Expression (2.22) cannot be used when the droplet surface temperature approaches boiling temperature when $\rho_{gs} = 0$ and B_M becomes infinitely large (e.g. [99]).

A more rigorous approach to the analysis of droplet evaporation was presented in [21], [22]. In the model suggested and developed in these papers, the requirement that ρ_{total} = const was relaxed. The species, momentum and energy conservation equations were solved assuming that all parameters depend only on the distance from the droplet centre, taking into account the dependence of gas/vapour density on temperature. As in the case of Expression (2.22), the problem was solved based on the quasi-steady state approximation (terms proportional to time partial derivatives were ignored in all equations) and the droplet surface temperature was assumed to be fixed during any time step. The effects of temperature gradient inside droplets was ignored (their thermal conductivity was assumed to be infinitely large).

An alternative expression for $\dot{m}_d$ was obtained based on the analysis of the heat balance equation. Assuming that the evaporating droplet is stationary, as in the case of Expression (2.22), this equation for an arbitrary distance $R > R_d$ from the centre of the droplet can be presented in the form [9]:

$$4\pi R^2 k_g \frac{dT}{dR} = -\dot{m}_d c_{pv}(T - T_s) - \dot{m}_d L(T_s) + \dot{q}_d, \qquad (2.53)$$

where k_g, c_{pv} and $L(T_s)$ are gas thermal conductivity, vapour specific heat capacity at constant pressure and latent heat of evaporation at the droplet surface temperature T_s. As in Expression (2.22), $\dot{m}_d \leq 0$. The left hand side of this equation shows the heat supplied from the surrounding gas to the droplet. The first term in the right hand side shows the heat required to heat fuel vapour from T_s to $T = T(R)$ (gas temperature at the distance R from the centre of the droplet). The second and third terms in the right hand side show the heat spent on droplet evaporation and raising its temperature (when $\dot{q}_d > 0$) respectively.

Rearranging this equation and its integration from $T = T_s$ to $T = T_g$ (ambient gas temperature) and from $R = R_d$ to $R = \infty$, assuming that the temperature dependence of k_g and c_{pv} can be ignored, gives [9]:

$$\dot{m}_d = \frac{-4\,\pi\,k_g R_d}{c_{pv}} \ln(1 + B_T), \tag{2.54}$$

where the Spalding heat transfer number is given by Equation (2.11). This equation can be rewritten in a slightly different format as:

$$B_T = \frac{c_{pv}(T_g - T_s)}{L(T_s) - (\dot{q}_d/\dot{m}_d)}, \tag{2.55}$$

and the relation between B_T and B_M is given in Equation (2.25). The combination of Equations (2.55) and (2.25) gives:

$$\dot{q}_d = -\dot{m}_d \left[\frac{c_{pv}(T_g - T_s)}{B_T} - L(T_s) \right] = -\dot{m}_d \left[\frac{c_{pv}(T_g - T_s)}{(1 + B_M)^\varphi - 1} - L(T_s) \right]. \tag{2.56}$$

Since the pioneering paper by Abramzon and Sirignano [9], Expression (2.56) has been widely used for modelling of heating of evaporating droplets.

The assumptions on which the derivation of this expression was based (e.g. the validity of Expression (2.22)) have been almost universally ignored. An obvious limitation of Expression (2.56) is that the value of $\dot{q}_d$ is not affected by the thermal conductivity of liquid, which contradicts the physical nature of $\dot{q}_d$, as discussed later in the section.

An alternative approach to the calculation of $\dot{q}_d$ could be based on the analysis of temperature distribution inside droplets, inferred from the direct

analysis of heating of evaporating droplets (see [5] for the details). This approach is restricted to the case when liquid thermal conductivity is finite, which can be expected for any realistic liquid. Nobody, to the best of our knowledge, has compared these 2 approaches to the calculation of $\dot{q}_d$ before publication of [59].

The focus of this section is on the comparison of these two approaches, following [59], and their implications to the modelling of droplet heating and evaporation in conditions typical for Diesel engines. The analysis is focused on stationary droplets, although it can be easily generalised to the case of the moving droplets, using the ETC model (see [5]).

The solution to the heat conduction equation inside droplets, assuming that all processes are spherically symmetric, is given by Equation (2.8). The convection heat transfer coefficient h for stationary evaporating droplets can be estimated as [5]:

$$h = \frac{k_g}{R_d} \frac{\ln(1+B_T)}{B_T}, \tag{2.57}$$

The rate of droplet heating, leading to the rise of their temperatures, can be estimated as

$$\dot{q}_d = 4\pi R_d^2 k_l \left.\frac{\partial T}{\partial R}\right|_{R=R_d-0}, \tag{2.58}$$

where $\dot{q}_d > 0$ when the droplet is heated. The substitution of Expression (2.8) into Expression (2.58) gives:

$$\dot{q}_d = 4\pi R_d^2 k_l \sum_{n=1}^{\infty} \left\{ \begin{array}{l} q_n \exp[-\kappa_R \lambda_n^2 t] - \frac{\sin \lambda_n}{\|v_n\|^2 \lambda_n^2} \mu_0(0) \exp[-\kappa_R \lambda_n^2 t] \\ - \frac{\sin \lambda_n}{\|v_n\|^2 \lambda_n^2} \int_0^t \frac{d\mu_{0(\tau)}}{d\tau} \exp[-\kappa_R \lambda_n^2(t-\tau)]d\tau \end{array} \right\} [-1 - h_0] \sin \lambda_n, \tag{2.59}$$

Expression (2.59) is applicable to any time step with $t = 0$ referring to the beginning of the time step, t refers to the end of the time step. The values of $\dot{q}_d$ at the beginning of each time step are equal to the values of $\dot{q}_d$ at the end of the previous time step or the start of the heating process. Hence, without loss of generality we can assume that $t = 0$ in Expression (2.59). The values of $\dot{q}_d$ predicted by Expression (2.59) were shown to coincide within the accuracy of

plotting with those predicted by Expression (2.59) using the numerical differentiation of the temperature predicted by Expression (2.8).

Expression (2.59) could be potentially generalised to take into account the effect of the moving droplet interface during the evaporation process, using the solution for the distribution of temperature inside a heated droplet presented in [100], [101]. The analysis of the contribution of this effect, however, is beyond the scope of this work.

Once, the values of $\dot{q}_d$ have been obtained, the values of $\dot{m}_d$ can be obtained from the numerical solution of Equation (2.54). The latter equation can be rewritten as:

$$\dot{m}_d = -\frac{4\pi k_g R_d}{c_{pv}} \ln \left(1 + \frac{c_{pv}(T_g - T_s)\dot{m}_d}{L(T_s)\dot{m}_d - \dot{q}_d}\right). \tag{2.60}$$

One can show that Equation (2.60) has 2 solutions, $\dot{m}_d = 0$ (non-evaporating droplet) and $\dot{m}_d < 0$ (evaporating droplet), when

$$\frac{4\pi k_g R_d (T_g - T_s)}{\dot{q}_d} > 1, \tag{2.61}$$

and only one trivial solution $\dot{m}_d = 0$ (non-evaporating droplet) when Condition (2.61) is not satisfied. In the limiting case when $B_T \ll 1$ Equation (2.61) has the analytical solution:

$$\dot{m}_d = \frac{1}{L(T_s)} \left[\dot{q}_d - 4\pi k_g R_d (T_g - T_s)\right]. \tag{2.62}$$

This solution does not have physical meaning unless Condition (2.61) is satisfied. Expression (2.22) can still be used in this approach if

$$B_M = (1 + B_T)^{1/\varphi} - 1. \tag{2.63}$$

Equations (2.8), (2.57), (2.59) and (2.60) are applied at each time step. All thermodynamic and transport properties for liquid and gas are assumed constant during each time step but their changes from one time step to another due to the corresponding changes in temperature are taken into account. The effects of thermal swelling are taken into account using the conventional approach (see Equation (25) of [64]).

The model described above has been applied to the analysis of heating of an evaporating n-dodecane droplet in air at the pressure 30 bars and temperature 700 K. Thermodynamic and transport properties of n-dodecane are taken the same as in [43], except the diffusion coefficient for n-dodecane vapour in air which was taken from [74]. The initial droplet temperature and radius are assumed equal to 300 K and 10 μm respectively.

The results predicted by Equations (2.59) and (2.60) (model 2) are compared with those predicted by the conventional model based on Expression (2.22) and (2.56) (model 1). In both cases the finite thermal conductivity of liquid has been taken into account and the distribution of temperature inside droplets has been predicted by Equation (2.8). The values of $\dot{q}_d$, predicted by these two approaches are shown in Figure 2.2.
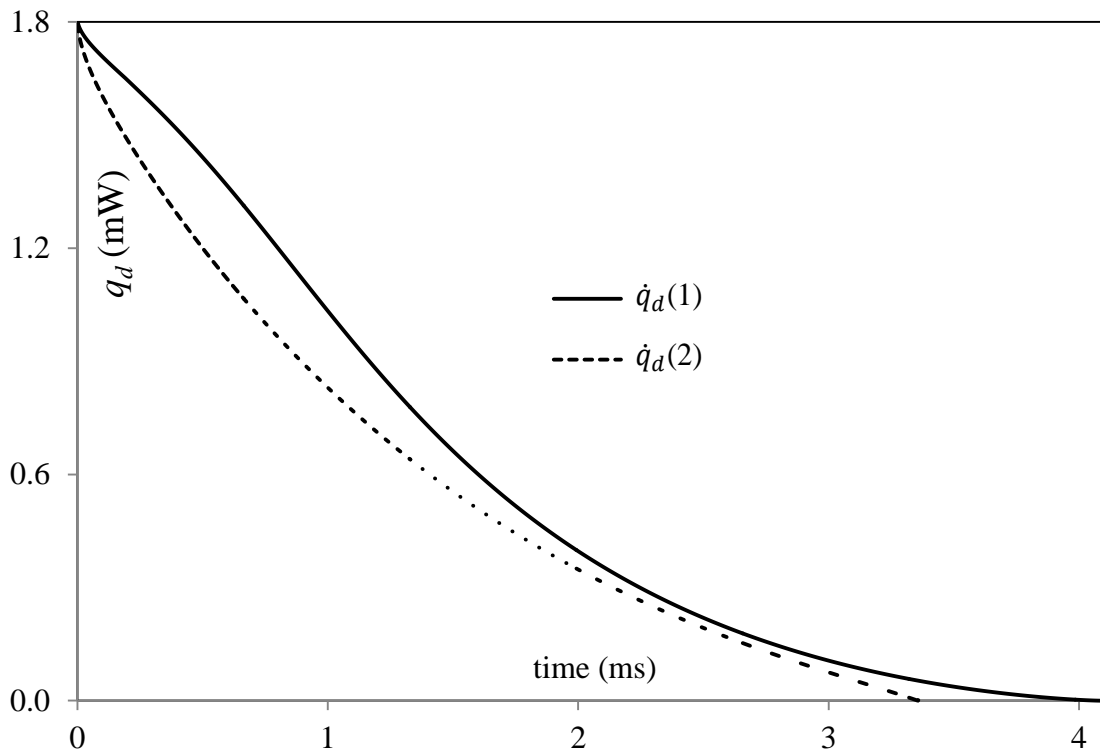
Figure 2.2 Plots of $\dot{q}_d$ versus time predicted by the model based on Expressions (2.22) and (2.56) (model 1) and Equations (2.60) and (2.61) (model 2) for an evaporating n-dodecane droplet heated in air at the pressure 30 bars and temperature 700 K. The initial droplet temperature and radius are assumed equal to 300 K and 10 μm respectively.

Note that at the very final stages of droplet evaporation the values of $\dot{q}_d$ predicted by the model, based on Equations (2.59) and (2.60), becomes negative (although close to zero) which eventually leads to the situation when Equation (2.60) had no real solutions. To avoid this situation the distribution of temperature inside droplets has been frozen at the moment when $\dot{q}_d = 0$. Also, at the very final stage of droplet evaporation, the predicted droplet temperature can approach the critical temperature and can even exceed it. This is partly remedied by assuming that once the value of T_{eff} has reached its minimal value it remains at this level until the droplet fully evaporates. These assumptions are expected to produce minor effects on the predicted values of surface temperatures and radii of droplets which are not important for practical applications. The problems with modelling droplet heating and evaporation at the final stages of droplet evaporation when $dR_d/dt \to \infty$ have been recognised in the previous studies (e.g. [100]).

As one can see from Figure 2.2, the time dependences of $\dot{q}_d$, predicted by both approaches are rather similar, but the actual values of $\dot{q}_d$ are noticeably different. This difference in the values of $\dot{q}_d$ leads to rather large differences in the corresponding values of droplet radii and surface temperatures versus time, shown in Figure 2.3.

As follows from Figure 2.3, the model based on Equations (2.59) and (2.60) predicts lower droplet surface temperatures and shorter evaporation times compared with the model based on Expressions (2.22) and (2.56). Lower droplet surface temperatures, predicted by model 2 compared with model 1 are expected to lead to lower values of the heat fluxes at the surface of the droplet. This is consistent with the predicted values of $\dot{q}_d$ shown in Figure 2.2.
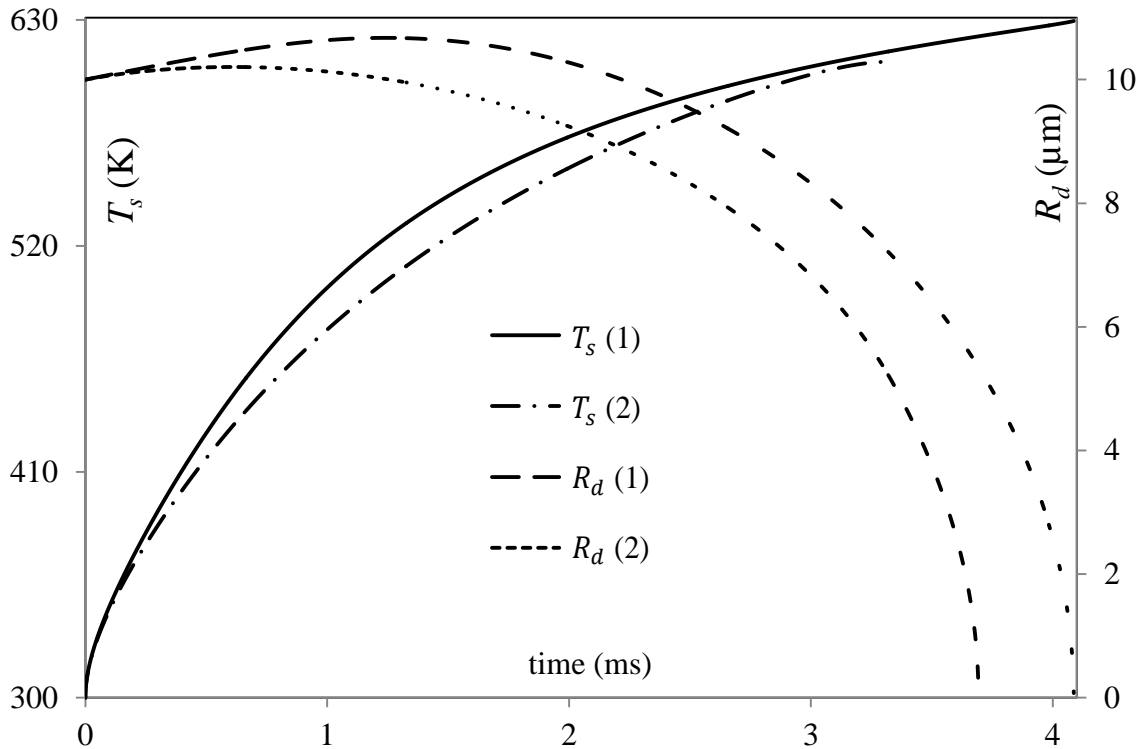
Figure 2.3 The same as in Figure 2.1 but for droplet surface temperatures (T_s) and radii (R_d).

Similar trends in time evolution of the parameters predicted by both models allows us to use them for qualitative analysis of droplet evaporation, but their reliability for quantitative analysis of the processes remains unclear. The limitations of this approximation for the case of non-evaporating droplet heating were discussed in [102], [103].

2.10   Kinetic effects

The previous analysis has been based on the hydrodynamic approximation, although the limitations of this approximation are well known (see [5], [6], [104]). In a number of studies, including [105]–[108], the evaporation of n-dodecane $C_{12}H_{26}$ (an approximation for Diesel fuel) is studied using a new model based on a combination of the kinetic and hydrodynamic approaches. In the immediate vicinity of droplet surfaces (up to about one hundred molecular mean free paths), the vapour and ambient gas dynamics were studied based on the Boltzmann equation (kinetic region); while at larger distances the analysis was based on the hydrodynamic equations (hydrodynamic region).

Mass, momentum and energy fluxes were conserved at the interface between these regions. The authors of [106]–[108] considered the problem of n-dodecane evaporation into air and developed a new numerical algorithm for the solution of a system of two Boltzmann equations for n-dodecane and air, taking into account elastic collisions between: n-dodecane molecules; between air molecules; and between n-dodecane and air molecules. A new approach to taking into account the effects of inelastic collisions was developed in [109] and applied to the problem of n-dodecane droplet heating and evaporation in [110].

One of the important limitations of the approaches described in [105]–[110] is that they were based on the assumption that Diesel fuel can be approximated by n-dodecane. A more detailed analysis of the composition of Diesel fuel showed that it can include hundreds of various hydrocarbon components [57], [111], [112], as will be demonstrated in Chapter 4. It is apparently not possible to take into account the contributions of all these components in the kinetic modelling. At the same time, one can see that the main contributors of these components can be subdivided into two main groups: alkanes and aromatics. The assumption that n-dodecane can approximate alkanes was widely used (see [112]–[114]); while aromatics could be approximated by p-dipropylbenzene [113]. In this case it was suggested that a more accurate approximation of Diesel fuel, compared with the one based on its approximation by n-dodecane, could be its approximation by a mixture of n-dodecane and p-dipropylbenzene. Mass fractions of n-dodecane in this mixture could vary from 0.8 to 0.7 [112], [113].

A new kinetic algorithm for modelling of a three component (two components, approximating Diesel fuel, and air, approximated by nitrogen) mixture was developed in [115]. Binary collisions between molecules were taken into account assuming that these collisions are elastic or inelastic. The functionality testing of the algorithm was performed using a simple test problem of heat and mass transfer in a mixture of n-dodecane, p-dipropylbenzene and nitrogen between two infinite parallel walls. It was concluded that the predictions of the new kinetic algorithm are qualitatively consistent with the predictions of more basic models of the phenomena for which it was tested.

The aim of this section is to investigate the kinetic effects on heating and evaporation of two-component droplets, approximating Diesel fuel, assuming that this approximation is a mixture of n-dodecane and p-dipropylbenzene. In our analysis we will follow the approach described in [60]. The numerical algorithm developed in [115] is used in the analysis. The results are compared with those based on the approximation of Diesel fuel droplets by n-dodecane droplets.

As in [105]–[110], two regions above the surface of an evaporating fuel droplet are considered: the kinetic and hydrodynamic regions. As in [110], this analysis takes into account that thermal conductivity of the liquid phase is finite, and identify the third region called the liquid phase region. All three regions are schematically shown in Figure 2.4.
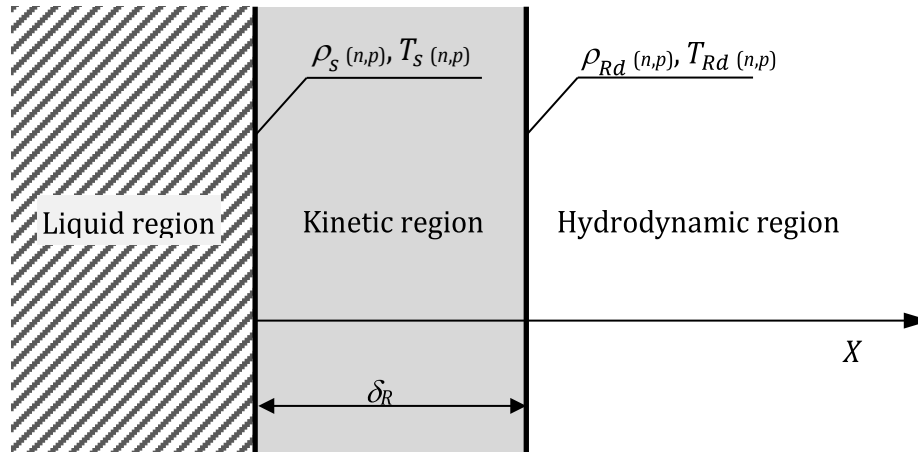
Figure 2.4 Liquid, kinetic and hydrodynamic regions near the surface of the droplet. T_s and ρ_s (n,p) refer to the surface temperature and vapour density (for n-dodecane (n) and p-dipropylbenzene (p)) in the immediate vicinity of the droplet surface; T_{Rd} and ρ_{Rd} (n,p) refer to the same parameters but at the interface between the kinetic and the hydrodynamic regions. δ_{Rd} is the thickness of the kinetic region.

In Figure 2.4, T_s and $\rho_{(n,p)}$ refer to the surface temperature and vapour density (for n-dodecane (n) and p-dipropylbenzene (p)) in the immediate vicinity of the droplet surface; T_{R_d} and $\rho_{R_d(n,p)}$ refer to the same parameters but at the interface between the kinetic and the hydrodynamic regions. δ_{R_d} is the thickness of the kinetic region. In contrast to [110], the diffusion of species in

the liquid phase and the presence of up to 3 components in the kinetic region are taken into account in this study. The conventional hydrodynamic analysis is applied in the liquid and hydrodynamic regions; while vapour and air dynamics in the kinetic region are described by the Boltzmann equations. The hydrodynamic and kinetic models used in the analysis are described below.

2.10.1. Hydrodynamic model

The hydrodynamic model for the liquid and gas phases, used in this work, is the same as described in Section 2.2 (Equations 2.1-2.8,). In the analysis of kinetic effects, the following approximations for saturated vapour pressure are used [60], [74]:

$$p_{v(\text{n})} = \exp[8.1948 - 7.8099(300/T_s) - 9.0098(300/T_s)^2] \times 10^5, \qquad (2.64)$$

for n-dodecane, and

$$\log_{10}\left[0.001 \times p_{v(\text{p})}(n)\right] = A(n) - \frac{B(n)}{T+C(n)}, \qquad (2.65)$$

where

$$A(n) = 0.0007\, n^2 - 0.0064\, n + 6.0715,$$
$$B(n) = 51.811\, n + 1049.1,$$
$$C(n) = 0.1215\, n^2 - 9.6892\, n + 11.161,$$

for p-dipropylbenzene.

Note that none of the expressions for p_v can be considered reliable at temperatures close to critical temperatures. Heating of the droplets above these temperatures, sometimes predicted by the model at the very final stage of droplet evaporation, does not describe accurately the physical background of the processes at this stage. The contribution of the processes at this stage of droplet heating and evaporation to the overall droplet heating and evaporation, however, is expected to be small. To mitigate this behaviour of droplet surface temperature, vapour pressures, predicted by Formula (2.64) and (2.65), have been artificially increased when the temperatures exceeded the corresponding critical temperatures. This has affected the very final stage of droplet

evaporation (when their mass becomes less than about 1% of the initial mass) and has produced negligible effects on the overall process of heating and evaporation.

The mass flux of individual components evaporating from the droplet surface is estimated as [60]:

$$j_{vi} = \frac{\epsilon_i |\dot{m}_d|}{4\pi R_d^2}. \tag{2.66}$$

2.10.2. Kinetic model

The kinetic model for a three component mixture, described in [115], is used in this analysis. A mixture of air (approximated by nitrogen), n-dodecane and p-dipropylbenzene is considered and exactly the same analysis can be applicable to any other mixture. The evolution of the molecular velocity distribution functions of these three components, $f_a \equiv f_a(\mathrm{r}, t, \mathrm{V})$, $f_n \equiv f_n(\mathrm{r}, t, \mathrm{V})$, and $f_p \equiv f_p(\mathrm{r}, t, \mathrm{V})$, is controlled by the following system of Boltzmann equations [116]:

$$\left.\begin{array}{l} \frac{\partial f_a}{\partial t} + \mathrm{V}_a \frac{\partial f_a}{\partial \mathrm{r}} = J_{aa} + J_{an} + J_{ap} \\[2mm] \frac{\partial f_n}{\partial t} + \mathrm{V}_n \frac{\partial f_n}{\partial \mathrm{r}} = J_{na} + J_{nn} + J_{np} \\[2mm] \frac{\partial f_p}{\partial t} + \mathrm{V}_p \frac{\partial f_p}{\partial \mathrm{r}} = J_{pa} + J_{pn} + J_{pp} \end{array}\right\} \tag{2.67}$$

where $J_{\alpha\beta}$ ($\alpha = a, n, p$; $\beta = a, n, p$) are collision integrals, taking into account the contribution of the collisions between molecules. The following explicit expressions for the collision integrals $J_{\alpha\beta}$ are used [108]:

$$J_{\alpha\beta} = \frac{\sigma_{\alpha\beta}^2}{2} \int_{-\infty}^{+\infty} d\mathrm{V}_1 \int_0^\pi \sin\theta \, d\theta \, \int_0^{2\pi} d\emptyset \big(\acute{f}_\alpha \acute{f}_{\beta1} - f_\alpha f_{\beta1}\big) |\mathrm{V}_\alpha - \mathrm{V}_{\beta1}|, \tag{2.68}$$

where $\sigma_{\alpha\beta} = (\sigma_\alpha + \sigma_\beta)/2$, σ_α and σ_β are the corresponding effective diameters of molecules of air 'a', n-dodecane 'n' and p-dipropylbenzene 'p', θ and $\emptyset$ are angular coordinates of molecules β relative to molecules α, superscript ´ indicates the velocities and the distribution functions after collisions,

34

subscript $_1$ indicates that the function f_α is modified under the influence of collisions with molecules of the type β. The first integral on the right hand side of (2.68) is calculated in the three dimensional velocity space. Expression (2.68) is the same as that used in [108], where the contribution of only 2 components in the kinetic region are taken into account. This is justified by the fact that triple collisions are ignored.

All collision integrals $J_{\alpha\beta}$ are calculated taking into account the contribution of internal degrees of freedom (inelastic collisions) as described in [109] . To further illustrate this approach, two molecules can be considered. Each of these molecules has three translational and a certain number of internal degrees of freedom. During the collision process, these molecules form a new system. The total number of degrees of freedom of this system is equal to a certain number N. Let us assume that none of these degrees of freedom has any preference over the others. For each of these degrees of freedom, one dimension in the N-dimensional space can be allocated describing all degrees of freedom. Thereafter, a sphere in this space with the centre in the origin (where energies of all degrees of freedom are equal to zero in the frame of reference moving with the centre of mass) and radius equal to square root of the sum of all energies (see Figure 2.5) can be considered. The redistribution of energy between the degrees of freedom during the collision process can be described in terms of the rotation of this vector in the n-dimensional space.

A degree of freedom is defined as a parameter corresponding to each independent variable necessary to describe the energy of a molecule [117]. A mono-atomic molecule has three degrees of freedom corresponding to its translational energies in x, y and z directions. Polyatomic molecules have additional degrees of freedom corresponding to their rotational and vibrational motions (see [118] for the analysis of degrees of freedom of CO_2 molecules). The total number of degrees of freedom in any molecule is equal to $3N_{at}$ where N_{at} is the total number of atoms in a molecule [80].
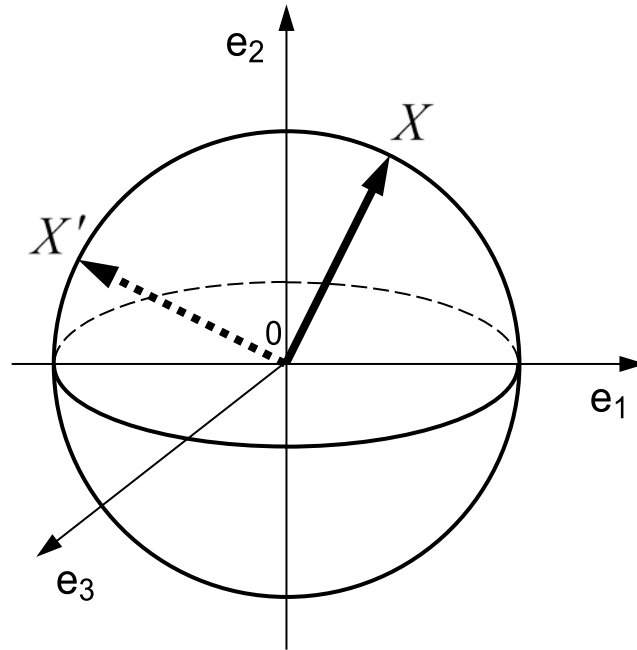
Figure 2.5 A schematic presentation of the rotation of vector X in the three dimensional space (e1; e2; e3). Reprinted from [119], with permission. Copyright Elsevier (2013).

It is assumed that air (approximated as nitrogen) has 2 internal degrees of freedom (because it has symmetric molecules); while both hydrocarbons (n-dodecane and p-dipropylbenzene) have 20 internal degrees of freedom each. As shown in [109], [110], taking into account larger numbers of internal degrees of freedom does not affect the results. As in [105]–[107], [110], the effects of the curvature of the droplet surface are ignored. This is justified by the fact that the thickness of the kinetic region is very small; in this work it is assumed equal to 10 mean free paths for n-dodecane molecules in saturated n-dodecane vapour at temperature equal to 600 K (ℓ) (see [6], [116]).

Equations (2.67) are solved subject to the boundary conditions at the interface between the kinetic and liquid regions and at the interface between the kinetic and hydrodynamic regions (see Figure 2.4). The first boundary condition for both components of the vapour can be presented as:

$$f_{vi(\text{out})} = \beta_i f_{vis} + (1 - \beta_i) f_{vir}, \tag{2.69}$$

where f_{vis} is the distribution function of molecules leaving the liquid surface assuming that β_i = 1, f_{vir} is the distribution function of reflected molecules.

Both f_{vis} and f_{vir} are assumed to be isotropic Maxwellian. The temperature for f_{vis} is assumed to be equal to T_s, while the temperature for f_{vir} is assumed to be equal to T_{R_d}. This is justified by the fact that the thickness of the kinetic region is small and the gas temperature just above the droplet surface is close to T_{R_d} [66], [104]. At the boundary between the kinetic and hydrodynamic regions the distribution function of vapour components and air molecules entering the kinetic region is assumed to be Maxwellian, controlled by ρ_{R_d} for both components and T_{R_d}.

The contributions of both mass and heat transfer in the kinetic region are taken into account following the approach described in [110]. In [110] the dependence of the evaporation coefficient for n-dodecane on temperature is taken into account, as inferred from previous molecular dynamics analysis [120]. Since no such analysis has been performed for p-dipropylbenzene, it would be more consistent to assume that in both cases the evaporation coefficients for both components are equal to 1 at this stage (See [6] for details). The kinetic calculations have been performed for 1) pure n-dodecane droplets, and the following n-dodecane and p-dipropylbenzene molar fractions: 2) 80% n-dodecane and 20% p-dipropylbenzene, and 3) 70% n-dodecane and 30% p-dipropylbenzene. Chemical formulae, molar masses and molecular diameters of these vapour components and nitrogen (approximating air), used in our analysis, are given in Table 2.1.

As in [110], the first step in the solution of Equations (2.67) is to perform an investigation of mass and heat transfer processes in the kinetic region for a set of values of ρ_{R_d} (for both vapour components) and T_{R_d}. The problem of heating and evaporation of droplets is considered in a hot gas (Diesel engine-like conditions) and these parameters are assumed to be in the ranges: $\rho_{R_d} < \rho_s$ and $T_{R_d} > T_s$. During the droplet heating process, the temperature increases away from the droplet; the evaporation process is possible when the vapour density decreases away from the droplet surface. For the chosen values of ρ_{R_d} and T_{R_d}, the solution to Equations (2.67) in the kinetic region allows us to calculate the normalised mass and heat fluxes at the outer boundary of this region:

$$\tilde{j}_{k(n,p)} = j_{k(n,p)}/\left(\rho_0\sqrt{R_v T_0}\right), \tag{2.70}$$

$$\tilde{q}_k = q_k/\left(p_0\sqrt{R_v T_0}\right), \tag{2.71}$$

where R_v is the gas constant referring to n-dodecane vapour, T_0 is the reference temperature chosen equal to 600 K, p_0 and ρ_0 are the saturated n-dodecane vapour pressure and density corresponding to T_0, ρ_0 is calculated from the ideal gas law, and subscript k stands for kinetic.

Table 2.1 Chemical formulae, molar masses and molecular diameters of n-dodecane, p-dipropylbenzene and nitrogen, used in our analysis.

Component	Chemical formula	Molar mass (g mol^{-1})	Molecular diameter (Å)
n-dodecane	$C_{12}H_{26}$	170.3	7.120
p-dipropylbenzene	$C_{12}H_{18}$	162.27	6.730
nitrogen	N_2	28.97	3.617

In [110], it has been shown that for the case of heating and evaporation of n-dodecane droplets, the values of $\tilde{q}_k$ are almost independent of $\tilde{\rho}_{R_d} \equiv \rho_{R_d}/\rho_s$ in a certain range of $\tilde{\rho}_{R_d}$ and the values of $\tilde{j}_k$ are almost independent of $\tilde{T}_{R_d} \equiv T_{R_d}/T_s$ in a certain range of $\tilde{T}_{R_d}$ relevant to the conditions typical for Diesel engines. In what follows (see [60]), it is demonstrated that this property is observed for the case of heating and evaporation of two-component (a mixture of n-dodecane and of p-dipropylbenzene) droplets.

Let us assume that molar fractions of n-dodecane and p-dipropylbenzene in the droplet are 80% and 20% respectively, droplet surface temperature is equal to 600 K, and $\tilde{\rho}_{R_d(n)} = \tilde{\rho}_{R_d(p)} \equiv \tilde{\rho}_{R_d}$. The plots of $\tilde{q}_k$ versus $\tilde{\rho}_{R_d}$ for $\tilde{T}_{R_d} = 1.05$ and 1.1 are shown in Figure 2.6. As one can see in this figure, the plots for these values of $\tilde{T}_{R_d}$ are the lines which are almost parallel to the $\tilde{\rho}_{R_d}$ axis. A similar conclusion was reached in the general case when $\tilde{\rho}_{R_d(n)} \neq \tilde{\rho}_{R_d(p)}$. The same result was obtained for the 70% n-dodecane and 30% p-dipropylbenzene mixture. This allows us to ignore the dependence of $\tilde{q}_k$ on $\tilde{\rho}_{R_d}$ in agreement with the similar result obtained in [110].
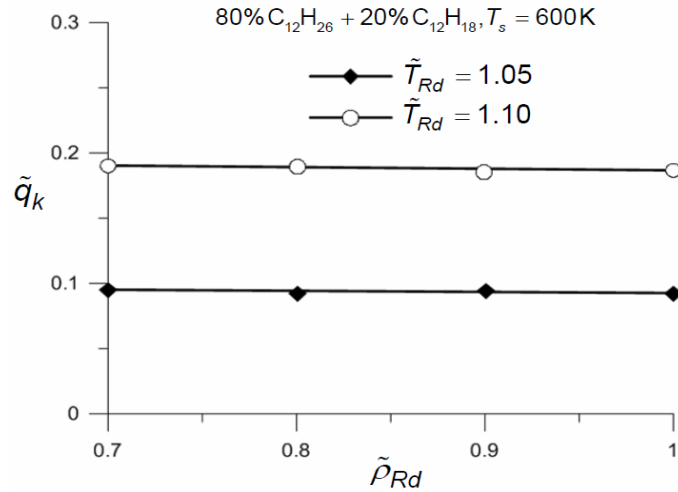
Figure 2.6 The plots of normalised heat flux $\tilde{q}_k$ versus $\tilde{\rho}_{R_d}$ for $\tilde{T}_{R_d} = 1.05$ and $\tilde{T}_{R_d} = 1.10$ for an 80% n-dodecane and 20% p-dipropylbenzene mixture at droplet surface temperature 600 K.

The plots of mass fluxes of n-dodecane and p-dipropylbenzene predicted by the kinetic model ($\tilde{j}_{k(n)}$ and $\tilde{j}_{k(p)}$) versus $\tilde{T}_{R_d}$ for $\tilde{\rho}_{R_d} = 0.7$ for both components under the same conditions as in Figure 2.6 are shown in Figure 2.7.
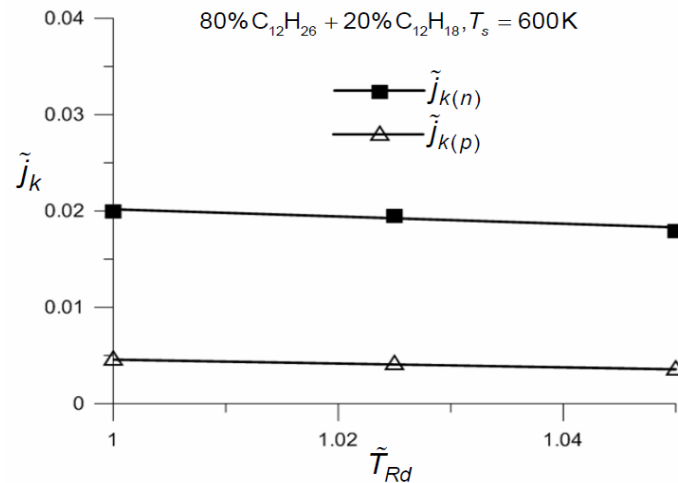
Figure 2.7 The plots of mass fluxes, predicted by the kinetic model, of n-dodecane $\tilde{j}_{k(n)}$ and p-dipropylbenzene $\tilde{j}_{k(p)}$ versus $\tilde{T}_{R_d}$ for $\tilde{\rho}_{R_d} = 0.7$ under the same conditions as in Figure 2.6.

As one can see in Figure 2.7, the plots for these values of $\tilde{\rho}_{R_d}$ and in the range of $\tilde{T}_{R_d}$ shown, are the lines which are almost parallel to the $\tilde{T}_{R_d}$ axis. In contrast to the case shown in Figure 2.6, a very weak dependence of j_k on $\tilde{T}_{R_d}$

can be observed, but this can be ignored in our analysis. A similar conclusion was reached in the general case when $\tilde{\rho}_{R_d(n)} \neq \tilde{\rho}_{R_d(p)}$. The same result was obtained for the 70% n-dodecane and 30% p-dipropylbenzene mixture. This allows us to ignore the dependence of $\tilde{j}_k$ on $\tilde{T}_{R_d}$. Thus the results shown in Figures 2.6 and 2.7 allow us to decouple the analysis of heat and mass fluxes in the kinetic region for $\tilde{\rho}_{R_d}$ in the range (0.7 – 1) and $\tilde{T}_{R_d}$ in the range (1–1.1).

The values of $\tilde{T}_{R_d}$ for two-component droplets have been obtained following the same procedure as described in [110] for mono-component droplets. This procedure is illustrated in Figure 2.8 for an 80% n-dodecane and 20% p-dipropylbenzene droplet of radius 5 μm, surface temperature 600 K and gas temperature 1000 K. The value of $\tilde{\rho}_{R_d}$ is taken equal to 0.7. Recalling Figure 2.6, the results are expected not to depend on the actual values of $\tilde{\rho}_{R_d}$. The plots of the heat flux predicted by the kinetic model, $\tilde{q}_k$, versus $\tilde{T}_{R_d}$, and the heat flux in the hydrodynamic region, $\tilde{q}_h = q_h / p_0 \sqrt{R_v T_0}$, versus $\tilde{T}_{R_d}$ (horizontal line), for these values of parameters are shown in Figure 2.8. The intersection between the horizontal and inclined lines gives the required value of $\tilde{T}_{R_d} = 1.022$.

The plots of the mass flux predicted in the kinetic region $\tilde{j}_k$ versus $\tilde{\rho}_{R_d}$ for $\tilde{T}_{R_d} = 1.05$ (as follows from the analysis based on Figure 2.7, the result is not expected to depend of $\tilde{T}_{R_d}$) and the mass flux predicted in the hydrodynamic region, $\tilde{j}_h = j_h / (\rho_0 \sqrt{R_v T_0})$, for n-dodecane ($\tilde{j}_{k(n)}$ and $\tilde{j}_{h(n)}$) and p-dipropylbenzene ($\tilde{j}_{k(p)}$ and $\tilde{j}_{h(p)}$) versus $\tilde{\rho}_{R_d}$ ($\tilde{\rho}_{R_d(n)}$ or $\tilde{\rho}_{R_d(p)}$) are shown in Figure 2.9. The mass fluxes predicted in the hydrodynamic region are shown by the horizontal lines. This figure is presented for the same parameters as in Figure 2.8.
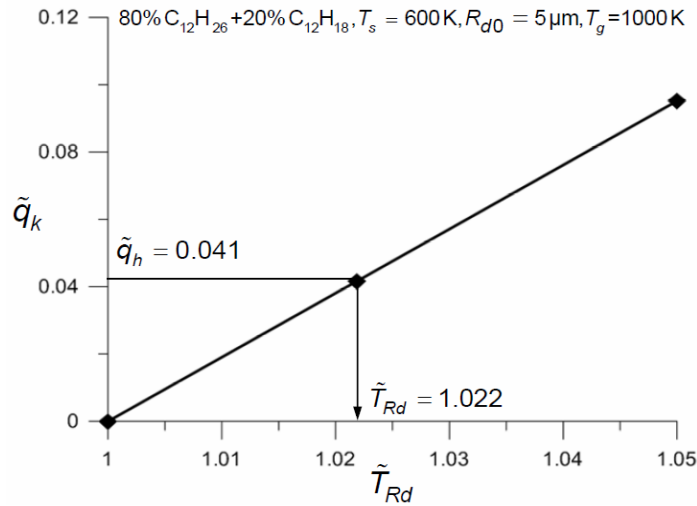
Figure 2.8 The plots of the heat flux predicted in the kinetic region, $\tilde{q}_k$, versus $\tilde{T}_{R_d}$ and the heat flux predicted in the hydrodynamic region, $\tilde{q}_h$, versus $\tilde{T}_{R_d}$ (horizontal line) for $\tilde{\rho}_{R_d} = 0.7$ and an 80% n-dodecane and 20% p-dipropylbenzene mixture droplet of radius 5 µm, surface temperature 600 K and gas temperature 1000 K. The intersection between the $\tilde{q}_k$ and $\tilde{q}_h$ gives the value of $\tilde{T}_{R_d} = 1.022$.
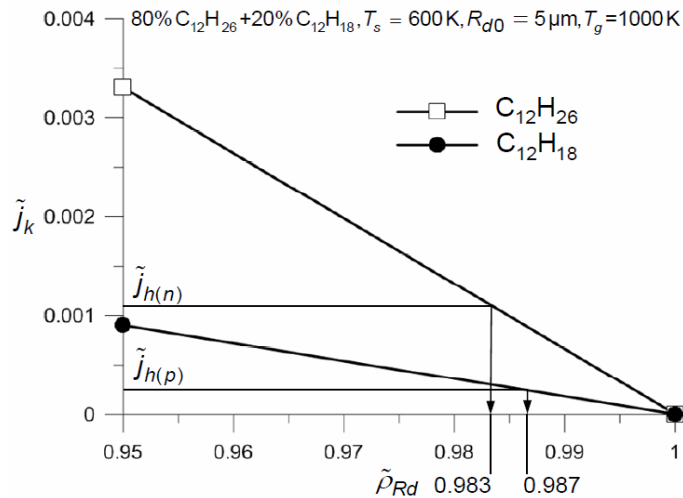
Figure 2.9 The plots of the mass flux of the components predicted in the kinetic region, $\tilde{j}_k$, versus $\tilde{\rho}_{R_d}$ for $\tilde{T}_{R_d} = 1.05$ and in the hydrodynamic region, $\tilde{j}_h$, for n-dodecane ($\tilde{j}_{h(n)}$) and p-dipropylbenzene ($\tilde{j}_{h(p)}$) versus $\tilde{\rho}_{R_d}$ ($\tilde{\rho}_{R_d(n)}$ and $\tilde{\rho}_{R_d(p)}$ for the same parameters as in Figure 2.6). $\tilde{j}_{h(n)}$ and $\tilde{j}_{h(p)}$ are shown by horizontal lines. The intersections between the horizontal and inclined lines give the required values of $\tilde{\rho}_{R_d}$: $\tilde{\rho}_{R_d(n)} = 0.983$ for n-dodecane and $\tilde{\rho}_{R_d(p)} = 0.987$ for p-dipropylbenzene.

Following [110], it is assumed that ρ_{R_d} in Equation (2.66) can be replaced with ρ_s. The intersections between the horizontal and inclined lines give the

required values of $\tilde{\rho}_{R_d}$ as: $\tilde{\rho}_{R_d(\text{n})} = 0.983$ for n-dodecane and $\tilde{\rho}_{R_d(\text{p})} = 0.987$ for p-dipropylbenzene. Similar values of $\tilde{T}_{R_d}$ and $\tilde{\rho}_{R_d}$ are obtained for other values of T_g, T_s and R_d relevant for Diesel engine conditions (T_g = 750 K, T_g = 700 K; for values of T_s in the range 300 K to temperatures close to critical temperature, and the range of molar fractions of n-dodecane and p-dipropylbenzene predicted by hydrodynamic calculations). The corresponding values of $\tilde{T}_{R_d}$ and $\tilde{\rho}_{R_d}$ are used for the analysis of heating and evaporation of mono- and two-components droplets in realistic Diesel engine-like conditions.

Following the above procedure, a set of values of $\tilde{\rho}_{R_d}$ and $\tilde{T}_{R_d}$ have been obtained for a number of specific pairs of values of droplet surface temperatures and radii, predicted by the hydrodynamic model. Once the values of $\tilde{\rho}_{R_d}$ are obtained, then for kinetic modelling the values of density at the surface of the droplet ρ_s (given as ρ_{vs} in Equation (2.23)) are replaced by ρ_{R_d}. For the intermediate values of these parameters the values of $\tilde{\rho}_{R_d}$ and $\tilde{T}_{R_d}$ are interpolated. The thickness of the kinetic region is assumed to be infinitely small. Since $\rho_{R_d} < \rho_s$, the value of B_M predicted by the kinetic model ($B_{M,k}$) is always less than the value of B_M predicted by the hydrodynamic model ($B_{M,h}$). Hence, the evaporation rate predicted by the kinetic model is expected to be always less than the one predicted by the hydrodynamic model for the same droplet surface temperature.

The decrease in the values of B_M predicted by the kinetic model is expected to lead to a corresponding decrease in the values of B_T and ultimately the values of the convection heat transfer coefficient (h). This will lead to a decrease in the values of T_{eff}. On the other hand, slowing down of the evaporation process, predicted by the kinetic model, will lead to a decrease in $|\dot{R}_d|$, and ultimately an increase in T_{eff}. The balance between these two processes will lead to either a decrease or an increase in the predicted droplet surface temperatures.

Note that the effect of changes in the droplet evaporation rates due to the changes in droplet surface temperatures predicted by the kinetic model is ignored. As a result, the corrected values of j_{vi} for the mass fluxes predicted by

the hydrodynamic model need to be considered. This correction leads to new values of $\tilde{\rho}_{R_d}$ and droplet surface temperature etc. The investigation of this effect is beyond the scope of this work.

The results of calculation of the radii and surface temperatures of a droplet with initial radius and temperature equal to 5 μm and 300 K, respectively, immersed into gas with temperature 1000 K are shown in Figure 2.10. In kinetic calculations both heat and mass transfer in the kinetic region and the effects of inelastic collisions are taken into account. The evaporation coefficient is assumed equal to 1 for both components. Since the values of ρ_{R_d} were estimated as perturbations of ρ_s predicted by the hydrodynamic model, the calculations of the droplet radii predicted by the kinetic model had to be terminated before the evaporation time predicted by the hydrodynamic model (which is always less than the evaporation time predicted by the kinetic model). Then the values of droplet radii predicted by the kinetic model were extrapolated until complete evaporation of the droplet.

As one can see from Figure 2.10, both the addition of p-dipropylbenzene and kinetic effects lead to an increase in the evaporation time of droplets. To investigate the effect of droplet composition on the kinetic effects, the following error function is introduced:

$$E \equiv \frac{t_{e(k)} - t_{e(h)}}{t_{e(k)}} \times 100\%, \tag{2.72}$$

where $t_{e(k,h)}$ is the evaporation time predicted by the kinetic/hydrodynamic models. E is estimated as a percentage. Note that $t_{e(k)} > t_{e(h)}$.

The values of E for the three mixtures presented in Figure 2.10 are the following: 100% n-dodecane, $E = 1.61\%$; 80% n-dodecane, $E = 1.70\%$; 70% n-dodecane, $E = 2.5\%$. Thus, the values of E increase with increasing p-dipropylbenzene contribution. In all cases, these values remain less than 3%, and they need to be taken into account only in the case of very accurate modelling of this process.
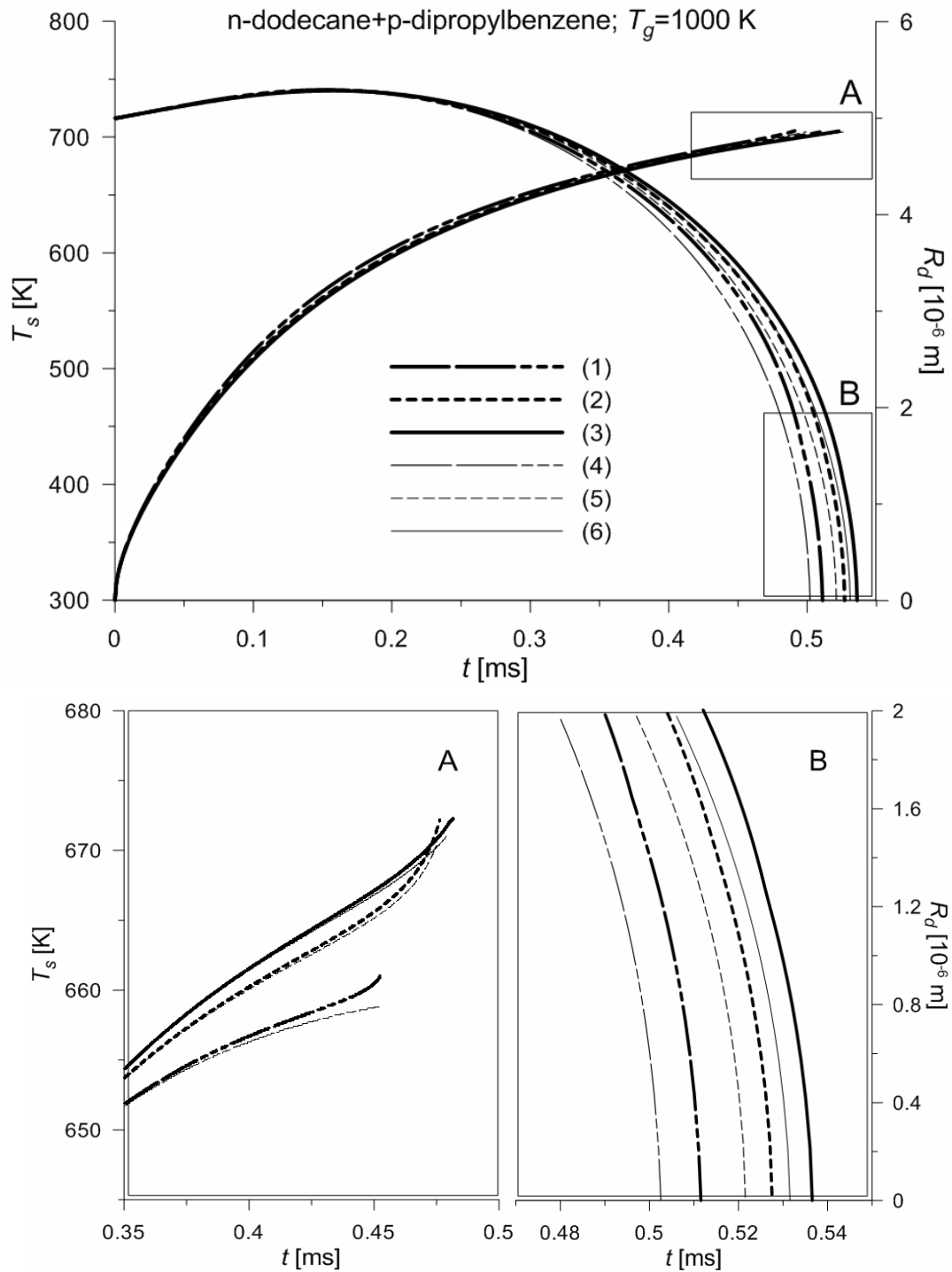
Figure 2.10 The plots of R_d and T_s versus time, as predicted by the kinetic and hydrodynamic models for droplets with initial radius and temperature equal to 5 μm and 300 K, respectively, immersed into gas with temperature 1000 K; pure n-dodecane and mixtures of n-dodecane and p-dipropylbenzene have been considered; the link between the modelling conditions and the plots is shown in Table 2.2. 'A' refers to the zoomed part of the figure for droplet surface temperatures; 'B' refers to the zoomed part of the figure for droplet radii. Reprinted from [60] with permission.

Table 2.2 The link between the modelling conditions and the plots shown in Figures 2.9 and 2.10.

Plots	model	Molar fraction of n-dodecane	Molar fraction of p-dipropylbenzene
1	Kinetic	100%	0%
2	Kinetic	80%	20%
3	Kinetic	70%	30%
4	Hydrodynamic	100%	0%
5	Hydrodynamic	80%	20%
6	hydrodynamic	70%	30%

The same plots as in Figure 2.10 but for gas temperature equal to 700 K are shown in Figure 2.11. Comparing Figures 2.10 and 2.11, one can see that the decrease in gas temperature from 1000 K to 700 K leads to more than doubling of the evaporation time and reduction of the kinetic effects for all three mixtures. For 100% n-dodecane, $E = 0.22\%$; 80% n-dodecane, $E = 0.32\%$; 70% n-dodecane, $E = 0.58\%$. As in the case of gas temperature equal to 1000 K, the values of E increase with increasing p-dipropylbenzene contribution. These errors can be safely ignored in sub-critical conditions.

The kinetic effects can become even more noticeable at temperatures greater than 1000 K. In this case, however, the droplet surface temperatures are expected to approach the critical temperature well before its final evaporation. In such conditions, this model is expected to be less reliable as it is based on the assumption that droplet surface temperature is not close to the critical temperature.
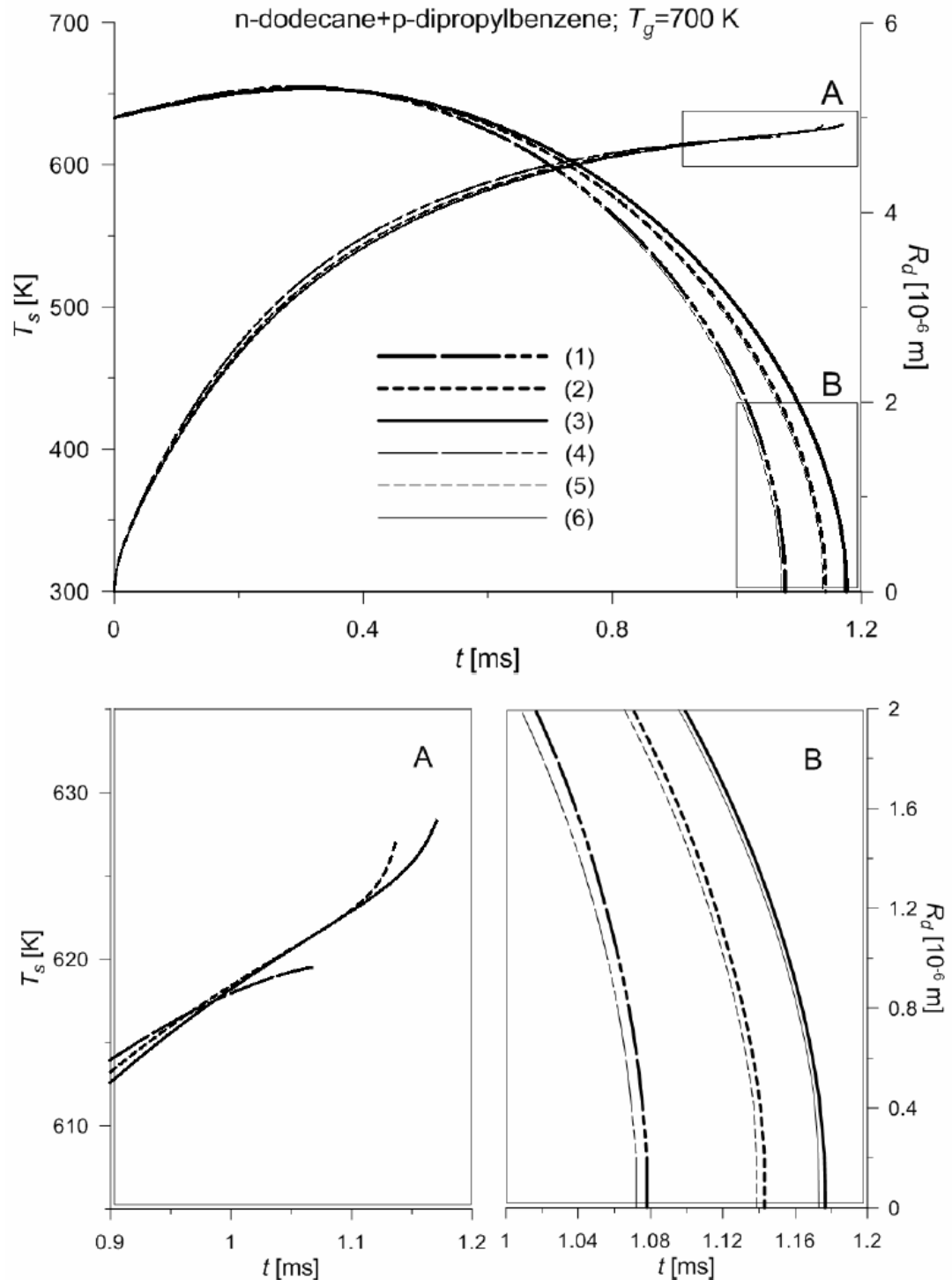
Figure 2.11 The same as Figure 2.10, but for the gas temperature 700 K. Reprinted from [60] with permission.

The main problem with approximation of Diesel fuel by a mixture of n-dodecane and p-dipropylbenzene is that the accuracy of this approximation for modelling droplet heating and evaporation has not yet been carefully investigated for a wide range of available Diesel fuels. In the case of Diesel fuel

considered in [110], the evaporation time of droplets with initial radii 5 µm in gas at temperature 700 K, predicted by this approximation, has turned out to be about one half of the evaporation time predicted for a Diesel fuel droplet in these conditions, although the prediction of this approximation is better than the one for a pure n-dodecane droplet. As shown in Chapter 4, a reasonably accurate approximation for both the evaporation time and time evolution of droplet surface temperature can be achieved when Diesel fuel is approximated by about 15 components/quasi-components. Of course, it is not feasible at this time to perform kinetic modelling for such a mixture; the approximation of Diesel fuel by a two-component mixture is bound to be crude; although nobody, to the best of authors' knowledge, has attempted to investigate this problem in depth and found an optimal two-component approximation of Diesel fuel (apart from the approximation presented in [116], used in this section).

Interestingly, the mixture 10% n-dodecane and 90% dodecylbenzene ($C_{18}H_{30}$) leads to the prediction of droplet evaporation times close to the one predicted for a Diesel fuel droplet. To achieve this, however, it is necessary to tolerate rather large differences in the predicted surface temperatures for this approximation and for the approximation of Diesel fuel considered in [57].

It is worth mentioning that these kinetic effects can be more noticeable for smaller sizes of droplets or near to the end of evaporation time, but they are insignificant for larger sizes of droplets (see [6]).

2.11   Solution algorithm

These are the main steps of the numerical algorithm for the hydrodymanic model used in our analysis

1. Assume an initial distribution of temperature and mass fractions of species inside the droplet or use the distributions obtained at the previous time step (in our case both initial distributions were assumed homogeneous). Recalculate the molar fractions of species into mass fractions of species.

2. Calculate the values of liquid thermal conductivity and effective thermal conductivity of the droplet using Equations (2.3) and (C.39, Section C8 in Appendix C8).

3. Calculate species partial pressures and molar fractions in the gas phase using Equation (2.61).

4. Calculate the value of the Spalding mass transfer number, using Equation (2.23).

5. Calculate the values of liquid heat capacity and diffusivity of the mixture of vapour species in the air, using Equations (2.47) and (2.44) respectively, and species evaporation rates (ϵ_i) using Equation (2.18).

6. Calculate the value of the Spalding heat transfer number using the iteration process based on Equations (2.25)-(2.28).

7. Calculate the values of the Nusselt and Sherwood numbers for isolated droplets using Equations (2.10) and (2.24).

8. Calculate the values of Nu* and Sh* using Equations (2.27) and (2.28).

9. Calculate the rate of change of droplet radius using Equations (2.29)-(2.31).

10. Calculate the effective temperature, using Equation (2.7).

11. Calculate the distribution of temperature inside the droplet based on Equation (2.8), using 33 terms in the series.

12. Calculate the distribution of species inside the droplet based on Equation (2.19), using 33 terms in the series. Note that the chosen number of terms adversely affects the accuracy of predicted distribution of species if this number is much less than 33. This effect is much weaker for the distribution of temperature in droplets.

13. Recalculate the droplet's radius at the end of the time step Δt. If this radius is negative then the time step is reduced and the calculations are repeated. If the ratio of this radius to the initial radius is less than an *à priori* chosen small number, $\varepsilon_s = 10^{-6}$, then the remaining part of the droplet is assumed

to be evaporated with all liquid species transferred into the gas phase with a corresponding decrease in gas temperature. If this ratio is greater than 10^{-6} then go to the next step.

14. Recalculate the distributions of temperature and species for the new droplet radius (e.g. $T(R) = T(RR_{d2}/R_{d1}) = T(\tilde{R})$, where $R_{d1,2}$ are droplet radii at the beginning and the end of the time step, $\tilde{R}$ is the new R used at the second time step, T are the values of temperature at the end of the first time step).

15. Return to Step 1 and repeat the calculations for the next time step.

2.12   Conclusions of Chapter 2

The previously suggested model for droplet heating and evaporation, taking into account temperature gradient, recirculation, and species diffusion inside droplets, is described. In contrast to the most commonly used models, which do not take these effects into account, this model is based on the analytical solutions to the heat transfer and species diffusion equations inside droplets.

Two approaches to modelling the heating of evaporated droplets are compared. In the first approach, the heat rate supplied to the droplets to raise their temperatures ($\dot{q}_d$) is derived from the requirement that the rates of droplet evaporation $\dot{m}_d$, inferred from steady-state equations for mass and heat balance in the gas phase, should be the same (in this approach the values of $\dot{q}_d$ do not depend on the value of liquid thermal conductivity). The second approach is based on the direct calculation of the distribution of temperature inside droplets assuming that their thermal conductivity is not infinitely large.

The implications of these two approaches are compared for the case of stationary droplets in conditions relevant to Diesel engines. It is pointed out that the trends of time evolution of $\dot{q}_d$, predicted by both approaches, are similar, but the actual values of $\dot{q}_d$ at any given time instant are visibly different. This difference can lead to noticeable differences in predicted droplet surface temperatures, radii and evaporation times. One of possible reasons for these differences is attributed to the fact that the calculations of the evaporation rate

in both approaches are based on the quasi-steady-state approximation. It is concluded that both approaches to the calculation of $\dot{q}_d$ can be applied for qualitative analysis of droplet heating and evaporation, but caution should be exercised when using any of them for the quantitative analysis.

The previously developed kinetic model for two-component droplet heating and evaporation into a high pressure background gas (air) is applied to the analysis of n-dodecane and p-dipropylbenzene mixture droplet heating and evaporation in Diesel engine-like conditions. The kinetic modelling of droplet heating and evaporation is based on the introduction of the kinetic region in the immediate vicinity of the droplets, where the dynamics of molecules are described in terms of the Boltzmann equations for vapour components and air, and the hydrodynamic region. The presence of two components in the vapour are taken into account. The boundary conditions at the outer boundary of the kinetic region are introduced by matching the mass fluxes of vapour components leaving the kinetic region and entering into the surrounding hydrodynamic region. The effects of finite thermal conductivity inside the droplets and inelastic collisions in the kinetic region are taken into account. Also, the effects of species diffusivity inside the droplets are considered. The evaporation coefficient for both components is assumed equal to 1.

It is pointed out that for the parameters typical for Diesel engine-like conditions, the heat flux in the kinetic region is a linear function of the vapour temperature at the outer boundary of this region, but is almost independent of the densities of vapour components at this boundary in a certain range of these densities, as in the case of mono-component droplets. The mass fluxes of both components in the kinetic region are shown to decrease almost linearly as their densities at the outer boundary of the kinetic region increase, but are almost independent of the temperatures at this boundary in a certain range of these temperatures, as in the case of mono-component droplets. Using the matching conditions at the outer boundary of the kinetic region, the values of temperature and densities of both components at this boundary are found.

The model is tested for the analysis of heating and evaporation of droplet with initial radius and temperature equal to 5 μm and 300 K, immersed into gas with temperatures 1000 K and 700 K for three droplet compositions (in terms of molar fractions): pure n-dodecane, a mixture of 80% n-dodecane and 20% p-dipropylbenzene, and a mixture of 70% n-dodecane and 30% pdipropylbenzene. It is shown that both the addition of p-dipropylbenzene and kinetic effects lead to an increase in the evaporation time of droplets. In all cases, the kinetic effects on the droplet evaporation times increase with increasing p-dipropylbenzene contribution and gas temperature.

3   BIODIESEL FUEL Droplets

3.1   Introductory comments

The interest to biodiesel fuels has been mainly stimulated by depletion of fossil fuels and the need to reduce carbon dioxide emissions, contributing to climate changes [121], [122]. The term 'biodiesel' typically refers to a fuel comprised of mono-alkyl esters of long-chain fatty acids produced by chemical conversion of animal fats or vegetable oils [121], [123]–[125]. The use of biodiesel fuel is expected to contribute to the reduction of global warming [126]. Also, using biodiesel fuel as an alternative to conventional fuels has a number of other advantages: it readily mixes with fossil Diesel fuels, it is less polluting, has higher lubricity, higher flash point, it is cost effective, and can be used in Diesel engines with minimal modifications [127]–[130]. According to the U.S. Environmental Protection Agency – Tier I and Tier II standards (see [131] for details), currently produced biodiesel types have passed the health effects testing requirements [132].

Most studies of biodiesel fuels have been focused on rapeseed, soybean and palm oil biodiesels [133]. The dominant oils for production of these fuels are rapeseed oil in Europe, soybean oil in the USA, and palm oil in Asia [124]. The term 'second-generation biodiesel' refers to biodiesel derived from inedible oil or algae [134], [135]. This analysis is focused on the modelling of biodiesel fuel droplet heating and evaporation, which is an important stage of the process leading from the injection of biodiesel fuel into a combustion chamber to its ultimate combustion and producing the driving force for internal combustion engines.

A number of models of biodiesel fuel heating and evaporation of various complexities have been suggested [23], [24], [26], [122], [136]. These models either ignored temperature gradients and species diffusion inside droplets or took them into account based on the numerical solutions of the underlying partial differential equations (e.g. [24]). The importance of taking into account

these effects has been discussed in a series of our studies, including [25], [46], [55], [69]. In contrast to most previously suggested models for these processes, the temperature gradients and species diffusion inside droplets are taken into account based on the analytical solutions to heat transfer and species diffusion equations, which are incorporated into a numerical algorithm of an in-house FORTRAN-based code.

Unlike typical fossil fuels, such as gasoline and Diesel fuels, which are composed of hundreds of components, biodiesel fuels are composed of a relatively small (6-14) number of fatty acid ethyl and methyl esters [123], [133], [134], [137] (only biodiesels composed of methyl esters are studied in this chapter). This allows us to analyse species diffusion inside droplets based on the Discrete Component (DC) model in which the diffusion of species is described without any additional approximations (cf. the analysis of Diesel fuel droplet heating and evaporation described in Chapter 4).

The model takes into account the effects of multi-component droplet heating by convection, its evaporation, the finite thermal conductivity, recirculation, and species diffusion in the liquid phase. Only the effects of ambient gas on droplets are taken into account, the effects of coupling between gas and droplets are ignored. A comparative analysis between the classical approach (single-dominant-component, single-component ITC and ITC/ID models) used in literature [20], [22], [54], [138] and the model used in this work (ETC/ED model) is presented.

The analyses of two cases are performed, following [46], [61], [62] 1) a preliminary investigation is focused on only five types of biodiesel fuel, using input parameters typical for the conditions in Diesel engines, and 2) an advanced analysis is performed for a much wider range of biodiesel fuels (19 types altogether) using the parameters typical to those inferred from the in-house Diesel engine experimental data.

The compositions of biodiesel fuels used in our analyses are presented in the following section.

3.2   Compositions of biodiesel fuels

As mentioned earlier, two cases of five and nineteen types of biodiesel fuels in two different engine conditions are used in our analysis. These types of biodiesel fuels and their compositions are described in the following sub-sections.

I.   Case 1

In this case study, the model is applied to five types of the most commonly used biodiesel fuels. These are: Palm Methyl Ester (PME), produced from palm oil [139]; Hemp Methyl Esters, produced from hemp seed oil in the Ukraine (HME1) [140] and European Union (HME2) [141]; Rapeseed oil Methyl Ester (RME) [133], produced from rapeseed oil in the Ukraine; and Soybean oil Methyl Ester (SME), produced from soybean oil [142]. Molar fractions of components of these (pure methyl esters) fuels are shown in Table 3.1.

The meaning of symbols of components, presented in Table 3.1, and their acid codes, molecular formulae, molar masses and boiling temperatures are shown in Table 3.2 (see [143]–[146] for more detailes about these molar fractions; the values of boiling temperatures in this table are taken from [46], [147]). The numbers of carbons in fatty acids (n_{acid}) and numbers of double bonds (DB) in each component are shown by the numbers on the left and on the right of ':' , respectively in the formulae for the components. For example, C16:1 M has $n_{acid} = 16$ and DB $= 1$ (see Table 3.2). The total number of carbon atoms in methyl esters is equal to $n_{acid} + 1$.

Since the composition of 'other' components has not been reported in the abovementioned papers, it would be reasonable to assume that all parameters of these 'other' components, including molar masses shown in Table 3.2, can be calculated as an arithmetic average of the corresponding values for all remaining components from C12:0 M to C18:3 M taking into account their average molar contributions. Chemical structures of three typical components shown in Tables 3.1 and 3.2 (C18:0 M, C18:1 M, C18:2), illustrating the meaning of DB, are shown in Figure 3.1.

54
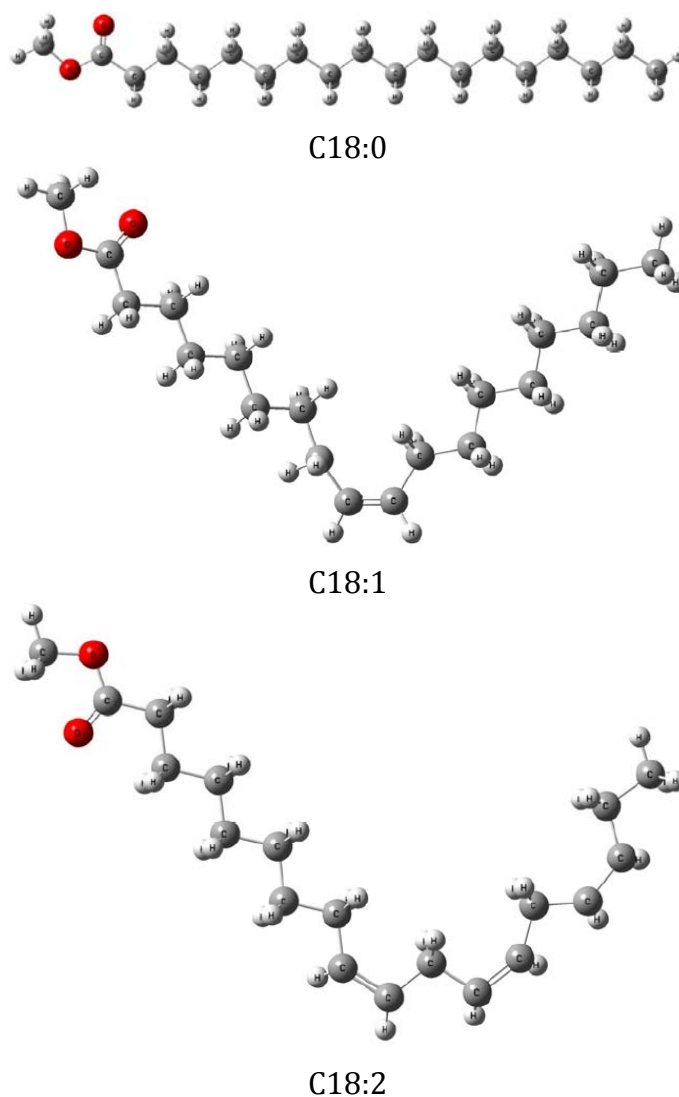
C18:0

C18:1

C18:2

Figure 3.1 Schematic presentations of the structures of C18:0 M, C18:1 M and C18:2 M molecules.

II.   Case 2

The following types of biodiesel fuels are used in this analysis: Tallow Methyl Ester (TME), Lard Methyl Ester (LME), Butter Methyl Ester (BME), Coconut Methyl Ester (CME), Palm Kernel Methyl Ester (PMK), Palm Methyl Ester (PME), Safflower Methyl Ester (SFE),   Peanut   Methyl Ester (PTE), Cottonseed Methyl Ester (CSE), Corn Methyl Ester (CNE), Sunflower Methyl Ester (SNE), Tung Methyl Ester (TGE), Hemp-oil Methyl Ester, produced from Hemp seed oil in Ukraine (HME1), Soybean Methyl Ester (SME), Linseed Methyl

Ester (LNE), Hemp-oil Methyl Ester, produced in European Union (HME2), Canola seed Methyl Ester (CAN), Waste cooking-oil Methyl Ester (WME) and Rapeseed Methyl Ester (RME). The molar fractions of the components of these fuels (in percent), inferred from averaging data presented in [46], [51], [125], [136], [148]–[150], are shown in Table 3.1.

As in Case 1, the molar fractions of unidentified additives in biodiesel fuels vary from 0 to around 8.7%. Since the exact nature of these components has not been identified, there is a certain freedom in selecting their transport and thermodynamic properties. In the preliminary analysis (Case 1 [25], [46], [64]), these properties are assumed as the arithmetic weighted mean of the corresponding values for all remaining components (C12:0M to C18:3M). In Case 2, these properties are assumed to be identical to those of C18:1M. The properties computed using this assumption turned out to be close to those obtained in Case 1 (see [68]), but the calculations are much simpler as they do not require an averaging procedure. Only 3 fuels have non-negligible molar fractions of unidentified components: RME, TGE, and to a lesser extent HME2. The molar fractions of unidentified components in other biodiesel fuels are either negligible or non-existent (see Table 3.1). The transport and thermodynamic properties of all components shown in Tables 3.1 and 3.2 are given in Appendix B. These properties are extrapolated to the cases of other fatty acids shown in Table 3.2, which have not been considered in Case 1.

There are other names used for some methyl esters shown in Table 3.2. For example, 'Methyl dodecanoate' is also known as 'Methyl laurate', 'Methyl tetradecanoate' is also known as 'Methyl myristate' and 'Methyl decosanoate' is also known as 'Methyl behenate' (see [46], [140], [151] for the details).

Table 3.1 Types of biodiesel fuels, their abbreviations, acid codes and molar fractions of the components (pure methyl esters). Symbols 'M' for the acid codes are omitted.

Methyl Esters	Abbreviations	Fatty Acids																	
		C8:0	C10:0	C12:0	C14:0	C16:0	C17:0	C18:0	C20:0	C22:0	C24:0	C16:1	C18:1	C20:1	C22:1	C24:1	C18:2	C18:3	Others
Tallow	TME	-	-	0.20	2.50	27.90	-	23.00	0.40	0.40	-	2.50	40.00	0.30	0.30	-	2.00	-	0.50
Lard	LME	-	-	-	1.00	26.00	-	14.00	-	-	-	2.80	44.00	2.00	2.00	-	8.00	-	0.20
Butter	BME	5.19	2.80	3.40	10.99	31.66	-	10.79	0.40	0.40	-	2.40	26.37	1.00	1.00	-	3.00	0.60	-
Coconut	CME	6.00	8.00	50.00	15.00	9.00	-	3.00	-	-	-	-	7.00	-	-	-	2.00	-	-
Palm Kernel	PMK	2.60	4.00	50.00	17.00	8.00	-	1.70	1.50	1.50	-	0.40	12.00	-	-	-	1.30	-	-
Palm	PME	-	-	0.26	1.29	45.13	-	4.47	0.35	0.17	-	0.21	38.39	-	-	-	9.16	0.19	0.38
Safflower	SFE	-	-	-	-	5.20	-	2.20	-	-	-	-	76.38	-	-	-	16.22	-	-
Peanut	PTE	-	-	-	0.50	8.00	-	4.00	7.00	7.00	-	1.50	49.00	-	-	-	23.00	-	-
Cottonseed	CSE	-	-	-	2.00	19.00	-	2.00	-	-	-	-	31.00	2.50	2.50	-	41.00	-	-
Corn	CNE	-	-	-	1.00	9.00	-	2.50	-	-	-	1.50	40.00	1.00	1.00	-	44.00	-	-
Sunflower	SNE	-	-	-	-	5.92	-	4.15	1.38	1.38	-	-	18.46	-	-	-	68.41	0.30	-
Tung	TGE	-	-	-	-	3.64	-	2.55	-	13.14	-	-	10.10	0.81	-	-	13.75	51.64	4.37
Hemp1	HME1	-	-	-	-	6.62	0.21	2.06	0.45	0.25	0.23	0.33	11.88	0.27	0.17	0.15	56.71	20.67	-
Soybean	SME	-	-	-	0.30	10.90	-	4.40	0.40	-	-	-	24.00	-	-	-	52.80	7.20	-
Linseed	LNE	-	-	-	0.20	6.20	-	0.60	-	-	-	-	18.00	-	-	-	16.00	59.00	-
Hemp2	HME2	-	-	-	-	6.51	-	2.46	0.90	-	-	-	11.88	0.90	-	-	54.82	20.07	2.46
Canola seed	CAN	-	-	-	-	4.48	0.14	1.99	0.62	0.35	0.16	0.36	59.66	1.49	0.42	-	20.89	9.44	-
Waste oil	WME	-	-	0.20	0.67	15.69	0.20	6.14	0.39	0.44	0.30	0.73	42.84	0.56	0.15	-	29.36	2.03	0.30
Rapeseed	RME	-	-	-	-	4.93	-	1.66	0.56	-	-	-	26.61	-	22.32	0.77	24.75	9.70	8.70

57

Table 3.2 Names, acid codes, molecular formulae, molar masses and boiling points of the components (pure methyl esters) presented in Table 3.1.

Fatty Acids	Acid code	Molecular Formula	Molar Mass (g/mol)	Boiling Point (K)
Methyl octanoate	C8:0 M	$C_9H_{18}O_2$	158.238	467.50
Methyl decanoate	C10:0 M	$C_{11}H_{22}O_2$	186.291	501.10
Methyl dodecanoate	C12:0 M	$C_{13}H_{26}O_2$	214.338	530.42
Methyl tetradecanoate	C14:0 M	$C_{15}H_{30}O_2$	242.39	554.20
Methyl palmitate	C16:0 M	$C_{17}H_{34}O_2$	270.442	577.98
Methyl heptadecanoate	C17:0 M	$C_{18}H_{36}O_2$	284.468	589.87
Methyl stearate	C18:0 M	$C_{19}H_{38}O_2$	298.494	601.76
Methyl eicosanoate	C20:0 M	$C_{21}H_{42}O_2$	326.546	625.55
Methyl decosanoate	C22:0 M	$C_{23}H_{46}O_2$	354.598	649.33
Methyl tetracosanoate	C24:0 M	$C_{25}H_{50}O_2$	382.65	673.11
Methyl palmitoleate	C16:1 M	$C_{17}H_{50}O_2$	268.426	577.57
Methyl oleate	C18:1 M	$C_{19}H_{50}O_2$	296.478	601.31
Methyl eicosenoate	C20:1 M	$C_{21}H_{50}O_2$	324.53	625.05
Methyl eurcate	C22:1 M	$C_{23}H_{44}O_2$	352.582	648.79
Methyl nervonate	C24:1 M	$C_{25}H_{48}O_2$	380.634	672.53
Methyl linoleate	C18:2 M	$C_{19}H_{34}O_2$	294.462	601.3
Methyl linolenate	C18:3 M	$C_{19}H_{32}O_2$	292.446	601.58
Others	–	–	296.478	601.31

3.3 Input parameters

The Sauter Mean Diameters (SMD) of biodiesel fuel droplets at temperature 80 °C, as reported in [46], [52], [140], [143], are shown in Table 3.3.

Table 3.3 The Sauter Mean Diameters (SMD) of biodiesel fuel droplets at 80 ℃.

Main References	PME	HME1	HME2	RME	SME
[52]	25.1 μm	-	-	28.8 μm	25.7 μm
[140]	-	23.55 μm	23.55 μm	26.69 μm	23.87 μm

According to Table 3.3, the values of the SMDs for all nineteen biodiesel fuels turned out to be rather close to the mean value of SMD which is equal to 25.32 μm. In the analysis of both cases (Case 1 and Case 2)   it is assumed that the initial values of droplet radii are equal to $R_{d0} = 12.66$ μm. Note that the same authors, as mentioned in Table 3.3, reported that the SMDs of Diesel fuel droplets, for the same conditions as those used for Table 3.3 (17.7 μm [52] and 18.3 μm [140]), are lower than those of biodiesel fuel droplets shown in Table 3.3. This can be attributed to the fact that the higher viscosity of biodiesel fuel leads to lower jet velocity and larger droplet sizes compared with Diesel fuel [152]. Other input parameters used in both cases are summarised below.

I.   Case 1

As reported in [153], the initial droplet temperatures (T_{d0}) could vary from 375 K to 440 K. In our analysis, it is assumed that $T_{d0} = 375$ K. As to the ambient air parameters, the following ranges of air density and temperature were reported in [153] for biofuels: 3.3–60 kg m^{-3} and 700–1300 K. Assuming that the ideal gas law is valid, this corresponds to the following range of air pressures: 6.63–223.9 bars (remembering that the gas constant for air is equal to 287 J kg^{-1}K^{-1}). Near the upper limits of these parameters, the analysis would require the application of the equation of state for real gases which is beyond the scope of this work. Our analysis is focused on the same values of parameters as in [43], [47] for Diesel engine conditions (assuming that the ideal gas law is valid): $\rho_a = 11.9$ kg m^{-3}, $T_a = 880$ K, $p_a = 30$ bar. These values are comparable with, although slightly lower than, those reported in [153].

II. Case 2

A droplet of initial temperature $T_{d0} = 360$ K is assumed to be moving through air at constant velocity of U_d= 28 m/s. In the case of Butter Methyl Ester (BME) the calculations have also been performed for stationary droplets. Ambient temperature and pressure are assumed equal to 700 K and 32 bar respectively. The droplet velocity was derived from the microscopic panorama images of Diesel spray interface [63], [154] based on the assumption that biodiesel and Diesel fuel droplets move at approximately the same velocities under the same ambient conditions.

3.4   Results of Case 1

The results presented in this section have been previously published in [25], [46], [51]. Using the values of the input parameters described in the previous section, the thermodynamic and transport properties of components described in Appendix B, the Effective Thermal Conductivity/Effective Diffusivity (ETC/ED) model is used for the analysis of biodiesel fuel droplet heating and evaporation. The values of droplet surface temperatures (T_s) and radii (R_d) versus time (t) were calculated for all 5 types of biodiesel fuels used in Case 1. The calculations were performed: (1) taking into account the contribution of up to 16 components shown in Table 3.1 (multi-component models); and (2) replacing these components by a single component with average transport and thermodynamic properties obtained as described in Appendix B (single component models).
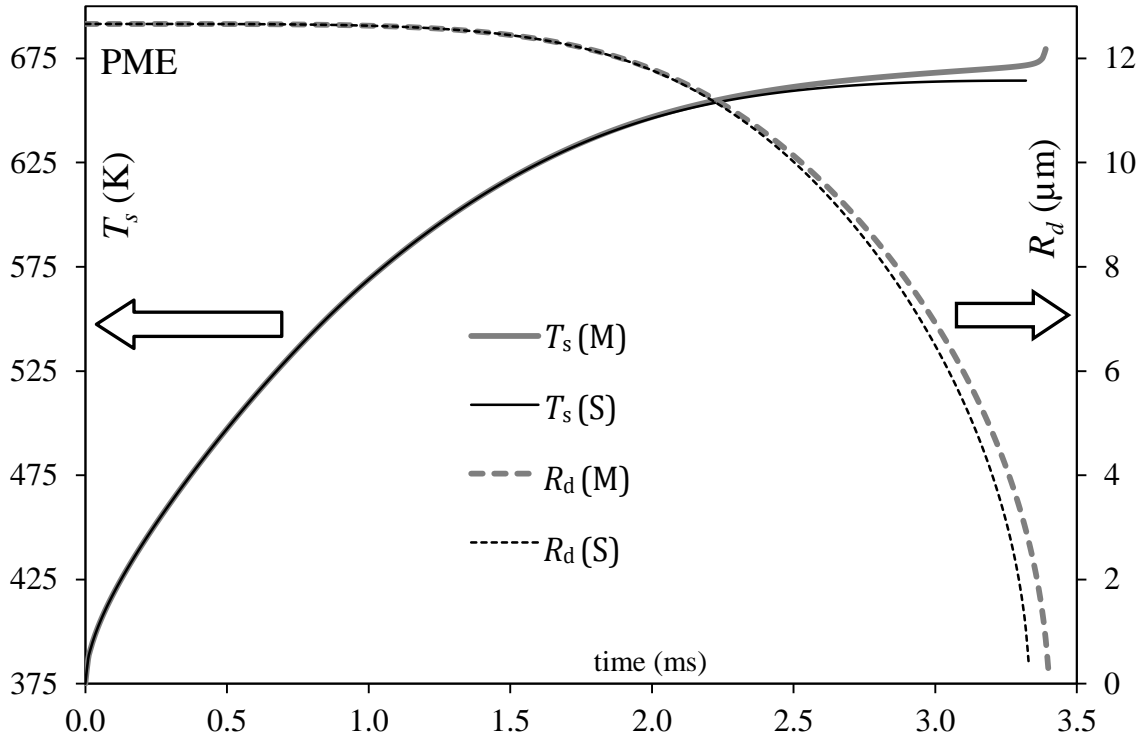
Figure 3.2 The plots of PME droplet surface temperatures (T_s) and radii (R_d) versus time predicted by the multi-component (M) and single component (S) models. Gas temperature and pressure are assumed to be equal to 880 K and 30 bar respectively. The initial droplet radius is assumed to be equal to 12.66 μm. The droplet is assumed to be stationary. The analysis is based on the ETC/ED model.

The results for PME for stationary droplets are shown in Figure 3.2. This figure shows that the multi-component model predicts higher droplet surface temperatures and longer evaporation times compared with the single component model. This result is consistent with the one earlier reported in [43], [45], [47] for Diesel and gasoline fuel droplets. As in the case of the abovementioned fuels, this behaviour of the droplet surface temperature and radius can be related to the fact that at the final stages of droplet evaporation the mass fraction of species with larger numbers of carbon atoms n (C20:1 M, C18:1 M, C18:2 M, C18:0 M) increases at the expense of species with smaller n (C16:0 M).

At the final stage of evaporation, for all species except C20:1 M, the mass fractions decrease with time. This is demonstrated in Figure 3.3, where the time evolution of surface mass fractions of four dominant species is presented.

The behaviour of surface mass fractions of the intermediate species (C18:1 M, C18:2 M, C18:0 M) when their mass fractions first increase and then start to decrease is similar to that observed for Diesel and gasoline fuel droplets (cf. Figure 11 of [43]). The species with larger n evaporate more slowly than the species with lower n and have higher wet bulb temperatures.
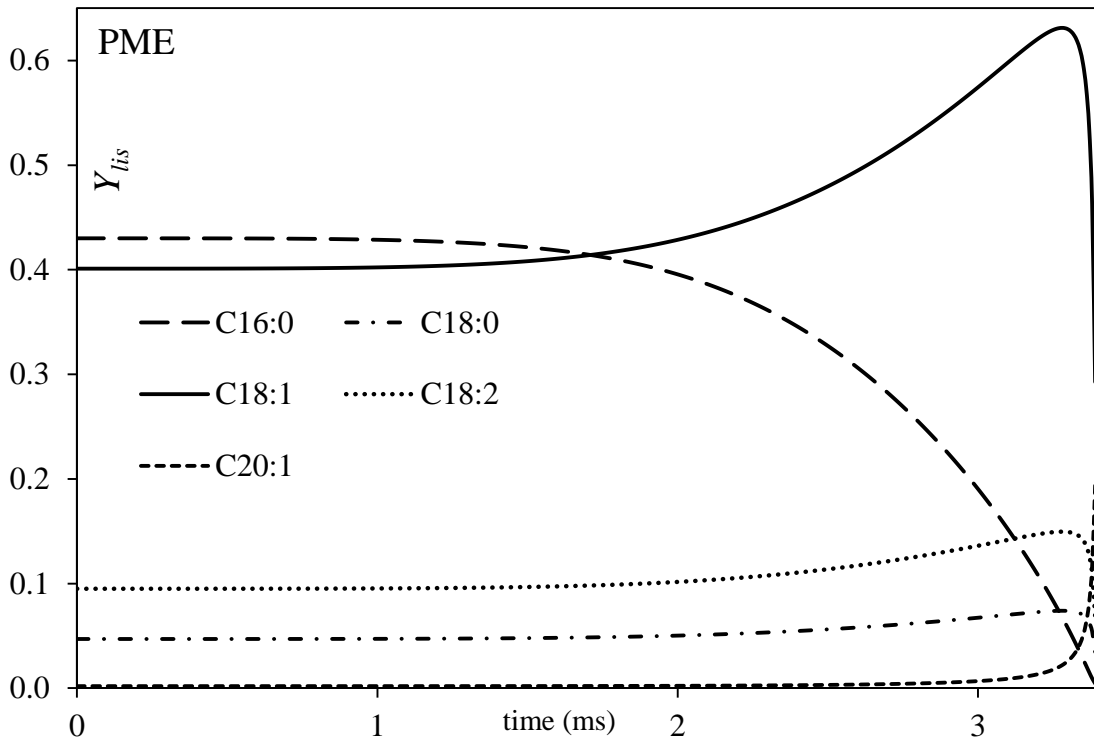
Figure 3.3 The plots of liquid surface mass fractions (Y_{lis}) of methyl palmitate (C16:0 M), methyl stearate (C18:0 M), methyl oleate (C18:1 M), methyl linoleate (C18:2 M) and methyl eicosenoate (C20:1 M) versus time for the same droplet as in Figure 3.2.

The plots of mass fractions of two dominant species in PME droplets (C16:0 M and C18:1 M) versus normalised radius R/R_d at three instants of time (0.3 ms, 1 ms and 2 ms) are shown in Figure 3.4. At $t = 0$ these plots are the lines parallel to the R/R_d axis. As one can see from this figure, at all three time instants the mass fractions of both components remain rather close to their initial values near the droplet centre, but the difference between them increases in the region close to the droplet surface, especially at $t = 2$ ms. The values of these mass fractions at the droplet surface are the same as those shown in Figure 3.3.

62
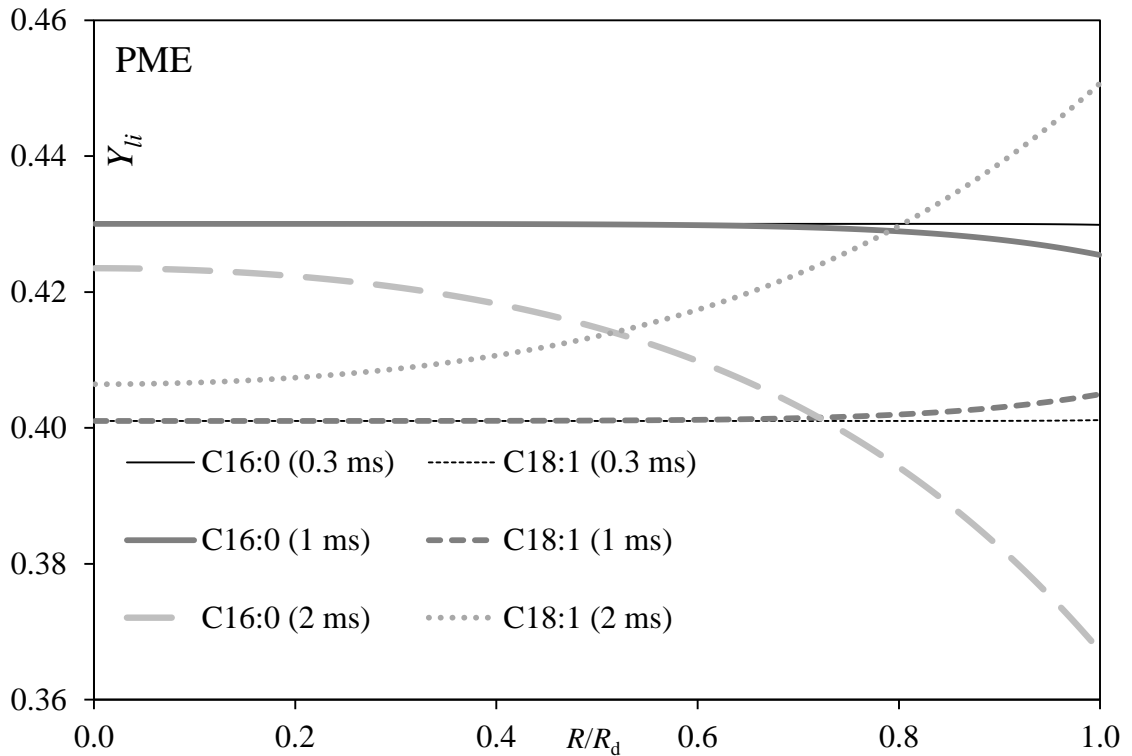
Figure 3.4 The plots of liquid mass fractions (Y_{li}) of methyl palmitate (C16:0 M) and methyl oleate (C18:1 M) versus normalised distance from the centre of the droplet R/R_d at three instants of time (0.3 ms, 1 ms and 2 ms) for the same droplet as in Figures 3.2 and 3.3.

The plots of temperatures in PME droplets versus normalised distance from the centre of the droplet R/R_d at five instants of time (0.02 ms, 0.3 ms, 0.5 ms, 1 ms and 2 ms) are shown in Figure 3.5. At $t = 0$ the plot reduces to the line parallel to the R/R_d axis ($T = 375$ K). As one can see from this figure the heating of the surface of the droplet is noticeable at very early times ($t = 0.03$ ms), while the gradient of temperature inside the droplet can be seen at all times up to $t = 2$ ms (approximately 60% of the evaporation time). This demonstrates the limitation of the widely used ITC model, in agreement with the earlier results [43], [44], [47], [55], [69].
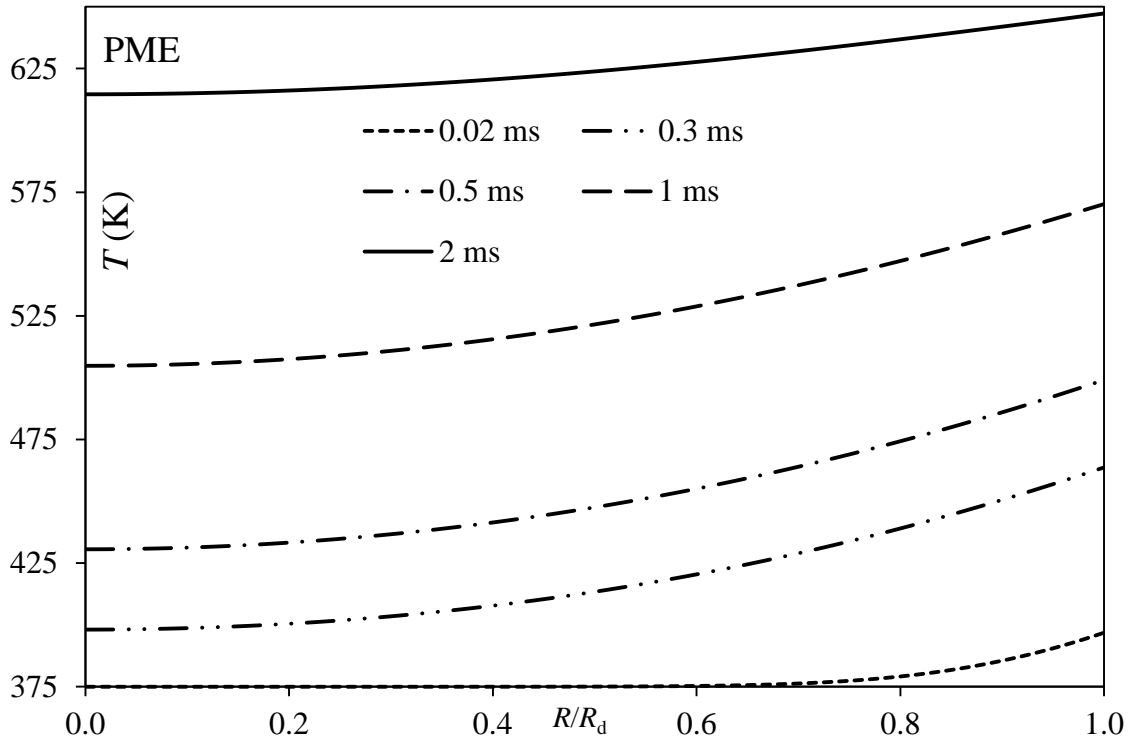
Figure 3.5 The plots of temperature (T) versus normalised distance from the centre of the droplet R/R_d at five instants of time (0.02 ms, 0.3 ms, 0.5 ms, 1 ms and 2 ms) for the same droplet as in Figures 3.2–3.4.

Note that the difference between the values of droplet surface temperatures (T_s) and radii (R_d) predicted by the multi-component and single component models is much smaller for PME than for Diesel and gasoline fuels (cf. Figures 2, 5 and 8 of [43]). The droplet evaporation times predicted by these models for PME droplets differ by 2.10% (relative to the prediction of the single component model). This can be related to the fact that in PME the dominant components have relatively close molar masses and corresponding boiling temperatures and enthalpies of evaporation, while in the case of Diesel and gasoline fuels the contributions of components in a wide range of molar masses, boiling temperatures and enthalpies of evaporation need to be taken into account. This implies that the approximation of PME with a single component is expected to be much more accurate compared with the case of Diesel and gasoline fuels.

The plots similar to those shown in Figure 3.2 but for HME1, are presented in Figure 3.6. Comparing Figures 3.2 and 3.6 one can see that HME1 droplets

take longer to evaporate completely than PME droplets and the surface temperatures of HME1 droplets, predicted by the multicomponent model at the final stage of droplet evaporation, are slightly higher than the ones predicted for the PME droplets.
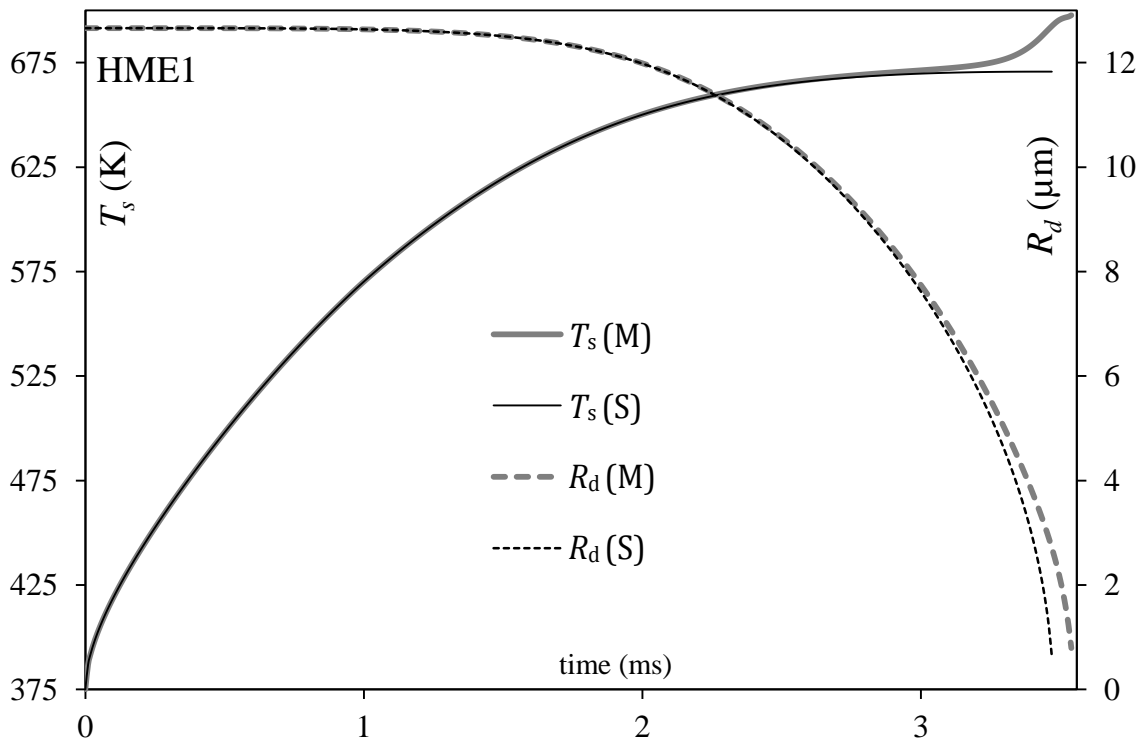
Figure 3.6 The plots of HME1 droplet surface temperatures (T_s) and radii (R_d) versus time predicted by the multi-component (M) and single component (S) models. The gas and initial droplet parameters are the same as in Figure 3.1. The analysis is based on the ETC/ED model.

Apart from the abovementioned remarks, the difference between the predictions of the multi-component and single component models for HME1 is rather similar to that for PME. However, the processes which take place in HME1 and PME droplets are rather different. This difference can be clearly seen when Figure 3.3 is compared with Figure 3.7. The latter figure shows the time evolution of surface mass fractions of five dominant species in HME1. The species with larger n (C24:0 M) evaporate more slowly than the species with smaller n (C18:2 M, C18:3 M, C18:1 M and C16:0 M) and have higher wet bulb temperatures. This leads to an increase in the surface mass fraction of C24:0 M

at the final stage of droplet heating and evaporation at the expense of the surface mass fractions of C18:2 M, C18:3 M, C18:1 M and C16:0 M.
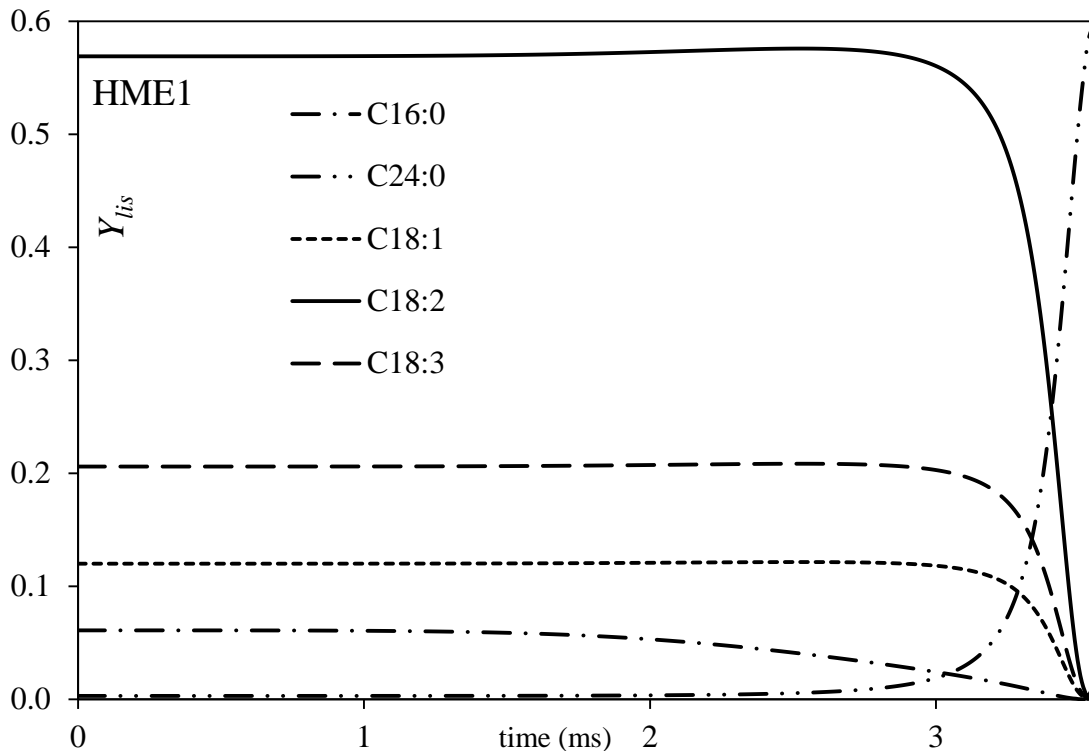
Figure 3.7 The plots of liquid surface mass fractions (Y_{lis}) of methyl palmitate (C16:0 M), methyl tetracosanoate (C24:0 M), methyl oleate (C18:1 M), methyl linoleate (C18:2 M) and methyl linolenate (C18:3 M) versus time for the same droplet as in Figure 3.6.

The plots of mass fractions of species and temperatures in HME1 droplets versus normalised distance from the centre of the droplet R/R_d at various instants of time show the same trends as in the case of PME but for different mass fractions, as shown in Figures 3.8 and 3.9. The same comment applies to HME2, RME and SME fuel droplets which are discussed below.
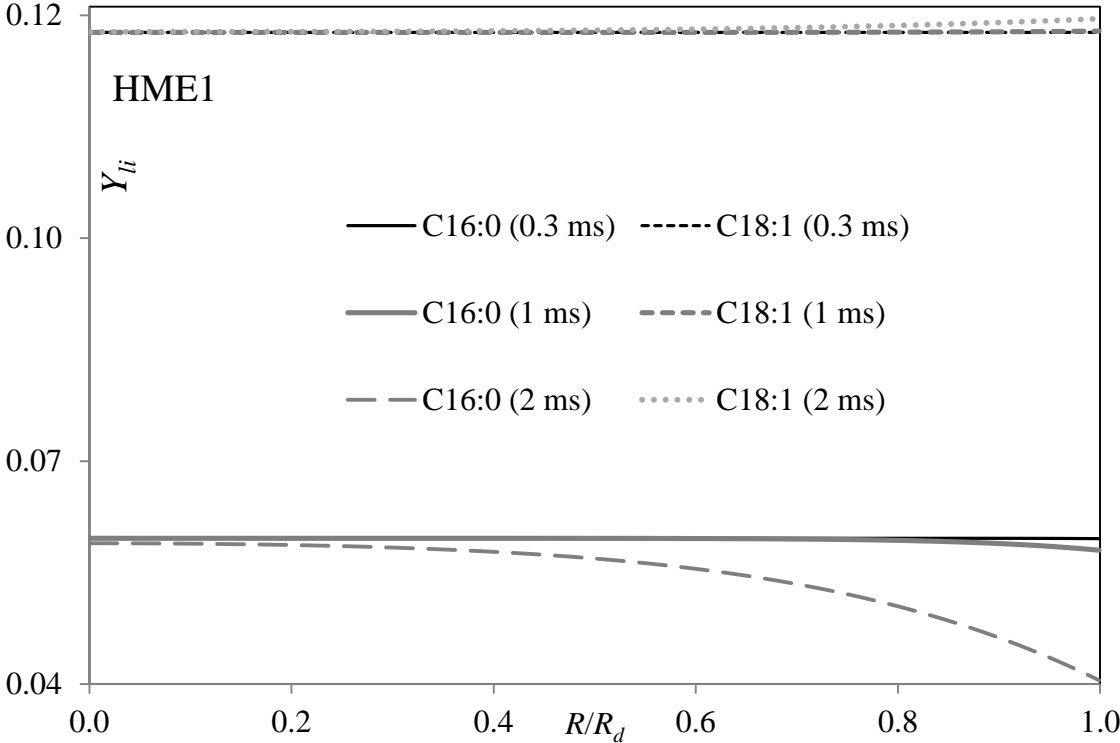
Figure 3.8 The plots of liquid mass fractions (Y_{li}) of the HME1 droplet versus normalised distance from the centre of the droplet R/R_d.
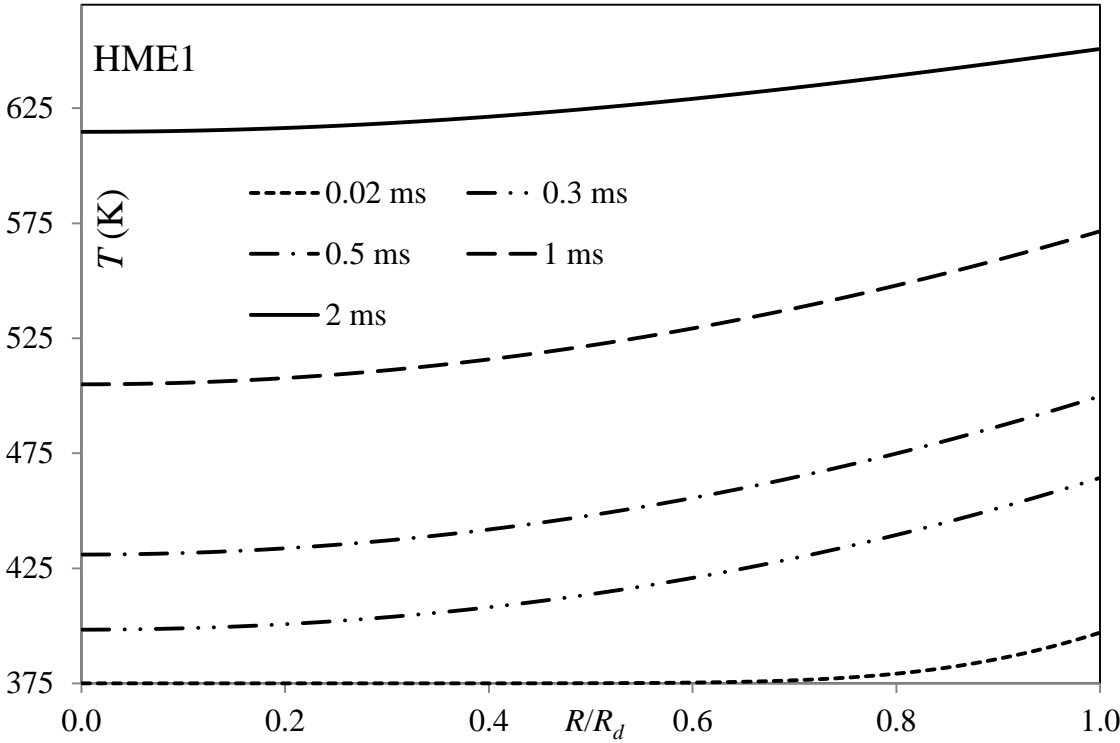
Figure 3.9 The plots of temperature (T) of the HME1 droplet versus normalised distance from the centre of the droplet R/R_d at five instants of time (0.02 ms, 0.3 ms, 0.5 ms, 1 ms and 2 ms).

The plots similar to those shown in Figures 3.2 and 3.6 but for HME2, are presented in Figure 3.10. The latter plots are rather similar to those referring to HME1, except that the results predicted by multi-component and single component models are much closer for HME2 than for HME1. The droplet evaporation times predicted by these models differ by 0.58%. This can be explained by the fact that there are no heaviest components (C22:1M and C24:1M) in HME2 while they are quite noticeable in HME1 (see Table 3.1).
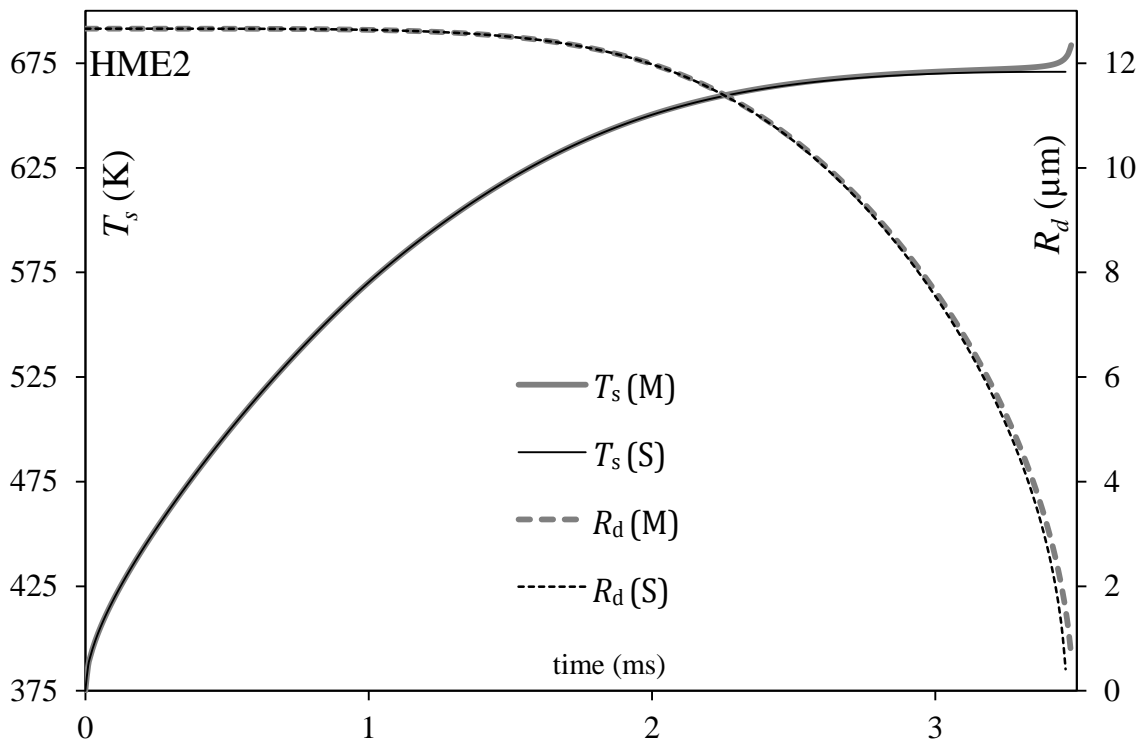
Figure 3.10 The plots of the HME2 droplet surface temperatures (T_s) and radii (R_d) versus time predicted by the multi-component (M) and single component (S) models. The gas and initial droplet parameters are the same as in Figure 3.2. The analysis is based on the ETC/ED model.

The time evolution of surface mass fractions of five dominant species in HME2 droplets is shown in Figure 3.10. As one can see in this figure, the mass fraction of the heaviest component C20:0 M increases with time at the final stage of droplet evaporation, while mass fractions of all other components decrease with time. These decreases and increases are less pronounced compared with the cases shown in Figures 3.3 and 3.7, which is reflected in the

closeness of the droplet surface temperatures and radii predicted by multi-component and single component models.
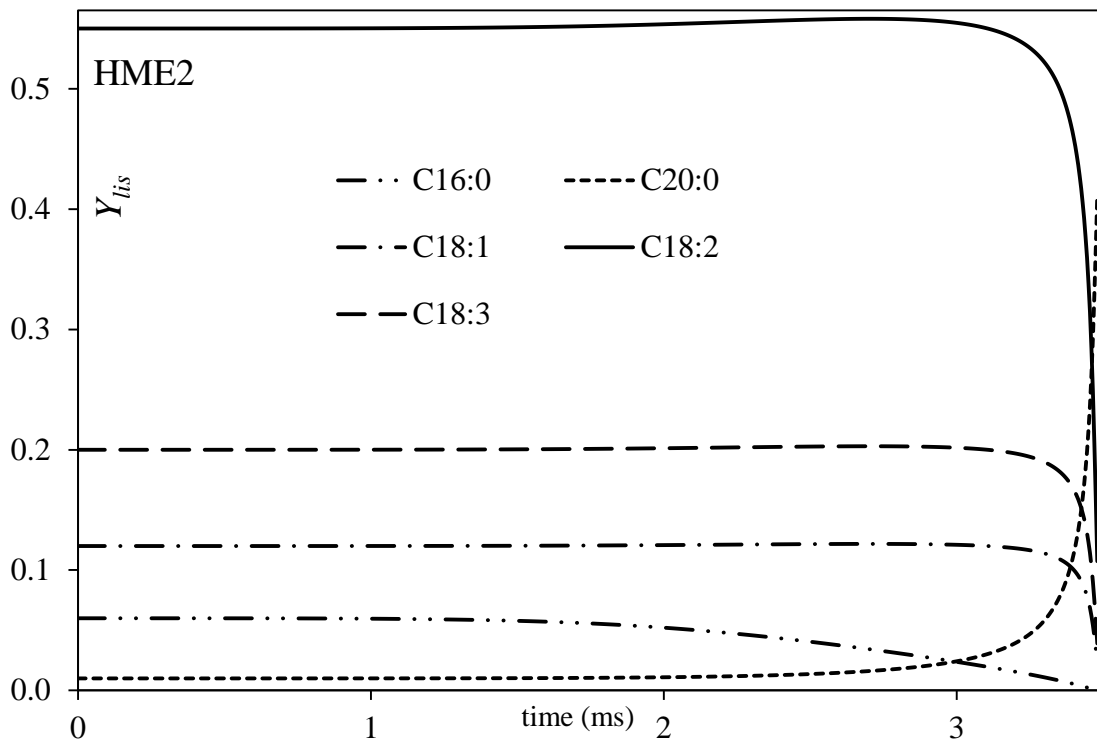
Figure 3.11 The plots of liquid surface mass fractions (Y_{lis}) of methyl palmitate (C16:0 M), methyl eicosanoate (C20:0 M), methyl oleate (C18:1 M), methyl linoleate (C18:2 M) and methyl linolenate (C18:3 M) versus time for the same droplet as in Figure 3.10.

The plots similar to those shown in Figures 3.2, 3.6 and 3.10 but for RME, are presented in Figure 3.12. The plots shown in this figure are rather similar to those referring to previously considered biodiesel fuels, except that the deviation between the results predicted by multi-component and single component models is larger than in the case of PME, HME1 and HME2. The droplet evaporation times predicted by these models for RME differ by 5.50%. This can be attributed to the presence in RME of two components, C22:1 M and C18:2 M, with almost equal initial mass fractions, but with different molar masses, boiling temperatures and enthalpies of evaporation.
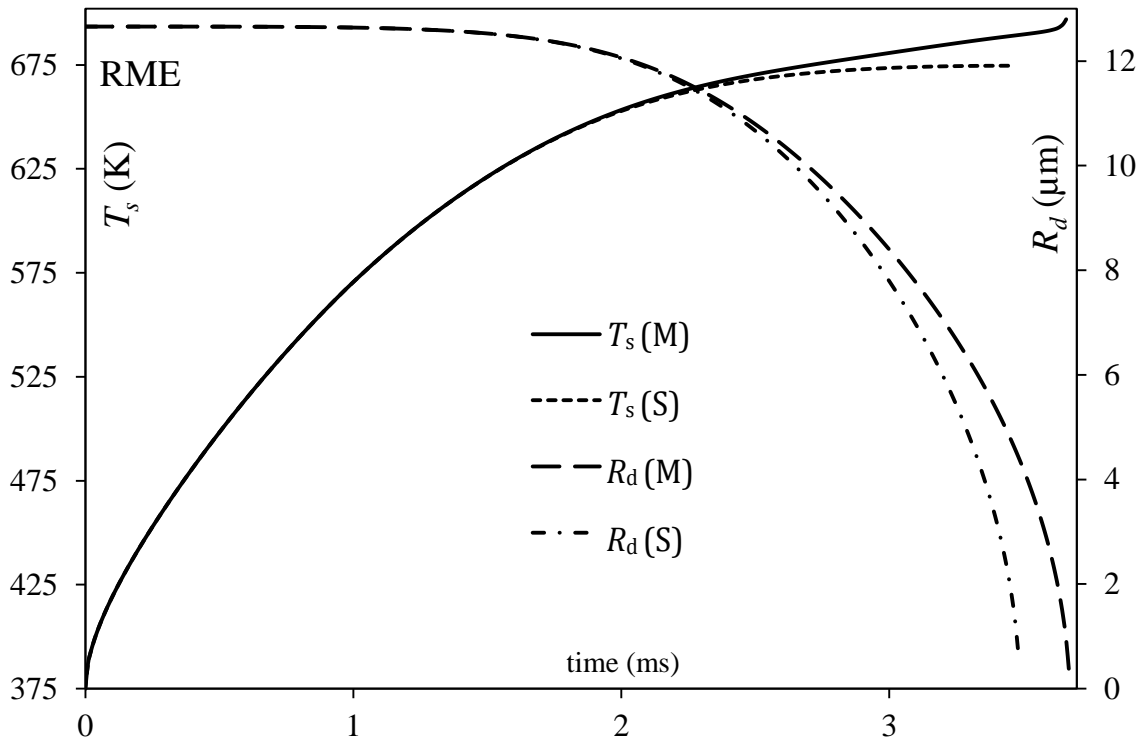
Figure 3.12 The plots of RME droplet surface temperatures (T_s) and radii (R_d) versus time predicted by the multi-component (M) and single component (S) models. The gas and initial droplet parameters are the same as in Figure 3.2. The analysis is based on the ETC/ED model.

Also, the mass fractions of species with larger number of carbons (n) (C22:1 M and C24:1 M) increase at the expense of species with smaller n (C16:0 M, C18:1 M, C18:2 M and C18:3 M) except at the very final stage of droplet evaporation. At this final stage, mass fractions of all species except C24:1 M start to decrease. This is demonstrated in Figure 3.13, where the time evolution of surface mass fractions of six dominant species is presented. As in the case of previously considered biodiesel fuels, the species with larger n evaporate more slowly than the species with lower n and have higher wet bulb temperatures.
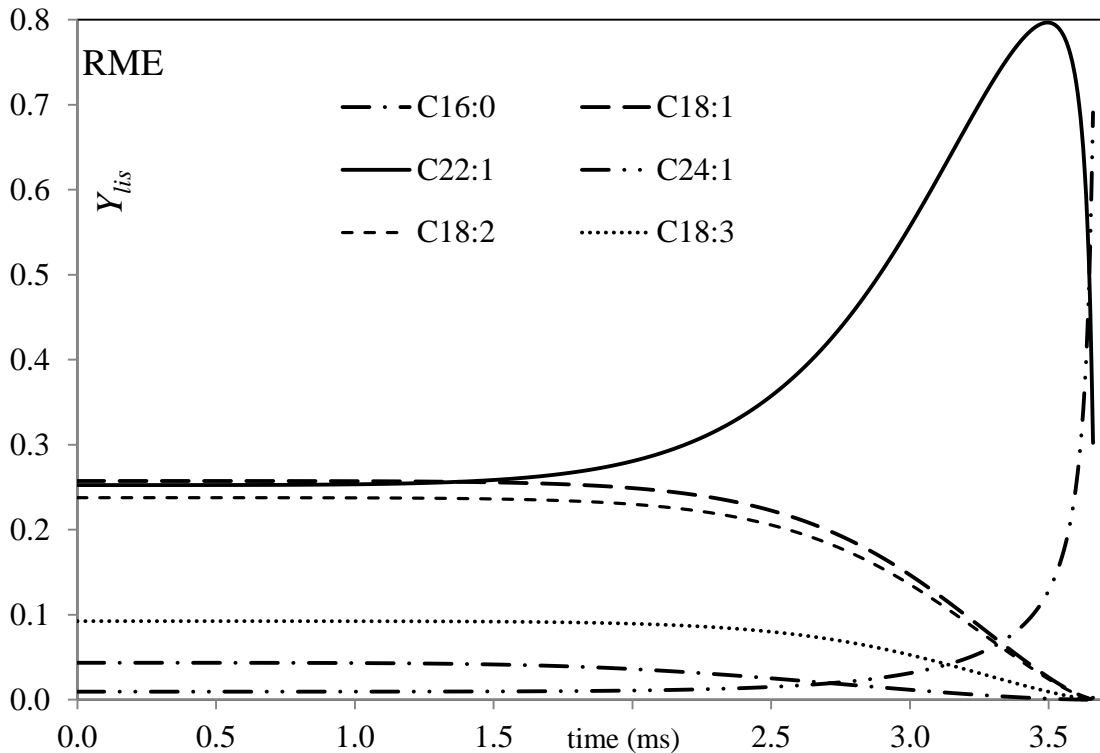
Figure 3.13 The plots of liquid surface mass fractions (Y_{lis}) of methyl palmitate (C16:0 M), methyl oleate (C18:1 M), methyl nervonate (C24:1 M), methyl linoleate (C18:2 M) and methyl linolenate (C18:3 M) versus time for the same droplet as in Figure 3.12.

The plots similar to those shown in Figures 3.2, 3.6, 3.10 and 3.12 but for SME, are presented in Figure 3.14. The plots shown in this figure are rather similar to those referring to previously considered biodiesel fuels, especially those for HME1. The droplet evaporation times predicted by these models differ by 1.16%.

The time evolution of surface mass fractions of six dominant species in SME droplets is shown in Figure 3.15. As one can see in this figure, the mass fraction of the heaviest component, C22:1 M, increases with time at the final stage of droplet evaporation, while mass fractions of all other components decrease with time. These decreases and increases are less pronounced compared with the cases shown in Figure 3.13, which is reflected in the relative closeness of the droplet surface temperatures and radii predicted by multi-component and single component models.
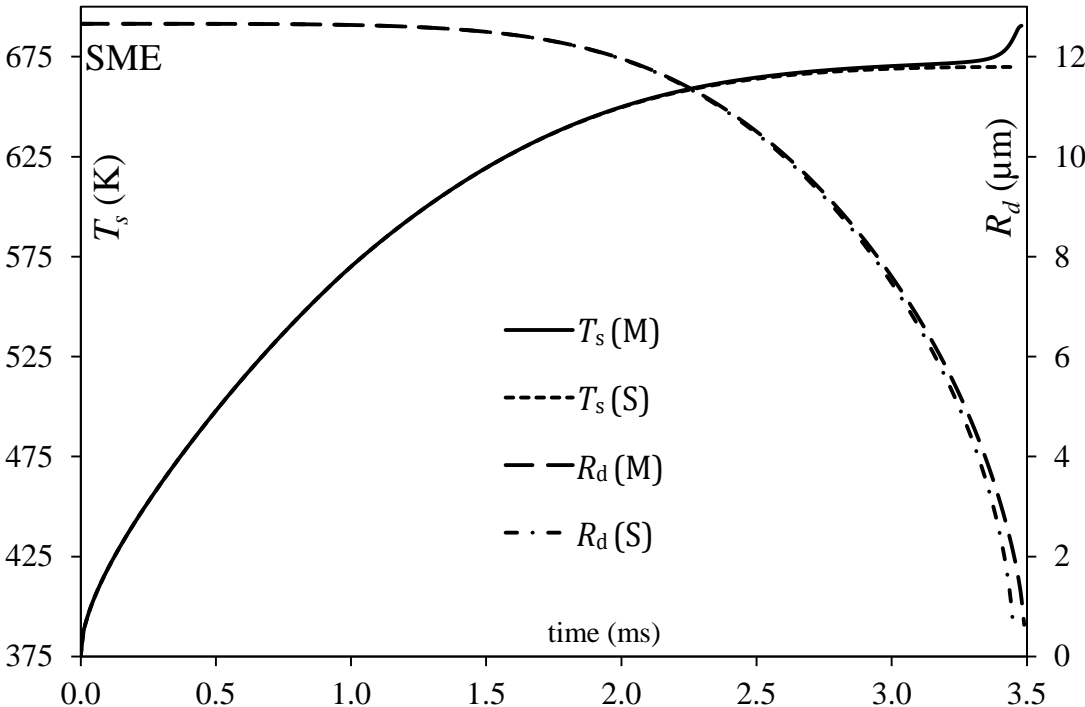
Figure 3.14 The plots of SME droplet surface temperatures (T_s) and radii (R_d) versus time predicted by the multi-component (M) and single component (S) models. The gas and initial droplet parameters are the same as in Figure 3.2. The analysis is based on the ETC/ED model.
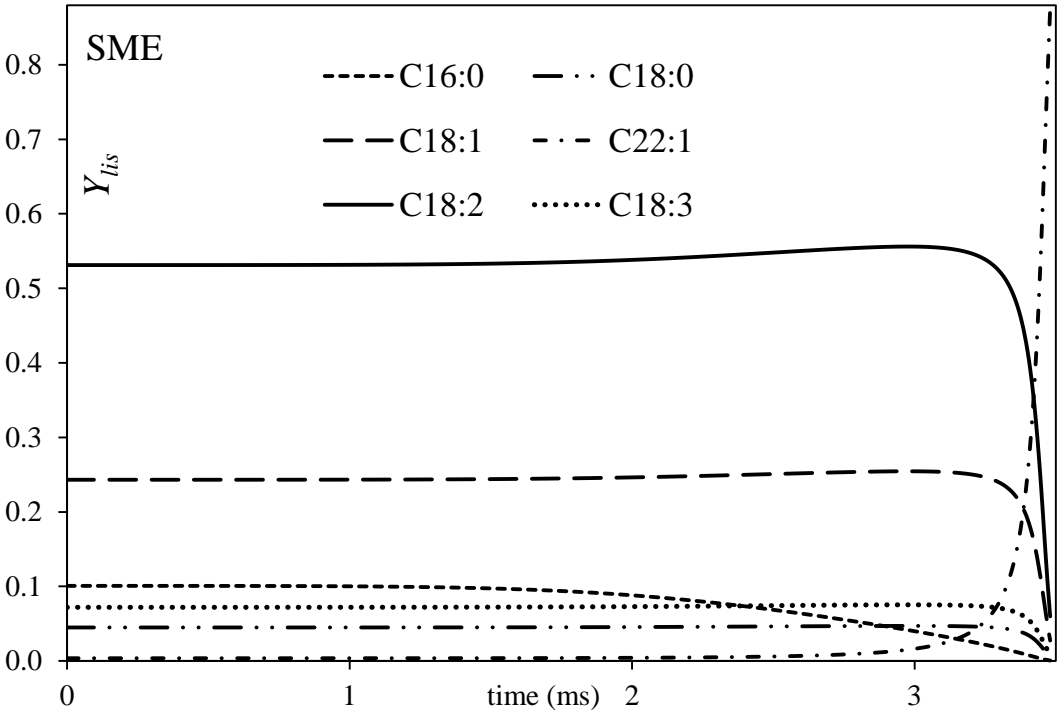
Figure 3.15 The plots of liquid surface mass fractions (Y_{lis}) of methyl palmitate (C16:0 M), methyl stearate (C18:0 M), methyl oleate (C18:1 M), methyl erucate (C22:1 M), methyl linoleate (C18:2 M) and methyl linolenate (C18:3 M) versus time for the same droplet as in Figure 3.14.

The plots for the same case as shown in Figure 3.2, but for a droplet moving with velocity 10 m/s, are presented in Figure 3.16. In the same figure the droplet surface temperatures T_s and radii R_d versus time, calculated using the multi-component model based on the ITC/ID and ETC/ED approaches, are shown.
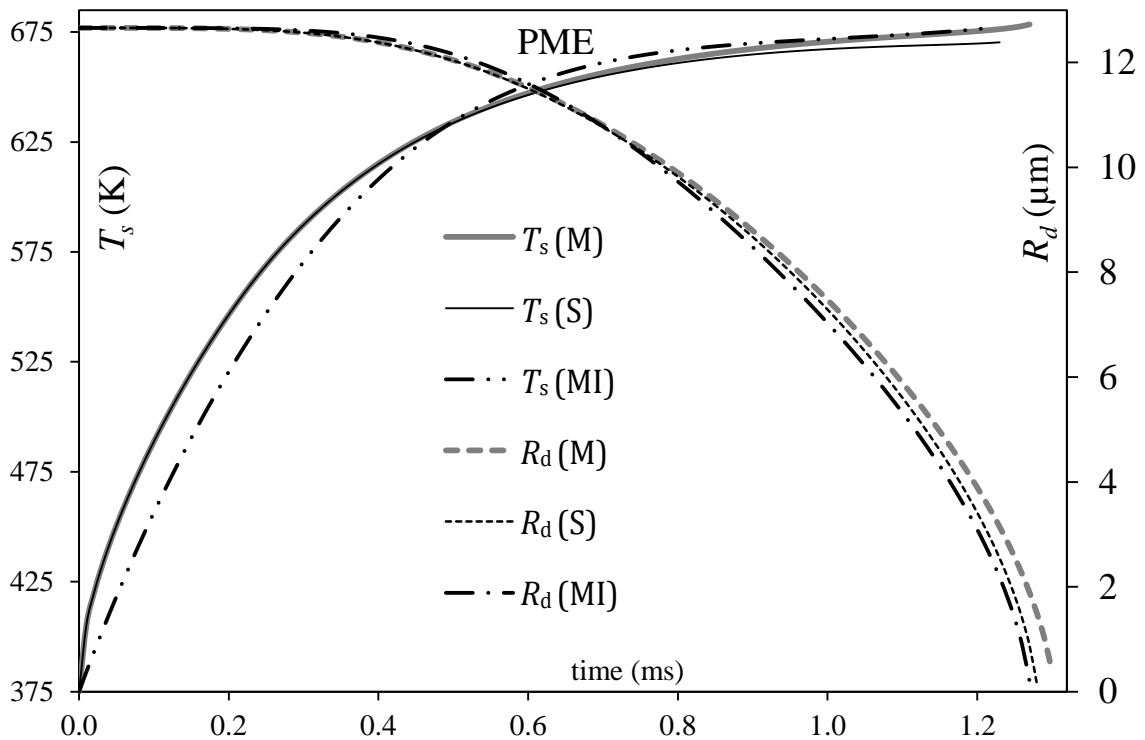
Figure 3.16 The plots of PME droplet surface temperatures (T_s) and radii (R_d) versus time predicted by the multi-component (M) and single component (S) models. Gas temperature and pressure are assumed to be equal to 880 K and 30 bar respectively. The initial droplet radius is assumed to be equal to 12.66 μm. The droplet is assumed to be moving with a constant velocity equal to 10 m/s. The analysis in both cases is based on the ETC/ED model and in the case of the multi-component model it is also based on the ITC/ID model (MI).

Comparing Figures 3.2 and 3.16 one can see that moving droplets evaporate about 3 times faster than stationary droplets as expected. As in the case of Diesel and gasoline fuel droplets [43], [47], there are noticeable differences in

predictions based on the ETC/ED and ITC/ID models, especially for temperatures at the initial stage of droplet heating. As mentioned in [43], [47] accurate prediction of these temperatures is particularly important for the prediction of the auto-ignition timing in Diesel engines. This brings into question the reliability of the models for heating and evaporation of biodiesel droplets, based on the ITC/ID approximations. These models are almost universally used for the analysis of these processes. As in the case shown in Figure 3.2, the multicomponent model predicts higher droplet surface temperatures and longer evaporation times compared with the single component model. The droplet evaporation times predicted by these models differ by 1.6%. This difference between the predictions of these models is slightly smaller than in the case of stationary droplets.

It should be emphasised that validation of the presented modelling results against experimental data was not performed, as was done in [55], [69] for bi-component droplets, as accurate measurements of time evolution of average biodiesel fuel droplet temperatures and radii have not been performed so far to the best of the author's knowledge. The main attention has been focused mainly on the validation of the predictions of simplified models (single component and/or ITC/ID models) against more general multi-component ETC/ED models. The predictions of the latter models, based on the analytical solution of the underlying equations, were verified against the predictions of the models based on the numerical solutions to these equations and validated againsts experimental data for bi-component droplets [54]. The limitations of the ETC/ED models were discussed in [155].

3.5 Results of Case 2

Most of the results presented in this section are published in [61], [68]. The model and numerical algorithm used in this analysis are exactly the same as the ones used in Case 1. In Case 2, the predictions of the following models are compared:

a) a model taking into account the contributions of all components of biodiesel fuels, their realistic diffusion, temperature gradient, and recirculation within the droplet, in the case of moving droplets (using the Effective Thermal Conductivity/Effective Diffusivity (ETC/ED) model); this model is referred to as the 'ME' model;

b) a model taking into account the contribution of all components of biodiesel fuels, but assuming that the diffusivity of species in droplets is infinitely fast and the liquid thermal conductivity is infinitely large (using the Infinite Thermal Conductivity/Infinite Diffusivity (ITC/ID) model); this model is referred to as the 'MI' model; and

c) a model ignoring transient diffusion of species (treating all species as a single component) and assuming that the liquid thermal conductivity is infinitely large (ITC model); this model is referred to as the 'SI' model. In the case of stationary droplets this model is further simplified assuming that biodiesel fuels can be approximated by a single dominant (with the largest molar fraction) component. The latter model is referred to as the 'DI' model.

The plots of time evolution of droplet surface temperature (T_s) and radius (R_d) for Tallow Methyl Ester (TME) are shown in Figure 3.17. The general trends of the curves shown in this figure are the same as presented in the previous case study (see [25], [46], [64] for further details). The ME model predicts longer evaporation times compared with the MI and SI models with the results predicted by the MI model being closer to those predicted by the ME model compared to the predictions of the SI model. The relative error in the evaporation times predicted by the SI model compared with the ME model is 9.0%. The same error for the MI model is 3.2%. That means that predictions of the models based on the assumption that species inside droplets mix infinitely fast are more reliable than the predictions of the models approximating TME by a single component. The MI model is one of the most widely used models for the analysis of heating and evaporation of complex hydrocarbon fuel mixtures (see, for example, [10], [34], [35], [37], [48], [49]). The deviations between the predictions of SI and ME models are larger than those reported in Case 1 (5.5%).
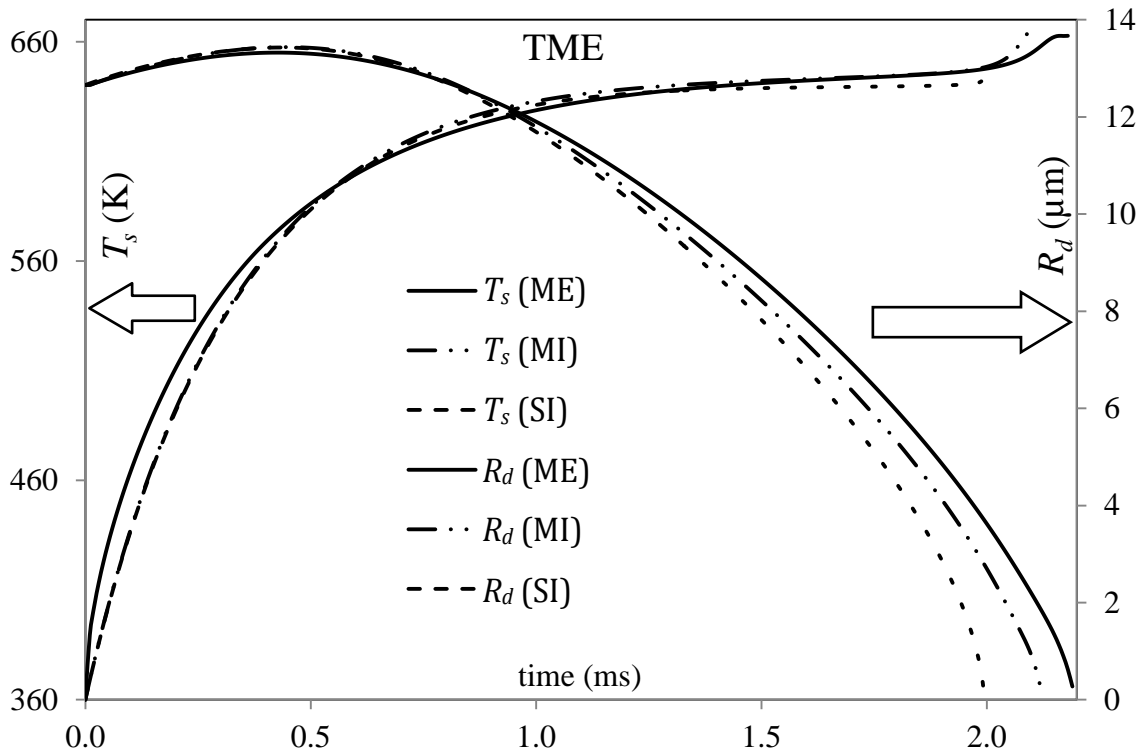
Figure 3.17 The plots of time evolution of surface temperature (T_s) and radius (R_d) for a Tallow Methyl Ester (TME) droplets predicted by the multi-component ETC/ED model (ME), single-component (zero diffusivity)/ITC model (SI), and multi-component ITC/ID model (MI). The droplet is assumed to have initial radius 12.66 μm and is moving at 28 m/s in still air at temperature and pressure equal to 700 K and 3.2 MPa respectively.

Note that, In Figure 3.17, both MI and ME models predict higher droplet surface temperatures at the final stages of droplet evaporation than the single-component model (SI). This is related to the fact that at the final stages of droplet evaporation the mass fractions of heavier species increase at the expense of lighter species. The heavier species evaporate more slowly than the lighter species and have higher boiling temperatures (see the results shown later in this chapter). The same behaviour of temperatures is observed for other types of biodiesel fuel discussed below.

The same plots as shown in Figure 3.17, but for Lard Methyl Ester (LME) are shown in Figure 3.18. The curves shown in Figure 3.17 are similar to those shown in Figure 3.18. As in the case of TME, the results predicted by the MI model are closer to those predicted by the ME model compared with the predictions of the SI model. The relative errors in the evaporation times

predicted by the SI and MI models compared with the ME model are slightly larger for LME compared with TME. These errors for the SI and MI models are found to be 11.1% and 4.0%, respectively.
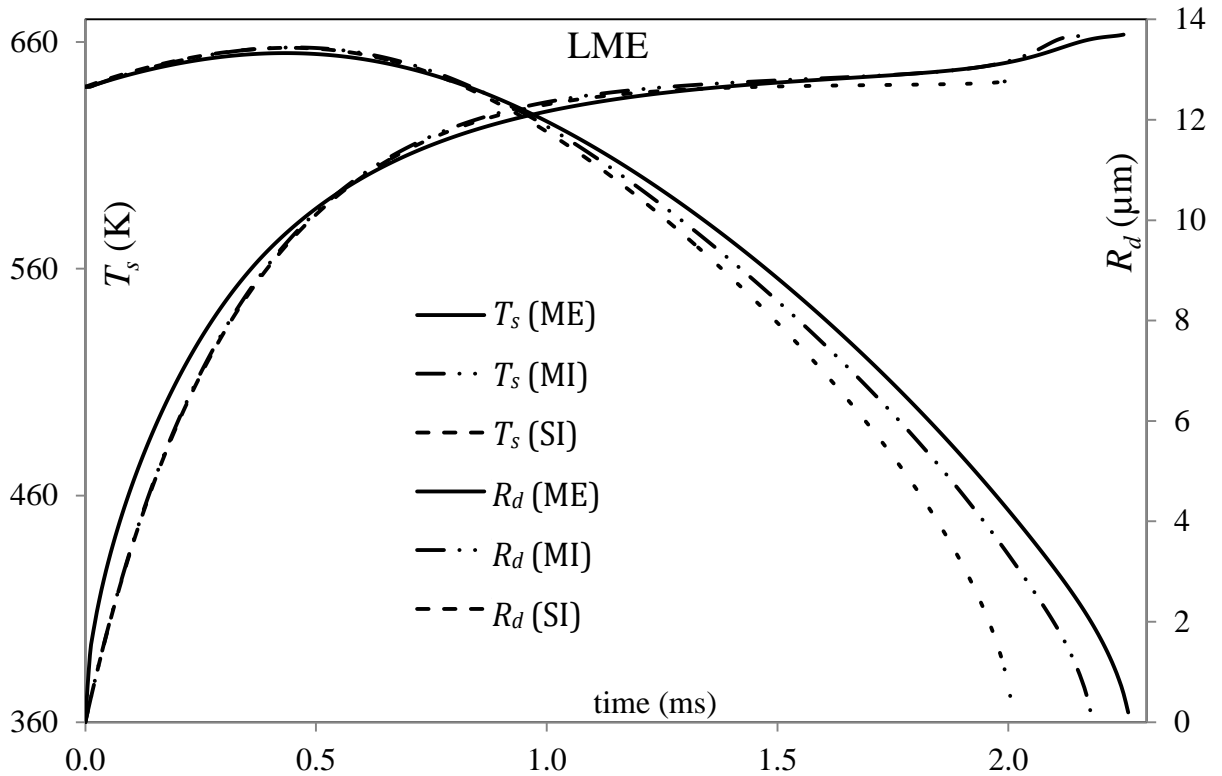
Figure 3.18 The same as Fig. 3.17 but for a Lard Methyl Ester (LME) droplet.

The same plots as shown in Figures 3.17 and 3.18, but for Butter Methyl Ester (BME) are presented in Figure 3.19. The trends of the curves presented in Figure 3.19 are similar to those shown in Figures 3.17 and 3.18, but the relative error in the evaporation time predicted by the SI model compared with the ME model is much larger for BME compared with TME and LME. This error for the SI model was found to be 25.2%. The importance of this result lies in the fact that it contradicts one of the main conclusions made in previous section (Case 1), based on the analysis of Palm Methyl Ester, Hemp Methyl Esters, Rapeseed oil Methyl Ester, and Soybean oil Methyl Ester. The analyses for Case 1 led us to the conclusion that biodiesel fuels can be safely approximated by single component fuels, which is not compatible with the results shown in Figure 3.19. The error of estimating the evaporation time using the MI model, compared

with the ME model, was found to be 3.7%. This is comparable with the results found for TME and LME.
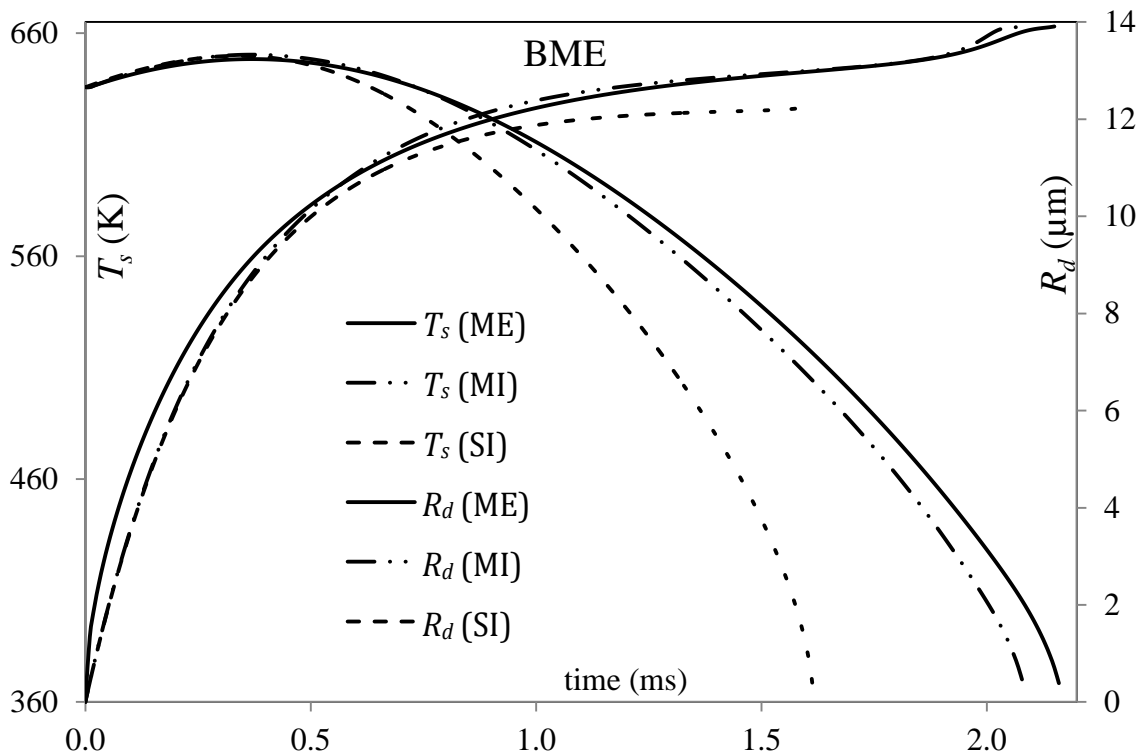
Figure 3.19 The same as Figures 3.17-3.18, but for a Butter Methyl Ester (BME) droplet.

The same plots as shown in Figures 3.17-3.19, but for Coconut Methyl Ester (CME) and Palm Kernel Methyl Ester (PMK) are presented in Figures 3.20 and 3.21 respectively. The shapes of the curves presented in these figures are rather similar to those shown in Figure 3.19.

In Figures 3.20 and 3.21, the errors of estimating the evaporation times using the SI model, compared with the ME model, for CME and PMK are found to be 23.0% and 26.3% respectively. Similar errors but for the MI model are found to be 3.8% and 5.0% respectively. The latter errors are comparable with those shown in Figures 3.17-3.19. Large errors of the estimations of the evaporation times for CME and PMK, using the SI model, reinforce the conclusion made based on the analysis of BME that the SI model cannot be used for the analysis of biodiesel droplet heating and evaporation unless errors of about 26% in predicted droplet evaporation times can be tolerated.

The shapes of the curves for time evolution of droplet surface temperature and radius, presented in Figures 3.22 and 3.23 for Palm Methyl Ester (PME) and Safflower Methyl Ester (SFE), are similar to those shown in Figures 3.17 and 3.18.
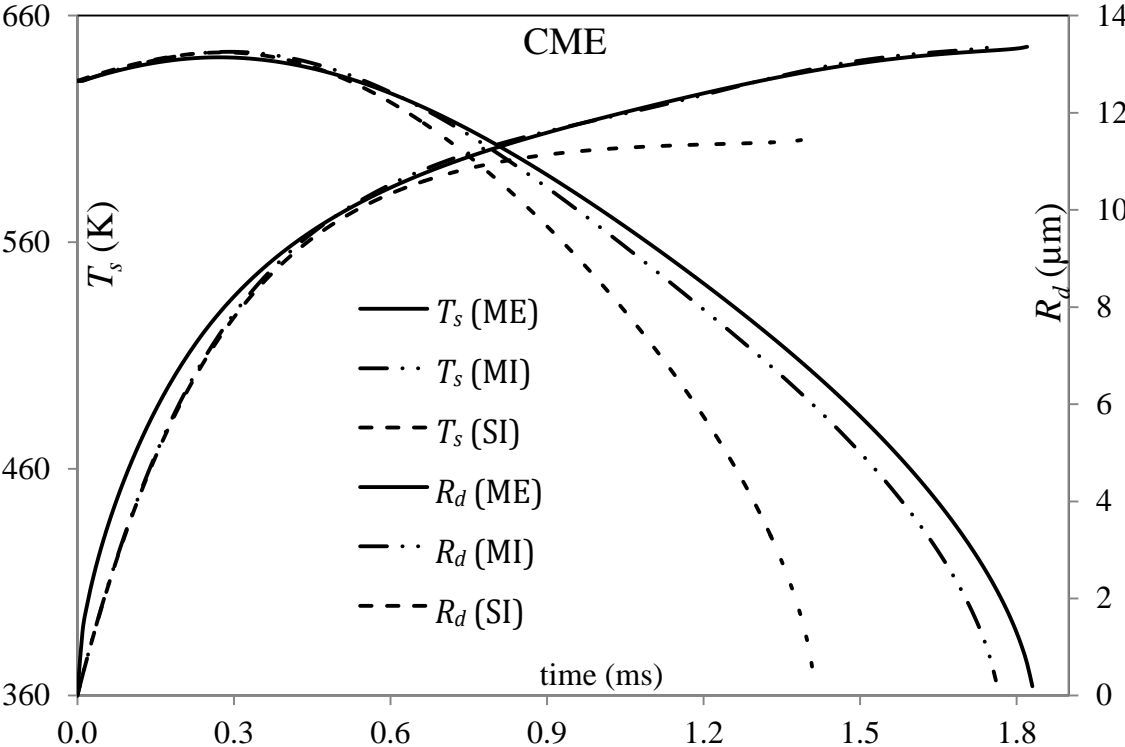
Figure 3.20 The same as Figures 3.17-3.19, but for a Coconut Methyl Ester (CME) droplet.
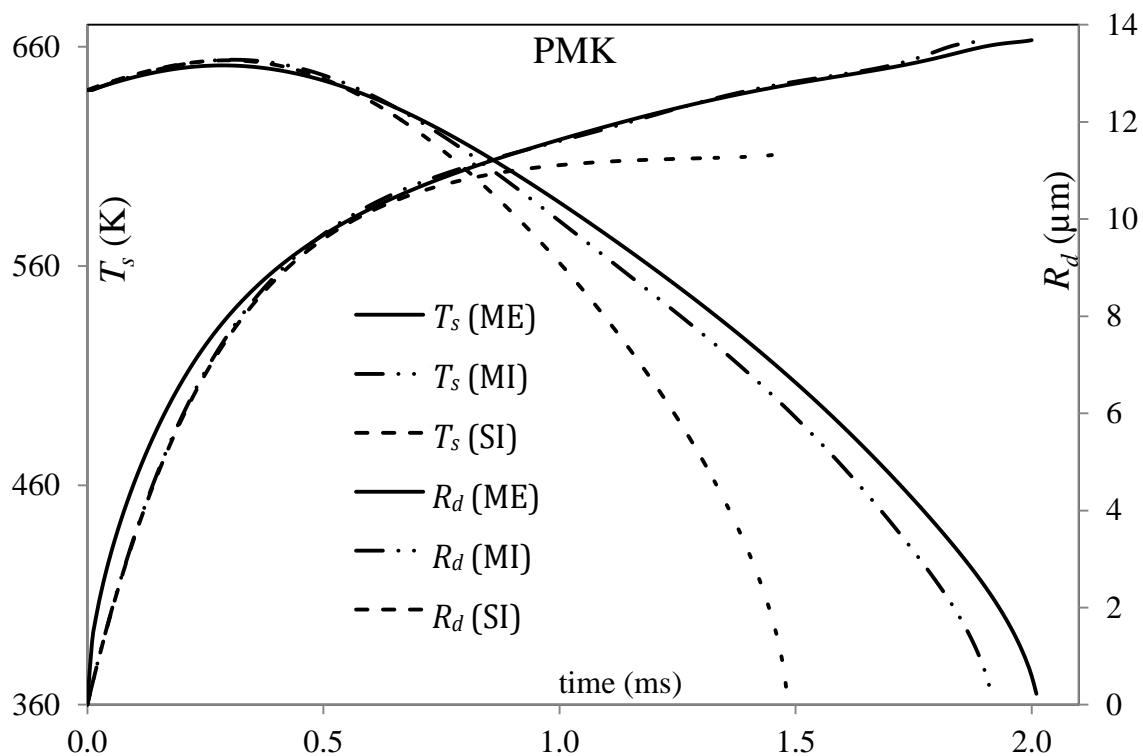
Figure 3.21 The same as Figures 3.17-3.20, but for a Palm Kernel Methyl Ester (PMK) droplet.
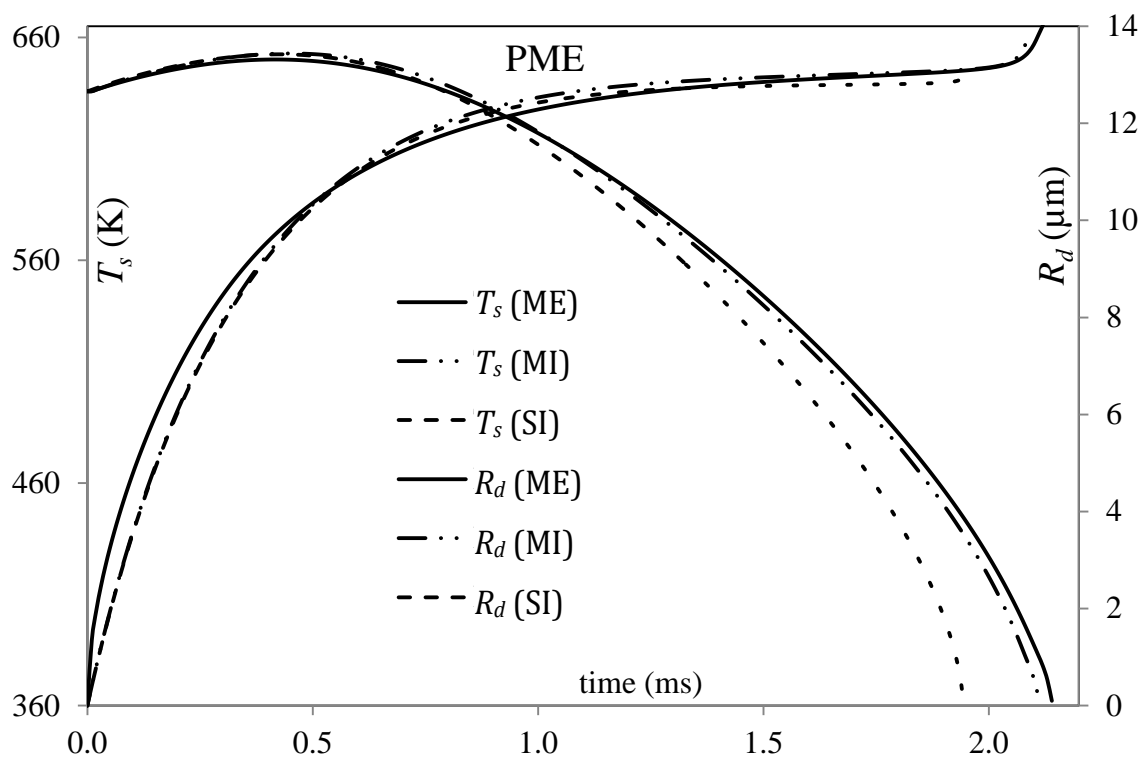
Figure 3.22 The same as Figures 3.17-3.21, but for a Palm Methyl Ester (PME) droplet.
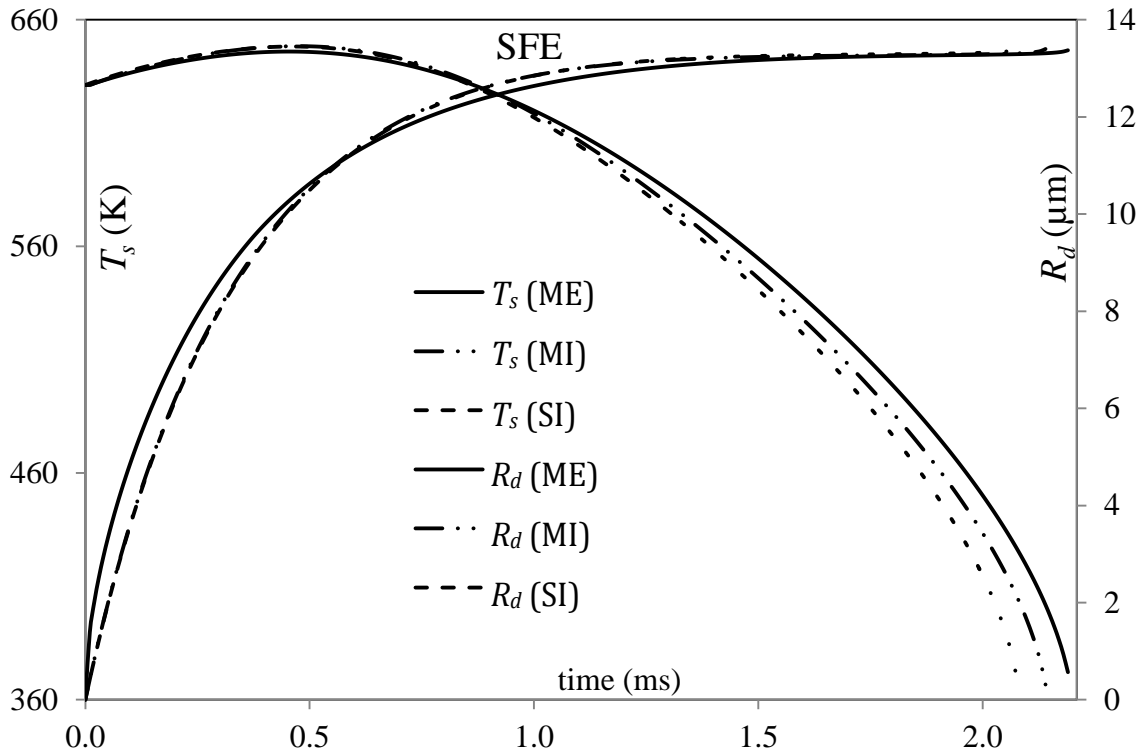
Figure 3.23 The same as Figures 3.17-3.22, but for a Safflower Methyl Ester (SFE) droplet.

As one can see from Figures 3.22 and 3.23, the evaporation times predicted by the SI model for PME and SFE are less than those predicted by the ME model by 9.3% and 5.1% respectively. At the same time, using the MI model for PME and SFE leads to under-estimation of these times by 1.4% and 2.3% respectively. The curve $R_d(t)$ predicted by the MI model for PME is very close to the one predicted by the ME model, although the curves for droplet surface temperatures, predicted by both models are noticeably different.

The curves shown in Figures 3.24-3.29 for Peanut Methyl Ester (PTE), Cotton-seed Methyl Ester (CSE), Corn Methyl Ester (CNE), Sunflower Methyl Ester (SNE), Tung Methyl Ester (TGE) and Hemp Methyl Ester 1 (HME1) are reasonably close to those shown in Figure 3.18.
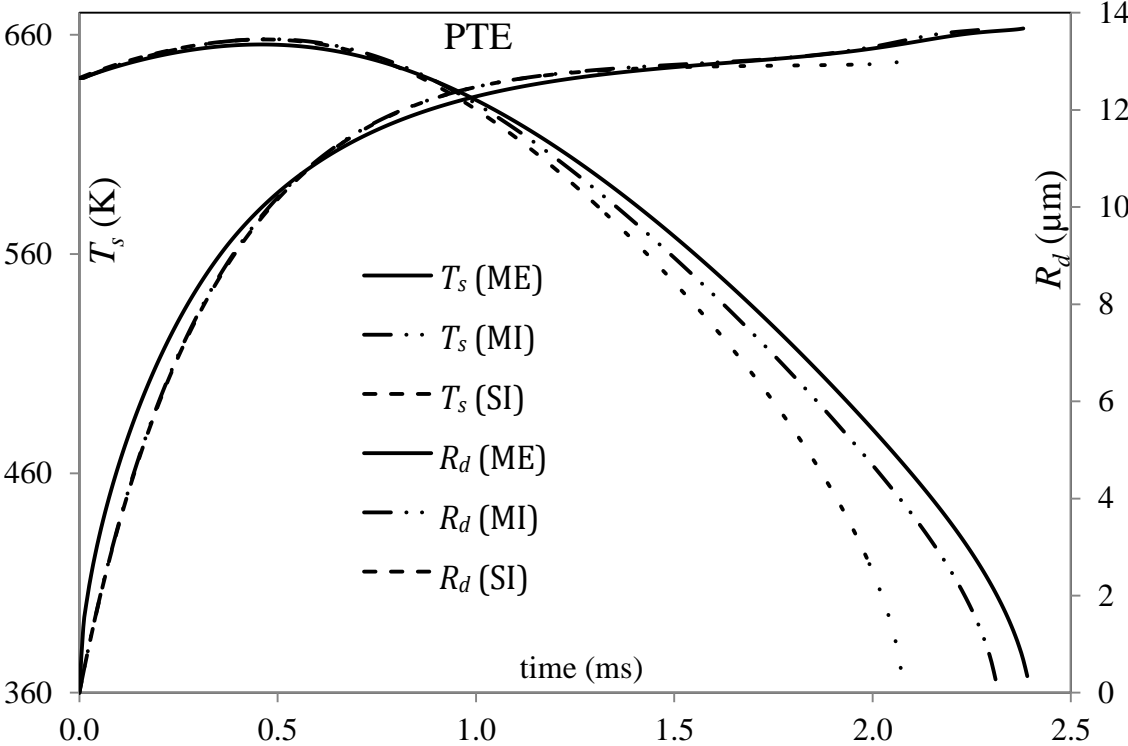
Figure 3.24 The same as Figures 3.17-3.23, but for a Peanut Methyl Ester (PTE) droplet.
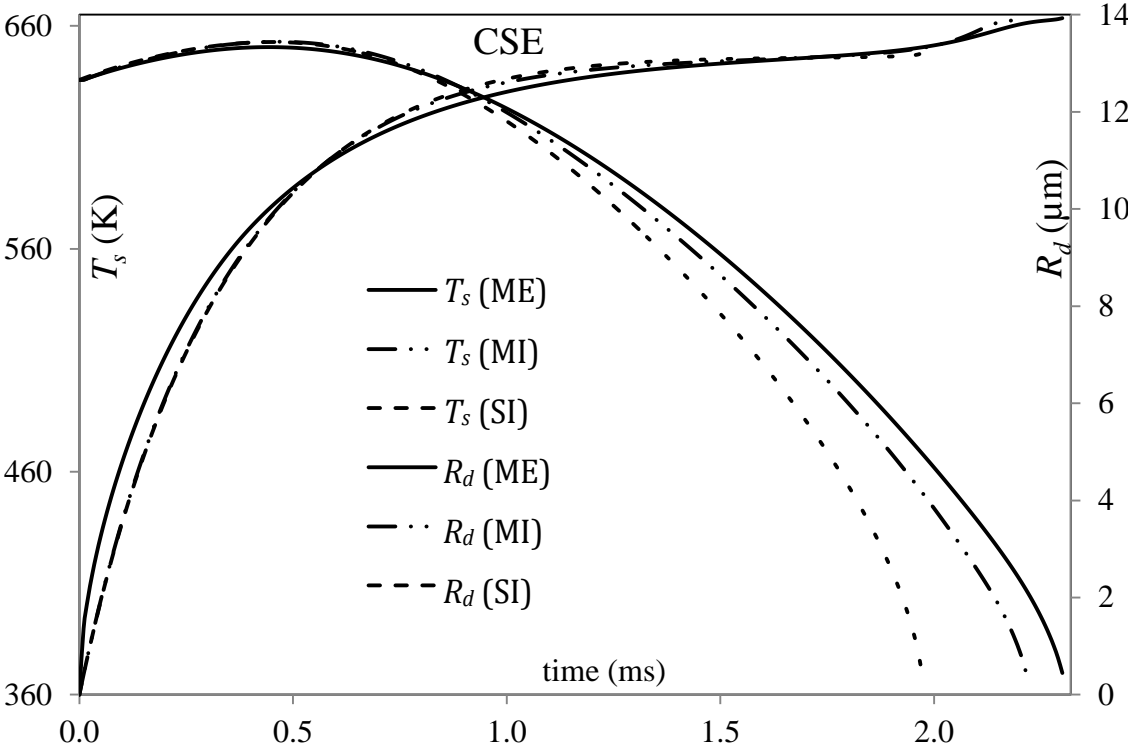
Figure 3.25 The same as Figures 3.17-3.24, but for a Cottonseed Methyl Ester (CSE) droplet.
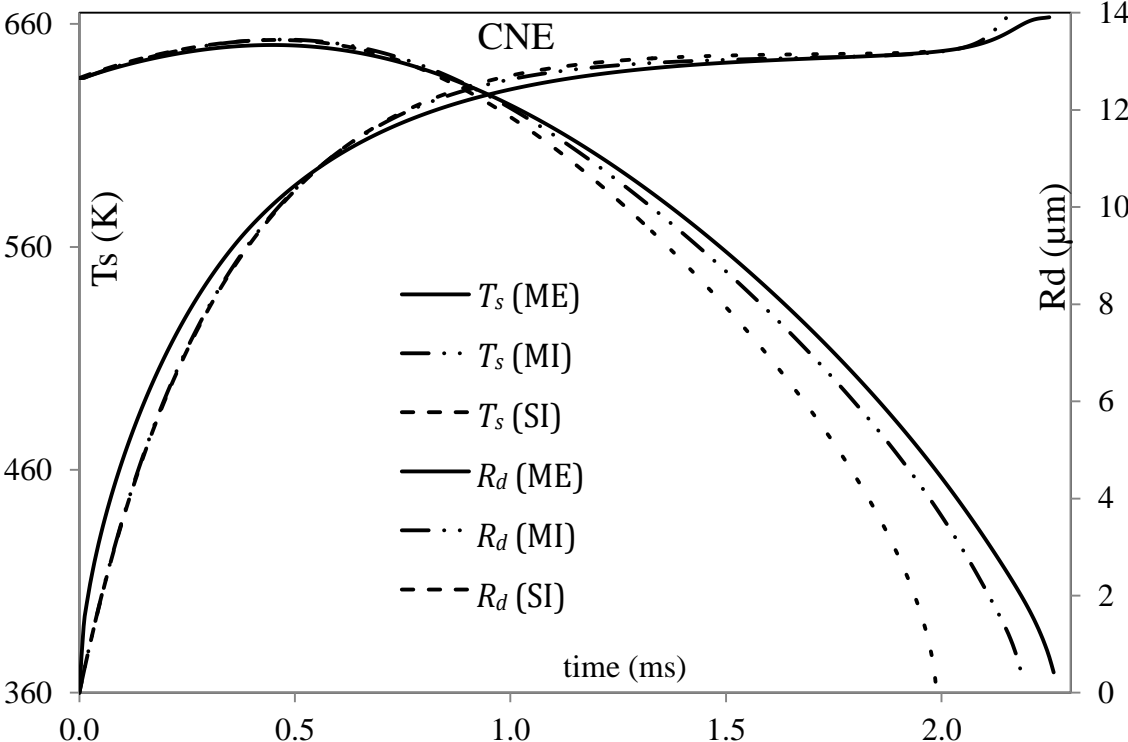
Figure 3.26 The same as Figures 3.17-3.25, but for a Corn Methyl Ester (CNE) droplet.
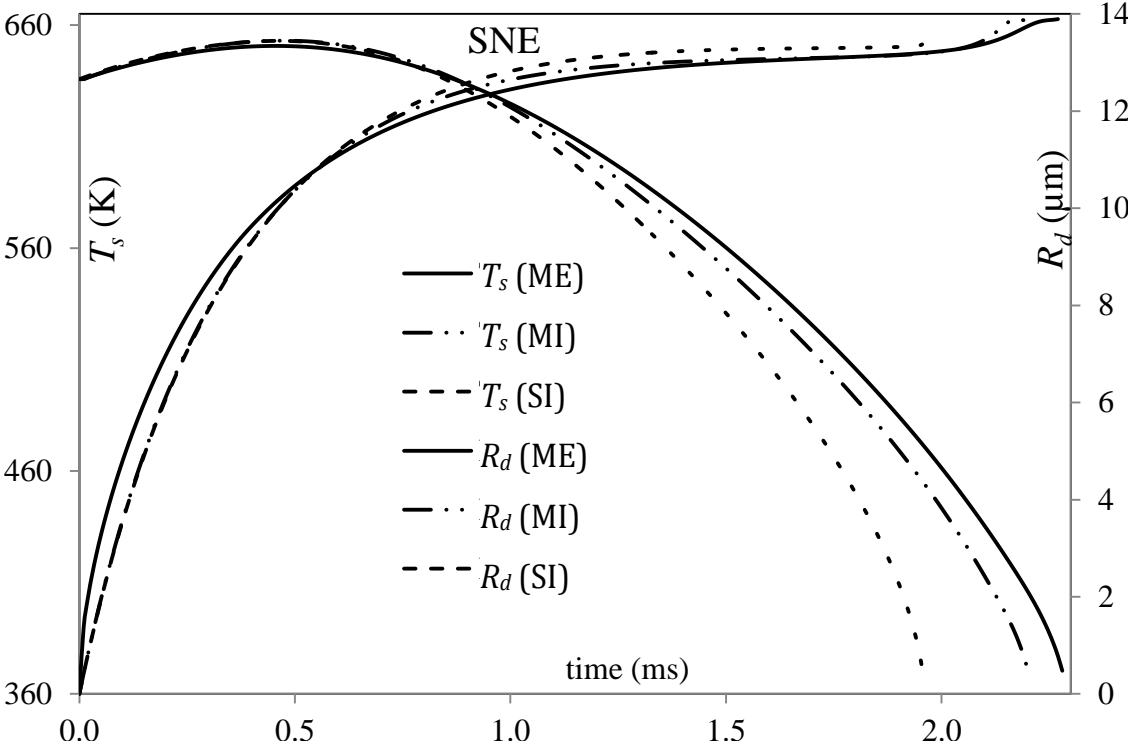
Figure 3.27 The same as Figures 3.17-3.26, but for a Sunflower Methyl Ester (SNE) droplet.
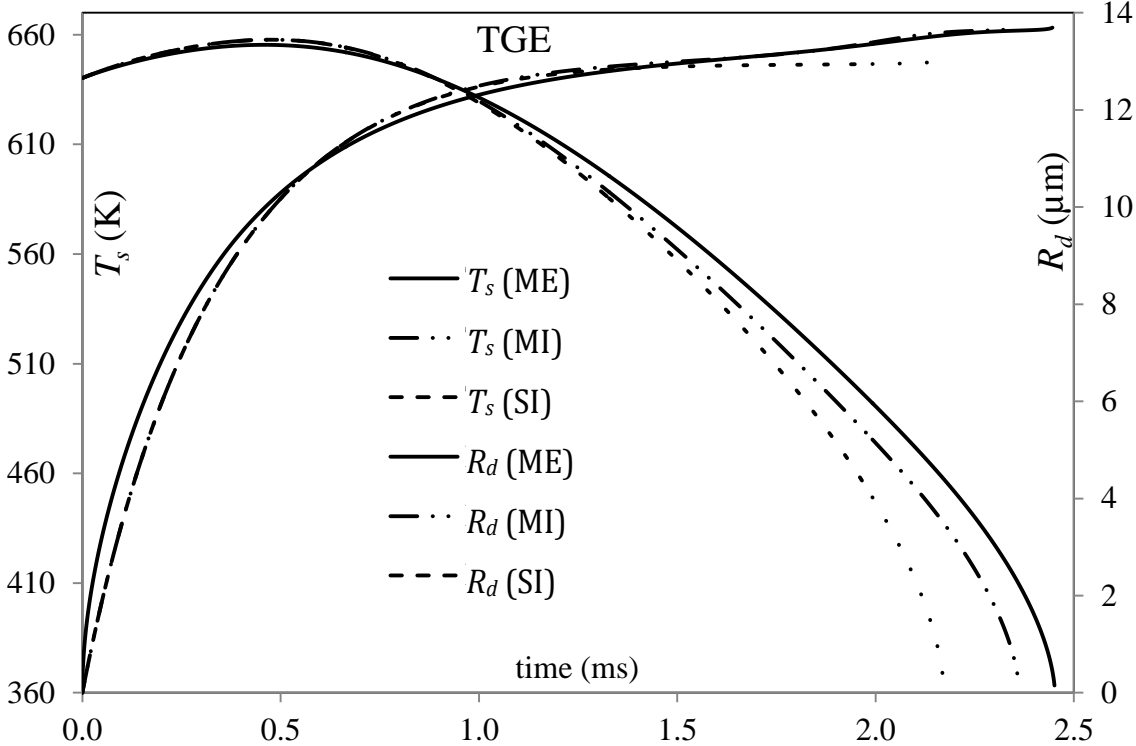
Figure 3.28 The same as Figures 3.17-3.27, but for a Tung Methyl Ester (TGE) droplet.
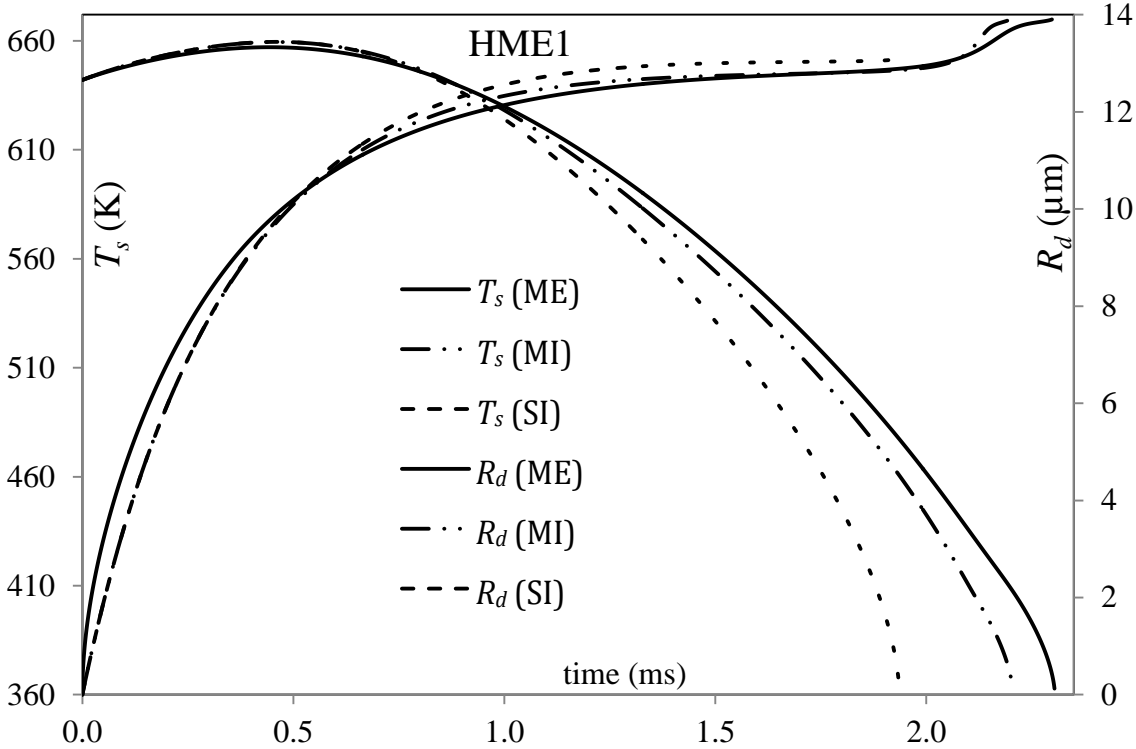
Figure 3.29 The same as Figures 3.17-3.28, but for a Hemp Methyl Ester 1 (HME1) droplet.

As one can see from Figures 3.24-3.29, the evaporation times predicted by the SI model for PTE, CSE, CNE, SNE, TGE and HME1 are less than those predicted by the ME model by 13.1%, 14.2%, 12.1%, 14.2%, 11.4% and 16.0% respectively. At the same time, using the MI model for PTE, CSE, CNE, SNE, TGE and HME1 leads to under-estimation of these times by 3.8%, 3.9%, 3.1%, 3.5%, 3.7% and 4.3% respectively.

The curves shown in Figures 3.30-3.34 for Soybean Methyl Ester (SME), Linseed Methyl Ester (LNE), Hemp Methyl Ester 2 (HME2), Canola Seed Methyl Ester (CAN), and Waste oil Methyl Ester (WME) are reasonably close to those shown in Figures 3.17 and 3.23. As one can see from these figures, the evaporation times predicted by the SI model for SME, LNE, HME2, CAN and WME are less than those predicted by the ME model by 4.1%, 3.5%, 4.0%, 6.8% and 8.7% respectively. At the same time, using the MI model for SME, LNE, HME2, CAN and WME leads to under-estimation of these times by 2.7%, 2.1%, 2.8%, 3.7% and 3.9% respectively.
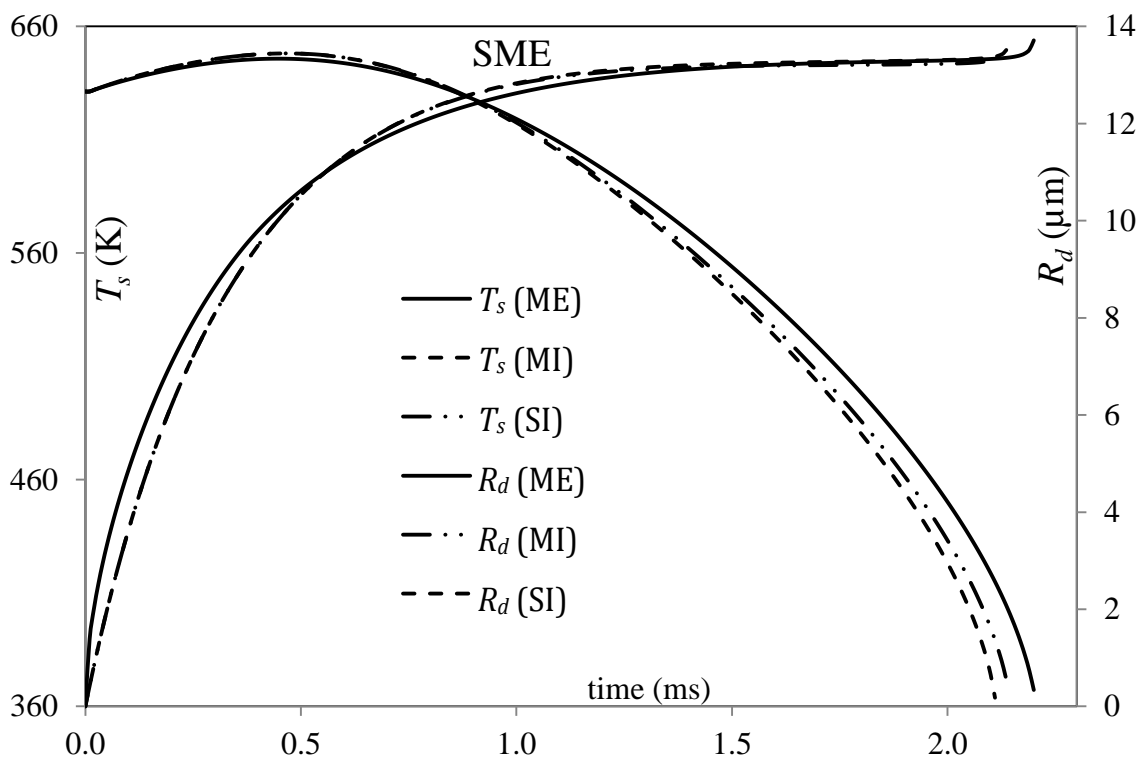
Figure 3.30 The same as Figures 3.17-3.29, but for a Soybean Methyl Ester (SME) droplet.

85
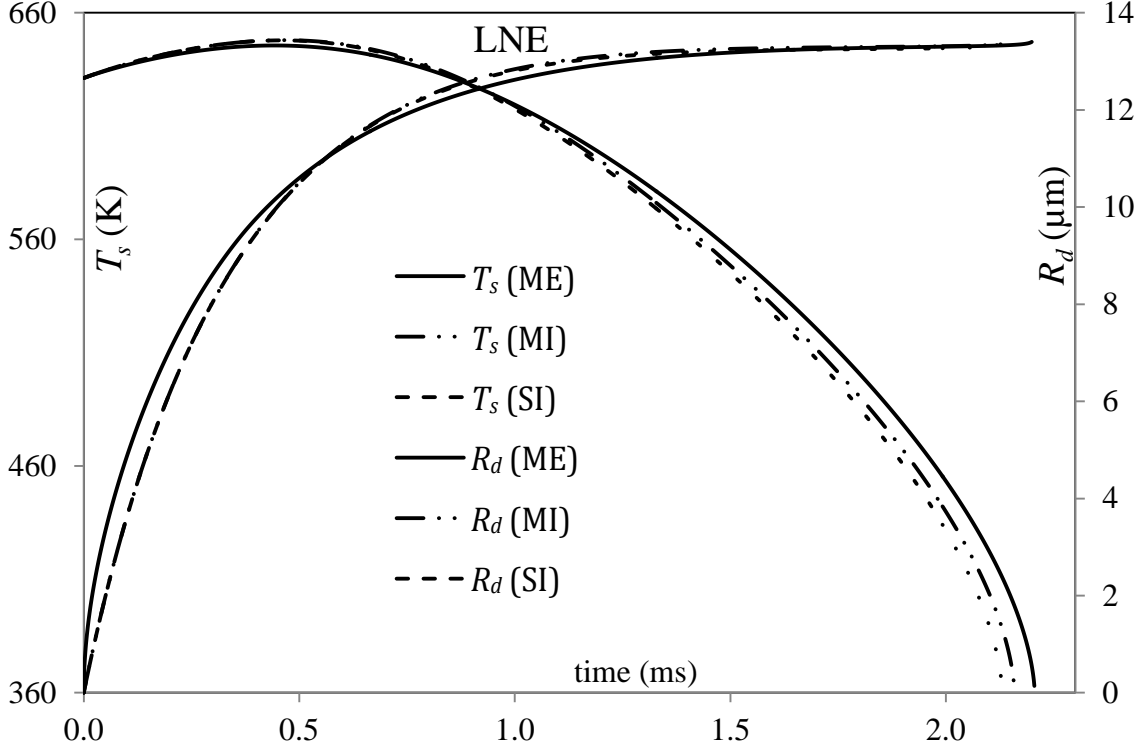
Figure 3.31 The same as Figures 3.17-3.30, but for a Linseed Methyl Ester (LNE) droplet.
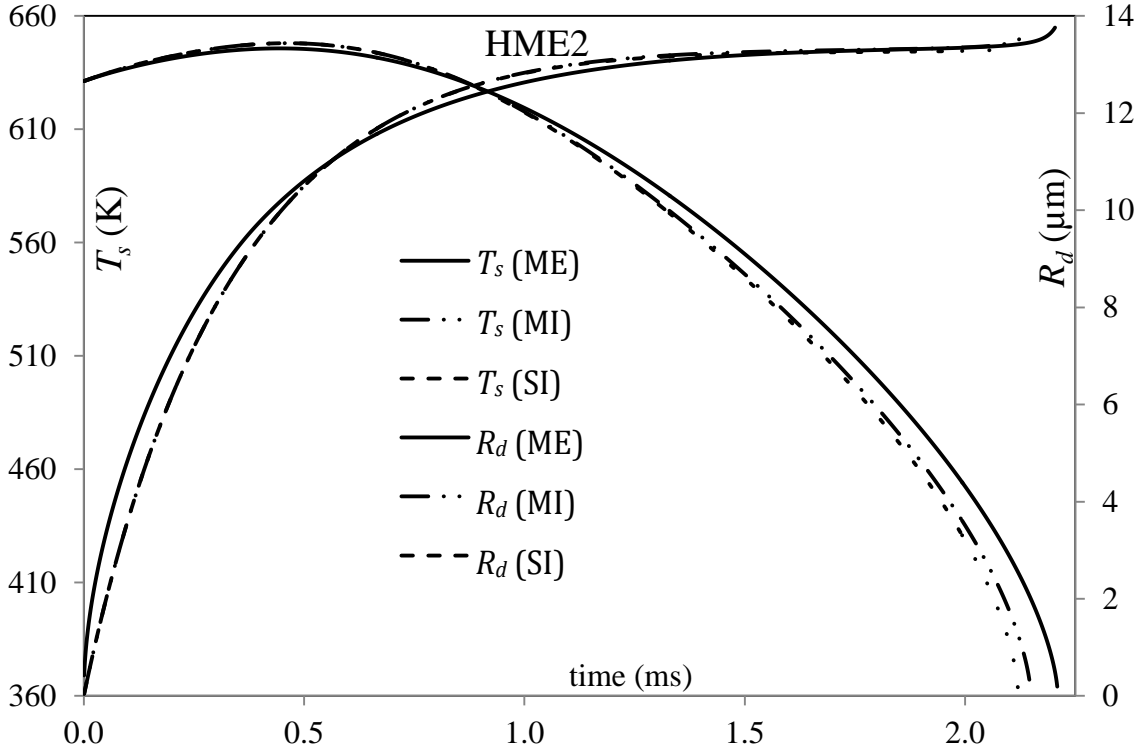
Figure 3.32 The same as Figures 3.17-3.31, but for a Hemp Methyl Ester 2 (HME2) droplet.
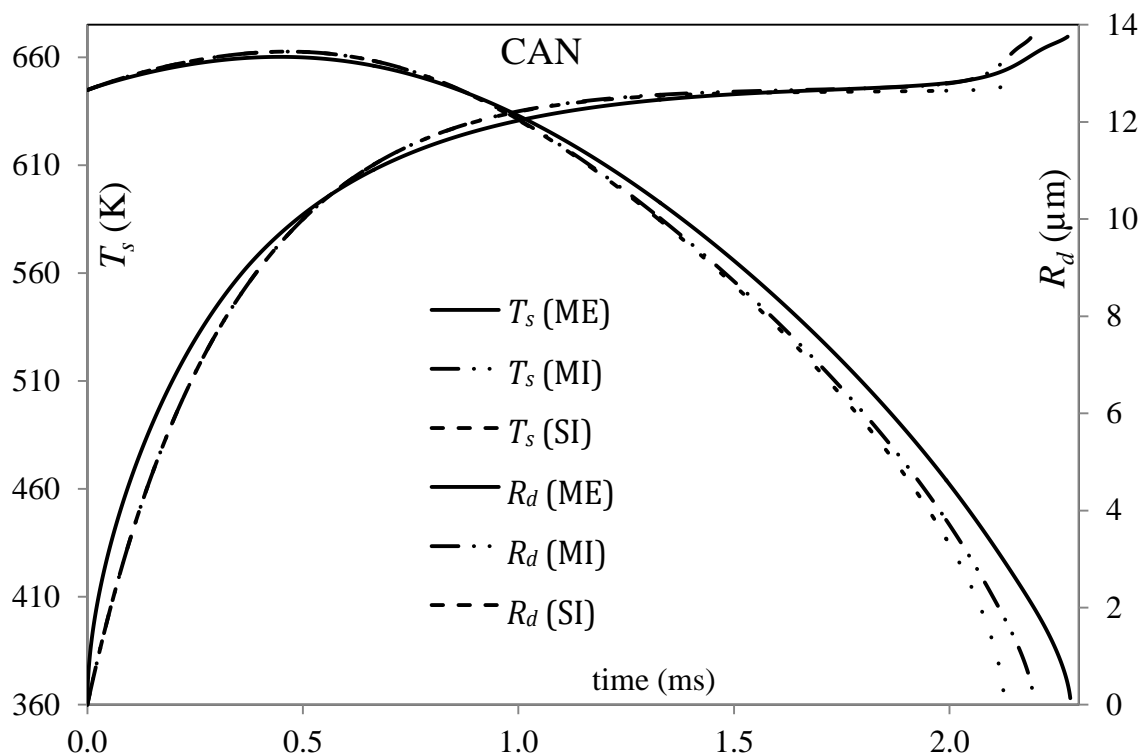
Figure 3.33 The same as Figures 3.17-3.32, but for a Canola Methyl Ester (CAN) droplet.
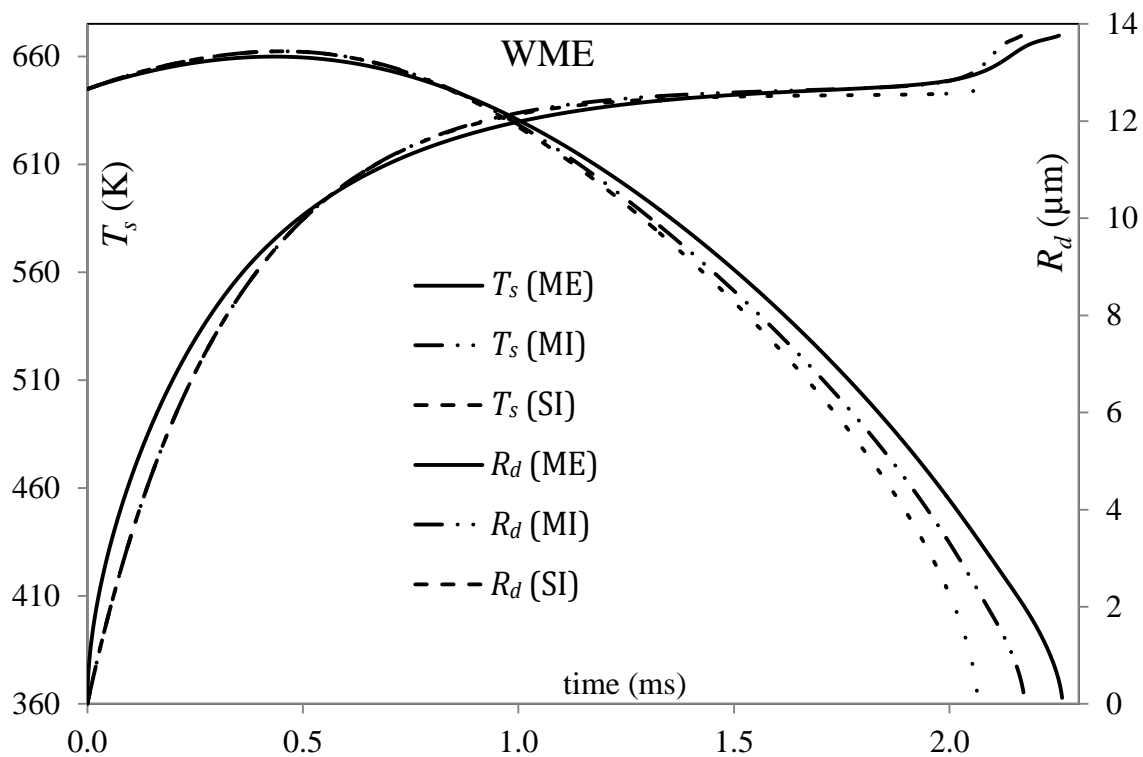
Figure 3.34 The same as Figures 3.17-3.33, but for a Waste-oil Methyl Ester (WME) droplet.

The curves shown in Figure 3.35 for Rapeseed Methyl Ester (RME) are different from the ones shown in the previous figures due to the fact that both SI and MI models under-estimate considerably the droplet evaporation times, compared with the prediction of the ME model. These errors for the SI and MI models were found to be 18.4% and 15.1%, respectively. This shows that not only the SI model, but also the MI model can lead to considerable errors in estimating droplet evaporation times. Both models cannot be considered reliable for the analysis of droplet heating and evaporation unless errors of more than 15% can be tolerated.

Note that the results shown in Figure 3.35 are expected to be less reliable than the ones presented in other figures as RME contains the largest amount of additives the properties of which cannot be properly specified (with molar fraction 8.7%).
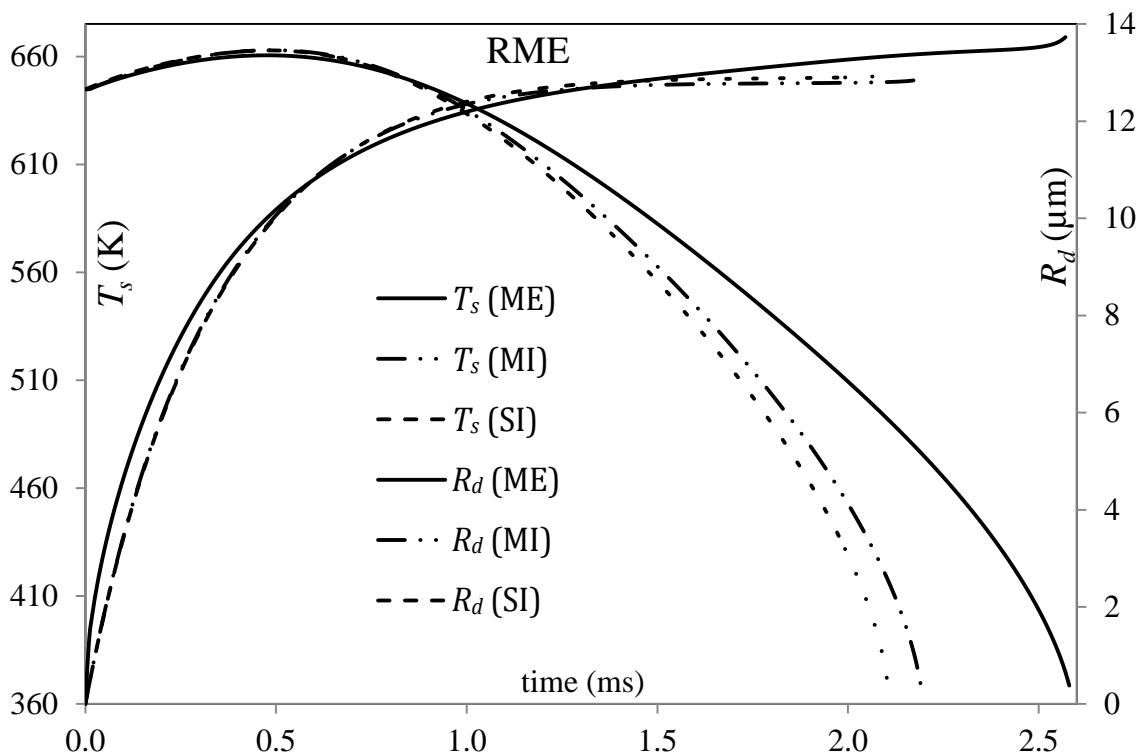
Figure 3.35 The same as Figures 3.17-3.34, but for a Rapeseed Methyl Ester (RME) droplet.

As one can see from Figure 3.35, the MI model shows more noticeable errors in the estimation of the evaporation time for the RME fuel compared to

the errors predicted for other types of biodiesel fuels. This can be attributed to the fact that RME contains larger amount of less volatile (heavier) components than other biodiesel fuel types as shown in Table 3.1.

Note that the evaporation times shown in Figures 3.17-3.35 cannot be directly compared with those shown in Case 1, as the latter have been obtained for the values of parameters different from those used in Case 2. Also, the comparison so far has been focused mainly on the evaporation times, although the difference in the shapes of the curves T_s versus time predicted by various models are equally important for the assessment of the accuracy of the models. In all cases shown in Figures 3.17-3.35 the ME model predicts higher droplet surface temperature at the initial stage of droplet heating and evaporation compared with the predictions of the MI and SI models (by about 7%). This is related to the fact that the ME model predicts that at the initial stage of droplet heating most of heat supplied to the droplet is spent on heating the region close to the surface of the droplet (e.g. Figure 3.38), while both SI and MI models are based on the assumption that the same heat is spread evenly over the whole volume of the droplet at any time.

The behaviour of the temperature at intermediate times predicted by all models appears to be rather complex and is controlled by several competing factor including the rate of evaporation, heat transfer inside the droplet and heat supplied to the droplet. At the final stage of droplet evaporation, however, the surface temperature predicted by the ME and MI models becomes larger than the one predicted by the SI model. This can be related to the fact that at the final stage of droplet heating and evaporation, the ME and MI models predict that droplet composition is dominated by the heaviest component with the highest boiling temperature (see Table 3.2). The surface temperatures predicted by the ME and MI models at the final stages of droplet evaporation are rather similar as the droplet compositions predicted by both models at this stage of droplet evaporation are expected to be rather close. Note that predictions of temperatures by all models at the very final stage of droplet evaporation are not expected to be very reliable due to large time derivatives of droplet radii (see [100] for more detailed discussion of this phenomenon).

To provide a deeper understanding of the processes taking place during biodiesel fuel droplet heating and evaporation, in Figures 3.36-3.38 the plots of surface mass fractions of selected components versus time, the plots of mass fractions of selected components versus normalised distance from the droplet centre at various time instants and temperatures versus normalised distance from the droplet centre at various time instants for the BME droplet are presented. The general shapes of these curves for other biodiesel fuels are similar to the ones for BME. All plots refer to the predictions of the ME model.
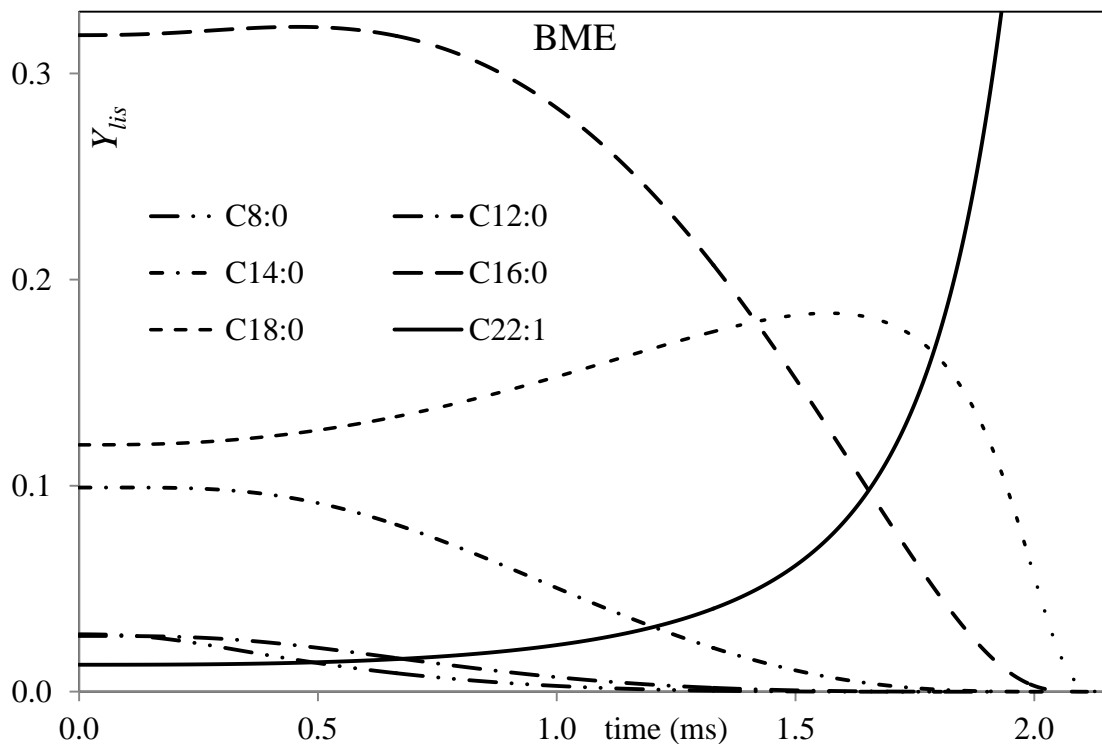
Figure 3.36 The plots of time evolution of surface mass fractions of C8:0M, C12:0M, C14:0M, C16:0M, C18:0M and C22:1M for a Butter Methyl Ester (BME) droplet for the same conditions as in Figures 3.17-3.35.

As follows from Figure 3.36, the surface mass fractions of the lightest components (C8:0M, C12:0M and C14:0M) monotonically decrease with time. The surface mass fraction of the heaviest component (C22:1M) monotonically in- creases with time. The surface mass fractions of the intermediate components (C16:0M and C18:0M) first increase and then decrease with time. At the end of the evaporation process, only the heaviest and least volatile component remains at the droplet surface. This component is mainly

responsible for prolonged droplet lifetime predicted by the ME model compared with the SI model, and higher surface temperatures at the final stage of droplet evaporation. The general shapes of the curves shown in Figure 3.36 are similar to those predicted for other biodiesel fuels including the ones studied in Case 1 (see [46]).
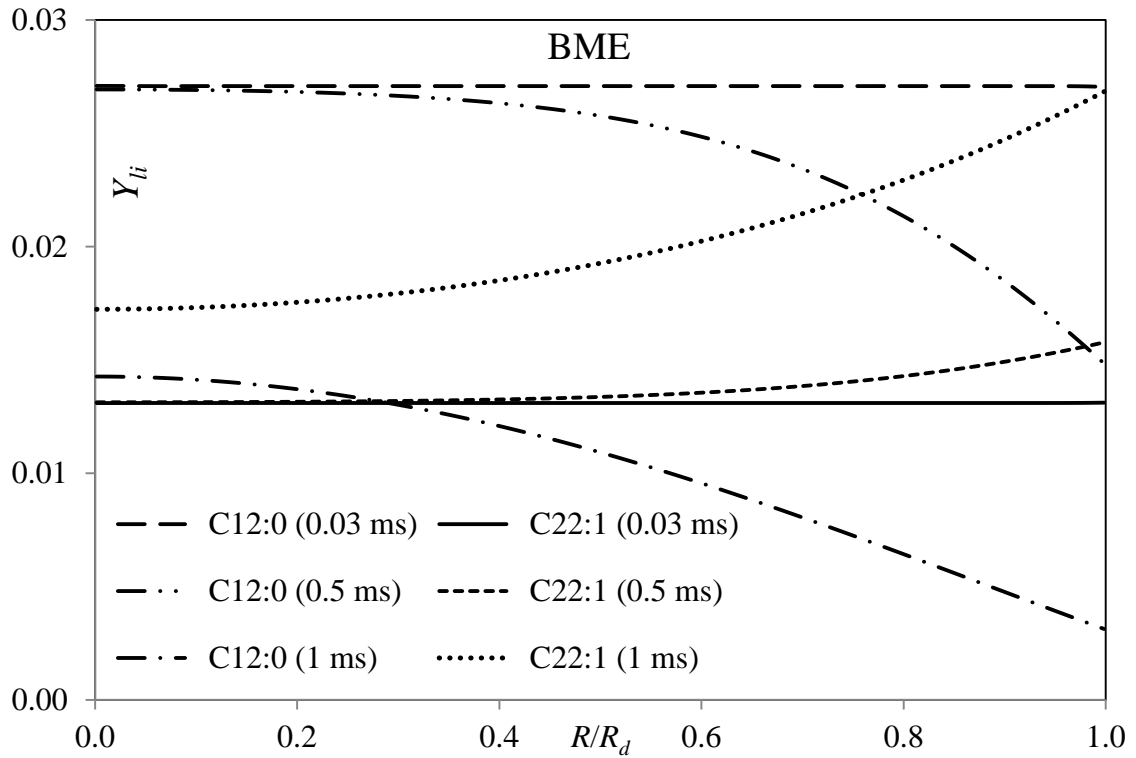
Figure 3.37 The plots of mass fractions of C12:0M and C22:1M versus normalised distance from the droplet centre at three time instants 0.03 ms, 0.5 ms and 1 ms for a Butter Methyl Ester (BME) droplet for the same conditions as in Figures 3.17-3.36.

As one can see in Figure 3.37, the decrease of the surface mass fraction of one of the lightest components (C12:0M) with time is accompanied by the corresponding decrease of the mass fraction of this component in the body of the droplet. The rate of this decrease, however, reduces in the regions close to the droplet centre. Thus a negative gradient of this mass fraction is formed inside the droplet, which leads to the diffusion of this component from the droplet centre to its surface. As can be inferred from the same figure, the increase of the surface mass fraction of the heaviest components (C22:1M) with time is accompanied by the corresponding increase of the mass fraction of this

component in the body of the droplet, although the rate of this increase reduces in the regions close to the droplet centre. Thus positive gradients of this mass fraction are formed inside the droplet, which lead to the diffusion of this component from the droplet surface to its centre. This leads to the formation of a droplet consisting mainly of the heaviest component (C22:1M) at the end of the evaporation process.

One can clearly see from Figure 3.37 that gradients of mass fractions of the components inside the droplet are initially small but increase with time. This observation shows the limitations of the well mixed models, including the MI model, widely used for the analysis of multi-component droplet heating and evaporation.
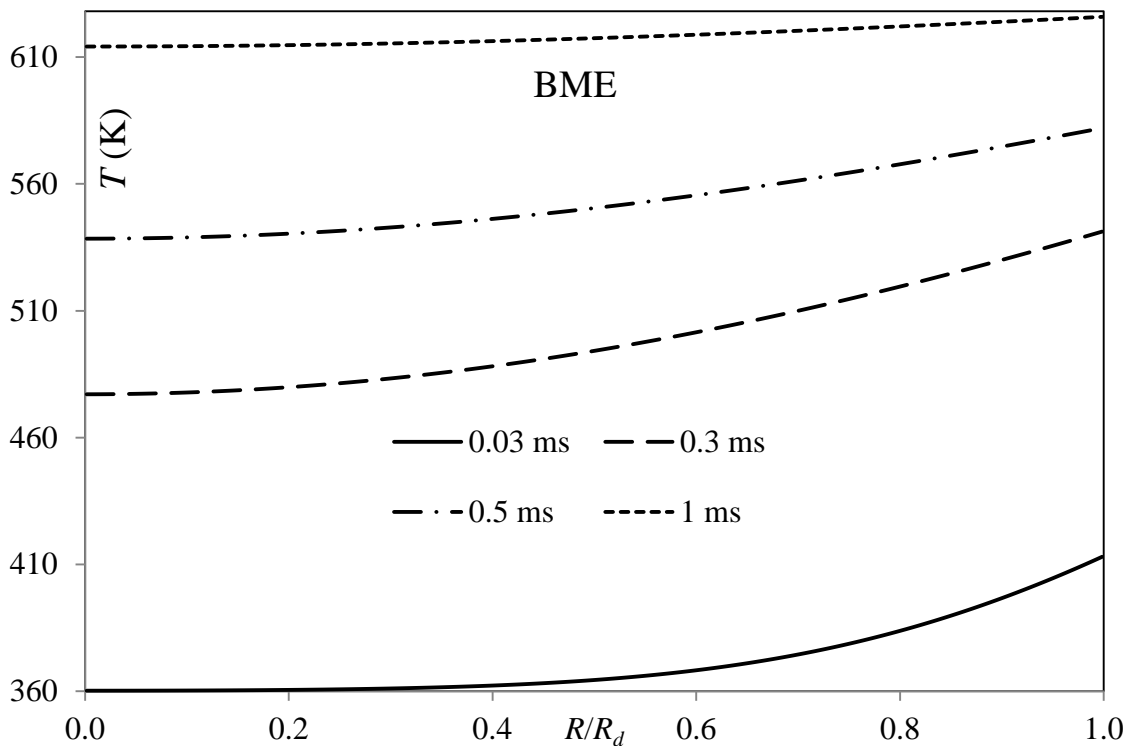
Figure 3.38 The plots of temperature versus normalised distance from the droplet centre at four time instants 0.03 ms, 0.3 ms, 0.5 ms and 1 ms for a Butter Methyl Ester (BME) droplet for the same conditions as in Figures 3.17-3.37.

As one can see in Figure 3.38, at the initial stage of droplet heating and evaporation (0.03 ms after the start of the process) rather large gradients of temperature inside the droplet close to droplet surface are formed. In contrast

to the case of species molar fractions, however, the gradients of temperature inside droplets decrease with time. These gradients are reasonably small at 1 ms after the start of the process. This means that the Infinite Thermal Conductivity model can be applied to the analysis of droplet heating and evaporation, except at the very beginning of the process, when high accuracy of calculations is not required.

The plots of time evolution of the surface temperature (T_s) and radius (R_d) for a BME droplet at the same conditions as shown in Figures 3.17-3.35 but assuming that the droplets is stationary are shown in Figure 3.39. The results predicted by the SI and ME models are shown, as in Figure 3.19. Apart from these, the results predicted by the model based on the assumption that BME can be approximated by the dominant component (C16:0M) and assuming that the thermal conductivity of liquid is infinitely large are shown in the same figure (DI model). Note that in the case of stationary droplets the ME model reduces to the so called conduction limit model. In our case, however, the term 'ME model' is used for both stationary and moving droplets.
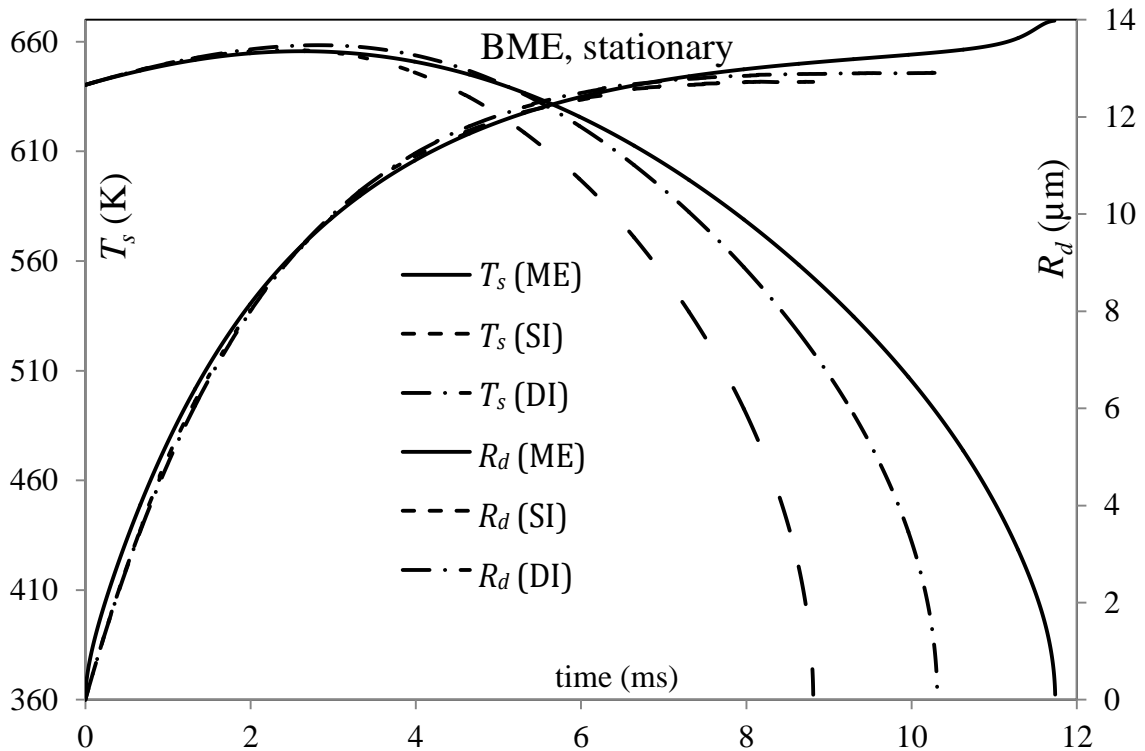
Figure 3.39 The plots of time evolution of surface temperature (T_s) and radius (R_d) for a Butter Methyl Ester (BME) droplet predicted by the multi- component ETC/ED model (ME), single-component (zero diffusivity)/ITC model (SI), and a model in which BME is approximated by the dominant component C16:0M and using the assumption of infinite liquid thermal conductivity (DI). The droplet is assumed to be stationary in still air at temperature and pressure equal to 700 K and 32 bar respectively; its initial radius is assumed equal to 12.66 μm.

Comparing Figures 3.19 and 3.39 one can see that moving droplets evaporate 5 times faster than stationary droplets, which can be attributed to increased Nusselt and Sherwood numbers of the moving droplets. At the same time the under-predictions of the evaporation times by the SI model compared with the ME model are about the same for moving (25.2%) and stationary (24.9%) droplets. The evaporation time predicted by the DI model turned out to be closer to the one predicted by the ME model than the evaporation time predicted by the SI model. The DI model under-predicted the evaporation time by 12.2%. This, however, is likely to be the case for this particular biodiesel fuel and cannot be generalised to other types of biodiesel fuels.

The plots similar to those shown in Figures 3.36-3.38 but for stationary droplets are presented in Figures 3.40-3.42.
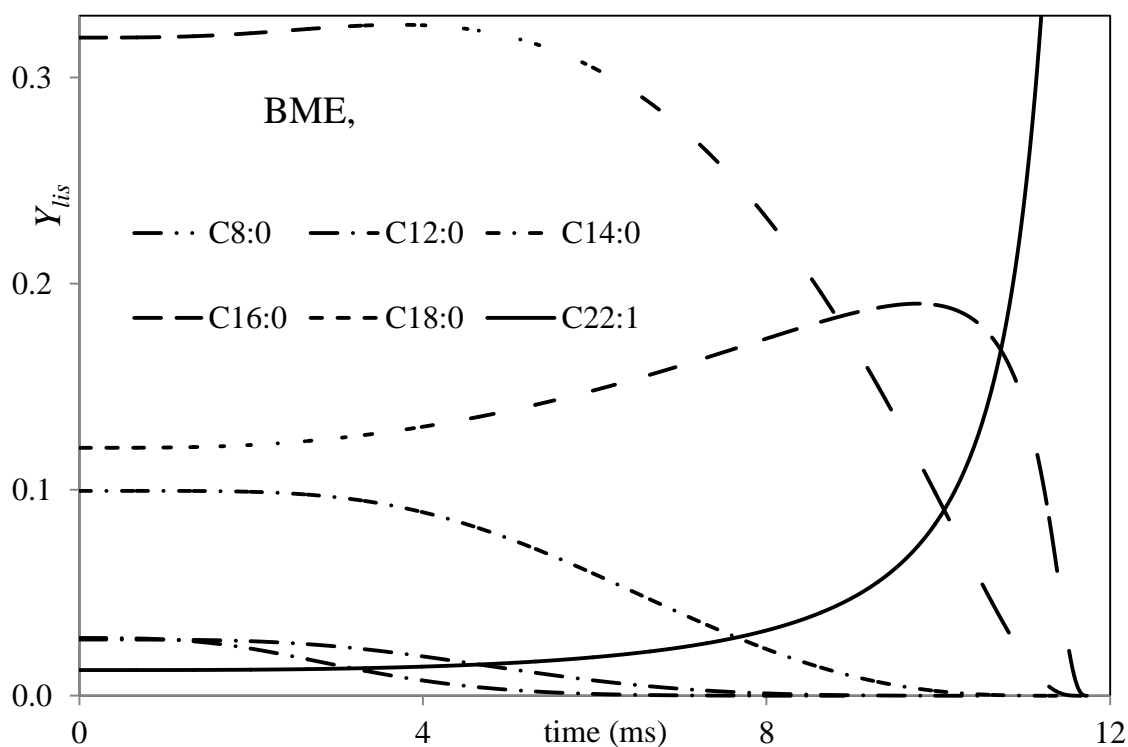
Figure 3.40 The same as Figure 3.36, but for a stationary Butter Methyl Ester (BME) droplet in the same conditions as in Figure 3.39.
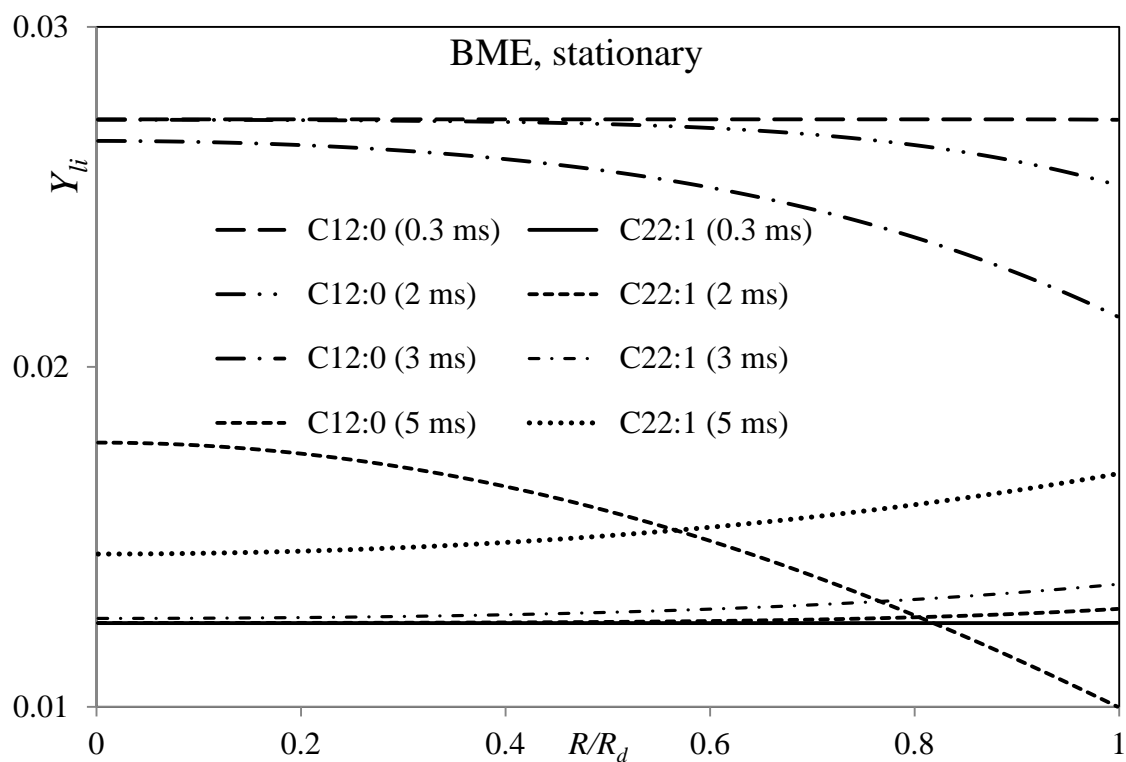
Figure 3.41 The same as Figure 3.37, but for a stationary Butter Methyl Ester (BME) droplet in the same conditions as in Figure 3.39.

95
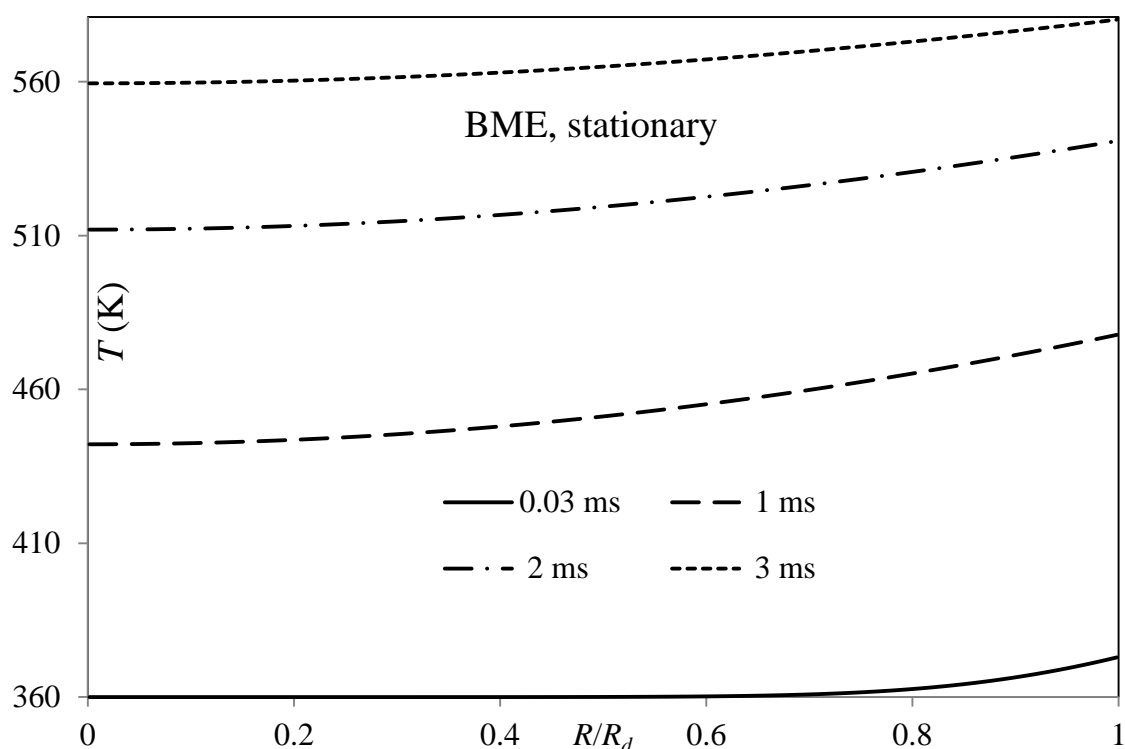
Figure 3.42 The same as Figure 3.38, but for a stationary Butter Methyl Ester (BME) droplet in the same conditions as in Figure 3.39.

The main conclusions which can be inferred from the latter figures are the same as those inferred from Figures 3.36-3.38. As one can see from Figure 3.40, the light components are expected to be the first to evaporate and the heavy components are expected to be the last to evaporate. In Figures 3.41 and 3.42 gradients of mass fractions of components inside droplets increase with time, while the gradients of temperature inside droplets decrease with time. This shows that limitations of the MI and SI models widely used in the analysis of biodiesel fuel droplet heating and evaporation.

3.6   Conclusions of Chapter 3

The previously suggested model for droplet heating and evaporation, taking into account temperature gradient, recirculation, and species diffusion inside droplets, has been applied to the analysis of biodiesel fuel droplet heating and evaporation in realistic Diesel engine-like conditions. In contrast to the most commonly used models to take into account these effects, the model used in the presented analysis is based on the analytical solutions to the heat transfer and species diffusion equations inside droplets.

Two (preliminary and more detailed) case studies have been performed based on the verities of input parameters and biodiesel fuels. In the preliminary case study, the analysis has been focused on five types of biodiesel fuels: Palm Methyl Ester (PME) produced from palm oil; Hemp Methyl Esters, produced from hemp seed oil in the Ukraine (HME1) and the European Union (HME2); Rapeseed oil Methyl Ester (RME), produced from rapeseed oil in the Ukraine; and Soybean oil Methyl Ester (SME), produced from soybean oil. These fuels contain up to 15 methyl esters and possibly small amounts of unspecified additives, which are treated as methyl esters with average characteristics. Calculations have been performed using two approaches. Firstly, a model taking into account the contribution of all components of biodiesel fuel is used. Secondly, a model in which biodiesel fuel is treated as a single-component fuel with averaged transport and thermodynamic coefficients.

In the the first case studied, the maximal deviations between the predictions of the multi-component and single component models have been observed for RME. Even in the latter case, however, the difference between the evaporation times predicted by these models has been less than about 5.5%.

In the second case, several models of biodiesel fuel droplet heating and evaporation in realistic Diesel engine-like conditions have been considered. Firstly, a model taking into account the contributions of all components of biodiesel fuels, their realistic diffusion, temperature gradient, and recirculation within the droplet, in the case of moving droplets (Effective Thermal Conductivity/Effective Diffusivity model), is used. In the second model, the

contribution of all components of biodiesel fuels are taken into account as in the first model, but the diffusivity of species in droplets is assumed to be infinitely fast and the liquid thermal conductivity is assumed to be infinitely large (Infinite Thermal Conductivity/Infinite Diffusivity model). In the third model, the transient diffusion of species is ignored and it is assumed that the liquid thermal conductivity is infinitely large. The fourth model is a simplified version of the third model in which it is assumed that biodiesel fuels can be approximated by a single dominant component (this model was used only for the analysis of stationary droplets).

Nineteen types of biodiesel fuel have been used in the analysis. These are Tallow Methyl Ester (TME), Lard Methyl Ester (LME), Butter Methyl Ester (BME), Coconut Methyl Ester (CME), Palm Kernel Methyl Ester (PMK), Palm Methyl Ester (PME), Safflower Methyl Ester (SFE), Peanut Methyl Ester (PTE), Cottonseed Methyl Ester (CSE), Corn Methyl Ester (CNE), Sunflower Methyl Ester (SNE), Tung Methyl Ester (TGE), Hemp-oil Methyl Ester, produced from Hemp seed oil in Ukraine (HME1), Soybean Methyl Ester (SME), Linseed Methyl Ester (LNE), Hemp-oil Methyl Ester, produced in European Union (HME2), Canola seed Methyl Ester (CAN), Waste cooking-oil Methyl Ester (WME) and Rapeseed Methyl Ester (RME).

It is shown that the third model under-predicts the droplet evaporation times compared with the first model (believed to be the most reliable one) by up to about 26%. This result does not support the earlier finding of Case 1, based on the analysis of only five types of biodiesel fuel in different engine conditions, that the deviations between the evaporation times predicted by these models do not exceed about 5.5%. The evaporation times predicted by the second model have been shown to be reasonably close to those predicted by the first model. The second model under-predicts this time by not more than 4.3% except for Rapeseed Methyl Ester (RME) for which this under- predictions reaches 15.1%. The predictions of the fourth model have been shown to be closer to the predictions of the first model than those of the third model.

The multi-component model predicts higher droplet surface temperatures and longer evaporation times than the single component model. This is related to the fact that at the final stages of droplet evaporation the mass fraction of heavier species increases at the expense of lighter species. The heavier species evaporate more slowly than the lighter species and have higher wet bulb temperatures.

4 DIESEL FUEL DROPLETS

4.1 Introductory comments

Diesel fuel droplet heating and evaporation is an important part of the processes leading to fuel combustion in Diesel engines [1]. Accurate modelling of these processes is essential for their understanding and ultimately improving engine design. As mentioned in Chapter 1, the main difficulty with modelling droplet heating and evaporation of Diesel fuels, compared with biodiesel fuels, lies in the fact that Diesel fuels contain many more components (over 100), compared with biodiesels (less than 16 in most cases [62], [123], [134], [135], [137]). This makes it rather difficult to calculate directly the mutual diffusion of individual components in Diesel fuel droplets.

Widely used models of Diesel fuel droplet heating and evaporation are based on a number of assumptions. These include the assumptions that: Diesel fuel can be approximated by a single component (n-dodecane in most cases); temperature gradients inside droplets can be ignored; the droplet interface is stationary during the time step; and kinetic effects during heating and evaporation can be ignored [2]. Some of these assumptions were relaxed in recent advanced models of multi-component droplet heating and evaporation (e.g. [54]). As illustrated in [43], [47], the most important of the abovementioned assumptions is that Diesel fuel can be approximated by a single component.

The early models, taking into account the effect of multiple components in Diesel fuels were based on the probabilistic analysis of a large number of components (e.g. the Continuous Thermodynamics (CT) approach [34], [35], [37] and the Distillation Curve Model [10]). In both of these approaches, additional simplifying assumptions were used, including the assumption that species inside droplets mix instantaneously or do not mix at all.

A new Quasi-Discrete (QD) model for the heating and evaporation of multi-component fuel droplets was suggested in [47]. Although the usefulness of the

QD model was clearly demonstrated in [43], [47], it still had a number of serious limitations. The most important of these limitations was the assumption that Diesel fuel consists only of alkanes and the distribution of mass/molar fractions as a function of the carbon number can be approximated by a smooth function. Both of these assumptions contradict the observed composition of realistic Diesel fuels [111]. An example of the composition of these fuels is shown in Figure 4.1. Our analysis if focused on this Diesel fuel, following [57].
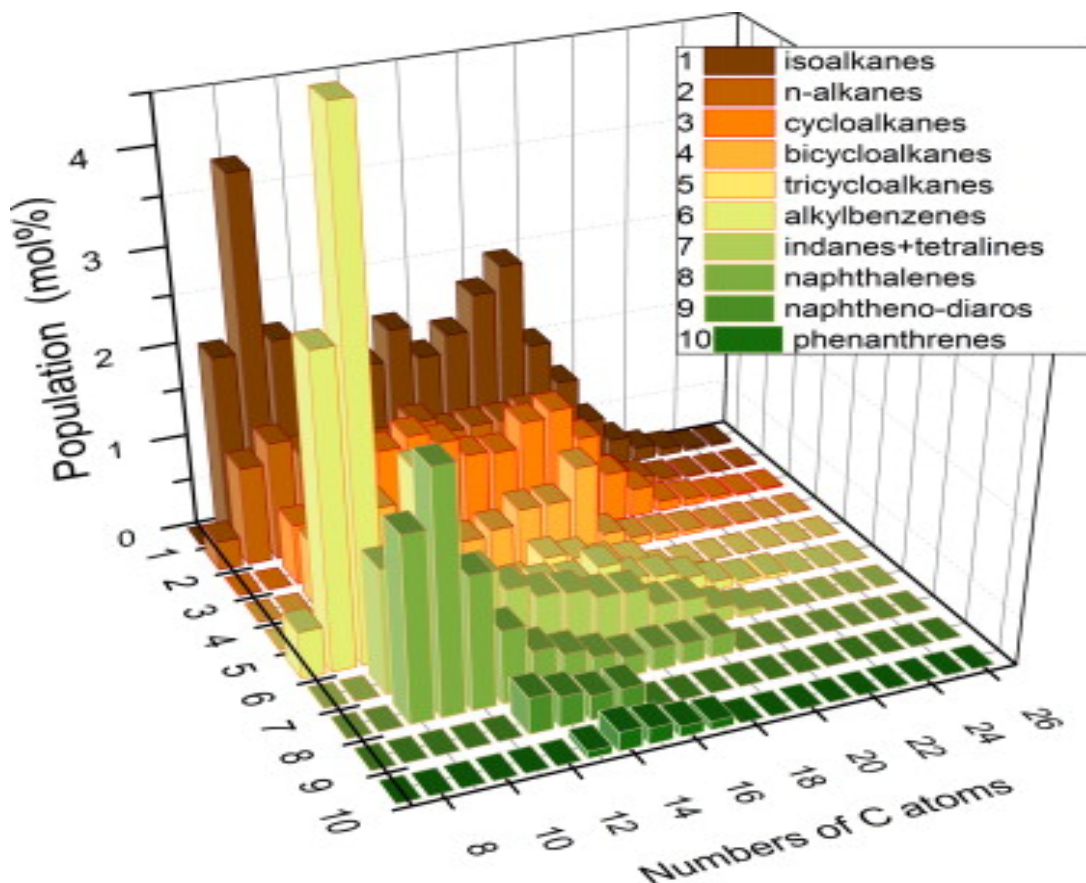
Figure 4.1 Molar fractions of various hydrocarbons versus the numbers of carbon atoms in a representative sample of commercial Diesel fuel [111].

The composition of Diesel fuel used in this analysis is described in Section 4.2. The main ideas of the QD model are described in Section 4.3. In the same section an alternative model to analyse Diesel droplet heating and evaporation, called Multi-Dimensional Quasi-Discrete (MDQD) model, is described. The input parameters and results of the calculations performed are presented in Sections 4.4 and 4.5. The main results of this chapter are summarised in Section 4.6.

4.2 Composition of Diesel fuel

The commercial Diesel fuel selected in the present work conforms to standard European Union fuel (EN590). The detailed chemical species composition was obtained using comprehensive two-dimensional gas chromatography (GCXGC) which is a very convenient tool for the characterisation of petroleum-based fuels [156]–[158]. Molar fractions of various components in this fuel are presented in Table 4.1 [112].

Table 4.1 The original composition (molar fractions) of a realistic Diesel fuel sample (gas chromatography data) [57], [111].

Number of C atoms	n-alkanes	Iso-alkanes	cycloalkanes	bicycloalkanes	tricycloalkanes	alkylbenzenes	Indanes & tetralines	naphthalenes	diaromatics	phenanthrenes
C8	0.3080	0	0	0	0	0.4970	0	0	0	0
C9	1.0513	1.9807	0	0	0	3.2357	0	0	0	0
C10	1.2635	3.7906	0.6408	0.6926	0	5.3584	1.3157	1.9366	0	0
C11	1.1002	2.0628	1.8745	1.0524	0	0.9492	1.3632	2.5290	0	0
C12	0.9866	1.6290	1.6951	0.9753	0	1.9149	1.1951	1.4012	0	0
C13	0.9646	1.5793	1.2646	0.6611	0	0.6873	1.0652	0.7692	0.3834	0
C14	1.0146	1.6351	1.3633	0.5631	0.0914	0.6469	0.8406	0.4879	0.3217	0.0768
C15	1.2051	1.9595	1.2353	0.4314	0.1799	0.4782	0.7051	0.3843	0.2589	0.2033
C16	1.0442	1.6137	1.0449	0.4921	0.1773	0.4564	0.6684	0.2854	0.2602	0.1705
C17	1.0564	1.8041	1.0162	0.6529	0.4001	0.4204	0.5598	0.2072	0	0.1154
C18	1.0596	2.1807	1.2848	0.6554	0.3304	0.5234	0.5357	0.2358	0	0.0917
C19	1.0916	2.4380	1.3566	0.9901	0.2159	0.3226	0.3403	0.2151	0	0
C20	0.7054	1.5284	0.9961	0.1965	0.1696	0.2848	0.3227	0.2256	0	0
C21	0.3756	1.0674	0.5374	0.0935	0	0.2032	0.1638	0	0	0
C22	0.2328	0.5662	0.3040	0.0701	0	0.0969	0.0781	0	0	0
C23	0.1083	0.2889	0.1090	0.0488	0	0.0494	0	0	0	0
C24	0.0461	0.1442	0.0755	0.0234	0	0.0473	0	0	0	0
C25	0.0221	0.0776	0.0445	0.0169	0	0	0	0	0	0
C26	0.0106	0.0319	0.0214	0	0	0	0	0	0	0
C27	0.0052	0.0257	0.0155	0	0	0	0	0	0	0
mol%	13.6518	26.4038	14.8795	7.6156	1.5646	16.1720	9.1537	8.6773	1.2242	0.6577

One can see in Table 4.1 that the contributions of tricycloalkanes, diaromatics and phenanthrenes to Diesel fuel are rather small (less than about 1.6% for each of these components). Hence, the dependence of the properties of these components on the number of carbon atoms can be ignored and these groups can be replaced with three characteristic components: tricycloalkane, diaromatic and phenanthrene, with arbitrary chosen values of carbon numbers. A simplified version of Table 4.1, in which n-alkanes and iso-alkanes are merged into one group of alkanes, and tricycloalkanes, diaromatics and phenanthrenes are excluded, is presented as Table 4.2.

Table 4.2 The simplified composition (molar fractions), used in the analysis, of the same Diesel fuel sample as presented in Table 4.1.

Number of C atoms	alkanes	cycloalkanes	bicycloalkanes	alkylbenzenes	Indanes & tetralines	naphthalenes
C8	0.308	0	0	0.497	0	0
C9	3.032	0	0	3.2357	0	0
C10	5.0541	0.6408	0.6926	5.3584	1.3157	1.9366
C11	3.163	1.8745	1.0524	0.9492	1.3632	2.529
C12	2.6156	1.6951	0.9753	1.9149	1.1951	1.4012
C13	2.5439	1.2646	0.6611	0.6873	1.0652	0.7692
C14	2.6497	1.3633	0.5631	0.6469	0.8406	0.4879
C15	3.1646	1.2353	0.4314	0.4782	0.7051	0.3843
C16	2.6579	1.0449	0.4921	0.4564	0.6684	0.2854
C17	2.8605	1.0162	0.6529	0.4204	0.5598	0.2072
C18	3.2403	1.2848	0.6554	0.5234	0.5357	0.2358
C19	3.5296	1.3566	0.9901	0.3226	0.3403	0.2151
C20	2.2338	0.9961	0.1965	0.2848	0.3227	0.2256
C21	1.443	0.5374	0.0935	0.2032	0.1638	0
C22	0.799	0.304	0.0701	0.0969	0.0781	0
C23	0.3972	0.109	0.0488	0.0494	0	0
C24	0.1903	0.0755	0.0234	0.0473	0	0
C25	0.0997	0.0445	0.0169	0	0	0
C26	0.0425	0.0214	0	0	0	0
C27	0.0309	0.0155	0	0	0	0
mol%	40.0556	14.8795	7.6156	16.172	9.1537	8.6773

Transport and thermodynamic properties of the components presented in Table 4.2 are summarised in Appendix C. Transport and thermodynamic properties of three components, tricycloalkane, diaromatic and phenanthrene, are summarised in Appendix C7. Based on the results presented in Table 4.1, the molar fraction of tricycloalkanes is assumed as 1.5647%, while the molar fraction of diaromatics and phenanthrenes are assumed equal to 1.2240% and 0.6577%, respectively. The analysis is based on the composition given in Table 4.2, in addition to the three discrete characteristic components: tricycloalkane, diaromatic and phenanthrene.

4.3   The model

In the original quasi-discrete model described by [43], [47], the contribution of various n-alkanes is described by the distribution function $f_m(n)$:

$$f_m(n) = C_m(n_0, n_f) \frac{(M(n)-\gamma)^{\alpha-1}}{\beta^\alpha \, \Gamma(\alpha)} \exp\left[-\left(\frac{M(n)-\gamma}{\beta}\right)\right], \tag{4.1}$$

where $n_0 \leq n \leq n_f$, subscripts 0 and f stand for initial and final, $\Gamma(\alpha)$ is the Gamma function, α and β are parameters that determine the shape of the distribution, M is molar mass, n is number of carbon atoms, γ determines the original shift, and the constant C_m is defined as:

$$C_m = \left\{ \int_{n_1}^{n_2} \frac{(M(n)-\gamma)^{\alpha-1}}{\beta^\alpha \Gamma(\alpha)} \exp\left[-\left(\frac{M(n)-\gamma}{\beta}\right)\right] dn \right\}^{-1}, \tag{4.2}$$

The expression for C_m is derived from the condition that:

$$\int_{n_1}^{n_2} f_m(n) \, dn = 1, \tag{4.3}$$

Assuming that the properties of hydrocarbons in a certain narrow range of n are close, the continuous distribution $f_m(n)$ can be replaced with a discrete one, consisting of N_f quasi-components (QC) with carbon numbers:

$$\bar{n}_j = \frac{\int_{n_{j-1}}^{n_j} n \, f_m(n) \, dn}{\int_{n_{j-1}}^{n_j} f_m(n) \, dn}, \tag{4.5}$$

and the corresponding molar fractions:

104

$$X_j = \int_{n_{j-1}}^{n_j} f_m(n) \, \mathrm{d}n, \tag{4.6}$$

where j is an integer in the range $\left(1 \leq j \leq N_f\right)$. Note that:

$$\sum_{j=1}^{j=N_f} X_j = 1. \tag{4.7}$$

The choice of n_j could be arbitrary. It was assumed that all $n_j - n_{j-1}$ are equal, i.e. all QC have the same range of values of n. For the case when $N_f = 1$ this approach reduces the analysis of multi-component droplets to that of mono-component droplets. These new QCs are not the actual physical hydrocarbon components ($\bar{n}_j$ in Equation (4.5) are not integers in the general case). Hence, this model was called a quasi-discrete model. These QC were treated as actual components in the conventional Discrete Component Model (DCM), including taking into account the diffusion of liquid QC in droplets, discussed later in this section. This model is expected to be particularly useful when N_f is much less than the number of actual species in the hydrocarbon mixture.

There are two main problems with the application of this approach to realistic Diesel fuels, the composition of which is shown in Figure 4.1 (see Tables 4.1 and 4.2 for further details). Firstly, even if the analysis is restricted only to alkanes, it does not appear to be easy to approximate this distribution with a reasonably simple distribution function $f_m(n)$, given by Expression (4.1) (similar to the one used in [43]–[45], [47]). Secondly, the contributions of the other eight hydrocarbon groups apart from alkanes, presented in Tables 4.1 and 4.2, cannot be ignored in any realistic model of Diesel fuels. In the new model described below both of these issues are addressed.

In this new model, the focus is shifted from the analysis of the distribution function to the direct analysis of molar fractions of the components. These are described by the matrix X_{nm}, where n refers to the number of carbon atoms, and m refers to the groups (e.g. alkanes) or individual characteristic components (tricycloalkane, diaromatic and phenanthrene). The link between the values of m and the components is shown in Table 4.3.

Table 4.3 The groups of multi-component Diesel fuel.

m	Group
1	alkanes
2	cycloalkanes
3	bicycloalkanes
4	alkylbenzenes
5	indanes
6	napthalenes
7	tricycloalkane
8	diaromatic
9	phenanthrene

For each m the values of $\bar{n}_{jm}$ of QC can be introduced as:

$$
\left.
\begin{aligned}
\bar{n}_{1m} &= \frac{\sum_{n=n_{1m}}^{n=n_{(\varphi_m+1)m}} (nX_{nm})}{\sum_{n=n_{1m}}^{n=n_{(\varphi_m+1)m}} X_{nm}}, \\[2mm]
\bar{n}_{2m} &= \frac{\sum_{n=n_{(\varphi_m+2)m}}^{n=n_{(2\varphi_m+2)m}} (nX_{nm})}{\sum_{n=n_{(\varphi_m+2)m}}^{n=n_{(2\varphi_m+2)m}} X_{nm}}, \\[2mm]
\bar{n}_{3m} &= \frac{\sum_{n=n_{(2\varphi_m+3)m}}^{n=n_{(3\varphi_m+3)m}} (nX_{nm})}{\sum_{n=n_{(2\varphi_m+3)m}}^{n=n_{(3\varphi_m+3)m}} X_{nm}}, \\[2mm]
&\ \vdots \\[2mm]
\bar{n}_{lm} &= \frac{\sum_{n=n_{((\ell-1)\varphi_m+\ell)m}}^{n=n_{km}} (nX_{nm})}{\sum_{n=n_{((\ell-1)\varphi_m+\ell)m}}^{n=n_{km}} X_{nm}},
\end{aligned}
\right\}
\tag{4.8}
$$

where $n_{1m} = n_{m(\min)}$ is the minimal value of n for which $X_{nm} \neq 0$, $n_{km} = n_{m(\max)}$ is the maximal value of n for which $X_{nm} \neq 0$ (see Table 4.2), $\ell = \text{integer}((k_m + \varphi_m)/(\varphi_m + 1))$. Parameter φ_m is assumed to be integer valued; $\varphi_m + 1$ is equal to the number of components to be included within each quasi-component, except possibly the last one in the group. φ_m is assumed to be the same for all QC within group m. If $\varphi_m = 0$ then $\ell = k_m$ and the number

of QC is equal to the number of actual components. φ_m and k_m depend on m in the general case.

The molar fractions of these C/QC are estimated as:

$$
\left.
\begin{aligned}
X_{1_m} &= \sum_{n=n_{1m}}^{n=n_{(\varphi_m+1)}} X_{nm}, \\[2mm]
X_{2_m} &= \sum_{n=n_{(\varphi_m+2)}}^{n=n_{(2\varphi_m+2)}} X_{nm}, \\[2mm]
&\quad\vdots \\[2mm]
X_{l_m} &= \sum_{n=n_{((\ell-1)\varphi_m+\ell)}}^{n=n_{k_m}} X_{nm}.
\end{aligned}
\right\}
\tag{4.9}
$$

This approach to generation of QC is based on the selection of the number of components $(\varphi_m + 1)$ within each quasi-component in most cases. An alternative approach to their generation is based on the selection of the number of QC n_q. In this case the number of components in each quasi-component, except possibly the last one, (n_c) is taken equal to the nearest integer of the ratio k_m/n_q. If k_m/n_q is not an integer then the number of components in the last quasi-component (n_{lc}) is either greater than n_c, if $(k_m/n_q) > n_c$, or less than n_c, if $(k_m/n_q) \leq n_c$. In application to Diesel fuel, the second approach is found to be more convenient and it is used in the analysis. The values of $\bar{n}_{im}$ were calculated using Equations (4.8).

As in the case of the original quasi-discrete model, $\bar{n}_{im}$ are not integers in the general case. In the case when mass fractions of components/quasi-components (C/QC) with large carbon numbers are small then these C/QC can be merged to form single QC. Due to the additional dimensions introduced by the subscript m in Equation (4.8), the new model is called the Multi-Dimensional Quasi-Discrete (MDQD) model.

The minimal number of $\bar{n}_{im}$ for the groups shown in Table 4.2 is 9 (when $\varphi_m = k_m - 1$ for all m). The multi-component model can be further simplified and approximated by the single-component model, assuming that the mass fractions of 9 C/QC are constant with time. The maximal number of these C/QC, providing the most accurate approximation of Diesel fuel shown in Figure 4.1

and Table 4.1, is 98. (see Table 4.2). In the current study, the reduction in the number of QCs is investigated, provided that the errors introduced by this reduction are acceptable for practical engineering applications. Note that in the model considered in [43], [47] the minimal and maximal numbers of QC for Diesel fuel were 1 and 20 respectively.

Note that in the case when the maximal $\ell = k_m$ is used, the new approach reduces to the conventional Discrete Component Model (DCM), while the previously suggested QD model does not have this property. In the case considered in [43], [47], Diesel fuel was approximated by 21 components (n-alkanes), but the maximal number of QC was just 20.

Once the C/QC have been introduced using the new approach they are treated in the same way as in [43], [47], using transport and thermodynamic properties of the components summarised in Appendix C. The mixtures are treated as ideal (Raoult's law is assumed to be valid, see Equations 2.46-2.52 in Section 2.8). In this case, partial pressures of individual C/QC are estimated as:

$$p_v(\bar{n}_{im}) = X_{lsim}(\bar{n}_{im})\, p^{sat}(\bar{n}_{im}), \tag{4.10}$$

where X_{lsim} are the molar fractions of liquid C/QC at the surface of the droplet, $p^{sat}(\bar{n}_{im})$ are calculated from the data presented in Appendix A. In the case of discrete components, these pressures do not depend on n (they are functions of temperature only).

As in the case of [43], [47], the temperature gradient and C/QC diffusion inside droplets are taken into account based on the analytical solutions to the heat conduction and species diffusion equations inside droplets as described previously. The analytical solutions and approximations of the model presented in Section 4.3 and Chapter 2 are used in the analysis below.

4.4   Input parameters

Following the results of measurements presented in [63], [154], the initial droplet radius is taken equal to $R_{d0} = $ 10 μm, which is compatible with Sauter Mean Diameters (SMD) of Diesel fuel droplets reported in [52], [140]. As in [47], the following values are assumed for ambient air density and pressure (assuming that the ideal gas law is valid):

$\rho_a = 11.9 \text{ kg m}^{-3}, T_a = 880\text{K}, p_a = 30 \text{ bar}.$

The MDQD model was applied to the analysis of heating and evaporation of Diesel fuel droplets of initial temperature $T_0 = $ 300 K, for (1) stationary droplets and (2) droplets moving at a relative velocity $U_d = 10$ m/s. As in the case of biodiesel fuel droplets (see [46], [64]), it is assumed that the gas temperature and pressure are equal to 880 K and 30 bars respectively.

4.5   Results

The calculations were initially based on the Effective Thermal Conductivity (ETC) model for stationary droplets (in this case the ETC model reduces to a pure conduction model). The plots of the droplet surface temperatures T_s and radii R_d versus time for various approximations of Diesel fuel composition, are shown in Figures 4.2-4.9. See Table 4.4 for details.

Table 4.4 The species contributions from different groups of Diesel composition based on the selected number of C/QC using the MDQD model.

number of QC/C	contribution of speacies from each group								
	alkanes	cycloalkanes	bicycloalkanes	alkylbenzenes	indanes/ tetralines	naphthalenes	tri- cycloalkane	diaromatic	phenanthrene
98	20	18	16	17	13	11	1	1	1
85	19	17	8	16	12	10	1	1	1
58	19	9	8	8	6	5	1	1	1
40	10	9	5	8	3	2	1	1	1
23	5	4	3	3	3	2	1	1	1
21	5	4	3	3	3	2	1	0	0
17	4	3	2	3	2	2	1	0	0
15	4	3	1	3	2	1	1	0	0
12	4	2	1	2	1	1	1	0	0
9	1	1	1	1	1	1	1	1	1
7	1	1	1	1	1	1	1	0	0
S (9 with ID/ITC)	1	1	1	1	1	1	1	1	1
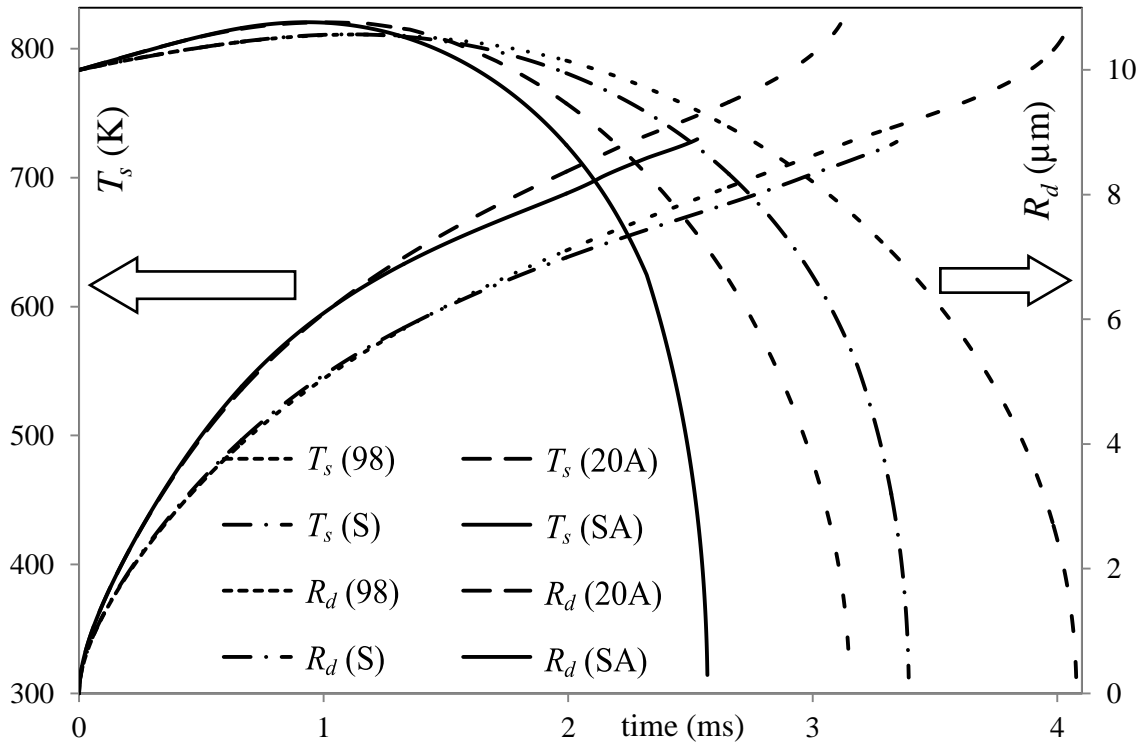
Figure 4.2 The plots of the droplet surface temperatures T_s (left arrow) and radii R_d (right arrow) versus time for four approximations of Diesel fuel composition: the contributions of all 98 components are taken into account (indicated as (98)); the contributions of only 20 alkane components (shown in Table 4.2) are taken into account (indicated as (20A)); the contribution of all 98 components are approximated by 9 quasi-components (corresponding to 9 groups shown in Tables 4.2 and 4.3) without taking into account the diffusion between them so that their mass fractions remain equal to the initial mass fractions and they behave like a single component (indicated as (S)); the contributions of only 20 alkane components (shown in Table 4.2) are taken into account and these are treated as a single quasi-component with the average value of the carbon number ($C_{14.763}H_{31.526}$; indicated as (SA)). Ambient gas pressure and temperature are assumed to be equal to 30 bar and 880 K respectively; the ETC/ED model was used for the analysis.

In Figure 4.2 these plots are shown for 4 cases: the contributions of all 98 components are taken into account (indicated as (98)); the contributions of only 20 alkane components shown in Table 4.2 are taken into account (standard approximation used in the original quasi-discrete model [43], [47]) (indicated as (20A)); the contribution of all 98 components is approximated by 9 QC, corresponding to 9 groups shown in Tables 4.2 and 4.3 without taking into account the diffusion between them so that their mass fractions remain equal to the initial mass fractions and they behave like a single quasi-component

(indicated as (S)); and the contributions of only 20 alkane components shown in Table 4.2 are taken into account and these are approximated by a single quasi-component with the average value of the carbon number ($C_{14.763}H_{31.526}$; indicated as (SA)). In the cases when only the contribution of alkanes was taken into account, the mass fractions of the components were recalculated to ensure that the total mass fractions of all alkanes were equal to 1. The same comment applies to the cases when other components are removed from the analysis.

As follows from Figure 4.2, the approximation of 98 actual components with a single quasi-component (formed of 9 components/quasi-components (C/QC); plots S) leads to a noticeable under-estimation of the droplet surface temperature, and an under- estimation of the evaporation time by about 17%. In the case when Diesel fuel is approximated with 20 alkane components, the predicted droplet surface temperatures appeared to be higher and the evaporation time shorter by about 23% than in the case of approximation of Diesel fuel with 98 components. This means that the approximation of Diesel fuel with alkanes, a widely used assumption in the modelling of Diesel fuels (see [43], [47] and the references therein), leads to results which are less accurate, compared with the approximation of Diesel fuel by a single QC. The approximation of Diesel fuel with a single alkane QC ($C_{14.763}H_{31.526}$) leads to under-prediction of the evaporation time by about 37% which is not acceptable even for qualitative analysis of the process. This leads us to question of the validity of the results of numerous papers where Diesel fuel was approximated with a single alkane component (e.g. [159]).

Note that in all cases shown in Figure 4.2 the droplet surface temperatures keep increasing with time until the droplets evaporate. This is consistent with our earlier studies of this process (e.g. [43], [74]). This result questions the applicability of the assumption that the droplet surface temperature remains constant during the evaporation process, in the general case, which is widely used in simplified models of this process (see e.g. [160], [161]). The well known d^2-law is implicitly based on this assumption (see [5]).

The results of calculations of the droplet surface temperatures T_s and radii R_d versus time for more refined approximations of Diesel fuel, compared with the case shown in Figure 4.2, are shown in Figure 4.3. The following approximations (see Table 4.4) were considered:

1. The contributions of all 98 components are taken into account as in the case shown in Figure 4.2 (indicated as (98)).
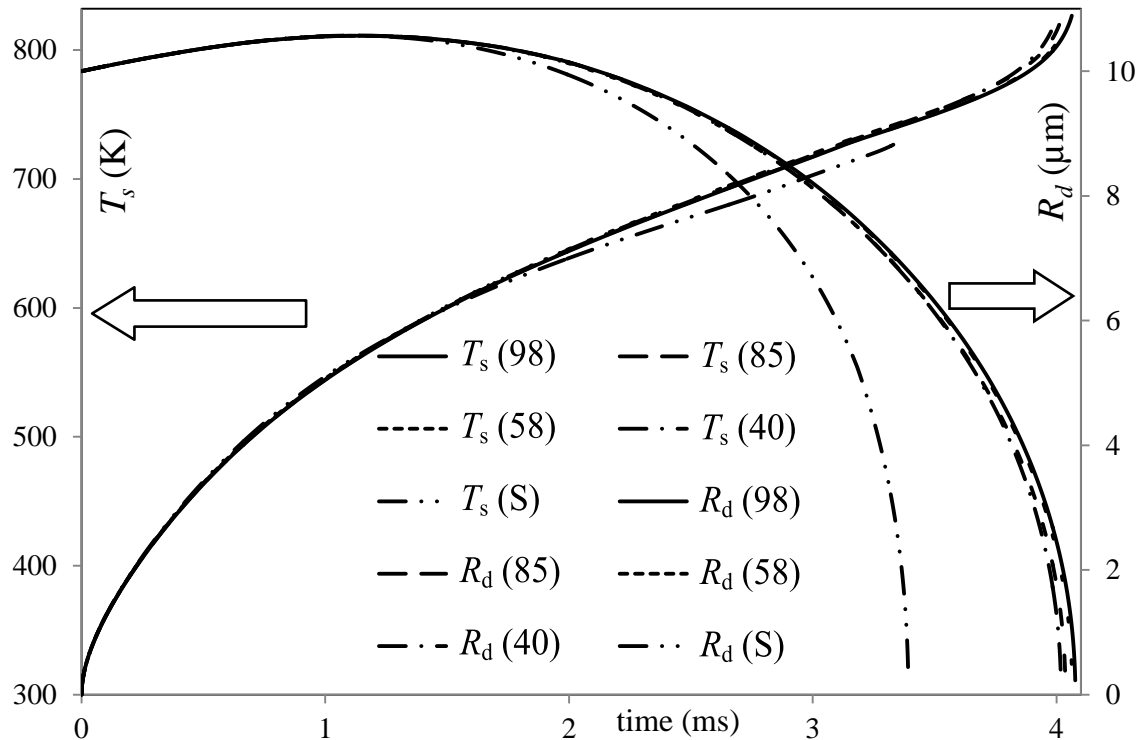
Figure 4.3 The plots of the droplet surface temperatures T_s and radii R_d versus time for five approximations of Diesel fuel composition: 98 components (indicated as (98)); 85 C/QC (indicated as (85)); 58 C/QC (indicated as (58)); 40 C/QC (indicated as (40)); the contribution of all 98 components is taken into account as that of a single component as in the case shown in Figure 4.2 (indicated as (S)) (see the details in the text of the paper). The same ambient conditions and model as in the case shown in Figure 4.2 were used for the analysis.

2. The contribution of alkanes is approximated by 19 components/ quasi-components (C/QC), 18 components and 1 QC incorporating 2 components with the largest values of n); the contribution of cycloalkanes is approximated by 17 C/QC (16 components and 1 QC incorporating 2 components with the largest values of n); the contribution of bicycloalkanes is approximated by 8 QC; the

contribution of alkylbenzenes is approximated by 16 C/QC (15 components and 1 QC incorporating 2 components with the largest values of n); the contribution of indanes & tetralines is approximated by 12 C/QC (11 components and 1 QC incorporating 2 components with the largest values of n); the contribution of naphthalenes is approximated by 10 C/QC (9 components and 1 QC incorporating 2 components with the largest values of n); the contributions of tricycloalkanes, diaromatics and phenanthrenes are taken into account; this leads to the model based on 85 C/QC (indicated as (85)).

3. The contribution of alkanes is approximated by 19 C/QC; the contribution of cycloalkanes is approximated by 9 QC; the contribution of bicycloalkanes is approximated by 8 QC; the contribution of alkylbenzenes is approximated by 8 QC; the contribution of indanes & tetralines is approximated by 6 QC; the contribution of naphthalenes is approximated by 5 QC; the contributions of tricycloalkane, diaromatic and phenanthrene are taken into account; this leads to the model based on 58 C/QC (indicated as (58)).

4. The contribution of alkanes is approximated by 10 QC; the contribution of cycloalkanes is approximated by 9 QC; the contribution of bicycloalkanes is approximated by 5 QC; the contribution of alkylbenzenes is approximated by 8 QC; the contribution of indanes & tetralines is approximated by 3 QC; the contribution of naphthalenes is approximated by 2 QC; the contributions of tricycloalkane, diaromatic and phenanthrene are taken into account; this leads to the model based on 40 C/QC (indicated as (40)).

5. The contributions of all 98 components are approximated with 9 single C/QC with average parameters, but diffusion between these C/QC is not allowed so that their mass fractions remain equal to the initial mass fractions and they behave like a single QC (indicated as (S) as in Figure 4.2).

The quasi-components in the abovementioned approximations were selected as described in Section 4.3. Zoomed parts of Figure 4.3 for droplet surface temperatures and radii are shown in Figures 4.4 and 4.5 respectively.
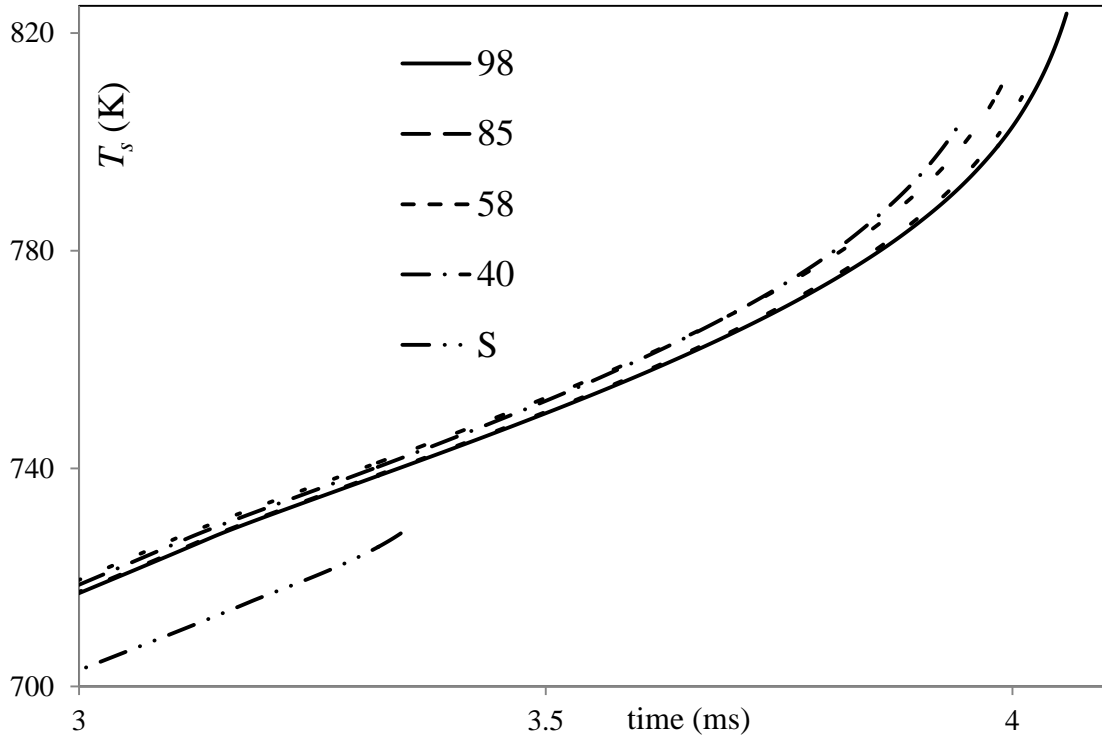
Figure 4.4 Zoomed part of Figure 4.3 referring to the droplet surface temperatures T_s.
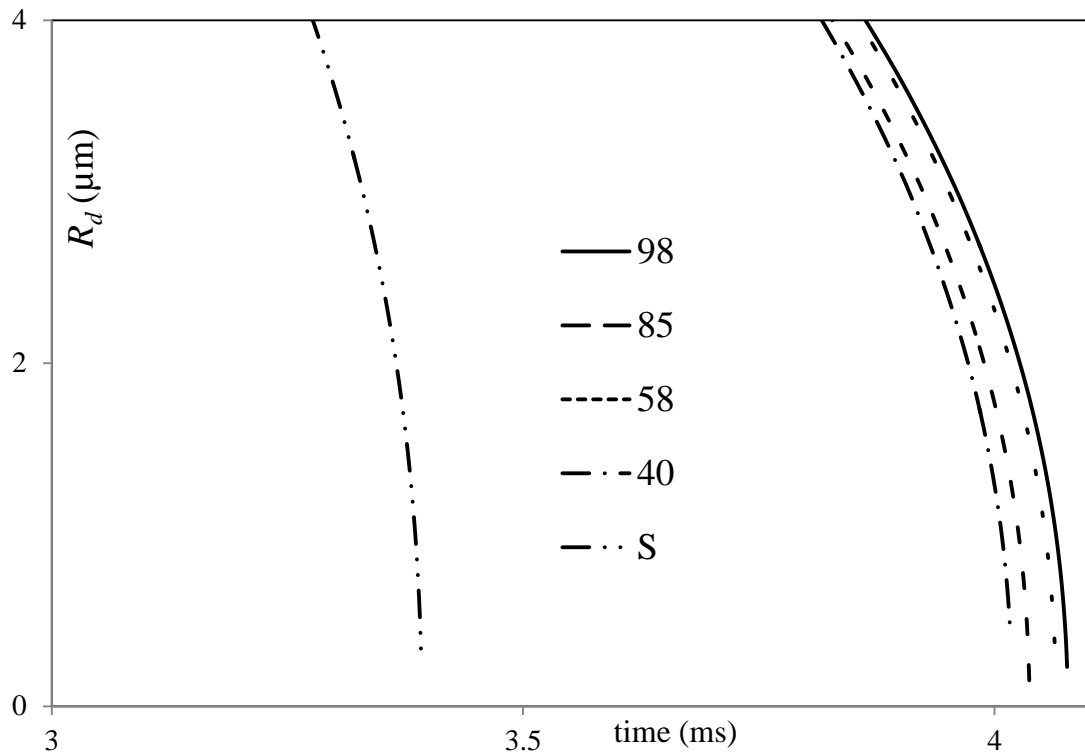
Figure 4.5 Zoomed part of Figure 4.3 referring to the droplet surface radii R_d.

As can be seen from Figures 4.3-4.5, the values of T_s and R_d predicted by all approximations, except the one of a single quasi-component, are very close. The temperatures predicted based on Approximations 2 are slightly higher than the ones predicted by the model taking into account the contributions of all 98 components. The calculations, based on Approximations 2-4 predict slightly shorter evaporation times than the ones predicted by the model taking into account the contributions of all 98 components. Even in the case of Approximation 4 (40 C/QC) the predicted evaporation time is only about 1.5% shorter than the evaporation time predicted by the model, taking into account the contributions of all 98 components. This difference can be safely ignored in most practical engineering applications. The longer evaporation times predicted by the model taking into account the contributions of all 98 components, compared with the models based on other approximations of Diesel fuel, can be attributed to the fact that at the final stages of droplet evaporation, the speed of evaporation is controlled by the least volatile component. When Diesel fuel is approximated with C/QCs, the least volatile of these quasi-components is never more volatile than the least volatile component of the Diesel fuel.

The results referring to the cases when the contributions of all 98 components are taken into account and the contribution of these 98 components is approximated with 9 single C/QC with average parameters, but diffusion between these C/QC is not allowed (Approximations 1 and 5), shown in Figures 4.2-4.5, are reproduced in Figures 4.6-4.9.
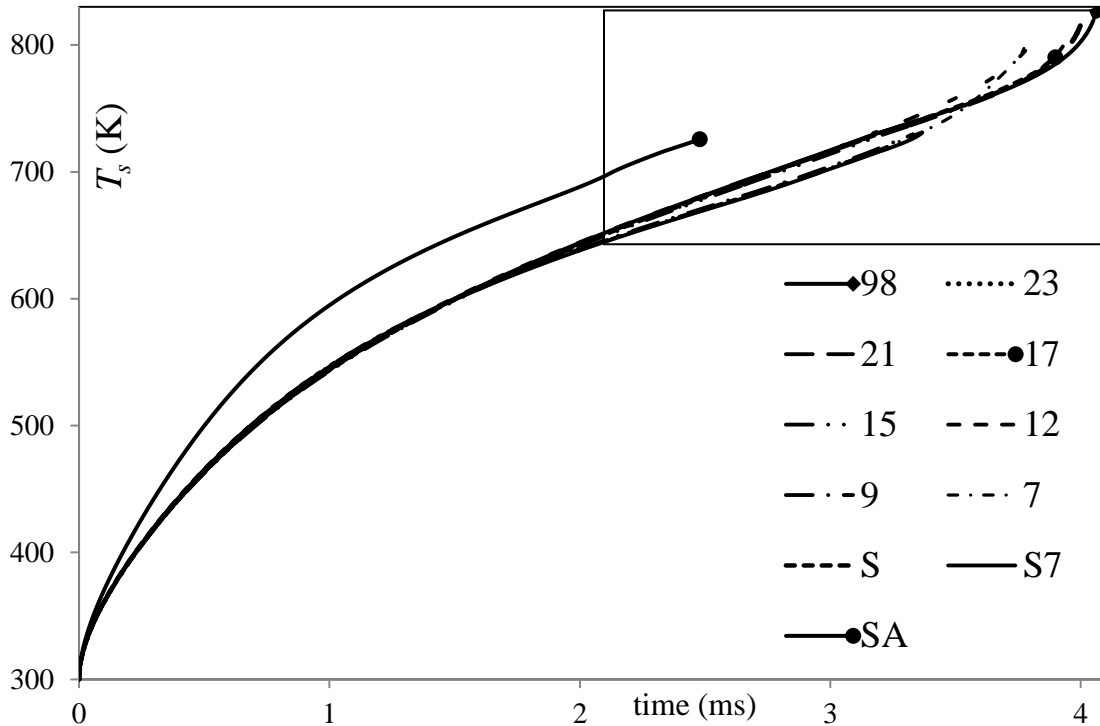
Figure 4.6 The plots of the droplet surface temperatures T_s versus time for ten approximations of Diesel fuel composition: 98 components (indicated as (98)); 23, 21, 17, 15, 12, 9 and 7 components/quasi-components (C/QC) (indicated as (23), (21), (17), (15), (12), (9) and (7) respectively); the contributions of all groups (shown in Tables 4.1, 4.2 and 4.3) are approximated by a single QC, to which the contribution of tricycloalkane is added, leading to 7 C/QC (indicated as (S7)); the contribution of all 98 components is taken into account as that of a single component as in the case shown in Figures 4.2 and 4.3 (indicated as (S)); the contributions of only 20 alkane components, shown in Table 4.2, are taken into account and these are treated as a single component, with the average value of the carbon number ($C_{14.763}H_{31.526}$; indicated as (SA)). The same ambient conditions and model as in the case shown in Figures 4.2-4.5 were used for the analysis.

The following additional approximations were considered for the plots shown in Figures 4.6-4.9:

6. The contribution of alkanes is approximated by 5 QC; the contribution of cycloalkanes is approximated by 4 QC; the contribution of bicycloalkanes is approximated by 3 QC; the contribution of alkylbenzenes is approximated by 3 QC; the contribution of indanes & tetralines is approximated by 3 QC; the contribution of naphthalenes is approximated by 2 QC and the contributions of

tricycloalkane, diaromatic and phenanthrene are taken into account. This leads to the model based on 23 C/QC (indicated as (23)).

7.   The same as above but without diaromatic and phenanthrene. This leads to the model based on 21 C/QC (indicated as (21)).

8.   The contribution of alkanes is approximated by 4 QC; the contribution of cycloalkanes is approximated by 3 QC; the contribution of bicycloalkanes is approximated by 2 QC; the contribution of alkylbenzenes is approximated by 3 QC; the contribution of indanes & tetralines is approximated by 2 QC; the contribution of naphthalenes is approximated by 2 QC and the contribution of tricycloalkane is taken into account but not that of diaromatic and phenanthrene. This leads to the model based on 17 C/QC (indicated as (17)).
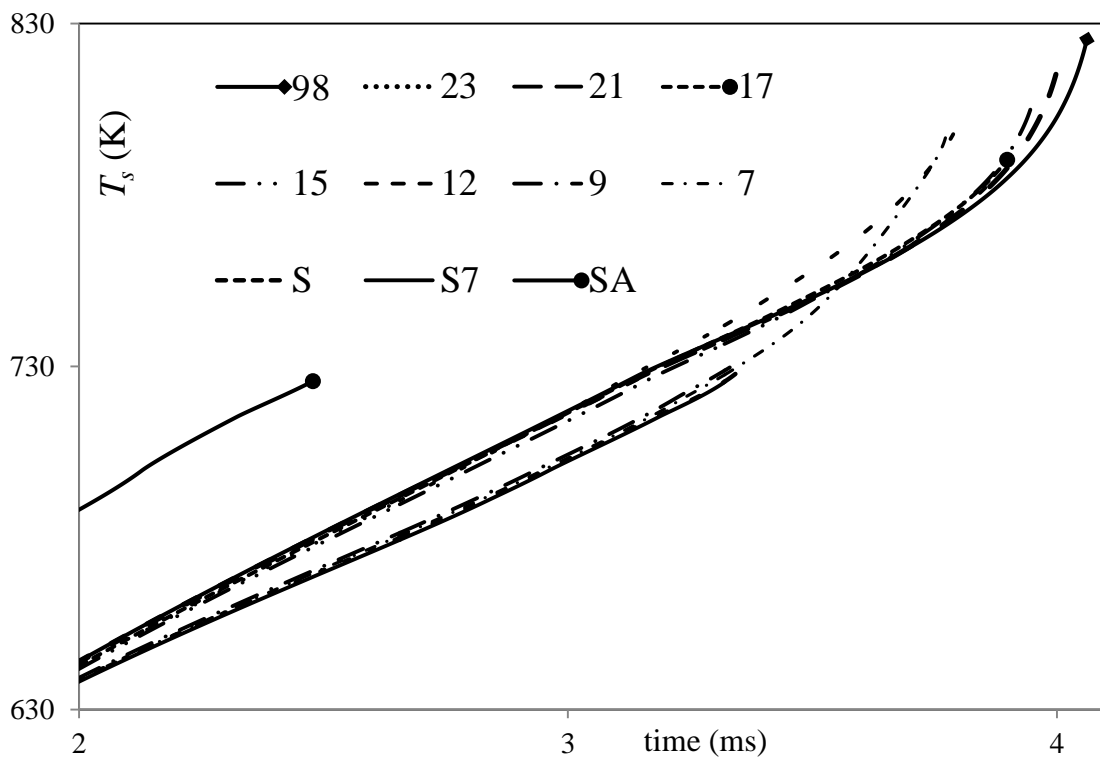
Figure 4.7 Zoomed part of Figure 4.6.
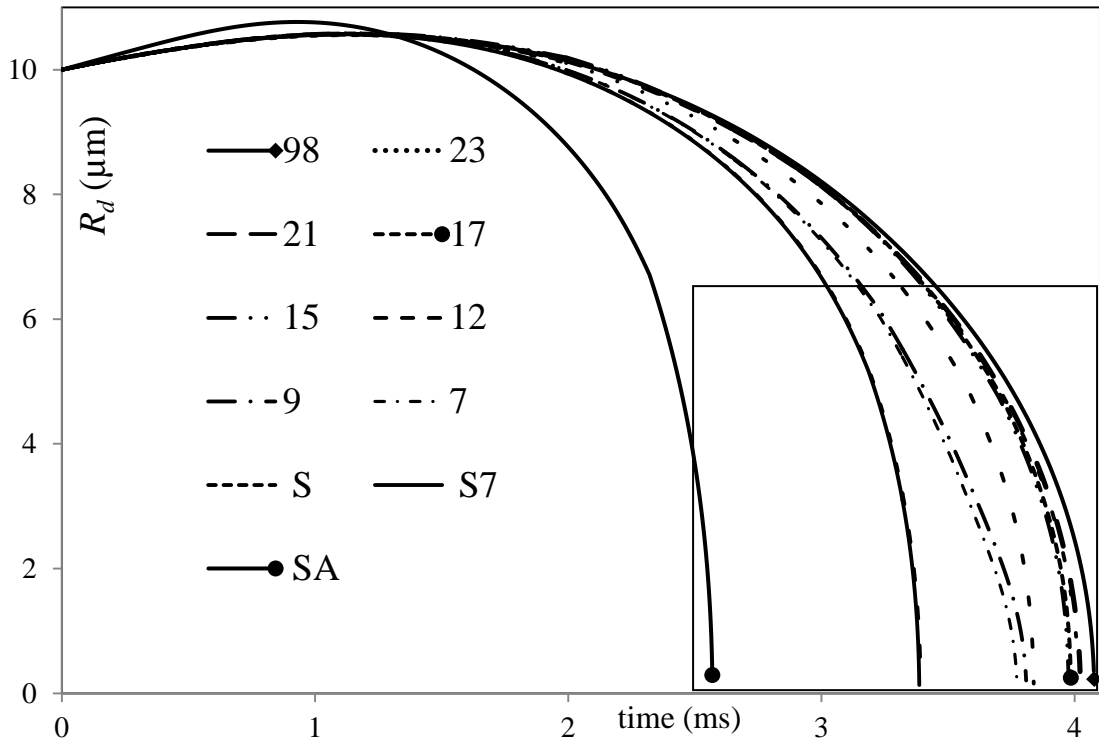
Figure 4.8 The same as Figure 4.6 but for the droplet radii R_d.
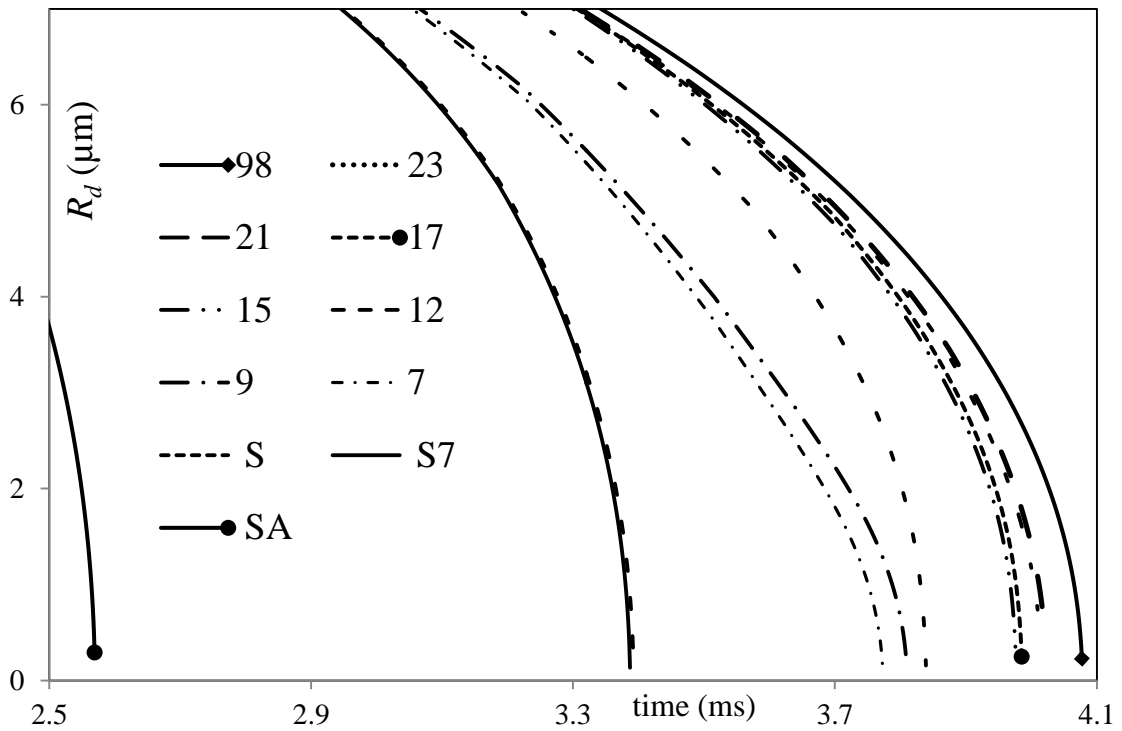
Figure 4.9 Zoomed part of Figure 4.8.

9. The contribution of alkanes is approximated by 4 QC; the contribution of cycloalkanes is approximated by 3 QC; the contribution of bicycloalkanes is approximated by 1 QC; the contribution of alkylbenzenes is approximated by 3 QC; the contribution of indanes & tetralines is approximated by 2 QC; the contribution of naphthalenes is approximated by 1 QC and the contribution of tricycloalkane is taken into account but not that of diaromatic and phenanthrene. This leads to the model based on 15 C/QC (indicated as (15)).

10. The contribution of alkanes is approximated by 4 QC; the contribution of cycloalkanes is approximated by 2 QC; the contribution of bicycloalkanes is approximated by 1 QC; the contribution of alkylbenzenes is approximated by 2 QC; the contribution of indanes & tetralines is approximated by 1 QC; the contribution of naphthalenes is approximated by 1 QC and the contribution of tricycloalkane is taken into account but not that of diaromatic and phenanthrene. This leads to the model based on 12 C/QC (indicated as (12)).

11. The contributions of all six groups shown in Table 4.2 are approximated by single QC and the contribution of tricycloalkane, diaromatic and phenanthrene are taken into account; this leads to the model based on 9 C/QC (indicated as (9)); in contrast to the single component approximation mentioned above, diffusions between C/QC are allowed in this case.

12. The contributions of all six groups shown in Table 4.2 are approximated by single QC and the contribution of tricycloalkane is taken into account but not that of diaromatic and phenanthrene. This leads to the model based on 7 C/QC (indicated as (7)).

13. Approximation 5 is further simplified by replacing the contributions of 9 C/QC with 7 C/QC excluding the contributions of diaromatic and phenanthrene. As in the case of Approximation 5, diffusion between C/QC is not allowed so that their mass fractions remain equal to the initial mass fractions and they behave like a single component (indicated as (S7)).

As in the cases shown in Figures 4.3-4.5, the components/quasi-components (C/QC) in the abovementioned approximations were selected rather arbitrarily.

As one can see from Figures 4.6-4.9, the plots for surface temperatures and radii based on Approximations 13 and 5 are almost indistinguishable. Also, the corresponding plots based on Approximations 11 and 12 are rather close. The same applies to the plots based on Approximations 6 and 7. This means that the contribution of diaromatic and phenanthrene can be safely ignored in the approximation of Diesel fuel when modelling the heating and evaporation of fuel droplets in realistic Diesel engine-like conditions. Both for droplet surface temperatures and radii, the accuracy of approximations improves as the number of C/QC increases. In the case of 15 C/QC the droplet evaporation time can be estimated with an error of about 2.5%. In the case of 21 C/QC, this error reduces to about 1.5%. This error is comparable with the one for the approximation of Diesel fuel with 40 C/QC. Thus when balancing simplicity with accuracy of the model we can recommend the approximation of Diesel fuel with 21 C/QC if errors less than about 2% can be tolerated. This number of C/QC can be reduced to 15 if errors less than about 3% can be tolerated.

The plots of the surface mass fractions Y_{lis} of 18 characteristic and/or dominant components, predicted based on the model, taking into account the contributions of all 98 components, for the same conditions as in Figures 4.2-4.9, are shown in Figures 4.10-4.11.

These are the components shown in Figure 4.10: alkanes $C_{18}H_{38}$ (1), $C_{25}H_{52}$ (2) and $C_{27}H_{56}$ (3), cycloalkanes $C_{20}H_{40}$ (4), $C_{24}H_{48}$ (5), $C_{26}H_{52}$ (6) and $C_{27}H_{54}$ (7), alkylbenzene $C_{10}H_{14}$ (8), and tricycloalkane $C_{19}H_{34}$ (9). These are the components shown in Figure 4.11: alkane $C_{10}H_{22}$ (1), bicycloalkanes $C_{11}H_{20}$ (2) and $C_{25}H_{48}$ (3), alkylbenzenes $C_{23}H_{40}$ (4) and $C_{24}H_{42}$ (5), indane or tetraline $C_{13}H_{18}$ (6), naphthalenes $C_{10}H_8$ (7), $C_{11}H_{10}$ (8) and $C_{19}H_{26}$ (9). Note that the scales in Figure 4.10 are about an order of magnitude larger compared with Figure 4.11.
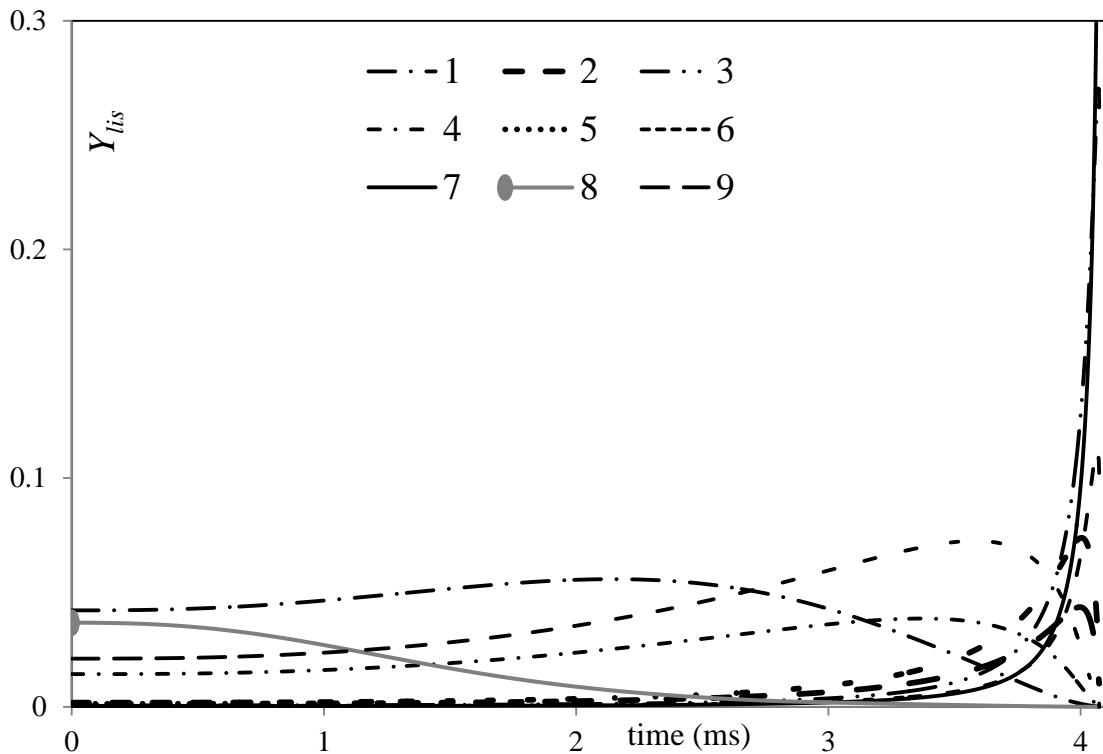
Figure 4.10 The plots of the surface mass fractions Y_{lis} of 9 characteristic and/or dominant components, predicted based on the model, taking into account the contributions of all 98 components, for the same conditions as in Figures 4.2-4.9: alkanes $C_{18}H_{38}$ (1), $C_{25}H_{52}$ (2), $C_{27}H_{56}$ (3), cycloalkanes $C_{20}H_{40}$ (4), $C_{24}H_{48}$ (5), $C_{26}H_{52}$ (6), $C_{27}H_{54}$ (7), alkylbenzene $C_{10}H_{14}$ (8) and tricycloalkane $C_{19}H_{34}$ (9).

As can be seen from Figures 4.10 and 4.11, the mass fractions of the lightest components, such as $C_{10}H_{14}$, $C_{10}H_{22}$, $C_{11}H_{10}$, $C_{10}H_8$ and $C_{11}H_{20}$, monotonically decrease with time, while the mass fraction of one of the heaviest components, $C_{27}H_{54}$, monotonically increases with time. The behaviour of the intermediate components appears to be more complex. Initially mass fractions of these components increase with time, but at the end of the evaporation period they start decreasing with time. At the very final stage of droplet evaporation only one, the least volatile component, remains in the liquid phase ($C_{27}H_{54}$ in the case shown in Figure 4.10). This behaviour of the surface mass fractions is consistent with that predicted by the simplified version of the model (QD model) described in [43], [47]. Note that strictly speaking the heaviest component in the mixture shown in Figure 4.10 is $C_{27}H_{56}$. This component, however, turned out to be slightly more volatile than $C_{27}H_{54}$. Hence, a rather

sharp increase in the mass fraction of $C_{27}H_{56}$ close to the end of the evaporation period is followed by an equally sharp decrease at the final stage of evaporation.
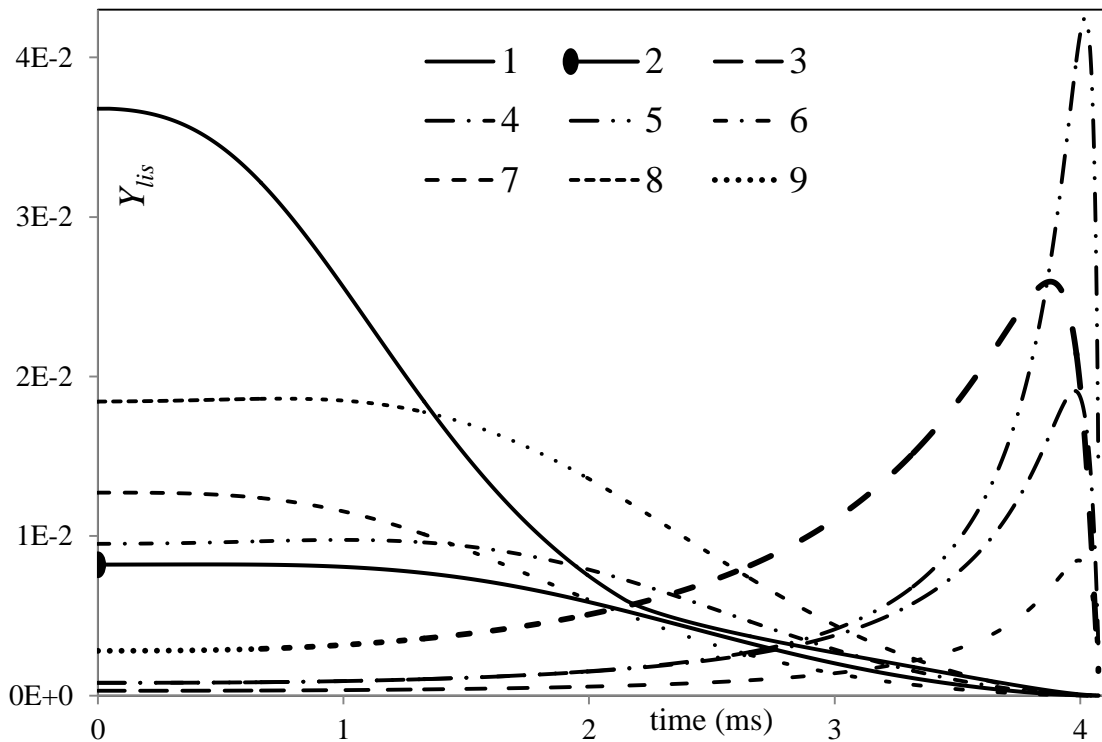
Figure 4.11 The same as Figure 4.10 but for alkane $C_{10}H_{22}$ (1), bicycloalkanes $C_{11}H_{20}$ (2) and $C_{25}H_{48}$ (3), alkylbenzenes $C_{23}H_{40}$ (4) and $C_{24}H_{42}$ (5), indane or tetraline $C_{13}H_{18}$ (6), naphthalenes $C_{10}H_8$ (7), $C_{11}H_{10}$ (8), and $C_{19}H_{26}$ (9).

Plots similar to those shown in Figures 4.10 and 4.11, but for 8 characteristic and/or dominant C/QC, as predicted by the model based on the approximation of Diesel fuel by 21 C/QC, are shown in Figure 4.12. These are the C/QC presented in this figure: alkane $C_{17.622}H_{37.244}$ (range $C_{16}H_{34} - C_{19}H_{40}$) (1), alkane $C_{20.869}H_{43.737}$ (range $C_{20}H_{42} - C_{23}H_{48}$) (2), cycloalkane $C_{25.644}H_{51.287}$ (range $C_{25}H_{50} - C_{27}H_{54}$) (3), bicycloalkane $C_{21.243}H_{40.485}$ (range $C_{20}H_{38} - C_{25}H_{48}$) (4), alkylbenzene $C_{10.207}H_{14.413}$ (range $C_8H_{10} - C_{13}H_{20}$) (5), indane or tetraline $C_{11.407}H_{14.814}$ (range $C_{10}H_{12} - C_{13}H_{18}$) (6), naphthalene $C_{11.533}H_{11.067}$ (range $C_{10}H_8 - C_{15}H_{18}$) (7), tricycloalkane $C_{19}H_{34}$ (8).
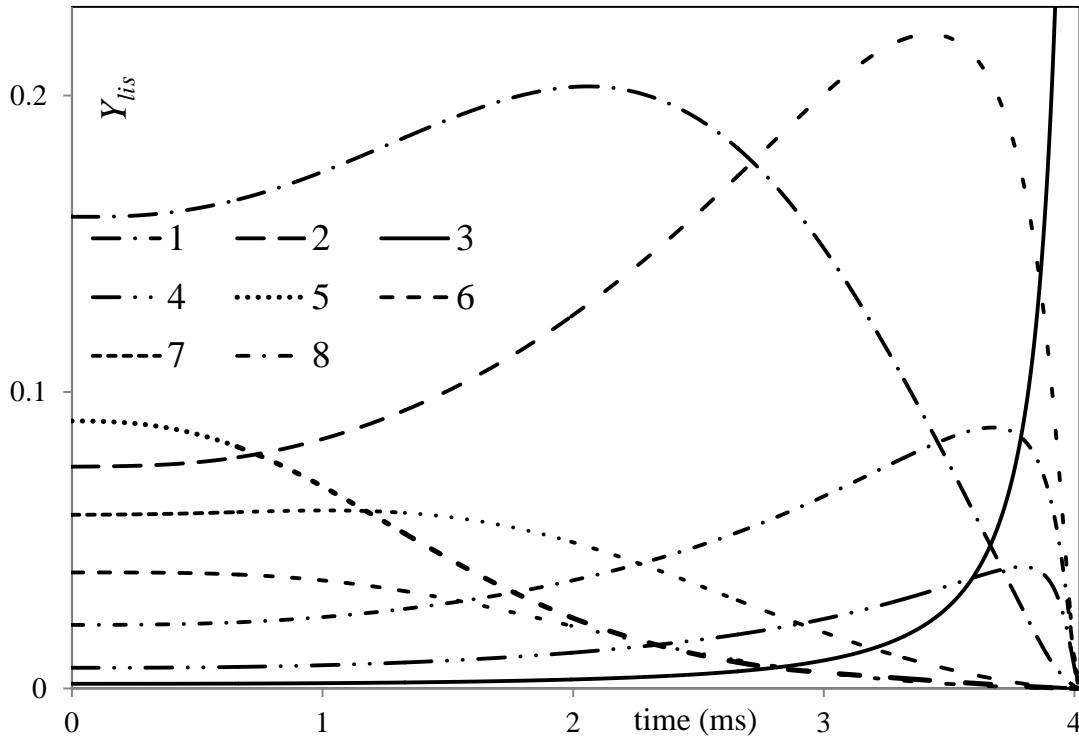
Figure 4.12 The same as Figures 4.10 and 4.11 but for the surface mass fractions Y_{lis} of 8 characteristic and/or dominant C/QC, predicted based on the model, taking into account the contributions of 21 C/QC; these are the C/QC: alkane $C_{17.622}H_{37.244}$ (range $C_{16}H_{34} - C_{19}H_{40}$) (1), alkane $C_{20.869}H_{43.737}$ (range $C_{20}H_{42} - C_{23}H_{48}$) (2), cycloalkane $C_{25.644}H_{51.287}$ (range $C_{25}H_{50} - C_{27}H_{54}$) (3), bicycloalkane $C_{21.243}H_{40.485}$ (range $C_{20}H_{38} - C_{25}H_{48}$) (4), alkylbenzene $C_{10.207}H_{14.413}$ (range $C_8H_{10} - C_{13}H_{20}$) (5), indane or tetraline $C_{11.407}H_{14.814}$ (range $C_{10}H_{12} - C_{13}H_{18}$) (6), naphthalene $C_{11.533}H_{11.067}$ (range $C_{10}H_8 - C_{15}H_{18}$) (7), tricycloalkane C19H34 (8).

As can be seen from Figure 4.12, the surface mass fractions of the lightest QCs, $C_{10.207}H_{14.413}$ and $C_{11.407}H_{14.814}$, monotonically decrease with time, while the surface mass fraction of the heaviest QC, $C_{25.644}H_{51.287}$, monotonically increases with time. The surface mass fractions of other C/QC initially increase and then decrease with time. This behaviour of the mass fractions is similar to that shown in Figures 4.10 and 4.11 for individual components.

Plots similar to those shown in Figure 4.12, but for 11 characteristic and/or dominant C/QC, as predicted by the model based on the approximation of Diesel fuel by 15 C/QC, are shown in Figure 4.13.
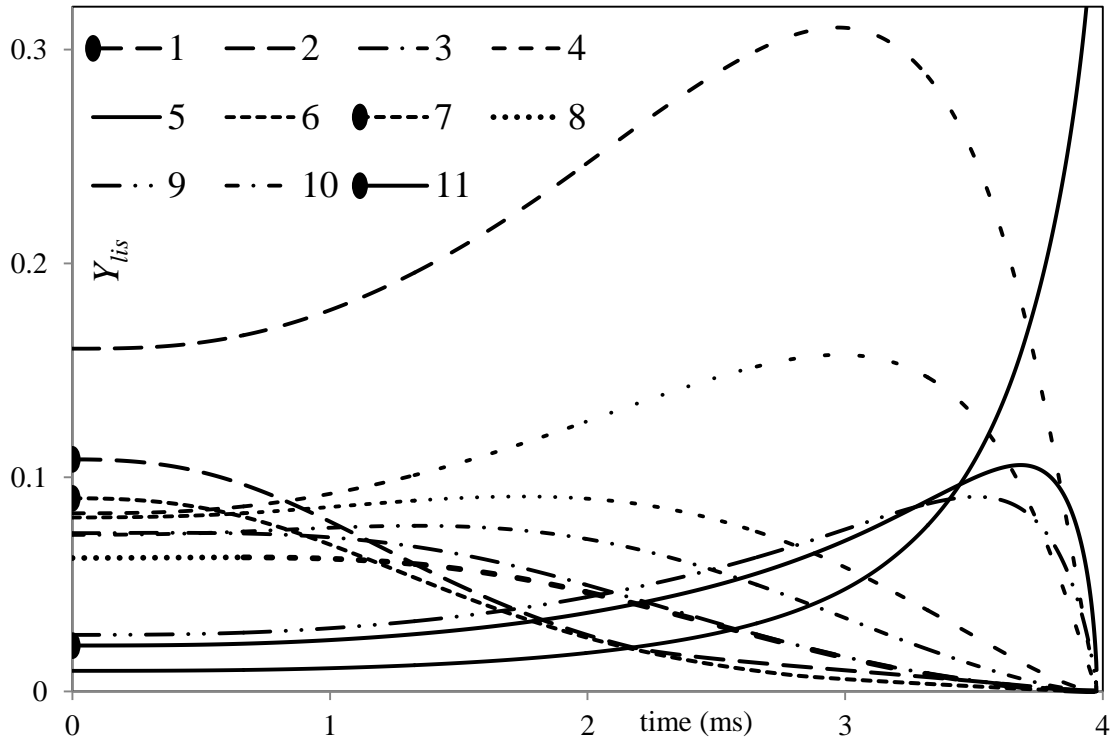
Figure 4.13 The same as Figure 4.12 but for the surface mass fractions Y_{lis} of 11 characteristic and/or dominant C/QC, predicted based on the model, taking into account the contributions of 15 C/QC; these are the C/QC: alkane $C_{10.335}H_{22.670}$ (range $C_8H_{18} - C_{12}H_{26}$) (1), alkane $C_{19.380}H_{40.760}$ (range $C_{18}H_{38} - C_{22}H_{46}$) (2), cycloalkane $C_{12.562}H_{25.125}$ (range $C_{10}H_{20} - C_{15}H_{30}$) (3), cycloalkane $C_{18.297}H_{36.595}$ (range $C_{16}H_{32} - C_{21}H_{42}$) (4), cycloalkane $C_{22.977}H_{45.953}$ (range $C_{22}H_{44} - C_{27}H_{54}$) (5), bicycloalkane $C_{14.743}H_{27.487}$ (range $C_{10}H_{18} - C_{25}H_{48}$) (6), alkylbenzene $C_{10.207}H_{14.413}$ (range $C_8H_{10} - C_{13}H_{20}$) (7), indane or tetraline $C_{12.495}H_{16.990}$ (range $C_{10}H_{12} - C_{16}H_{24}$) (8), indane or tetraline $C_{18.615}H_{29.229}$ (range $C_{17}H_{26} - C_{22}H_{36}$) (9), naphthalene $C_{12.392}H_{12.783}$ (range $C_{10}H_8 - C_{20}H_{28}$) (10), tricycloalkane $C_{19}H_{34}$ (11).

These are the C/QC presented in Figure 4.13: alkane $C_{10.335}H_{22.670}$ (range $C_8H_{18} - C_{12}H_{26}$) (1), alkane $C_{19.380}H_{40.760}$ (range $C_{20}H_{42} - C_{23}H_{48}$) (2), cycloalkane $C_{12.562}H_{25.125}$ (range $C_{10}H_{20} - C_{15}H_{30}$) (3), cycloalkane $C_{18.297}H_{36.595}$ (range $C_{16}H_{32} - C_{21}H_{42}$) (4), cycloalkane $C_{22.977}H_{45.953}$ (range $C_{22}H_{44} - C_{27}H_{54}$) (5), bicycloalkane $C_{14.743}H_{27.487}$ (range $C_{10}H_{18} - C_{25}H_{48}$) (6), alkylbenzene $C_{10.207}H_{14.413}$ (range $C_8H_{10} - C_{13}H_{20}$) (7), indane or tetraline $C_{12.495}H_{16.990}$ (range $C_{10}H_{12} - C_{16}H_{24}$) (8), indane or tetraline $C_{18.615}H_{29.229}$ (range $C_{17}H_{26} - C_{22}H_{36}$) (9), naphthalene $C_{12.392}H_{12.783}$ (range $C_{10}H_8 - C_{20}H_{28}$) (10), tricycloalkane $C_{19}H_{34}$ (11).

As can be seen from Figure 4.13, the surface mass fractions of the lightest QCs, $C_{10.335}H_{22.670}$, $C_{10.207}H_{14.413}$, and $C_{12.495}H_{16.990}$, monotonically decrease with time, while the surface mass fraction of the heaviest QC, $C_{22.977}H_{45.953}$, monotonically increases with time. The surface mass fractions of other C/QC initially increase and then decrease with time. This behaviour of the mass fractions is similar to that shown in Figures 4.10 and 4.11 for individual components and Figure 4.12 for C/QCs in the model based on the approximation of Diesel fuel by 21 C/QC.

Plots of the mass fractions of alkylbenzene $C_{10}H_{14}$ and tricycloalkane $C_{19}H_{34}$ versus normalised distance from the droplet centre (R/R_d) at four instants of time as predicted by the model, taking into account the contributions of all 98 components, are shown in Figure 4.14. These components were chosen as typical high-volatile and low-volatile components.
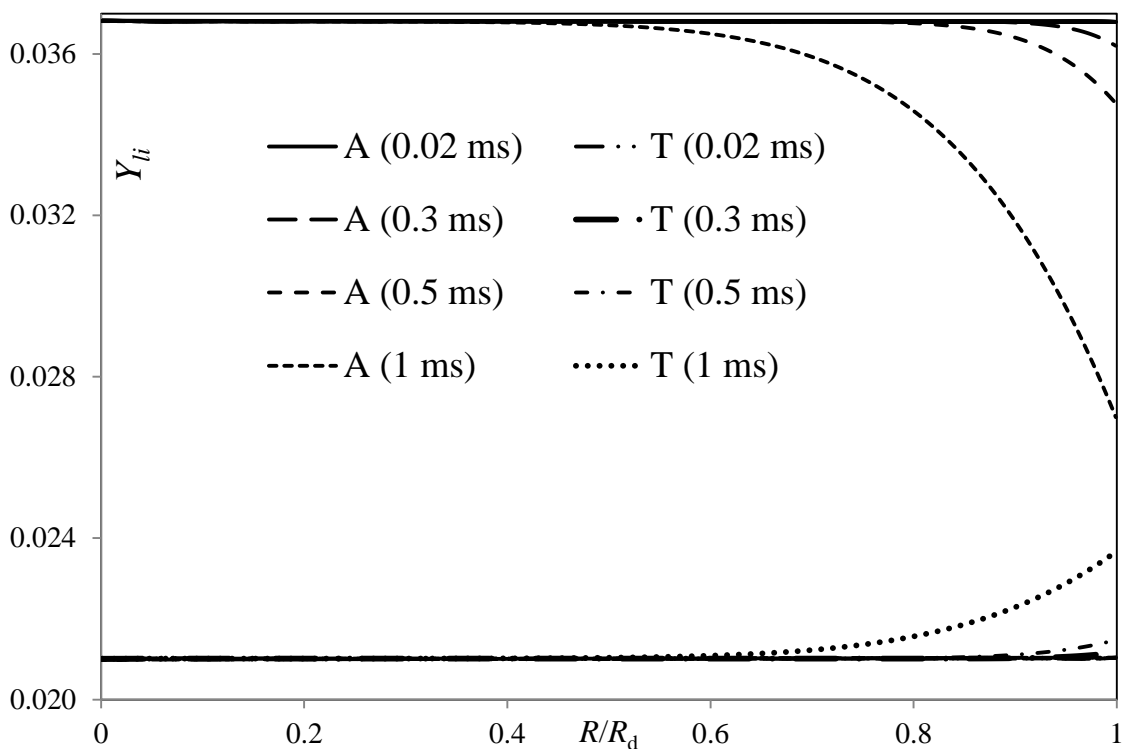
Figure 4.14 The plots of the mass fractions of alkylbenzene $C_{10}H_{14}$ (indicated as A) and tricycloalkane $C_{19}H_{34}$ (indicated as T) versus normalised distance from the droplet centre (R/R_d) at four instants of time 0.02 ms, 0.3 ms, 0.5 ms and 1 ms (indicated near the plots) as predicted by the model, taking into account the contributions of all 98 components. The same ambient conditions and model as in the case shown in Figures 4.2-4.13 were used for the analysis.

126

As can be seen from Figure 4.14, the surface mass fraction of $C_{10}H_{14}$ decreases, while the surface mass fraction of $C_{19}H_{34}$ increases with time, in agreement with the results shown in Figure 4.10. Also, these changes in the surface mass fractions of $C_{10}H_{14}$ and $C_{19}H_{34}$ lead to corresponding changes in mass fractions inside the droplets, leading to the formation of the gradients of the corresponding mass fractions. This clearly demonstrates the limitation of the Infinite Diffusivity (ID) model and the model based on the approximation of Diesel fuel with a single quasi-component, which are widely used for the analysis of Diesel fuel droplet heating and evaporation.

Plots of temperature versus normalised distance from the droplet centre (R/R_d) at four instants of time as predicted by the model, taking into account the contributions of all 98 components, are shown in Figure 4.15.
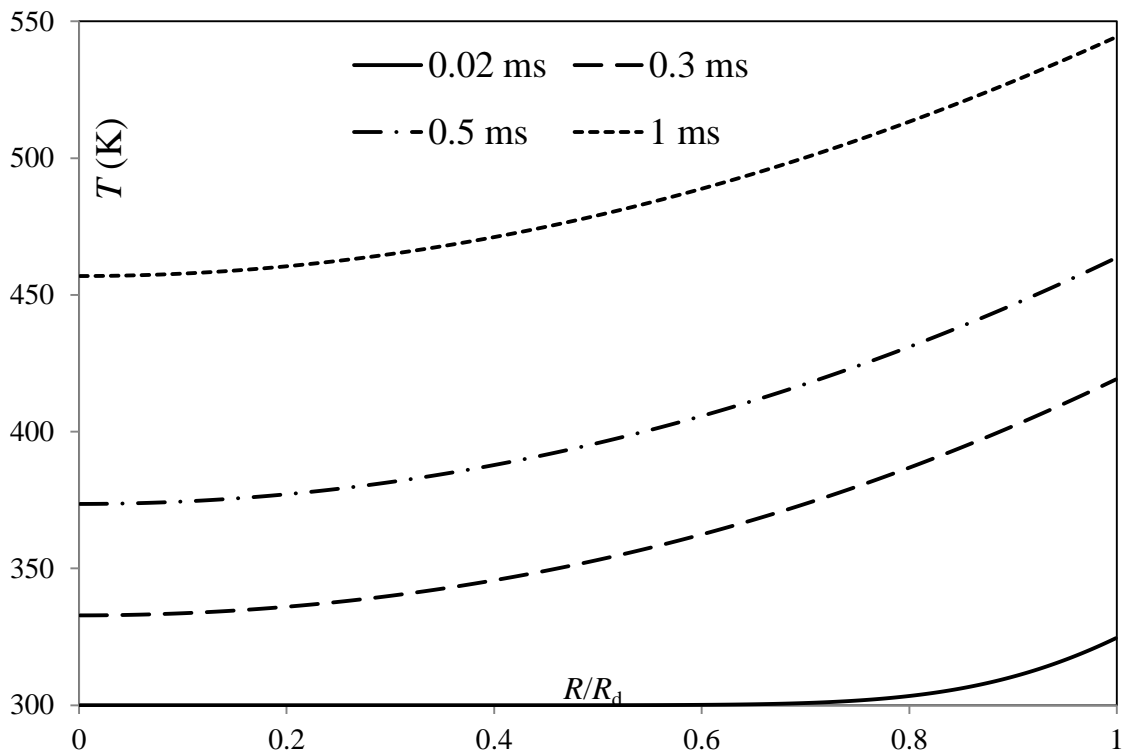
Figure 4.15 The plots of temperature versus normalised distance from the droplet centre (R/R_d) at four instants of time 0.02 ms, 0.3 ms, 0.5 ms and 1 ms (indicated near the plots) as predicted by the model, taking into account the contributions of all 98 components. The same ambient conditions and model as in the case shown in Figures 4.2-4.14 were used for the analysis.

As can be seen from Figure 4.15, temperatures throughout the droplet increase with time, and the temperature gradients can be plainly seen at all instants of time. This clearly shows the limitations of the Infinite Thermal Conductivity (ITC) model, which is widely used for the analysis of droplet heating and evaporation (see [123] and the references therein). The droplet surface temperatures predicted by this figure are the same as those shown in Figure 4.2, as expected.

Plots similar to those shown in Figure 4.14, but for the mass fractions of alkylbenzene quasi-component $C_{10.207}H_{14.413}$ (range C_8H_{10} – $C_{13}H_{20}$) and tricycloalkane $C_{19}H_{34}$, predicted by the model based on the approximation of Diesel fuel by 15 C/QC, are presented in Figure 4.16.
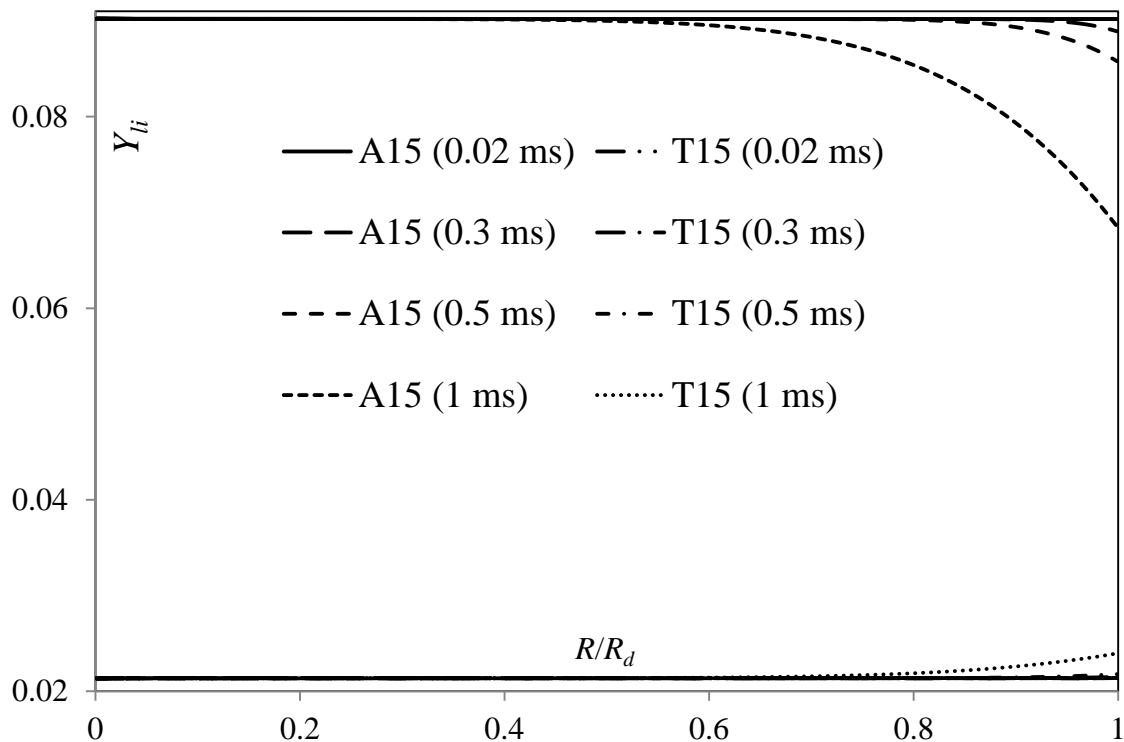
Figure 4.16 The plots of the mass fractions of alkylbenzene QC $C_{10.207}H_{14.413}$ (range $C_8H_{10} - C_{13}H_{20}$) and tricycloalkane $C_{19}H_{34}$, versus normalised distance from the droplet centre (R/R_d) at four instants of time 0.02 ms, 0.3 ms, 0.5 ms and 1 ms (indicated near the plots) as predicted by the model based on the approximation of Diesel fuel by 15 C/QC. The same ambient conditions and model as in the case shown in Figures 4.1-4.14 were used for the analysis.

The plots presented in Figures 4.14 and 4.16 show the same trends, although the mass fraction of the quasi-component $C_{10.207}H_{14.413}$ is clearly

larger than that of alkylbenzene $C_{10}H_{14}$. Plots similar to those shown in Figure 4.15, but predicted by the model based on the approximation of Diesel fuel by 15 C/QC, are presented in Figure 4.17.
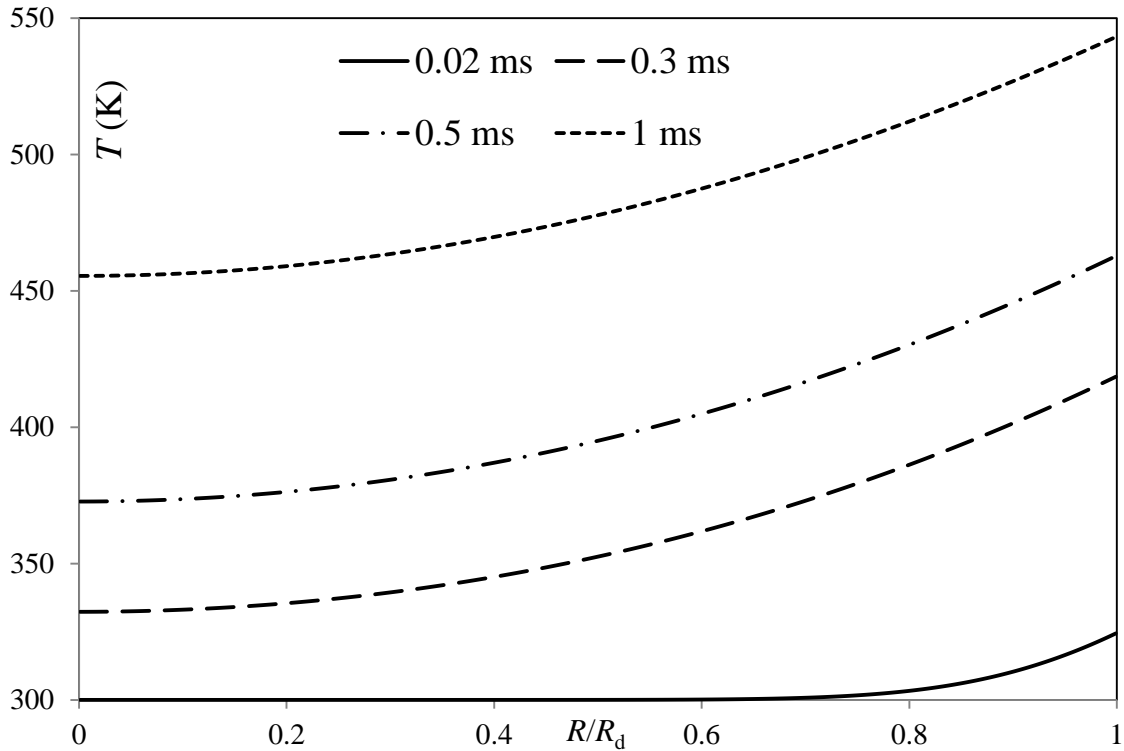
Figure 4.17 The same as Figure 4.15, but predicted by the model based on the approximation of Diesel fuel by 15 C/QC.

The trends of the plots shown in Figures 4.15 and 4.17 are rather similar; the droplet surface temperatures inferred from Figure 4.17 are the same as those inferred from Figure 4.6 as expected.

It has been noticed that the results, similar to those presented in Figures 4.16 and 4.17 for alkylbenzene QC $C_{10.207}H_{14.413}$, tricycloalkane $C_{19}H_{34}$ and temperature, but for the model based on the approximation of Diesel fuel by 21 C/QC, do not show any qualitatively new features compared with those presented in Figures 4.16 and 4.17. These plots are presented in Figures 4.18 and 4.19.
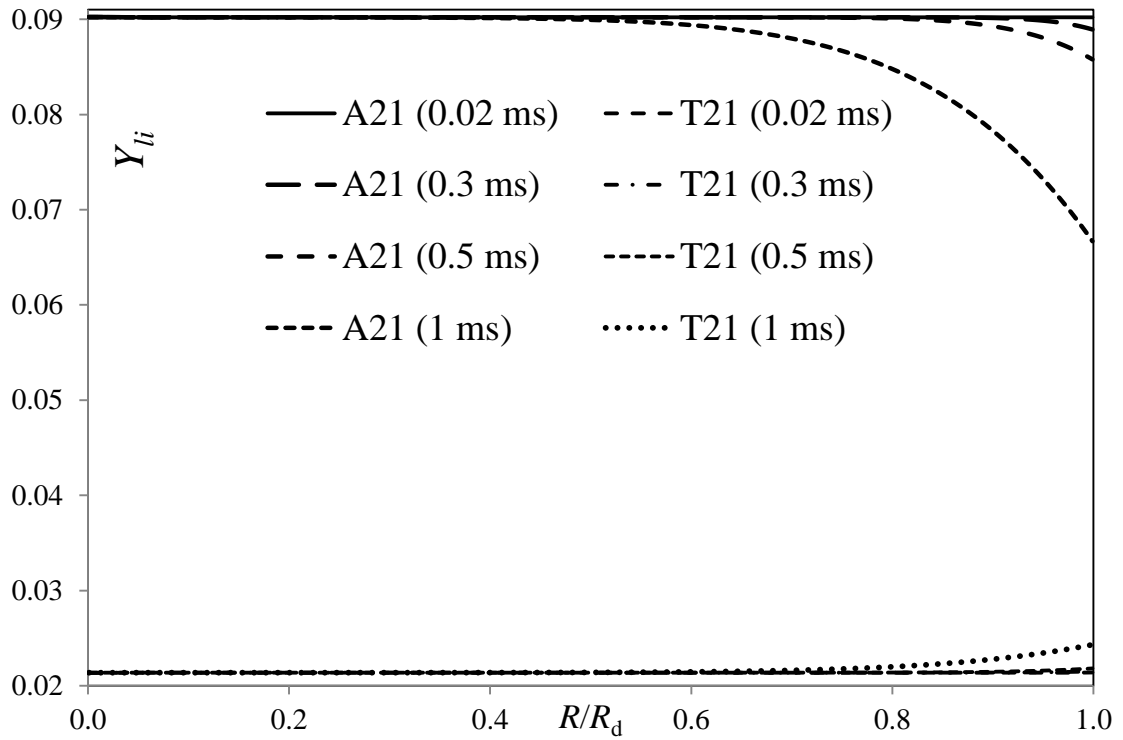
Figure 4.18 The same as in Figure 4.16, but for 21 C/QC.
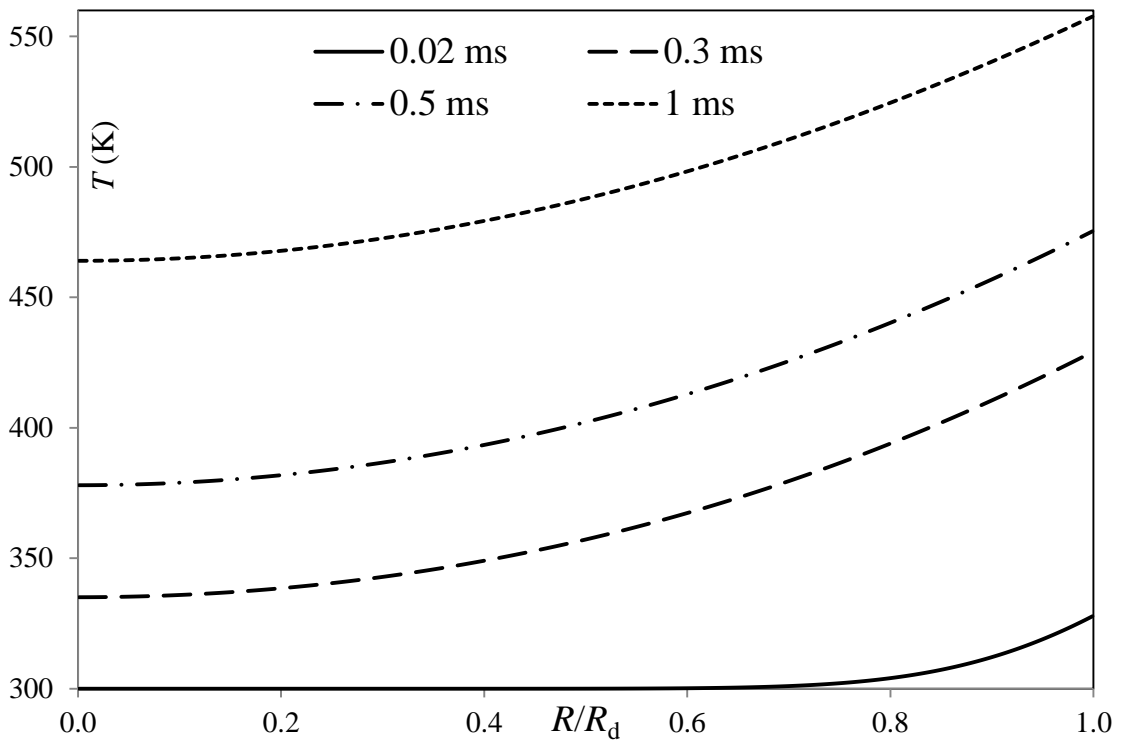
Figure 4.19 The same as in Figure 4.17, but for 21 C/QC.

The values of droplet surface temperatures T_s and radii R_d versus the number of C/QC, predicted by the ETC/ED model for stationary droplets at time instants t = 0.02 ms, t = 0.5 ms, t = 1 ms, t = 2 ms and t = 2.5 are shown in Figures 4.20-4.24.

As follows from Figures 4.20-4.24, the predictions of the models based on the approximation of Diesel fuel by about or more than 21 C/QC are reasonably close to the prediction of the model taking into account the contribution of all 98 components. The values of droplet radii at these time instants show trends similar to those observed for the surface temperatures. This is consistent with the results shown in Figures 4.8 and 4.9 for the droplet evaporation time. This confirms the previous conclusion, inferred from Figures 4.8 and 4.9, that a realistic Diesel fuel can be approximated by about 21 C/QC. Moreover, the number of these C/QC can be reduced to 15 if the errors of about 3.7% for the surface temperature and 2.5% for evaporation time can be tolerated. The errors in the estimates of T_s and R_d appear to be particularly large in the case when the number of C/QC is less than 15 at t = 2 ms.
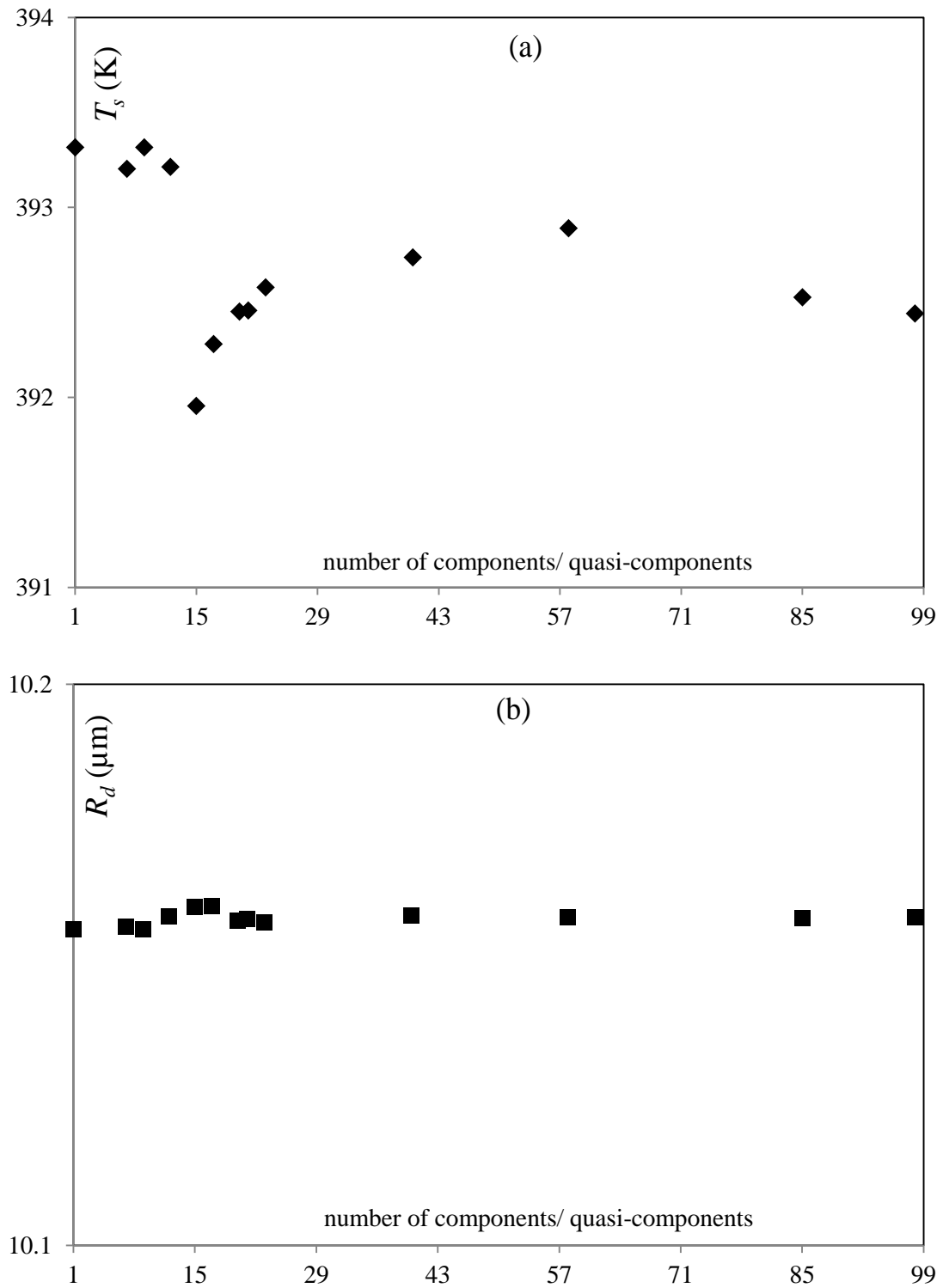
Figure 4.20 The values of droplet surface temperatures (a) and radii (b) versus the number of C/QC used for the approximation of Diesel fuel for the time instant 0.02 ms for the same conditions as in Figures 4.2-4.19.
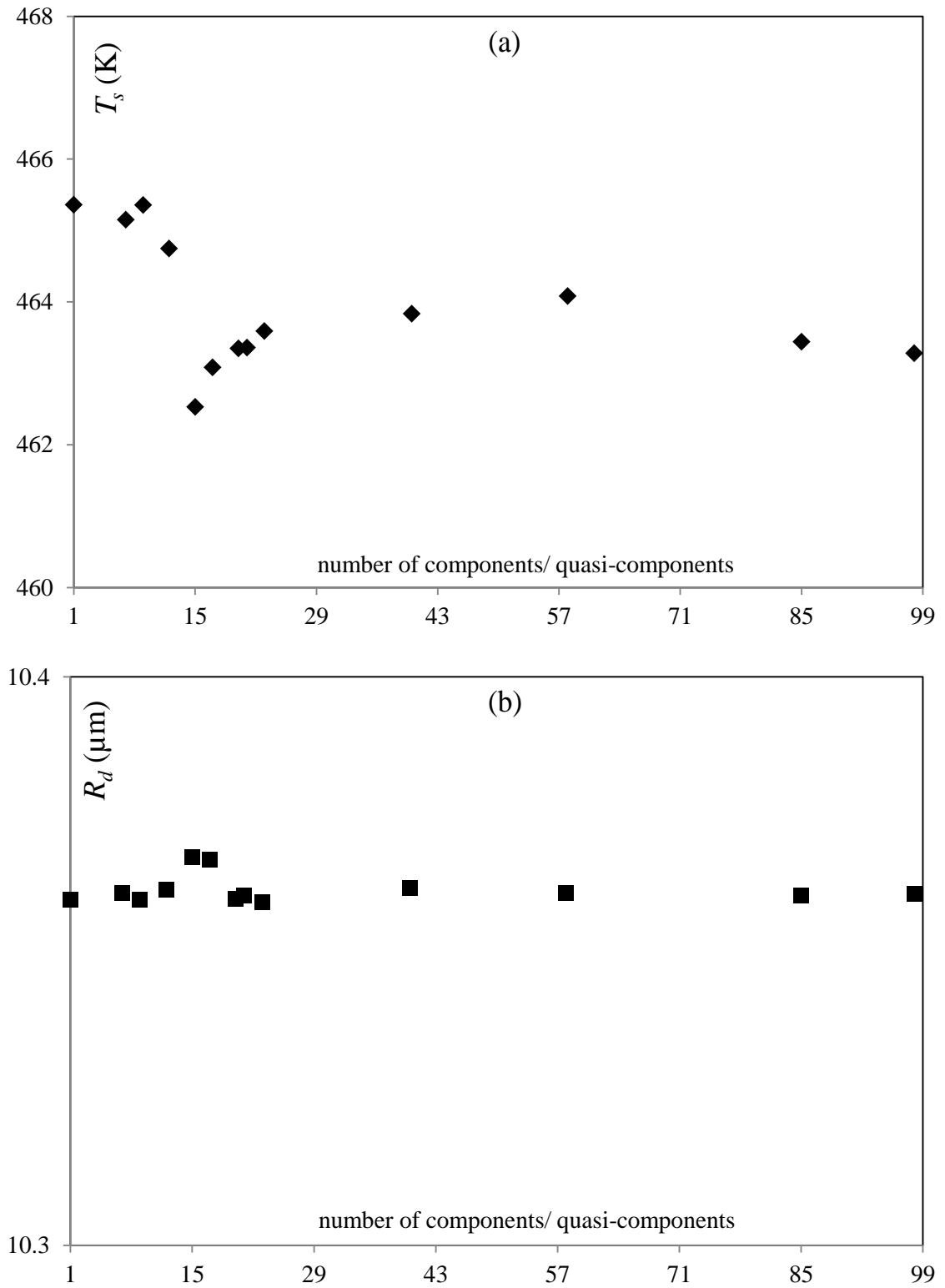
Figure 4.21 The same as Figure 4.20 but for the time instant 0.5 ms.
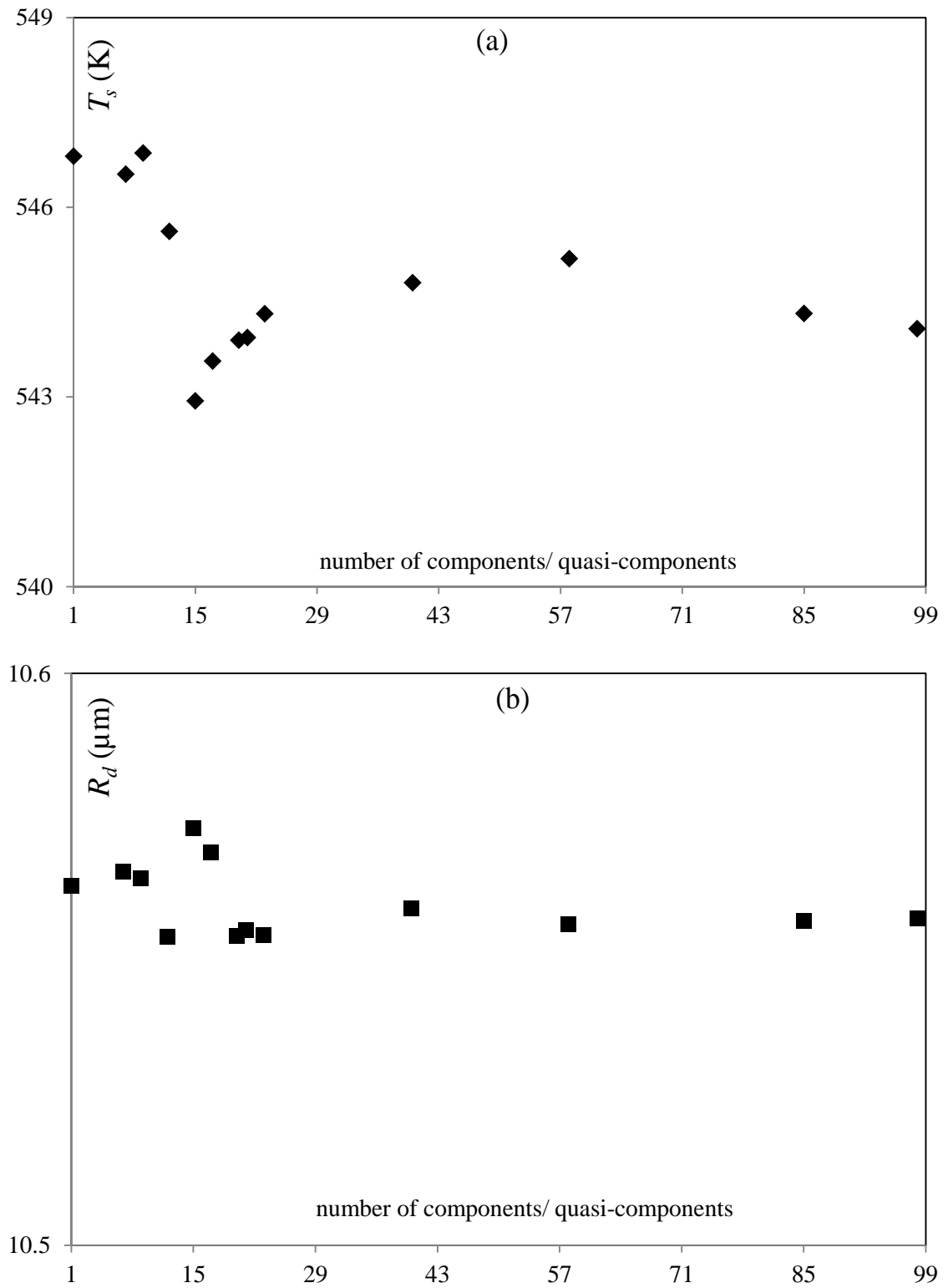
Figure 4.22 The same as Figures 4.19 and 4.21 but for the time instant 1 ms.
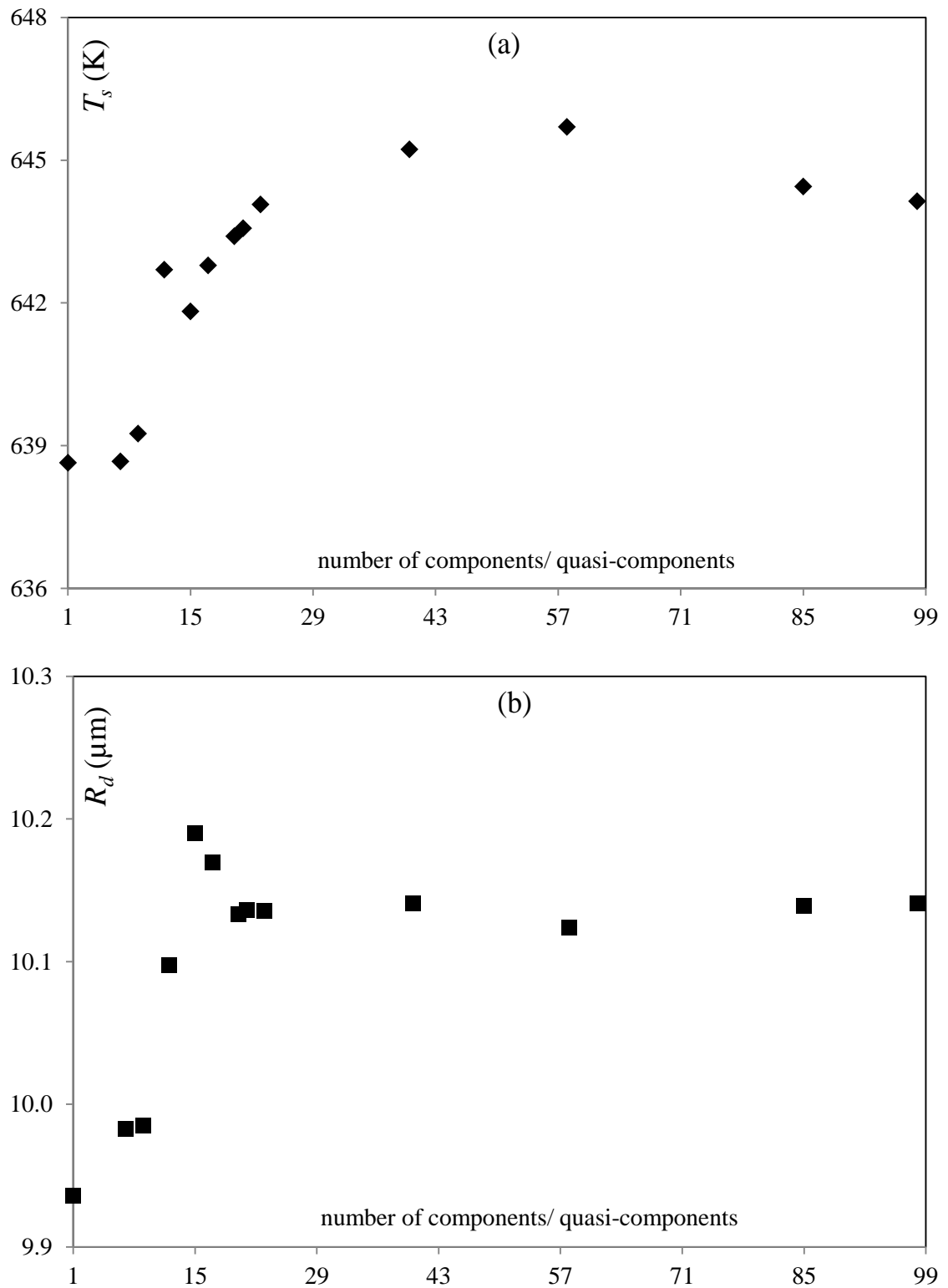
Figure 4.23 The same as Figures 4.19-4.22 but for the time instant 2 ms.
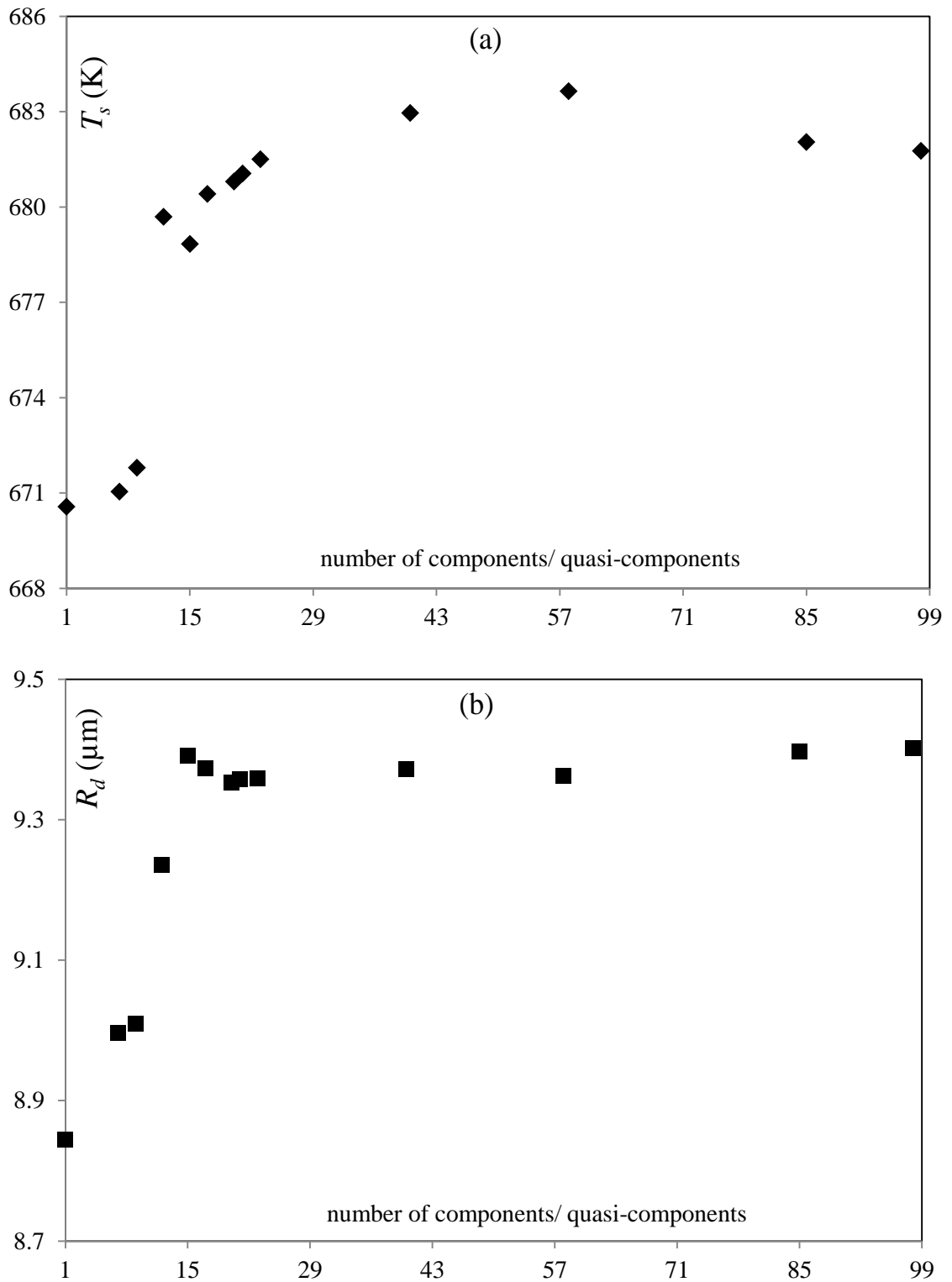
Figure 4.24 The same as Figures 4.19-4.23 but for the time instant 2.5 ms.

Note that, in contrast to the case when Diesel fuel is approximated by alkanes only (see [43], [45], [47]), in the presented case there is no clear reduction in errors observed with increasing numbers of C/QC. For example, in

the case shown in Figure 4.20, the value of the surface temperature predicted by the model based on the approximation of Diesel fuel with 58 C/QC is clearly less accurate than the value of this temperature predicted by the model based on the approximation of Diesel fuel with 21 C/QC. This can be attributed to the fact that mole fractions of components in realistic Diesel fuel cannot be approximated by a smooth function of the carbon numbers for various groups shown in Table 4.2. These errors are generally reasonably small (not more than about 26 K for surface temperatures and not more than about 1.8 μm for droplet radii) when the number of C/QC is approaching or more than 21 for the cases shown in Figures 4.20-4.24 and can be safely ignored in most practical engineering applications. These errors can increase at the very final stage of droplet evaporation, but are generally not important in engineering applications. These errors increase slightly when the number of C/QC approaches 15 (not more than 29.5 K for surface temperatures and not more than about 2.5 μm for droplet radii), but even in this case they can be tolerated in most engineering applications.

Plots similar to those shown in Figure 4.6, but for a droplet moving with velocity 10 m/s, and based on the assumptions that Diesel fuel can be approximated by 98 and 15 C/QC and a single quasi-component, are presented in Figure 4.25. In the same figure the plots calculated using the multicomponent model, based on the Infinite Thermal Conductivity/Infinite Diffusivity (ITC/ID) approach, are shown.
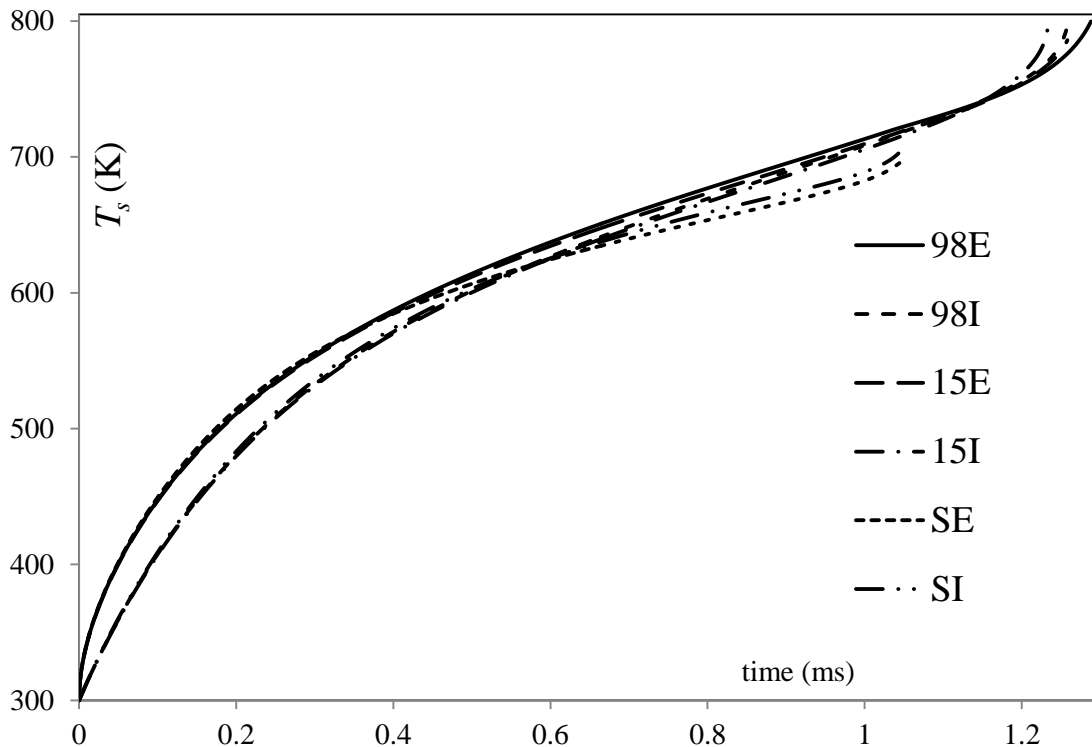
Figure 4.25 The plots of the droplet surface temperatures T_s versus time for 3 approximations of Diesel fuel composition: the contributions of all 98 components is taken into account (indicated as (98)); 15 C/QC (indicated as (15)); the contributions of all 98 components are taken into account as that of a single-component as in the case shown in Figures 4.2, 4.3 and 4.6 (indicated as (S)) for the same conditions as in Figures 4.2-4.17 except that the droplet is assumed to be moving with a velocity equal to 10 m/s and using both the Effective Thermal Conductivity/Effective Diffusivity model (indicated as E) and the Infinite Thermal Conductivity/ Infinite Diffusivity model (indicated as I).

Comparing Figures 4.6 and 4.25, one can see that moving droplets are heated up faster than stationary droplets and reach higher temperatures. Note that at the final stages of evaporation of droplets for which Diesel fuel is approximated by 98 and 15 C/QC, temperatures can approach or even exceed the critical temperatures of some components. In this case the results become less reliable. As in the cases considered in [43], [47], there are noticeable differences in the predictions based on the ETC/ED and ITC/ID models, especially for temperatures at the initial stage of droplet heating. As mentioned in [2], accurate prediction of these temperatures is particularly important for the prediction of the auto-ignition timing in Diesel engines. This brings into question the reliability of the models for heating and evaporation of Diesel fuel

droplets based on the ITC/ID approximations. These models are almost universally used for the analysis of these processes.

Plots similar to those shown in Figure 4.25, but for droplet radii are presented in Figure 4.26. Comparing Figures 4.8 and 4.26 it can be seen that moving droplets evaporate about 3 times faster than stationary droplets. Similar to the case shown in Figures 4.8 and 4.9, the model based on the approximation of Diesel fuel by a single quasi-component leads to under-prediction of the droplet evaporation time. For the case shown in Figure 4.26 this under-prediction was estimated to be about 19% for the ETC/ED model. At the same time, the evaporation time is not very sensitive to the choice of ETC/ED or ITC/ID models. In the case when Diesel fuel is approximated by 98 components, the application of the ITC/ID model leads to under-estimation of the evaporation time by only about 3%. This is consistent with the results earlier reported in [76].
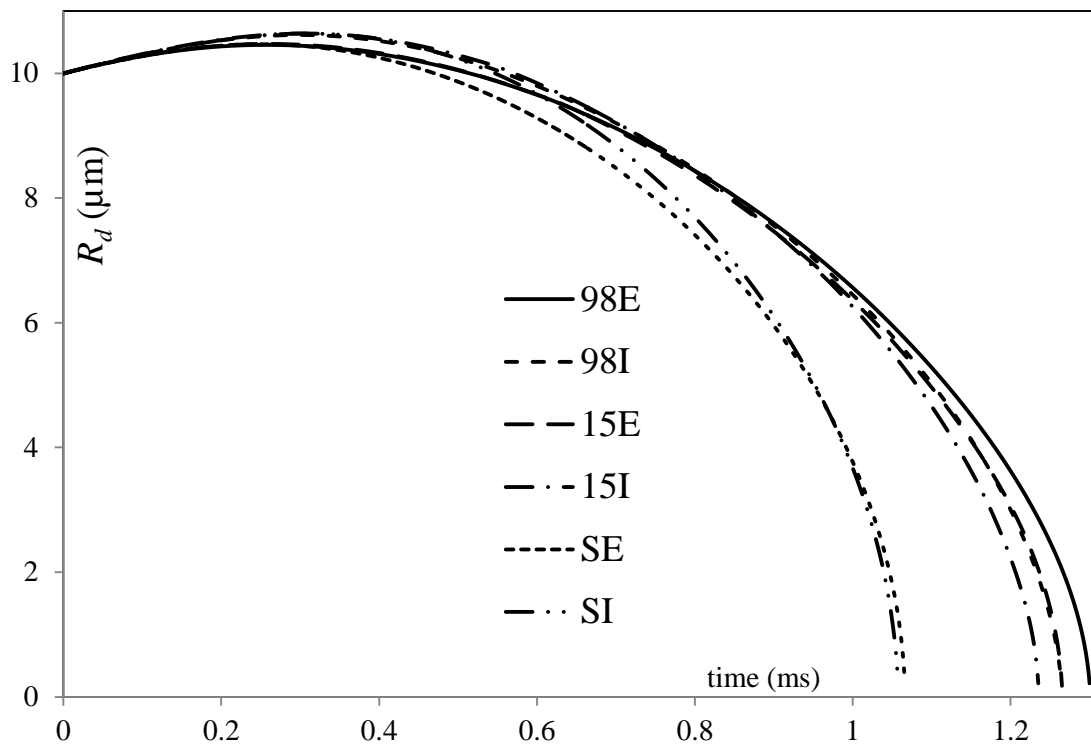
Figure 4.26 The same as Figure 4.25 but for the droplet radii R_d.

As in the case shown in Figures 4.8 and 4.9, the approximation of Diesel fuel with 15 C/QC leads to under-estimation of the evaporation time by about 2.5%

(see Figure 4.26). This confirms our earlier conclusion, based on the analysis of stationary droplets, that 15 C/QC can reasonably accurately approximate realistic Diesel fuel for the analysis of heating and evaporation of droplets.

To illustrate the computational efficiency of the new model, a diagram of CPU time, required for calculation of stationary droplet heating and evaporation with parameters specified earlier in the paper, versus the number of C/QC is shown in Figure 4.27. Intel Xeon (core duo) E8400, 3 GHz and 3 GB RAM, was used. The time step was set as 1 µs in a FORTRAN based serial code. As one can see from this figure, the CPU time of the 15 C/QC model is almost 1/6th of the CPU time needed for the 98 component model. This illustrates the efficiency of the new model.
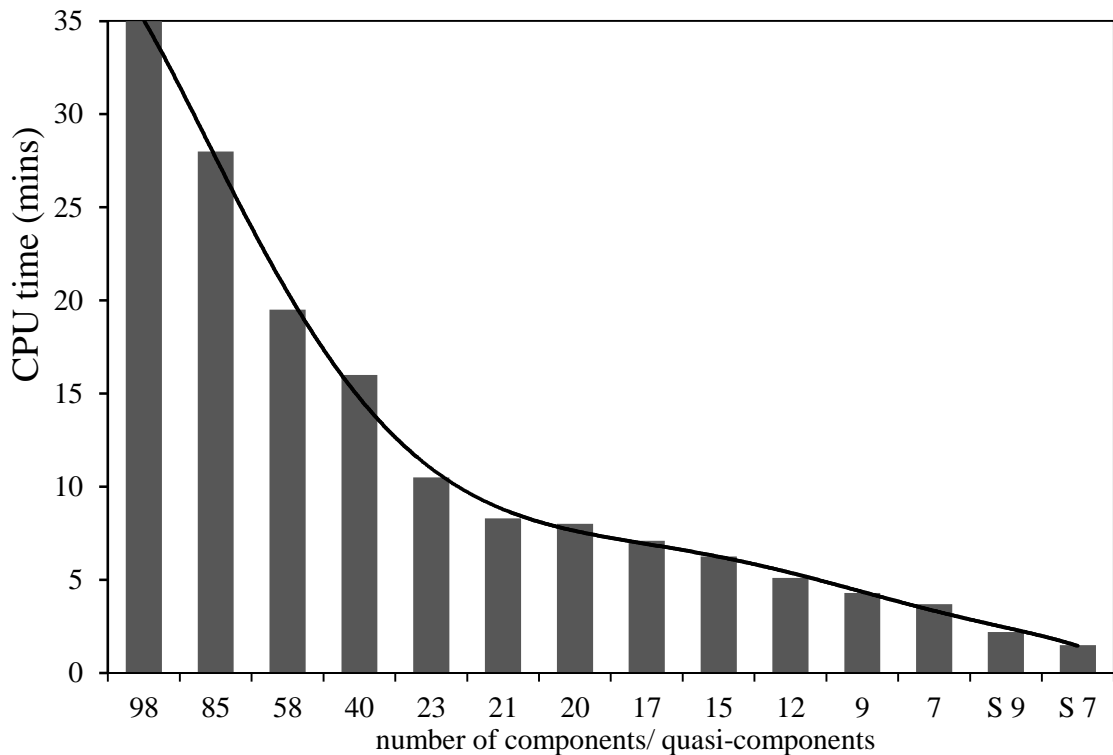
Figure 4.27 The plot of CPU time, required for calculations of stationary droplet heating and evaporation for the same parameters as in Figures 4.2-4.24, versus the number of C/QC used in the model.

4.6 Conclusions of Chapter 4

A new multi-dimensional quasi-discrete model is suggested and tested for the analysis of heating and evaporation of Diesel fuel droplets. As in the original quasi-discrete model suggested earlier, the components of Diesel fuel with close thermodynamic and transport properties are grouped together to form quasi-components. In contrast to actual components, these quasi-components are allowed to have non-integer values of carbon atoms. This, however, does not prohibit their treatment as actual components, and the modelling of the diffusion of these quasi-components inside the droplets.

In contrast to the original quasi-discrete model, the new model takes into account the contributions of various groups of hydrocarbons in Diesel fuels; quasi-components are formed within individual groups. Hence, the term 'multi-dimensional' is used to describe the new model. Also, in contrast to the original quasi-discrete model, the contribution of individual components is not approximated by the distribution function of carbon numbers. The formation of quasi-components is based on directly taking into account the contributions of individual components. Groups contributing small molar fractions to the composition of Diesel fuel (less than about 1.6%) are replaced by individual components.

The application of the new model is illustrated for one specific type of Diesel fuel, containing the following molar fractions of the groups of components: 13.6518% of n-alkanes, 26.4039% of iso-alkanes, 14.8795% of cycloalkanes, 7.6154% of bicycloalkanes, 1.5647% of tricycloalkanes, 16.1719% of alkylbenzenes, 9.1537% of indanes & tetralines, 8.6773% of naphthalenes, 1.2240% of diaromatics, and 0.6577% of phenanthrenes. Since the contributions of tricycloalkanes, diaromatics, and phenanthrenes are less than about 1.6%, they are replaced with individual components $C_{19}H_{34}$ (tricycloalkane), $C_{13}H_{12}$ (diaromatic), and $C_{14}H_{10}$ (phenanthrene). The difference between the thermodynamic and transport properties of n-alkanes and iso-alkanes is ignored and they are treated as alkanes. This led us to a simplified presentation of Diesel fuel with the following six groups: alkanes (molar fraction 40.0556%), cycloalkanes (molar fraction 14.8795%),

141

bicycloalkanes (molar fraction 7.6154%), alkylbenzenes (molar fraction 16.1719%) indanes & tetralines (molar fraction 9.1537%), and naphthalenes (molar fraction 8.6773%), and 3 components, $C_{19}H_{34}$ (molar fraction 1.5647%), $C_{13}H_{12}$ (molar fraction 1.2240%), and $C_{14}H_{10}$ (molar fraction 0.6577%).

The total number of components in the simplified approximation of Diesel fuel is equal to 98. Thermodynamic and transport properties of all these components are presented. Mixing rules are used for calculation of properties of the mixtures of the components, except for the thermal conductivity. The latter is based on the approximation of the results of experimental studies of typical Diesel fuels. Several further approximations of the above simplified approximation of Diesel fuel were considered. These include the approximation of Diesel fuel by a single quasi-component (mass fractions of all components inside the droplet do not change with time), the approximation of Diesel fuel by only alkanes, ignoring the contributions of all other components, the approximation of each of the above-mentioned six groups by single quasi-components with average values of carbon numbers (9 quasi-components and components altogether), and the approximation of each of the above-mentioned six groups by one or more quasi-components, leading to numbers between 9 and 98 quasi-components and components. All these approximations were used for the analysis of heating and evaporation of a Diesel fuel droplet in Diesel engine-like conditions.

It is pointed out that the approximation of Diesel fuel with only alkanes leads to less accurate modelling results compared with the approximation of Diesel fuel by a single quasi-component. This questions the applicability of the previously developed quasi-discrete model based on the former approximation (see [43], [45], [47]). Also, it is pointed out that the approximations of Diesel fuel by less than about 15 components/quasi-components lead to unacceptably large errors (relative to the prediction of the model, taking into account the contributions of all 98 components) in predicting droplet temperatures and evaporation times and are not recommended for practical engineering applications. The approximation of Diesel fuel by 15 components/quasi-components, leads to errors in estimated temperature and evaporation times

not exceeding about 1.6% and 2.5% respectively, which is acceptable for most engineering applications. This model requires about 1/6th CPU time compared with the model taking into account the contributions of all 98 components.

5   GASOLINE FUEL DROPLETS

5.1   Introductory comments

Gasoline is the most widely used automotive fuel [45], [56], [162], [163]. It is a middle distillate of petroleum, mainly containing C4-C12 hydrocarbons [163], [164]. Gasoline fuel droplet heating and evaporation are crucial processes leading to fuel combustion in automotive engines; hence, the accuracy of modelling of these processes is important for improving the design of these engines [7], [45], [74]. There have been several approaches to accurate modelling of fuel droplet heating and evaporation [5], [6], [43], [46], [47], [54], [57], [59], [60], [165]. In many studies, gasoline fuels have been approximated with iso-octanes (2,2,4-trimethylpentane structure) (see [166]–[168]); whilst commerical gasoline fuel generally comprise of tens of hydrocarbons [169]. A typical example of gasoline fuel composition used as Fuel for Advanced Combustion Engines (FACE) is shown in Table 5.1 (see [164] for the details of other compositions of FACE gasoline fuels).

In this chapter, the MDQD model, described in the previous chapter, is applied to the analysis of gasoline fuel droplet heating and evaporation. In contrast to the approach used in Chapter 4 (see [57], [63]), the contributions of the two groups of alkanes, n-alkanes (n-paraffin) and iso-alkanes (iso-paraffin), are considered separately, taking into account the differences in their thermodynamic and transport properties.

In the following section, the composition of FACE gasoline fuel used in the thesis is described. The main ideas of the model used in our analysis are summarised in Section 5.3. The results of calculations are presented in Section 5.4, and the main results of the chapter are summarised in Section 5.5.

5.2   Composition of gasoline fuel

Our analysis is focused on FACE gasoline fuel the composition of which is shown in Table 5.1 [162] (the unidentified components (with up to 0.087% of total molar fractions) are ignored). Data presented in this table is close to average contributions of species for several types of gasoline fuels [169].
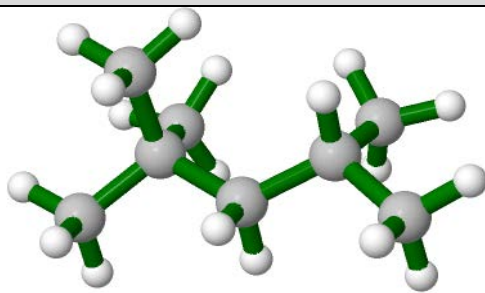
Table 5.1 The original and simplified compositions of gasoline fuel used in the analysis.
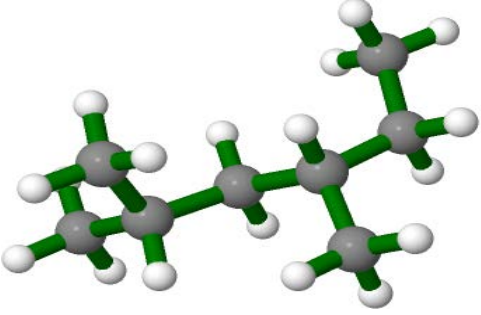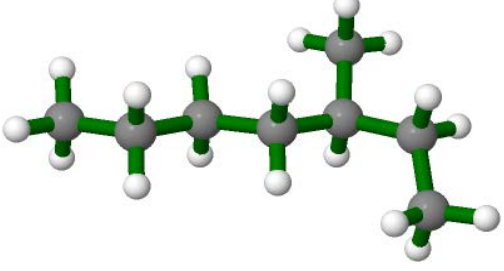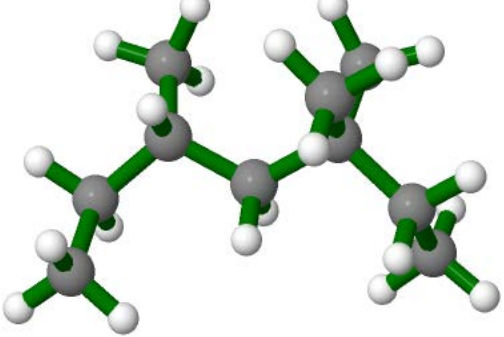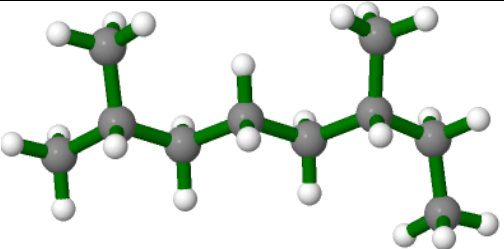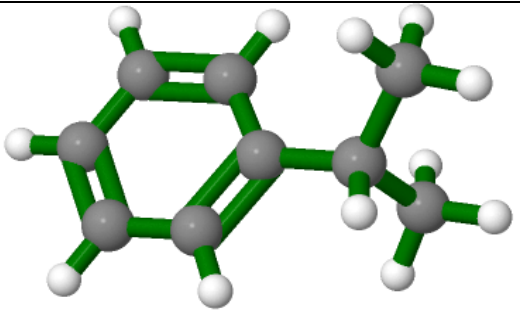
group	components	carbon numbers	molar fractions (%)	approximations	molar fractions (%)
n-alkanes	n-butane	4	3.905436784	same	3.905436784
	n-pentane	5	13.87020578	same	13.87020578
	n-hexane	6	10.84154056	same	10.84154056
	n-decane	10	0.010008808	same	0.010008808
	n-dodecane	12	0.012010569	same	0.012010569
iso-alkanes	i-butane	4	0.092081031	same	0.092081031
	2,2-dimethylpropane	5	0.012010569	averaged	7.456561774
	i-pentane	5	7.444551205		
	2,3-dimethylbutane	6	2.021779166	averaged	2.979622067
	2-methylpentane	6	0.604531988		
	3-methylpentane	6	0.353310914		
	2,4-dimethylpentane	7	4.271759148	averaged	11.66826808
	2,2,3-trimethylbutane	7	0.044038754		
	2-methylhexane	7	0.253222836		
	2,3,-dimethylpentane	7	6.883057090		
	3-methylhexane	7	0.216190247		
	2,2,4-trimethylpentane	8	23.23644807	averaged	42.17311234
	2,5-dimethylhexane	8	1.739530787		
	2,2,3-trimethylpentane	8	0.550484426		
	2,4-dimethylhexane	8	2.369084795		
	2,3,4-trimethylpentane	8	6.905076467		
	2,3,3-trimethylpentane	8	4.947353671		
	2,3-dimethylhexane	8	1.888662023		
	2-methyl-3-ethylpentane	8	0.068059893		
	2-methylheptane	8	0.060052847		
	4-methylheptane	8	0.021018496		
	3-methyl-3-ethylpentane	8	0.152133878		
	3,4-dimethylhexane	8	0.175154136		
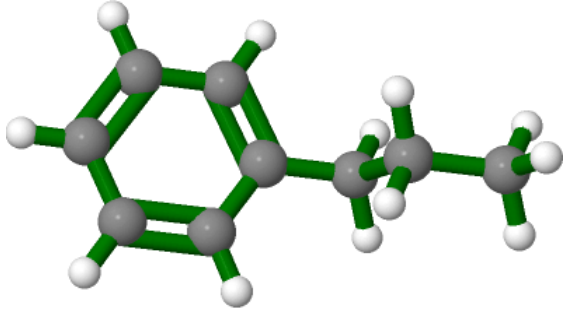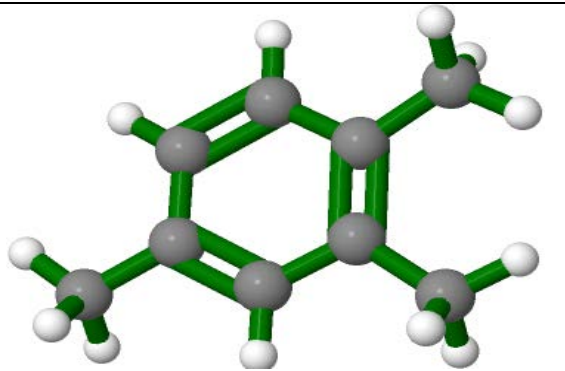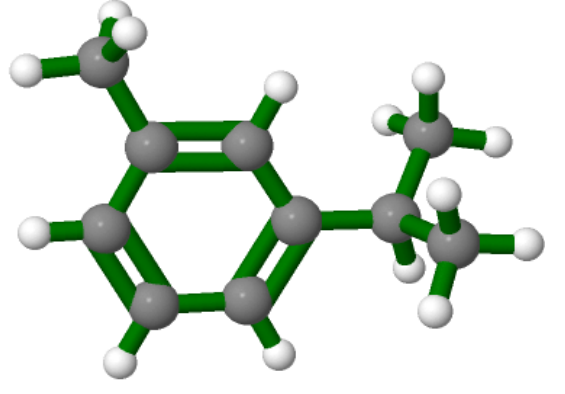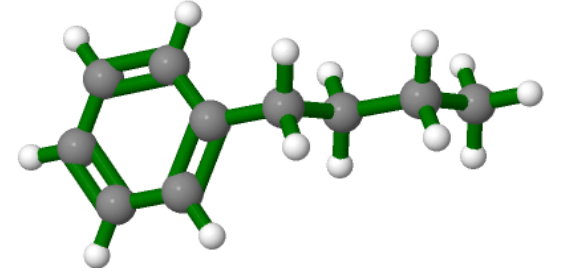
group	components	carbon numbers	molar fractions (%)	approximations	molar fractions (%)
	3-methylheptane	8	0.060052847		
	2,3,4-trimethylhexane	9	0.179157659		
	2,2,3-trimethylhexane	9	0.02602290	averaged	0.317279206
	2,5-dimethylheptane	9	0.069060773		
	2,3,-dimethylheptane	9	0.043037873		
	c10 - isoparaffin-1	10	0.025022019		
	c10 - isoparaffin-2	10	0.128112739		
	3,3,5-trimethylheptane	10	0.096084554		
	2,3,6-trimethylheptane	10	0.05204580	averaged	0.360317079
	c10 - isoparaffin-1	10	0.016014092		
	2,6-dimethyloctane	10	0.029025542		
	c10 - isoparaffin-7	10	0.014012331		
	2,3,3,trimethyloctane	11	0.012010569		
	2,5-dimethylnonane	11	0.081071343	averaged	0.113099528
	3-ethylnonane	11	0.020017616		
aromatics	o-xylene	8	0.242213148	same	0.242213148
	i-propylbenzene	9	0.046040516		
	n-propylbenzene	9	0.172151493		
	3-ethyl-1-methylbenzene	9	0.621546961		
	4-ethyl-1-methylbenzene	9	0.287252782	averaged	3.521098567
	1,3,5-trimethylbenzene	9	0.383337337		
	2-ethyl-1-methylbenzene	9	0.462406918		
	1,2,4-trimethylbenzene	9	1.304147650		
	1,2,3-trimethylbenzene	9	0.244214909		
	sec-butylbenzene	10	0.012010569		
	3-isopropyl-1-	10	0.033029066		
	4-isopropyl-1-	10	0.009007927		
	1,3-diethylbenzene	10	0.030026423		
	3-propyl-1-methylbenzene	10	0.080070462		
	4-propyl-1-methylbenzene	10	0.035030827		
	n-butylbenzene	10	0.016014092	averaged	0.440387541
	5-ethyl-1,3-dimethylbenzene	10	0.059051966		
	2-propyl-1-methylbenzene	10	0.021018496		
	2-ethyl-1,4-dimethylbenzene	10	0.038033469		
	4-ethyl-1,3-dimethylbenzene	10	0.033029066		
	4-ethyl-1,2-dimethylbenzene	10	0.059051966		
	3-ethyl-1,2-dimethylbenzene	10	0.015013212		
	4-isoproyl-1-ethylbenzene	11	0.023020258	averaged	0.055048443
	1-butyl-1-methylbenzene	11	0.032028185		

group	components	carbon numbers	molar fractions (%)	approximations	molar fractions (%)
indanes/ naphthalenes	5-methylindan	10	0.010008808	indane (C_9H_{10})	0.104091601
	2-methylindan	10	0.009007927		
	naphthalene	10	0.019016735		
	indane (indenes)	9	0.066058131		
cycloalkanes	3c-ethylmethylcyclopentane	8	1.345183762	3c-ethyl-methyl-cyclopentane (C_8H_{16})	1.491312355
	1,1,methylethylcyclopentane	8	0.022019377		
	c8 - mononaph - 3	8	0.060052847		
	methylcycloheptane	8	0.046040516		
	1-methyl-2-	10	0.018015854		
olefins	1-pentene	5	0.046040516	1-nonene (C_9H_{18})	0.346304748
	c-pentene-2	5	0.016014092		
	1-hexene	6	0.007006165		
	1-nonene	9	0.195171751		
	(z) 2-decene	10	0.056049323		
	3-ethyl-2-methyl-2-heptene	10	0.013011450		
	c-10-isoolefin-9	10	0.013011450		

Some components shown in Table 5.1 have similar carbon numbers, chemical formulae and very close thermodynamic and transport properties. The main differences between these components are in their molecular structures, as illustrated for some molecules in Figure 5.1. This allows us to replace these groups of similar components with single components (with averaged properties, based on averaged molar weights; or the ones with the highest molar contributions in the groups with molar fractions up to 1.5%); see the penultimate column in Table 5.1.

component	Structure	Shape
iso-octane (C_8H_{18})	2,2,4-trimethylpentane	

component	Structure	Shape
iso-decane ($C_{10}H_{22}$)	2,4-dimethylhexane	
	3-methylheptane	
	3,3,5-trimethylheptane	
	2,6-dimethyloctane	
C_9H_{12}	i-propylbenzene,	

component	Structure	Shape
C$_{10}$H$_{14}$	n-propylbenzene	
	1,2,4-trimethylbenzene	
	3-isopropyl-1-methylbenzene	
	n-butylbenzene	
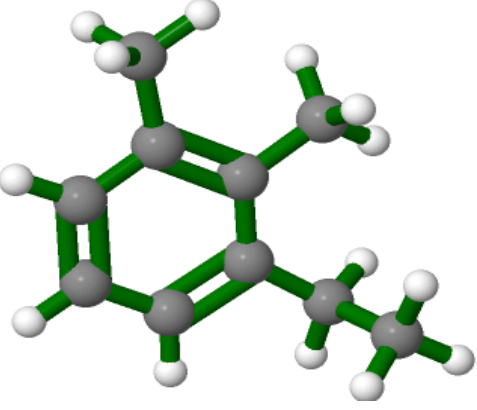
component	Structure	Shape
	3-ethyl-1,2-dimethylbenzene	

Figure 5.1 The structures of some organic components of gasoline fuel, generated using software described in [170].

This approach allows us to reduce the number of species in gasoline fuel to 20 components. These components are allocated to 3 groups, n-alkanes (5 components), iso-alkanes (8 components), and aromatics (4 components); and 3 components approximating groups with small molar fractions (indanes/naphthalenes, cycloalkanes and olefins). Molar fractions of these groups and components are shown in Table 5.2.

5.3   The model

As with Diesel fuel droplets (Chapter 4), following [6], [9], [25], [46], [55], [57], the analyses are based on the assumption that droplets are spherically symmetric, temperature gradient and species diffusions in the liquid phase and the effect of internal recirculation due to relative velocity between ambient gas and droplets are taken into account. The interaction effect of coupling between ambient gas and droplets are ignored.

The previously developed multi-dimensional quasi-discrete (MDQD) model, in which the actual composition of fuel is reduced to a much smaller number of representative components/quasi-components (C/QC), is used in this analysis. In this model, the effects of finite liquid thermal conductivity, C/QC diffusivity and recirculation are taken into account using the Effective Thermal Conductivity and Effective Diffusivity (ETC/ED) models. The analyses are based

on the previously obtained analytical solutions to the heat transfer and species diffusion equations within droplets (see [5], [7], [70], [76]). In contrast to [57], [63], where the MDQD model was applied to 9 groups of components, our analysis is focused on 6 groups (shown in Table 5.2). Three of these groups are approximated by single components, while QC are generated for three remaining groups of alkanes: n-alkanes (n-paraffins), iso-alkanes (i-paraffins) and aromatics.

Similarly to Equations 4.8 (Chapter 4), for each group m ($m = 1$ to 3), the values of carbon numbers $\bar{n}_{jm}$ for QC can be introduced, as in System (4.8).

Table 5.2 The groups of component of gasoline fuel, their molar fractions, and the numbers of components in the groups, as inferred from Table 5.1.

m	group	molar fractions (%)	number of components
1	n-alkanes	28.73	5
2	iso-alkanes	65.07	8
3	aromatics	4.26	4
4	indanes/naphthalenes	0.10	1
5	cycloalkanes	0.49	1
6	olefins	0.35	1

As in Chapter 3, the molar fractions of quasi-components are estimated based on System (4.9). The mixtures are treated as ideal (Raoult's law is assumed to be valid, see Equations 2.46-2.52 in Section 2.8). The thermodynamic and transport properties of gasoline fuel components are calculated as shown in Appendix D.

As assumed in our previous studies (eg. [43], [47], [55], [57]), gasoline fuel vapour diffuses from the surface of the droplet, without changing its composition, based on averaged binary diffusion of fuel into dry air. The gasoline fuel vapour can be replaced with the vapour of iso-octane; the binary diffusion coefficient can be estimated using the following expression [171]:

$$D_{va} = (A + B\,T + C\,T^2) \times 10^{-4} \ (\text{m}^2 \ \text{s}^{-1}), \tag{5.1}$$

where $A = -0.0578$, $B = 3.0455E - 4$ and $C = 3.4265E - 7$, which depend on the type of hydrocarbons, and T is vapor temperature in the vicinity of the droplet.

The results of calculations, using the above-described model, will be compared to the predictions of simplified models based on the assumptions that liquid thermal conductivity is infinitely high (Infinite Thermal Conductivity (ITC) model) and liquid species diffusivity is infinitely high (Infinite Diffusivity (ID) model) or infinitely small (Single Component (SI) model).

5.4 Results

The initial modelling parameters were determined from a set of experimental data of fuel droplets and gas velocity measured in an optically accessed, direct injection research engine, at part and full load, engine-like conditions at an engine speed of 1000 rpm. The axial velocity component of the fuel droplets and gas seeding particles (up to the instance of fuel injection) in the axial direction of the cylinder, at locations along the axis of the fuel injector, were recorded with respect to time using the Phase and Laser Doppler Anemometry techniques. The fuel droplet size distributions were measured from the start of fuel injection. The results applicable to the model were selected for a part load engine case, whereby fuel injection occurred during the late stages of the compression stroke. The fuel droplet data was ensemble-averaged within the first crank angle interval, immediately following the start of fuel injection, that contained at least 50 measurement records. The mean diameter of droplets at the initial stage of evaporation is taken equal to 24 µm, their axial velocity component and initial temperatures are assumed equal to U_{drop}= 20 m/s and T_d = 296 K, respectively, air axial velocity component (at the instance prior to fuel injection) is assumed equal to U_{air}= -4 m/s (leading to a relative droplet axial velocity component of 24 m/s), ambient air (gas) pressure and temperature are assumed equal to p_g = 9 bar and T_g = 545 K, respectively.

The plots of the droplet surface temperatures T_s and radii R_d versus time are presented in Figure 5.2. Four cases are shown in Figure 5.2: (1) the contributions of all 20 components are taken into account using the ETC/ED model (indicated as (ME)); (2) the contributions of 20 components are taken into account using the ITC/ID model (indicated as (MI)); (3) the thermodynamic and transport properties of 20 components are averaged to form a single component and temperature gradient is ignored (ITC model) (indicated as (SI)); and (4) the ITC model in which gasoline fuel is approximated with iso-octane (2,2,4-trimethylpentane) is used (indicated as (IO)).
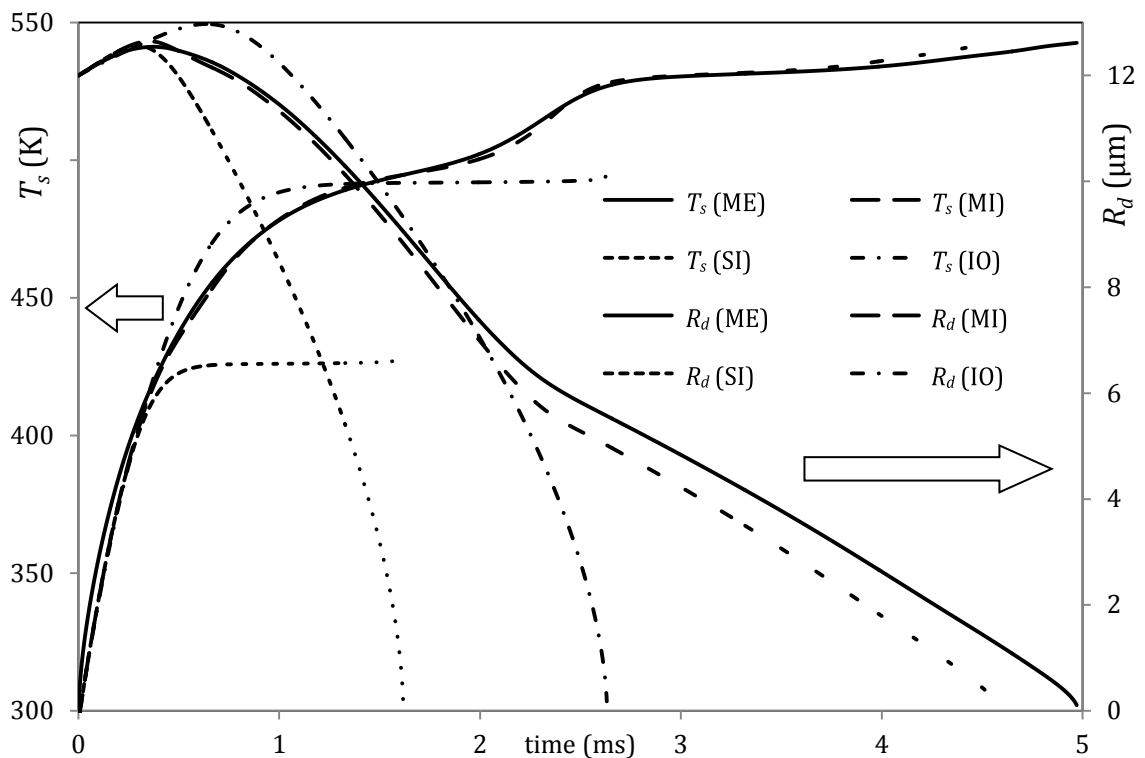
Figure 5.2 The droplet surface temperatures T_s and radii R_d versus time for the cases when 1) the contributions of all 20 components are taken into account using the ETC/ED model (ME); 2) the contribution of 20 components are taken into account using the ITC/ID model (MI), 3) the 20 component are approximated by a single component with average thermodynamic and transport properties in combination with the ITC model (SI); 4) gasoline fuel is approximated by iso-octane in combination with the ITC model (IO). The droplet with the initial radius 12 μm and initial homogeneous temperature 296 K is assumed to be moving with relative velocity 24 $m\,s^{-1}$ in air. Ambient pressure and temperature are equal to 0.9 MPa and 545 K respectively.

As one can see from Figure 5.2, the errors in droplet surface temperatures and evaporation times predicted by the SI model, compared to ME model, are 13.6% and 67.5% respectively. For the IO model these errors reduce to 6.3% and 47.1%, respectively, and reduce further to 4.8% and 8%, respectively, when the MI model was used. Although the accuracy of the latter model might be acceptable in some engineering applications, this model cannot describe adequately the underlying physics of the processes inside droplets (heat conduction and species diffusion) as demonstrated later in this section.

The same plots as in Figure 5.2, but for the cases when 20 components of gasoline fuel are approximated by 15 (3 C/QC of n-alkanes, 6 C/QC of iso-alkanes, 3 C/QC of aromatics, and 3 components representing Groups 4-6; see Table 5.2), 11 (2 C/QC of n-alkanes, 4 C/QC of iso-alkanes, 2 C/QC of aromatics, and 3 charecteristic components representing Groups 4-6) and 7 (2 QC of alkanes, 3 QC of iso-alkanes, and 2 QC of aromatics) C/QC, using the ETC/ED model are shown in Figure 5.3.
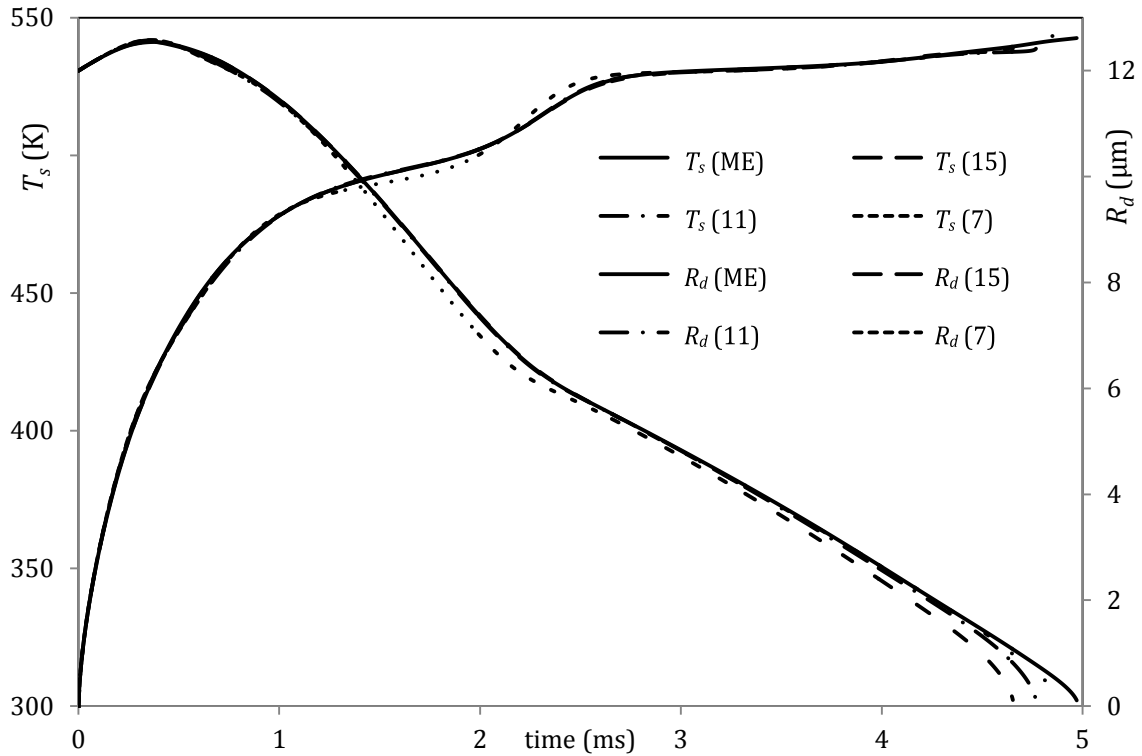
Figure 5.3 The same as Figure 5.2 but for the cases when the ETC/ED model was used taking into account the contributions of all 20 components of gasoline fuel (indicated as ME) and assuming that these components are approximated by 15, 11 and 7 C/QC (numbers are indicated near the plots).

As can be seen in Figure 5.3, the errors in surface temperatures and evaporation times predicted by the model using 15 C/QC are 0.3% and 1.3%, respectively. These errors increase to 0.5% and 4%, respectively, when gasoline fuel is approximated by 11 C/QC, and further increase to 0.8% and 6.4%, respectively, when gasoline fuel is approximated by 7 C/QC. Even in the latter case, however, these errors can be tolerated in some engineering applications. The accuracy of this model is better compared with the accuracy of the MI model, and it describes adequately the underlying physics of the processes in droplets.

The same plots as in Figure 5.3 but for the cases when 20 components of gasoline fuel are approximated by 6 (2 QC of n-alkanes, 2 QC of iso-alkanes, and 2 QC of aromatics), 5 (2 QC of n-alkanes, 1 QC of iso-alkane, and 2 QC of aromatics), 4 (1 QC of n-alkanes, 1 QC of iso-alkanes, and 2 QC of aromatics) and

3   (1 QC of n-alkanes, 1 QC of iso-alkanes, and 1 QC of aromatics) C/QC, using the ETC/ED model are shown in Figures 5.4 and 5.5.
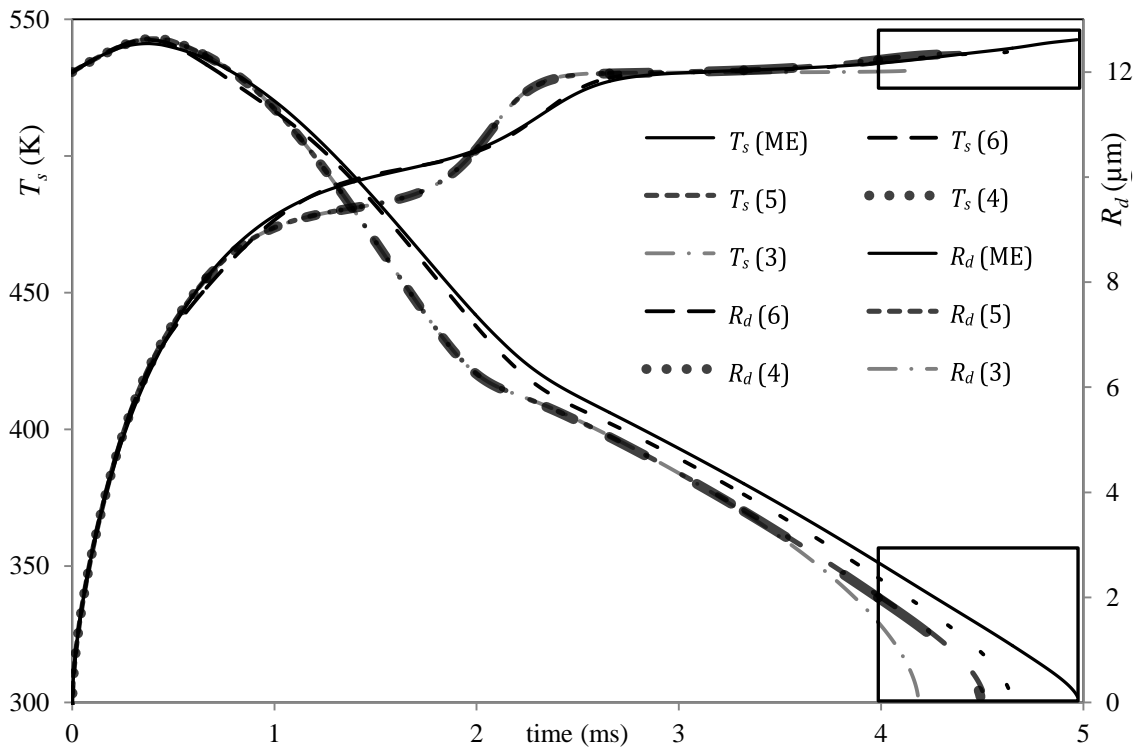
Figure 5.4 The same as Figure 5.3 but for the cases when 20 components of gasoline fuel (ME) are approximated by 6, 5, 4 and 3 C/QC.
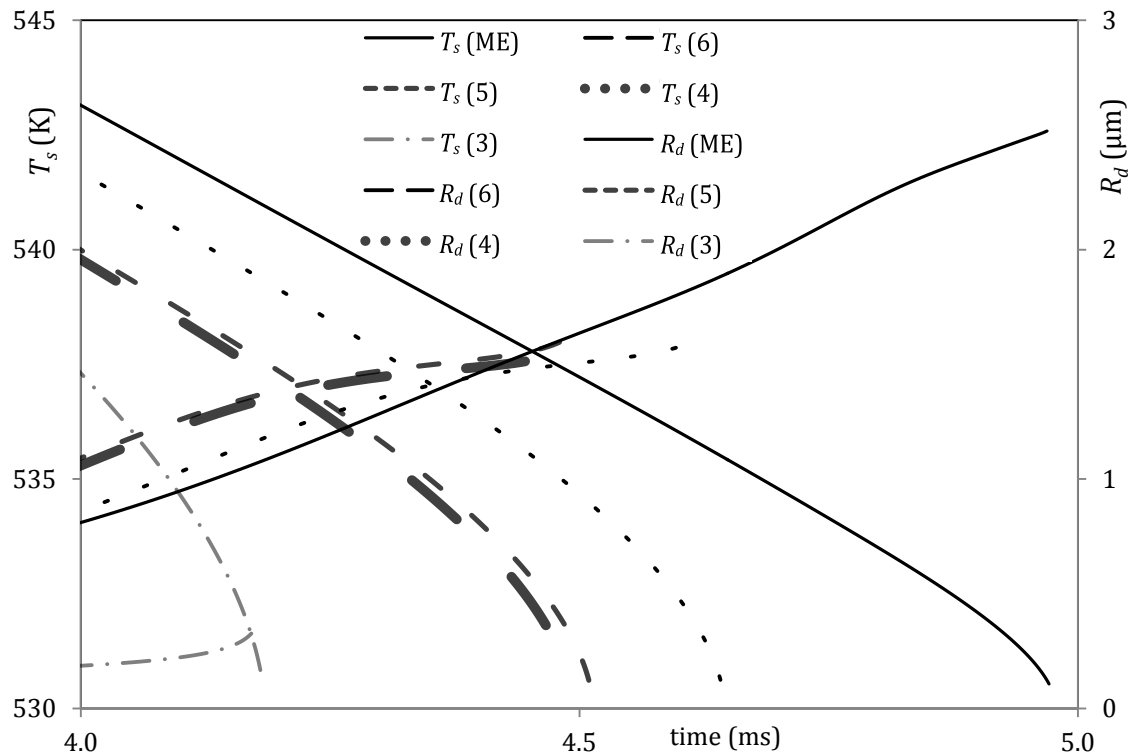
Figure 5.5 The zoomed parts of Figure 5.4.

As can be seen in Figures 5.4 and 5.5, the errors in surface temperatures and evaporation times predicted by the model using 6 C/QC are 0.8% and 6.6%, respectively. These errors increase to 2.3% and 9.3%, respectively, when gasoline fuel is approximated by 5 C/QC, and further increase to 2.3% and 9.7%, respectively, when gasoline fuel is approximated by 4 C/QC, and to 2.4% and 15.8%, respectively, when gasoline fuel is approximated by 3 QC. In the latter 3 cases, these errors are larger than those for the MI model and cannot be tolerated in most engineering applications.

The mass fractions of several components, selected out of 20 components, at the surface of the droplet versus time for the same conditions as in Figures 5.2-5.5, are shown in Figure 5.6.
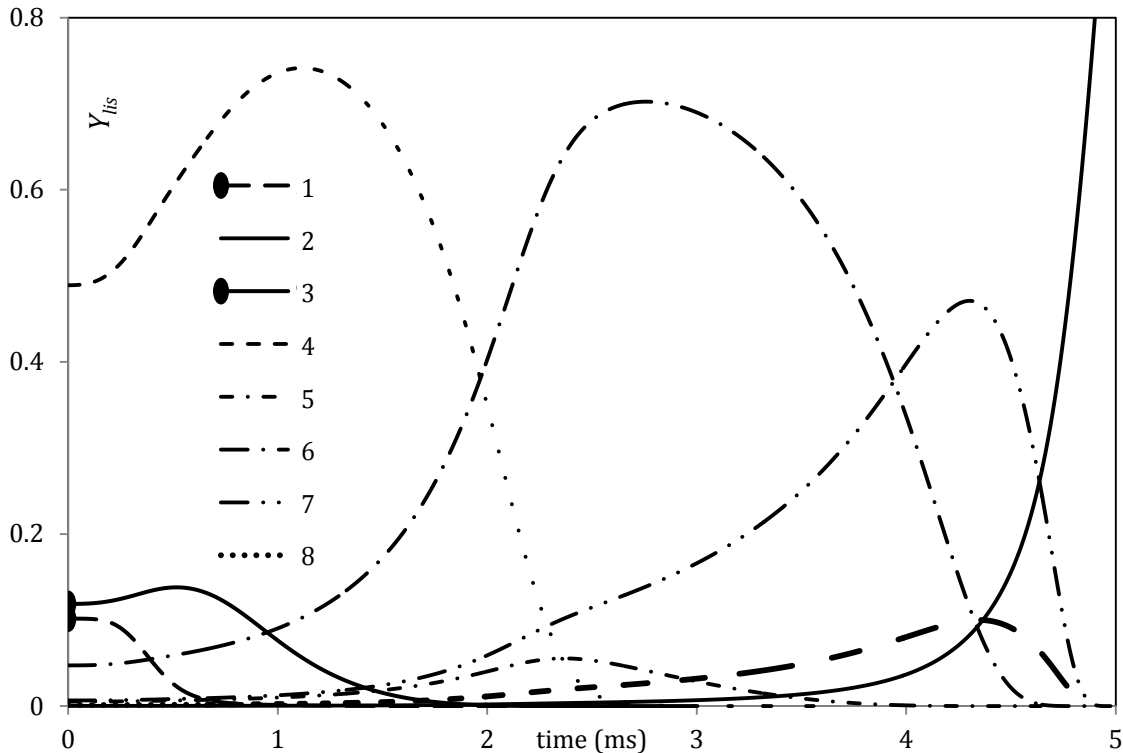
Figure 5.6 The surface mass fractions Y_{lis} versus time for C_5H_{12} (1), $C_{12}H_{26}$ (2), iso $- C_7H_{16}$ (3), iso $- C_8H_{18}$ (4), iso $- C_{10}H_{22}$ (5), C_9H_{12} (6), $C_{10}H_{14}$ (7) and indane C_9H_{10} (appproximation for indanes/naphthenes) (8), predicted by the ETC/ED model taking into account the contributions of all 20 components of gasoline fuel.

As can be seen from Figure 5.6, the surface mass fraction of the heaviest component, $C_{12}H_{26}$, increases with time at the expense of the surface mass fractions of the light components, C_5H_{12} and C_7H_{16}, which decrease with time; the mass fractions of intermediate components first increase and then decrease with time. This behaviour is similar to the one observed for the components in Diesel fuel droplets [13].

Mass fractions of n-pentane C_5H_{12} and propylbenzene C_9H_{12} versus normalised distance from the centre of droplet (R/R_d) at four time instants, 0.02 ms, 0.3 ms, 0.5 ms and 1 ms are shown in Figure 5.7. As can be seen from this figure, the decrease of mass fraction of n-pentane with time at the surface of the droplet leads to the generation of n-pentane mass fraction gradient in the body of the droplet. This, in its turn, leads to n-pentane diffusion from the centre of the droplet to its surface. Similarly, the increase of mass fraction of propylbenzene with time at the surface of the droplets leads to the generation

of propylbenzene negative mass fraction gradient in the body of the droplet and to propylbenzene diffusion from the surface of the droplet to its centre.
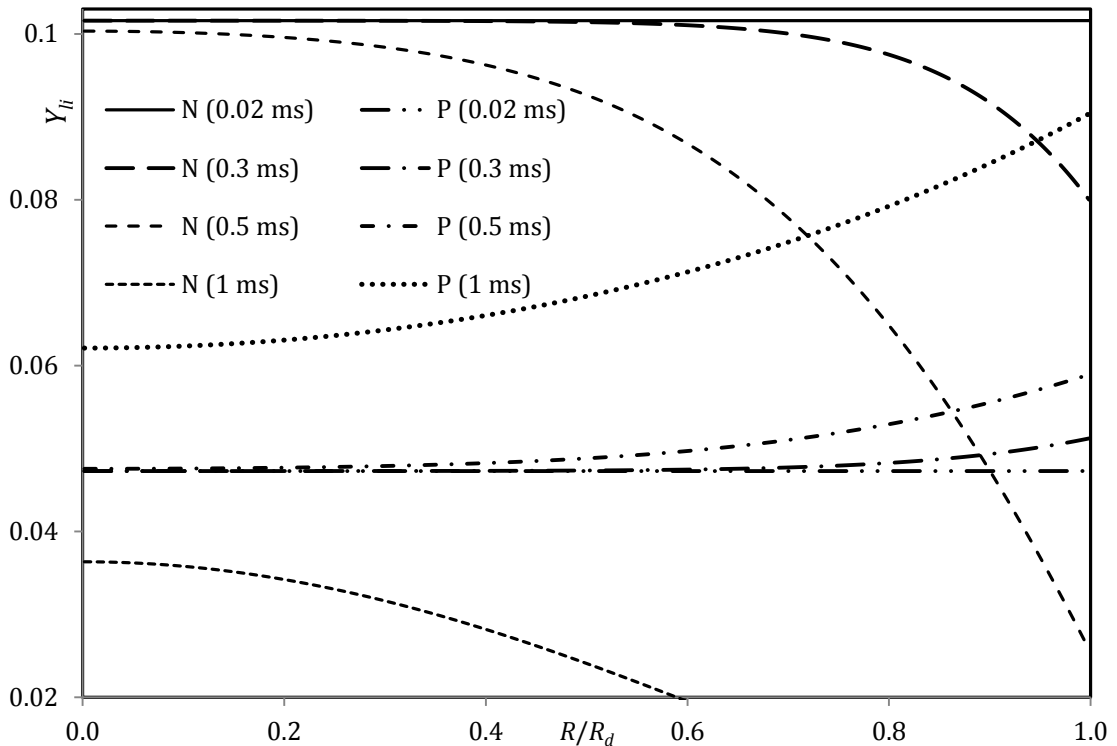
Figure 5.7 Mass fractions of n-pentane C_5H_{12} (N) and propylbenzene C_9H_{12} (P) versus normalised distance from the centre of droplet (R/R_d) at four time instants, 0.02 ms, 0.3 ms, 0.5 ms and 1 ms (indicated near the plots), predicted by the ETC/ED model taking into account the contributions of all 20 components of gasoline fuel.

The plots of temperatures versus normalised distance from the centre of the droplet at four time instants are shown in Figure 5.8. As one can see from this figure, the effect of temperature gradient due to finite thermal conductivity inside the droplet cannot be ignored, especially at the initial stage of evaporation. This questions the applicability of the widely used Infinite Thermal Conductivity (ITC) model of droplet heating and evaporation to the analysis of gasoline fuel droplets.
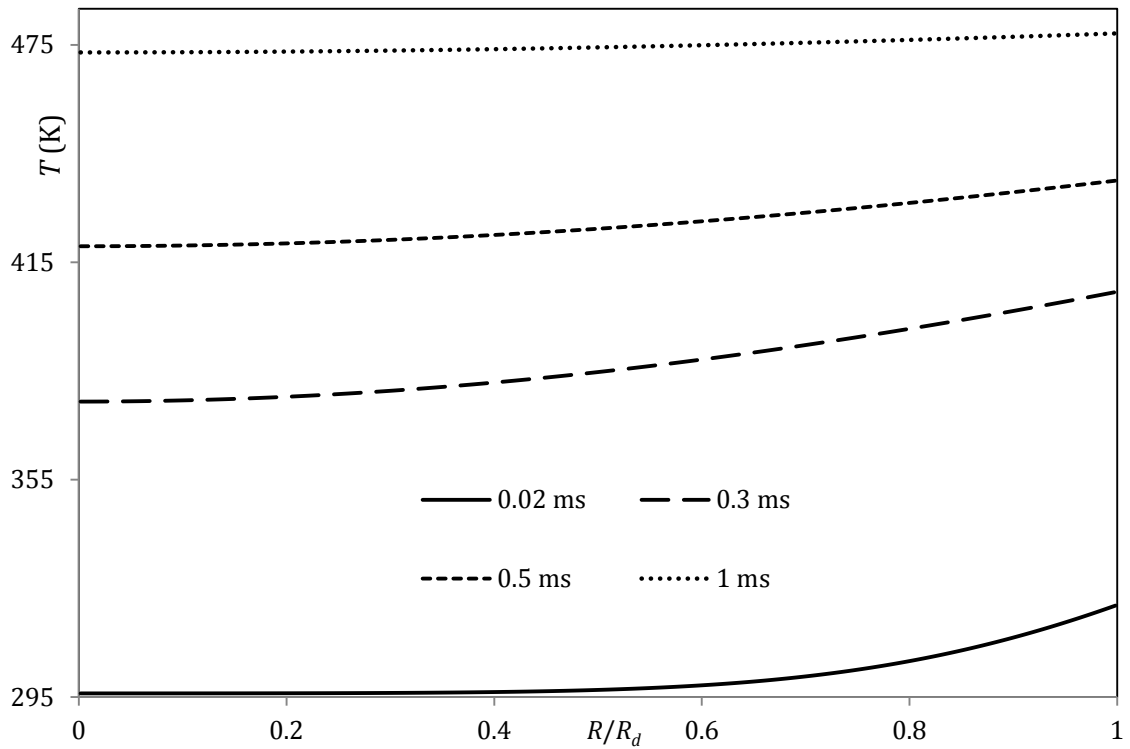
Figure 5.8 The plots of temperature versus normalised distance from the droplet centre (R/R_d) at three instants of time 0.02 ms, 0.3 ms and 0.5 ms (indicated near the plots) as predicted by the ETC/ED model, taking into account the contributions of all 20 components.

The predicted values of droplet radii (R_d) versus the number of C/QC at four time instants are shown in Figure 5.9. As can been seen from this figure, the predictions of the model based on the approximation of gasoline fuel by 6 or more C/QC give reasonably good agreements with the predictions of the model taking into account all 20 components of gasoline fuel.
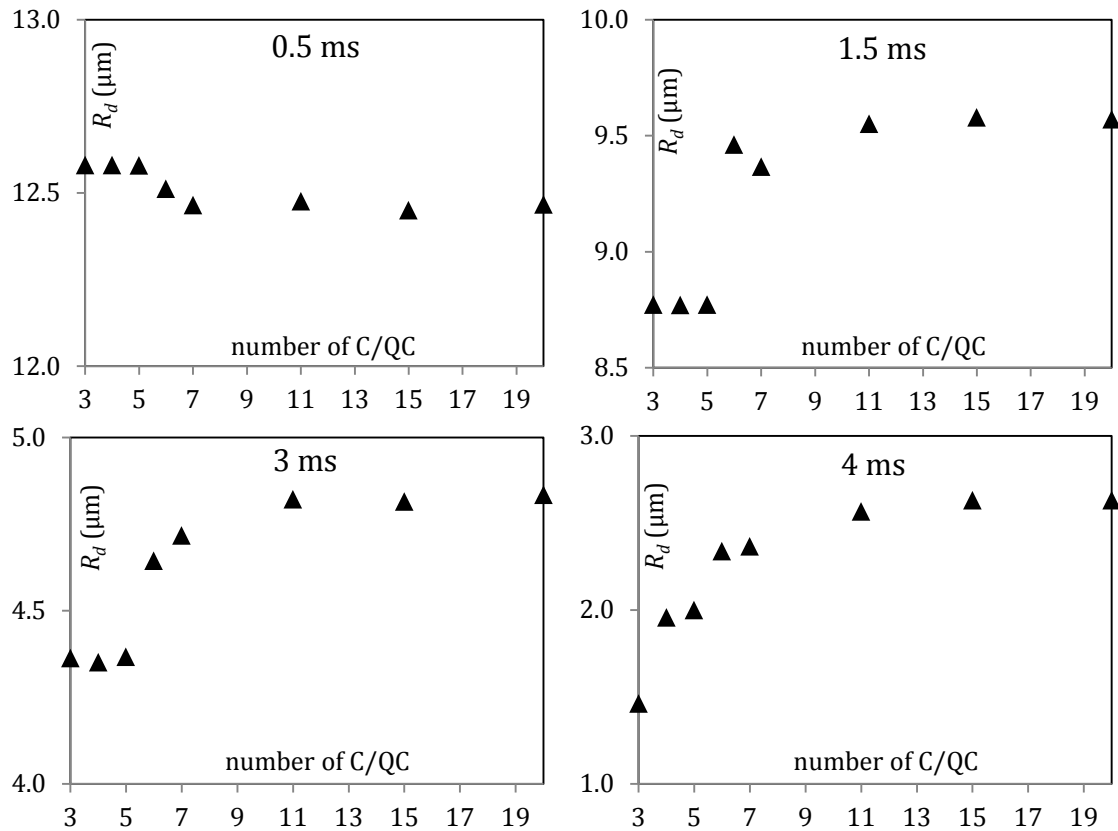
Figure 5.9 The droplet radii versus the number of C/QC, used for the approximation of gasoline fuel, at four time instants, 0.5 ms, 1.5 ms, 3 ms, and 4 ms.

The plots similar to those shown in Figure 5.9, but for droplet surface temperatures, are presented in Figure 5.10. As in the case shown in Figure 5.9, we can see from Figure 5.10 that the approximations of gasoline fuel by 6 or more C/QC give reasonably good agreements with the predictions of the model taking into account the contributions of all 20 components of gasoline fuel. These results are compatible with those inferred from the analysis of Figures 5.3-5.5.
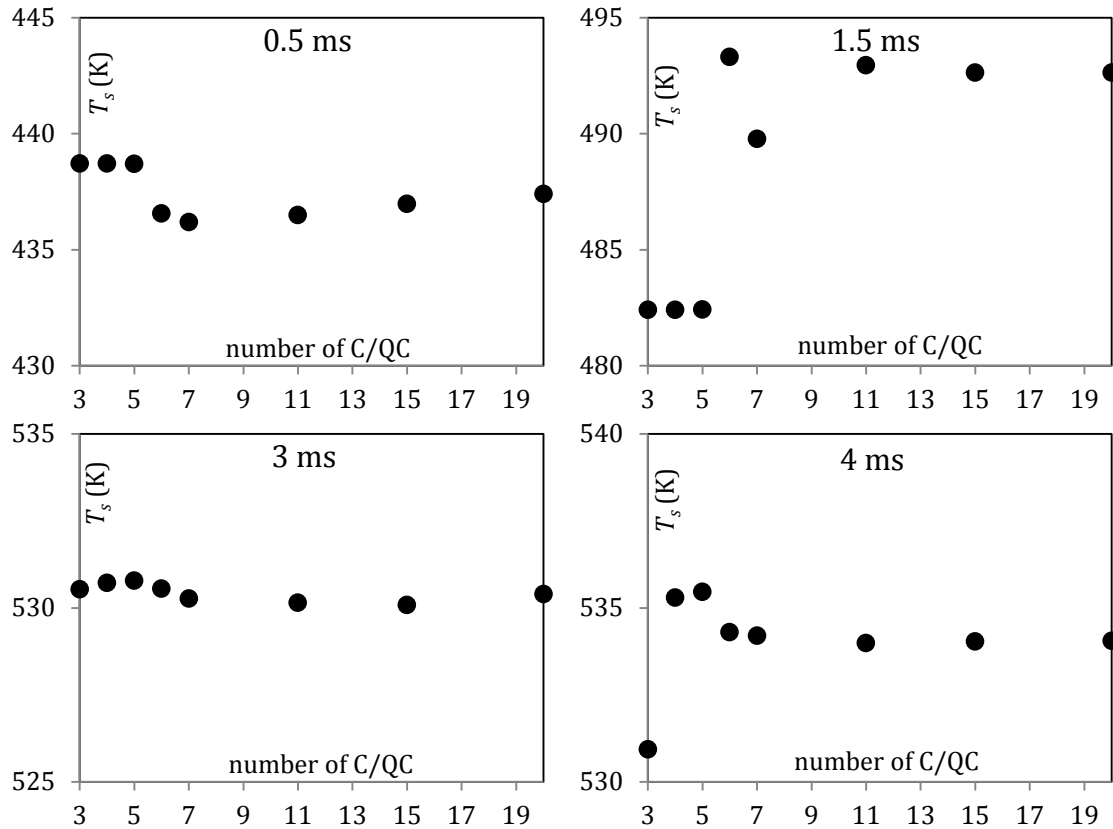
Figure 5.10 The droplet surface temperatures versus the number of C/QC, used for the approximation of gasoline fuel, at four time instants, 0.5 ms, 1.5 ms, 3 ms, and 4 ms.

The CPU efficiencies of the model versus the numbers of C/QC are shown in Figure 5.11 (PC used is Intel Xeon (core duo) E8400, 3 GHz and 3 GB RAM). As can be seen from this figure, approximating 20 components of gasoline fuel by 6 C/QC reduces the required CPU time by more than 70% compared with the model taking into account the contributions of all 20 components. As can be inferred from the above analysis, the choice of 6 C/QC can ensure a good compromise between CPU efficiency of the model and its accuracy.

CPU time (Sec)
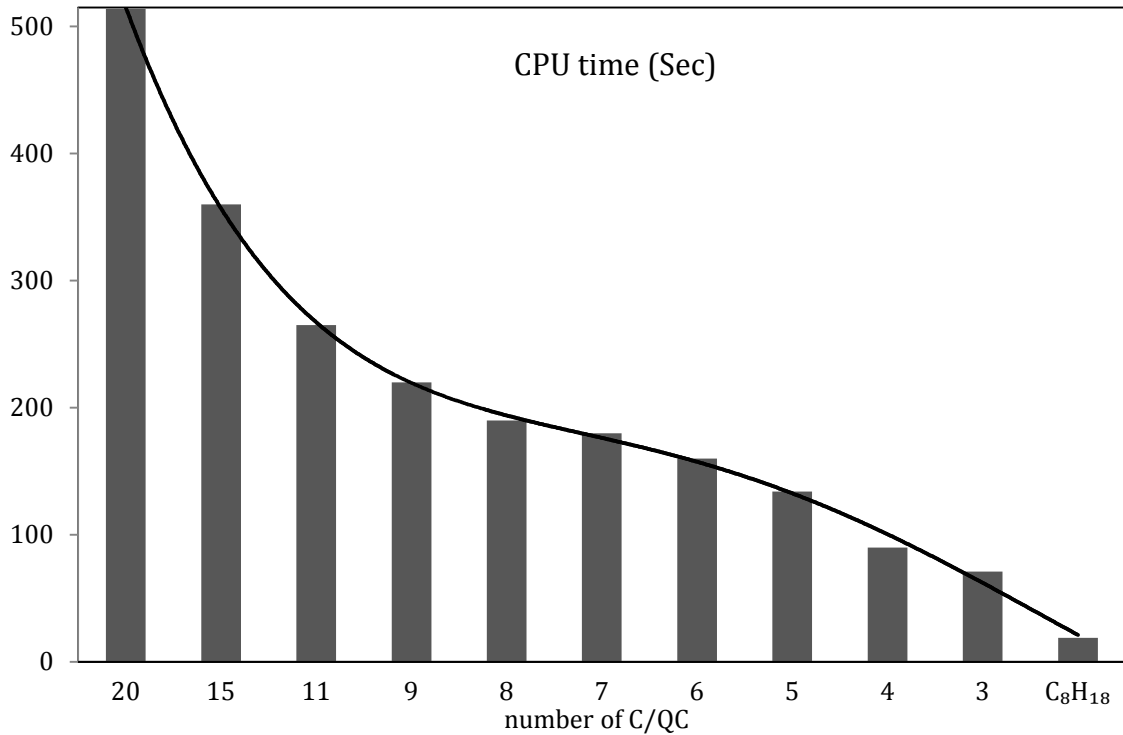
Figure 5.11 Plot of CPU time required for calculations of droplet heating and evaporation versus the number of C/QC used in the model for the same input parameters as in Figures 5.2-5.10.

5.5   Conclusions of Chapter 5

A new approach to modelling of the heating and evaporation of gasoline fuel droplets in realistic internal combustion engine environment is described. The components with similar molecular formulae but different molecular structures are replaced with single components, leading to the reduction of the total number of components used in modelling to just 20. As in the previously suggested multi-dimensional quasi-discrete (MDQD) model, these 20 components of the fuel are replaced with a smaller number of hypothetical quasi-components and components. Transient diffusion of these components/quasi-components in the liquid phase, temperature gradient and recirculation inside droplets due to relative velocities between droplets and ambient air are all taken into account.

In contrast to the original MDQD model, where n-alkanes and iso-alkanes are merged into one group of alkanes, in our approach separate contributions of

163

these two groups are taken into account. The results are compared with the predictions of several simplified models. In these models, the contributions of 20 components are taken into account using the infinite thermal conductivity/infinite species diffusivity (ITC/ID) model; the thermodynamic and transport properties of 20 components are averaged to form a single component and temperature gradient is ignored (ITC model); and the ITC model in which gasoline fuel is approximated with iso-octane (2,2,4-trimethylpentane). It is shown that the application of the latter two simplified models leads to under-prediction of the droplet evaporation time by up to 67% and 47% respectively, which are not acceptable in most engineering applications. The ITC/ID model leads to under-prediction of this evaporation time by 8%, which can be acceptable in some engineering applications. This model, however, cannot describe adequately the underlying physics of the processes inside droplets (heat conduction and species diffusion).

It is shown that the approximation of the actual composition of gasoline fuel by 6 components/quasi-components, using the MDQD model, leads to errors in estimated droplet surface temperatures and evaporation times of about 0.9% and 6.6% respectively, for the same engine conditions, which can be tolerated in many engineering applications. It is shown that the application of the latter model leads to about 70% reduction in CPU time compared to the model taking into account the contributions of all 20 components of gasoline fuel.

6 CONCLUSIONS AND RECOMMENDATIONS

6.1 Conclusions

Two approaches to modelling heating of evaporated droplets have been compared. In the first approach, the heat rate supplied to the droplets to raise their temperatures, $\dot{q}_d$, is derived from the requirement that the rates of droplet evaporation $\dot{m}_\mathrm{d}$, inferred from steady-state equations for mass and heat balance in the gas phase, should be the same. The second approach is based on the direct calculation of the distribution of temperature inside droplets.

The implications of these two approaches have been compared for the case of stationary droplets in conditions relevant to Diesel engines. It is pointed out that the time evolution of $\dot{q}_d$, predicted by both approaches, were similar, but the actual values of $\dot{q}_d$ at any given time instant were visibly different in the graphs presented in this thesis. This difference can lead to noticeable differences in predicted droplet surface temperatures, radii and evaporation times. It is concluded that both approaches to the calculation of $\dot{q}_d$ can be applied for qualitative analysis of droplet heating and evaporation, but caution should be exercised when using any of them for the quantitative analysis.

The previously developed kinetic model for two-component droplet heating and evaporation has been applied to the analysis of n-dodecane and p-dipropylbenzene mixture droplets. In contrast to most recently introduced kinetic models, the presence of two components in the vapour are taken into account. The effects of finite thermal conductivity inside the droplets and inelastic collisions in the kinetic region are taken into account. Also, in contrast to previously suggested kinetic models, the effects of species diffusivity inside the droplets are considered. The model is tested for the analysis of heating and evaporation of droplets in two typical engine conditions, considering several mixtures of n-dodecane and p-dipropylbenzene. It is shown that both the addition of p-dipropylbenzene and kinetic effects lead to an increase in the evaporation time of droplets. In all cases, the kinetic effects on the droplet

evaporation times increase with increasing p-dipropylbenzene contribution and gas temperature.

The previously suggested 'discrete component' model for droplet heating and evaporation, taking into account temperature gradient, recirculation, and species diffusion inside droplets, has been applied to the analysis of biodiesel fuel droplet heating and evaporation in realistic Diesel engine like conditions. In contrast to the most commonly used numerical models which take these effects into account, the model used in this analysis is based on the analytical solutions to the heat transfer and species diffusion equations inside droplets.

The analyses of biodiesel fuel droplets heating and evaporation have been focused on two cases, preliminary and advanced, which are categorised based on the engine conditions and biodiesel types. The preliminary analysis (Case 1) has been performed for five types of biodiesel fuels: Palm Methyl Ester (PME) produced from palm oil; Hemp Methyl Esters, produced from hemp seed oil in the Ukraine (HME1) and the European Union (HME2); Rapeseed oil Methyl Ester (RME), produced from rapeseed oil in the Ukraine; and Soybean oil Methyl Ester (SME), produced from soybean oil. These fuels contain up to 15 methyl esters and possibly small amounts of unspecified additives, which are treated as methyl esters with average characteristics. The maximal deviation between the predictions of the multi-component and single component models have been observed for RME. Even in the latter case, however, the difference between the evaporation times predicted by these models has been less than 5.5%.

In the advanced analysis (Case 2), a comparative analysis of predictions of several models of biodiesel fuel droplet heating and evaporation in realistic Diesel engine-like conditions has been presented. Nineteen types of biodiesel fuel have been used. These are Tallow Methyl Ester (TME), Lard Methyl Ester (LME), Butter Methyl Ester (BME), Coconut Methyl Ester (CME), Palm Kernel Methyl Ester (PMK), Palm Methyl Ester (PME), Safflower Methyl Ester (SFE), Peanut Methyl Ester (PTE), Cottonseed Methyl Ester (CSE), Corn Methyl Ester (CNE), Sunflower Methyl Ester (SNE), Tung Methyl Ester (TGE), Hemp-oil Methyl Ester, produced from Hemp seed oil in Ukraine (HME1), Soybean Methyl Ester (SME), Linseed Methyl Ester (LNE), Hemp-oil Methyl Ester, produced in

European Union (HME2), Canola seed Methyl Ester (CAN), Waste cooking-oil Methyl Ester (WME) and Rapeseed Methyl Ester (RME).

It is pointed out that the simplified approaches under-predict the droplet evaporation times compared with our model (believed to be the most reliable one) by up to about 26%. This result does not support our earlier finding, based on the analysis of only five types of biodiesel fuel in different engine conditions, that the deviations between the evaporation times predicted by these models do not exceed about 5.5%. The multi-component model predicts higher droplet surface temperatures at the final stages of evaporation (in most cases) and longer evaporation times than the single component model. This is related to the fact that at the final stages of droplet evaporation the mass fraction of heavier species, which evaporate more slowly than the lighter species and have higher boiling temperatures, increases at the expense of lighter species.

The application of discrete component models to biodiesel has been possible in principle due to the limited number of components contained within this fuel. However, the application of the same model to realistic Diesel fuel (potentially containing up to hundreds of components) droplets is computationally expensive. A new (multi-dimensional quasi-discrete) model is introduced to model heating and evaporation of these droplets, to take into account the abovementioned effects, but using a computationally cost-effective approach. As in the original quasi-discrete model suggested earlier, the components of Diesel fuel with close thermodynamic and transport properties are grouped together to form quasi-components. In contrast to actual components, these quasi-components are allowed to have non-integer values of carbon atoms. This, however, does not prohibit their treatment as actual components, and the modelling of the diffusion of these quasi-components inside the droplets.

Also, in contrast to the original quasi-discrete model, the contribution of individual components has not been approximated by the distribution function of carbon numbers. The formation of quasi-components has been based on directly taking into account the contributions of individual components. Groups contributing small molar fractions to the composition of Diesel fuel (less than

about 1.5%) have been replaced by individual components. The total number of components in the simplified approximation of Diesel fuel has been equal to 98.

Several further approximations of the above simplified approximation of Diesel fuel have been considered. These included the approximation of Diesel fuel by a single quasi-component (mass fractions of all components inside the droplet do not change with time), the approximation of Diesel fuel by only alkanes, ignoring the contributions of all other components, the approximation of each of the above-mentioned six groups by single quasi-components with average values of carbon numbers (9 quasi-components and components altogether), and the approximation of each of the above-mentioned six groups by one or more quasi-components, leading to sets of numbers between 9 and 98 quasi-components and components. All these approximations have been used for the analysis of heating and evaporation of a typical Diesel fuel droplet in Diesel engine-like conditions.

It is shown that approximations of Diesel fuel with only alkanes lead to less accurate modelling results compared with the approximation of Diesel fuel by a single quasi-component. This finding questions the applicability of the previously developed quasi-discrete model based on the former approximation. Also, it is shown that the approximations of Diesel fuel by less than about 15 components/quasi-components led to unacceptably large errors (relative to the prediction of the model, taking into account the contributions of all 98 components) in predicting droplet temperatures and evaporation times and are not recommended for practical engineering applications. The approximation of Diesel fuel by 15 components/quasi-components, has led to errors in estimated temperature and evaporation times not exceeding about 1.6% and 2.5% respectively, which is acceptable for most engineering applications. This model requires about 1/6th of the CPU time compared with the model taking into account the contributions of all 98 components.

Application of the MDQD model to the analysis of the heating and evaporation of gasoline fuel droplets in realistic internal combustion engine environment is described. The components with similar molecular formulae but different molecular structures are replaced with single components, leading to the reduction of the total number of components used in the modelling to just

20. The results of droplet heating and evaporation analyses are compared with the predictions of several simplified models. It is shown that the application of the simplified models leads to under-prediction of the droplet evaporation time by up to 67% and 47% respectively, which cannot be accepted in most engineering applications. Also, the approximation of the actual composition of gasoline fuel by 6 components/quasi-components, leads to errors in estimated droplet surface temperatures and evaporation times of about 0.9% and 6.6% respectively, which can be tolerated in many engineering applications. It is shown that the application of the latter model leads to about 70% reduction in CPU time compared to the model taking into account the contributions of all 20 components of gasoline fuel.

6.2 Recommendation and future work

The benefits and usefulness of the discrete component and multi-dimensional quasi-discrete (MDQD) models have been clearly demonstrated in the thesis. However, it remains unclear how these models, more specifically MDQD model, can be linked with approximations of automotive fuels by surrogate-fuels (widely used for modelling these fuels auto-ignition). Also, no rigorous algorithm for the selection of quasi-components in the MDQD model has been developed; the selection of quasi-components has been based on a trial and error approach.

The recommended future work is to address all the above-mentioned points. Also, a feasibility of implementing the MDQD model and abovementioned effects into a commercial CFD code for a full-cycle simulation would be important for practical applications. These are our more specific suggestions:

- The investigation of the applicability of the multi-dimensional quasi-discrete (MDQD) model to a wider range of typical automotive fuels, including surrogates and blended fuels.

- The optimisation of the MDQD model by developing a mathematical algorithm for the auto-selection of quasi-components.

- Development of a new algorithm for the auto-selection of quasi-components of the MDQD model.

- The generalisation of the MDQD model to take into account other effects, such as thermal radiation, moving droplet interface during evaporation and non-spherical droplet shapes.

- Investigation of the performance of the generalised MDQD model for a wider range of automotive fuels, such as surrogates and blended fuels (e.g. Diesel and biodiesel blends).

- The implementation of the generalised MDQD model into a commercial (e.g. ANSYS-FLUENT) CFD code to perform a full cycle simulation in engine-like conditions. This work is in progress and some preliminary results are presented in Appendix E.

REFERENCES

[1] P. F. Flynn, R. P. Durrett, G. L. Hunter, A. O. zur Loye, O. C. Akinyemi, J. E. Dec, and C. K. Westbrook, "Diesel Combustion: An Integrated View Combining Laser Diagnostics, Chemical Kinetics, And Empirical Validation," SAE International, Warrendale, PA, 1999-01-0509, Mar. 1999.

[2] E. M. Sazhina, S. S. Sazhin, M. R. Heikal, V. I. Babushok, and R. J. R. Johns, "A Detailed Modelling of the Spray Ignition Process in Diesel Engines," *Combust. Sci. Technol.*, vol. 160, no. 1, pp. 317–344, 2000.

[3] M. Shahabuddin, A. M. Liaquat, H. H. Masjuki, M. A. Kalam, and M. Mofijur, "Ignition delay, combustion and emission characteristics of diesel engine fueled with biodiesel," *Renew. Sustain. Energy Rev.*, vol. 21, pp. 623–632, May 2013.

[4] R. Cataluna and R. da Silva, "Effect of Cetane Number on Specific Fuel Consumption and Particulate Matter and Unburned Hydrocarbon Emissions from Diesel Engines," *J. Combust.*, vol. 2012, p. e738940, Oct. 2012.

[5] S. S. Sazhin, "Advanced models of fuel droplet heating and evaporation," *Prog. Energy Combust. Sci.*, vol. 32, no. 2, pp. 162–214, 2006.

[6] S. S. Sazhin, *Droplets and Sprays*. London: Springer, 2014.

[7] W. A. Sirignano, *Fluid Dynamics and Transport of Droplets and Sprays*. Cambridge, U.K: Cambridge University Press, 1999.

[8] R. Stone, *Introduction to Internal Combustion Engines*. Basingstoke, England: Macmillan, 1992.

[9] B. Abramzon and W. A. Sirignano, "Droplet vaporization model for spray combustion calculations," *Int. J. Heat Mass Transf.*, vol. 32, no. 9, pp. 1605–1618, Sep. 1989.

[10] M. Burger, R. Schmehl, K. Prommersberger, O. Schäfer, R. Koch, and S. Wittig, "Droplet evaporation modeling by the distillation curve model: accounting for kerosene fuel and elevated pressures," *Int. J. Heat Mass Transf.*, vol. 46, no. 23, pp. 4403–4412, Nov. 2003.

[11] C. K. Law, "Recent advances in droplet vaporization and combustion," *Prog. Energy Combust. Sci.*, vol. 8, no. 3, pp. 171–201, Jan. 1982.

[12] W. L. H. Hallett, "A simple model for the vaporization of droplets with large numbers of components," *Combust. Flame*, vol. 121, no. 1–2, pp. 334–344, Apr. 2000.

[13]   V. Deprédurand, "Approche experimentale de l' évaporation de sprays de combustibles multicomposant," Vandoeuvre-Les- Nancy, France, 2009.

[14]   V. Deprédurand, G. Castanet, and F. Lemoine, "Heat and mass transfer in evaporating droplets in interaction: Influence of the fuel," *Int. J. Heat Mass Transf.*, vol. 53, no. 17–18, pp. 3495–3502, Aug. 2010.

[15]   C. Maqua, "Contribution à la compréhension de l'évaporation de gouttes de combustible bi-composant à l'aide de méthodes optiques," Thèse de doctorat : Mécanique et énergétique, Nancy- Université, 2007.

[16]   C. Maqua, G. Castanet, F. Grisch, F. Lemoine, T. Kristyadi, and S. S. Sazhin, "Monodisperse droplet heating and evaporation: Experimental study and modelling," *Int. J. Heat Mass Transf.*, vol. 51, no. 15–16, pp. 3932–3945, Jul. 2008.

[17]   C. Maqua, V. Depredurand, G. Castanet, M. Wolff, and F. Lemoine, "Composition measurement of bicomponent droplets using laser-induced fluorescence of acetone," *Exp. Fluids*, vol. 43, no. 6, pp. 979–992, Nov. 2007.

[18]   C. Maqua, G. Castanet, F. Lemoine, N. Doué, and G. Lavergne, "Temperature measurements of binary droplets using three-color laser-induced fluorescence," *Exp. Fluids*, vol. 40, no. 5, pp. 786–797, May 2006.

[19]   H. Nomura, Y. Ujiie, H. J. Rath, J. Sato, and M. Kono, "Experimental study on high-pressure droplet evaporation using microgravity conditions," *Symp. Int. Combust.*, vol. 26, no. 1, pp. 1267–1273, Jan. 1996.

[20]   S. S. Sazhin and P. A. Krutitskii, "A Conduction Model for Transient Heating of Fuel Droplets," in *proceedings of the 3rd ISAAC Congress*, River Edge, NJ, 2003, pp.   1231–1240.

[21]   S. Tonini and G. E. Cossali, "An analytical model of liquid drop evaporation in gaseous environment," *Int. J. Therm. Sci.*, vol. 57, pp. 45–53, Jul. 2012.

[22]   S. Tonini and G. E. Cossali, "A novel vaporisation model for a single-component drop in high temperature air streams," *Int. J. Therm. Sci.*, vol. 75, pp. 194–203, Jan. 2014.

[23]   W. L. H. Hallett and N. V. Legault, "Modelling biodiesel droplet evaporation using continuous thermodynamics," *Fuel*, vol. 90, no. 3, pp. 1221–1228, Mar. 2011.

[24]   K. Saha, E. Abu-Ramadan, and X. Li, "Multicomponent evaporation model for pure and blended biodiesel droplets in high temperature convective environment," *Appl.   Energy*, vol.   93, pp.   71–79,   May   2012.

[25] M. Al Qubeissi, R. Kolodnytska, and S. S. Sazhin, "Biodiesel fuel droplets: modelling of heating and evaporation processes," in *25th European Conference on Liquid Atomization and Spray Systems*, Crete, Greece, 2013, vol. 4 (CD).

[26] Y. Ra and R. D. Reitz, "A vaporization model for discrete multi-component fuel sprays," *Int. J. Multiph. Flow*, vol. 35, no. 2, pp. 101–117, Feb. 2009.

[27] J. Abraham and V. Magi, "A Model for Multicomponent Droplet Vaporization in Sprays," SAE International, Warrendale, PA, 980511, Feb. 1998.

[28] S. K. Aggarwal and H. C. Mongia, "Multicomponent and High-Pressure Effects on Droplet Vaporization," *J. Eng. Gas Turbines Power*, vol. 124, no. 2, p. 248, 2002.

[29] G. Continillo and W. A. Sirignano, "Unsteady, Spherically-Symmetric Flame Propagation Through Multicomponent Fuel Spray Clouds," in *Modern Research Topics in Aerospace Propulsion*, G. Angelino, L. D. Luca, and W. A. Sirignano, Eds. Springer New York, 1991, pp. 173–198.

[30] M. Klingsporn and U. Renz, "Vaporization of a binary unsteady spray at high temperature and high pressure," *Int. J. Heat Mass Transf.*, vol. 37, pp. 265–272, Mar. 1994.

[31] P. L. C. Lage, C. M. Hackenberg, and R. H. Rangel, "Nonideal vaporization of dilating binary droplets with radiation absorption," *Combust. Flame*, vol. 101, no. 1–2, pp. 36–44, Apr. 1995.

[32] C. Maqua, G. Castanet, and F. Lemoine, "Bicomponent droplets evaporation: Temperature measurements and modelling," *Fuel*, vol. 87, no. 13–14, pp. 2932–2942, Oct. 2008.

[33] A. Y. Tong and W. A. Sirignano, "Multicomponent Transient Droplet Vaporization with Internal Circulation: Integral Equation Formulation and Approximate Solution," *Numer. Heat Transf.*, vol. 10, no. 3, pp. 253–278, 1986.

[34] Z. Abdel-Qader and W. L. H. Hallett, "The role of liquid mixing in evaporation of complex multicomponent mixtures: modelling using continuous thermodynamics," *Chem. Eng. Sci.*, vol. 60, no. 6, pp. 1629–1640, Mar. 2005.

[35] M. Arias-Zugasti and D. E. Rosner, "Multicomponent fuel droplet vaporization and combustion using spectral theory for a continuous mixture," *Combust. Flame*, vol. 135, no. 3, pp. 271–284, Nov. 2003.

[36] A. M. Lippert and R. D. Reitz, "Modeling of multicomponent fuels using continuous distributions with application to droplet evaporation and sprays," SAE International, Warrendale, PA, SAE Technical Paper 972882, Oct. 1997.

[37] E. Rivard and D. Brüggemann, "Numerical investigation of semi-continuous mixture droplet vaporization at low temperature," *Chem. Eng. Sci.*, vol. 65, no. 18, pp. 5137–5145, Sep. 2010.

[38] J. Tamim and W. L. H. Hallett, "A continuous thermodynamics model for multicomponent droplet vaporization," *Chem. Eng. Sci.*, vol. 50, no. 18, pp. 2933–2942, Sep. 1995.

[39] L. Zhang and S.-C. Kong, "Modeling of multi-component fuel vaporization and combustion for gasoline and diesel spray," *Chem. Eng. Sci.*, vol. 64, no. 16, pp. 3688–3696, Aug. 2009.

[40] G.-S. Zhu and R. D. Reitz, "A model for high-pressure vaporization of droplets of complex liquid mixtures using continuous thermodynamics," *Int. J. Heat Mass Transf.*, vol. 45, no. 3, pp. 495–507, Jan. 2002.

[41] L. S. Ott, B. L. Smith, and T. J. Bruno, "Composition-Explicit Distillation Curves of Waste Lubricant Oils and Resourced Crude Oil: A Diagnostic for Re-Refining and Evaluation," *Am. J. Environ. Sci.*, vol. 6, no. 6, pp. 523–534, Jun. 2010.

[42] B. L. Smith and T. J. Bruno, "Advanced Distillation Curve Measurement with a Model Predictive Temperature Controller," *Int. J. Thermophys.*, vol. 27, no. 5, pp. 1419–1434, Sep. 2006.

[43] A. E. Elwardany and S. S. Sazhin, "A quasi-discrete model for droplet heating and evaporation: Application to Diesel and gasoline fuels," *Fuel*, vol. 97, pp. 685–694, Jul. 2012.

[44] A. E. Elwardany, "Modelling of multi-component fuel droplets heating and evaporation," PhD thesis, University of Brighton, UK, 2012.

[45] A. E. Elwardany, S. S. Sazhin, and A. Farooq, "Modelling of heating and evaporation of gasoline fuel droplets: A comparative analysis of approximations," *Fuel*, vol. 111, pp. 643–647, Sep. 2013.

[46] S. S. Sazhin, M. Al Qubeissi, R. Kolodnytska, A. E. Elwardany, R. Nasiri, and M. R. Heikal, "Modelling of biodiesel fuel droplet heating and evaporation," *Fuel*, vol. 115, pp. 559–572, Jan. 2014.

[47] S. S. Sazhin, A. E. Elwardany, E. M. Sazhina, and M. R. Heikal, "A quasi-discrete model for heating and evaporation of complex multicomponent hydrocarbon fuel droplets," *Int. J. Heat Mass Transf.*, vol. 54, no. 19–20, pp. 4325–4332, Sep. 2011.

[48] C. Laurent, G. Lavergne, and P. Villedieu, "Continuous thermodynamics for droplet vaporization: Comparison between Gamma-PDF model and QMoM," *Comptes Rendus Mécanique*, vol. 337, no. 6–7, pp. 449–457, Jun. 2009.

[49] L. Zhang and S.-C. Kong, "Vaporization modeling of petroleum–biofuel drops using a hybrid multi-component approach," *Combust. Flame*, vol. 157, no. 11, pp. 2165–2174, Nov. 2010.

[50] L. Zhang, "Multicomponent drop vaporization modeling of petroleum and biofuel mixtures," Iowa State University, 2011.

[51] R. Kolodnytska, M. Al Qubeissi, and S. S. Sazhin, "Biodiesel fuel droplets: transport and thermodynamic properties," in *25th European Conference on Liquid Atomization and Spray Systems*, Crete, Greece, 2013, vol. No. 7 (CD).

[52] C. E. Ejim, B. A. Fleck, and A. Amirfazli, "Analytical study for atomization of biodiesels and their blends in a typical injector: Surface tension and viscosity effects," *Fuel*, vol. 86, no. 10–11, pp. 1534–1544, Jul. 2007.

[53] S. Choi and Y. Oh, "The spray characteristics of unrefined biodiesel," *Renew. Energy*, vol. 42, pp. 136–139, Jun. 2012.

[54] A. E. Elwardany, I. G. Gusev, G. Castanet, F. Lemoine, and S. S. Sazhin, "Mono- and multi-component droplet cooling/heating and evaporation: comparative analysis of numerical models," *At. Sprays*, vol. 21, no. 11, pp. 907–931, 2011.

[55] S. S. Sazhin, A. Elwardany, P. A. Krutitskii, G. Castanet, F. Lemoine, E. M. Sazhina, and M. R. Heikal, "A simplified model for bi-component droplet heating and evaporation," *Int. J. Heat Mass Transf.*, vol. 53, no. 21–22, pp. 4495–4505, Oct. 2010.

[56] S. T. Teng, A. D. Williams, and K. Urdal, "Detailed hydrocarbon analysis of gasoline by GC-MS (SI-PIONA)," *J. High Resolut. Chromatogr.*, vol. 17, no. 6, pp. 469–475, Jun. 1994.

[57] S. S. Sazhin, M. Al Qubeissi, R. Nasiri, V. M. Gun'ko, A. E. Elwardany, F. Lemoine, F. Grisch, and M. R. Heikal, "A multi-dimensional quasi-discrete model for the analysis of Diesel fuel droplet heating and evaporation," *Fuel*, vol. 129, pp. 238–266, 2014.

[58] M. Al Qubeissi, S. S. Sazhin, J. Turner, S. Begg, C. Crua, and M. R. Heikal, "Modelling of gasoline fuel droplets heating and evaporation," *Fuel*, vol. 159, pp. 373–384, Nov. 2015.

[59] S. S. Sazhin, M. Al Qubeissi, and J.-F. Xie, "Two approaches to modelling the heating of evaporating droplets," *Int. Commun. Heat Mass Transf.*, vol. 57, pp. 353–356, Oct. 2014.

[60] S. S. Sazhin, I. N. Shishkova, and M. Al Qubeissi, "Heating and evaporation of a two-component droplet: Hydrodynamic and kinetic models," *Int. J. Heat Mass Transf.*, vol. 79, pp. 704–712, Dec. 2014.

[61] M. Al Qubeissi, S. S. Sazhin, C. Crua, and M. R. Heikal, "Modelling of heating and evaporation of biodiesel fuel droplets," *Int. J. Mech. Aerosp. Ind. Mechatron. Eng.*, vol. 9, no. 1, pp. 46–49, Jan. 2015.

[62] M. Al Qubeissi, S. S. Sazhin, C. Crua, J. Turner, and M. R. Heikal, "Modelling of biodiesel fuel droplet heating and evaporation: effects of fuel composition," *Fuel*, vol. 154, pp. 308–318, Aug. 2015.

[63] M. Al Qubeissi, S. S. Sazhin, G. de Sercey, and C. Crua, "Multi-dimensional quasi-discrete model for the investigation of heating and evaporation of Diesel fuel droplets," in *26th European Conference on Liquid Atomization and Spray Systems*, Bremen, Germany, 2014, vol. ABS-135 (CD).

[64] S. S. Sazhin, M. Al Qubeissi, and M. R. Heikal, "Modelling of biodiesel and diesel fuel droplet heating and evaporation," in *15th International Heat Transfer Conference, IHTC-15*, Kyoto, Japan, 2014, vol. IHTC15–8936.

[65] S. S. Sazhin and M. Al Qubeissi, "Modelling of automotive fuel droplet heating and evaporation," in *MURPHYS-HSFS-2014 - 7th International Workshop on Multi-Rate Processes & Hysteresis, 2nd International Workshop on Hysteresis and Slow-Fast Systems, Preliminary Program*, Berlin, Germany, 2014.

[66] S. S. Sazhin, I. N. Shishkova, and M. Al Qubeissi, "Kinetic modelling of Diesel fuel droplet heating and evaporation: effects of the approximation of fuel composition," in *26th European Conference on Liquid Atomization and Spray Systems*, Bremen, Germany, 2014, vol. ABS-148 (CD).

[67] B. Duret, M. Al Qubeissi, S. S. Sazhin, and C. Crua, "Evaporating droplets: comparison between DNS and modelling," in *26th European Conference on Liquid Atomization and Spray Systems*, Bremen, Germany, 2014, vol. ABS-187 (CD).

[68] M. Al Qubeissi, S. S. Sazhin, C. Crua, and M. R. Heikal, "Modelling of heating and evaporation of biodiesel fuel droplets," in *ICHTA 2015 : XIII International Conference on Heat Transfer and Applications*, London, UK, 2015, vol. 2 (9), p. 667.

[69] S. S. Sazhin, A. E. Elwardany, P. A. Krutitskii, V. Deprédurand, G. Castanet, F. Lemoine, E. M. Sazhina, and M. R. Heikal, "Multi-component droplet heating and evaporation: Numerical simulation versus experimental data," *Int. J. Therm. Sci.*, vol. 50, no. 7, pp. 1164–1180, Jul. 2011.

[70] S. S. Sazhin, W. A. Abdelghaffar, P. A. Krutitskii, E. M. Sazhina, and M. R. Heikal, "New approaches to numerical modelling of droplet transient heating and evaporation," *Int. J. Heat Mass Transf.*, vol. 48, no. 19–20, pp. 4215–4228, Sep. 2005.

[71] S. S. Sazhin, P. A. Krutitskii, W. A. Abdelghaffar, E. M. Sazhina, S. V. Mikhalovsky, S. T. Meikle, and M. R. Heikal, "Transient heating of diesel fuel

droplets," *Int. J. Heat Mass Transf.*, vol. 47, no. 14–16, pp. 3327–3340, Jul. 2004.

[72] H. S. Carslaw, *Conduction of Heat in Solids*, 2nd ed. Oxford: New York: Clarendon Press; Oxford University Press, 1986.

[73] E. M. Kartashov, *Analytical Methods in Heat Transfer Theory in Solids.* Moscow: Vysshaya Shkola, 2001.

[74] B. Abramzon and S. S. Sazhin, "Convective vaporization of a fuel droplet with thermal radiation absorption," *Fuel*, vol. 85, no. 1, pp. 32–46, Jan. 2006.

[75] W. A. Sirignano, *Fluid Dynamics and Transport of Droplets and Sprays.* Cambridge, U.K: Cambridge University Press, 2010.

[76] S. S. Sazhin, T. Kristyadi, W. A. Abdelghaffar, and M. R. Heikal, "Models for fuel droplet heating and evaporation: Comparative analysis," *Fuel*, vol. 85, no. 12–13, pp. 1613–1630, Sep. 2006.

[77] W. A. Sirignano, "Fuel droplet vaporization and spray combustion theory," *Prog. Energy Combust. Sci.*, vol. 9, no. 4, pp. 291–322, 1983.

[78] G. M. Faeth, "Evaporation and combustion of sprays," *Prog. Energy Combust. Sci.*, vol. 9, no. 1–2, pp. 1–76, 1983.

[79] D. B. Spalding, *Convective Mass Transfer: an Introduction.* London: Edward Arnold Publ. Ltd, 1963.

[80] P. W. Atkins and J. De Paula, *Atkins' Physical Chemistry.* Oxford: Oxford University Press, 2002.

[81] M. C. Rogers and G. G. Brown, *Raoult's Law and the Equilibrium Vaporization of Hydrocarbon Mixtures.* University of Michigan, 1929.

[82] B. E. Poling, J. M. Prausnitz, and J. P. O'Connell, *The properties of gases and liquids.* New York: McGraw-Hill, 2001.

[83] V. Sanchez and M. Clifton, "Mutual diffusion coefficients in binary mixtures of carbon tetrachloride and alcohols at 20.degree.C," *J. Chem. Eng. Data*, vol. 23, no. 3, pp. 209–212, Jul. 1978.

[84] V. Sanchez and M. Clifton, "An Empirical Relationship for Predicting the Variation with Concentration of Diffusion Coefficients in Binary Liquid Mixtures," *Ind. Eng. Chem. Fundam.*, vol. 16, no. 3, pp. 318–320, Aug. 1977.

[85] R. Kneer, *Grundlegende Untersuchungen zur Sprühstrahlausbreitung in Hochbelasteten Brennräumen: Tropfenverdunstung und Sprühstrahlcharakterisierung.* Karlsruhe: Dissertation Doktors der Ingenieur-

wissenschaften, 1993.

[86] A. Vignes, "Diffusion in Binary Solutions. Variation of Diffusion Coefficient with Composition," *Ind. Eng. Chem. Fundam.*, vol. 5, no. 2, pp. 189–199, May 1966.

[87] R. B. Bird, W. E. Stewart, and E. N. Lightfoot, *Transport Phenomena*. New York: J. Wiley, 2002.

[88] C. R. Wilke and P. Chang, "Correlation of diffusion coefficients in dilute solutions," *AIChE J.*, vol. 1, no. 2, pp. 264–270, 1955.

[89] C. M. Silva, H. Liu, and E. A. Macedo, "Models for self-diffusion coefficients of dense fluids, including hydrogen-bonding substances," *Chem. Eng. Sci.*, vol. 53, no. 13, pp. 2423–2429, Jul. 1998.

[90] S. Dooley, M. Uddi, S. H. Won, F. L. Dryer, and Y. Ju, "Methyl butanoate inhibition of n-heptane diffusion flames through an evaluation of transport and chemical kinetics," *Combust. Flame*, vol. 159, no. 4, pp. 1371–1384, Apr. 2012.

[91] A. L. Magalhães, F. A. Da Silva, and C. M. Silva, "New models for tracer diffusion coefficients of hard sphere and real systems: Application to gases, liquids and supercritical fluids," *J. Supercrit. Fluids*, vol. 55, no. 3, pp. 898–923, Jan. 2011.

[92] P. Diévart, S. H. Won, S. Dooley, F. L. Dryer, and Y. Ju, "A kinetic model for methyl decanoate combustion," *Combust. Flame*, vol. 159, no. 5, pp. 1793–1805, May 2012.

[93] F. A. Perdomo and A. Gil-Villegas, "Molecular thermodynamics of biodiesel fuel compounds," *Fluid Phase Equilibria*, vol. 293, no. 2, pp. 182–189, Jun. 2010.

[94] K. Seshadri, T. Lu, O. Herbinet, S. Humer, U. Niemann, W. J. Pitz, R. Seiser, and C. K. Law, "Experimental and kinetic modeling study of extinction and ignition of methyl decanoate in laminar non-premixed flows," *Proc. Combust. Inst.*, vol. 32, no. 1, pp. 1067–1074, Jan. 2009.

[95] C. R. Wilke and C. Y. Lee, "Estimation of Diffusion Coefficients for Gases and Vapors," *Ind. Eng. Chem.*, vol. 47, no. 6, pp. 1253–1257, Jun. 1955.

[96] J. O. Hirschfelder, C. F. Curtiss, and R. B. Bird, *Molecular Theory of Gases and Liquids.* New York; London; Sydney: J. Wiley and Sons, 1967.

[97] L. Grunberg and A. H. Nissan, "Mixture law for viscosity," *Nature*, vol. 164, no. 4175, p. 799, Nov. 1949.

[98] R. Lin and L. L. Tavlarides, "Thermophysical properties needed for the development of the supercritical diesel combustion technology: Evaluation of diesel fuel surrogate models," *J. Supercrit. Fluids*, vol. 71, pp. 136–146, Nov. 2012.

[99] C. Lemofack, J. M. Lacome, J. Reveillon, and F. X. Demoulin, "Numerical modelling of liquid jets atomisation due to leakage of liquefied gas storage," in *Proceedings of ICLASS 2012*, Heidelberg, Germany, 2012.

[100] S. S. Sazhin, P. A. Krutitskii, I. G. Gusev, and M. R. Heikal, "Transient heating of an evaporating droplet with presumed time evolution of its radius," *Int. J. Heat Mass Transf.*, vol. 54, no. 5–6, pp. 1278–1288, Feb. 2011.

[101] S. S. Sazhin, P. A. Krutitskii, I. G. Gusev, and M. R. Heikal, "Transient heating of an evaporating droplet," *Int. J. Heat Mass Transf.*, vol. 53, no. 13–14, pp. 2826–2836, Jun. 2010.

[102] S. S. Sazhin, I. G. Gusev, P. A. Krutitskii, and M. R. Heikal, "Transient heating of a semitransparent spherical body immersed into a gas with inhomogeneous temperature distribution," *Int. J. Therm. Sci.*, vol. 50, no. 7, pp. 1215–1222, Jul. 2011.

[103] S. S. Sazhin, P. A. Krutitskii, S. B. Martynov, D. Mason, M. R. Heikal, and E. M. Sazhina, "Transient heating of a semitransparent spherical body," *Int. J. Therm. Sci.*, vol. 46, no. 5, pp. 444–457, May 2007.

[104] N. A. Fuchs, *Evaporation and Droplet Growth in Gaseous Media*. London: Pergamon Press, 1959.

[105] A. P. Kryukov, V. Y. Levashov, and S. S. Sazhin, "Evaporation of diesel fuel droplets: kinetic versus hydrodynamic models," *Int. J. Heat Mass Transf.*, vol. 47, no. 12–13, pp. 2541–2549, Jun. 2004.

[106] S. S. Sazhin and I. N. Shishkova, "Kinetic algorithm for modeling the droplet evaporation process in the presence of heat flux and background gas," *At. Sprays*, vol. 19, no. 5, pp. 473–489, 2009.

[107] S. S. Sazhin, I. N. Shishkova, A. P. Kryukov, V. Y. Levashov, and M. R. Heikal, "Evaporation of droplets into a background gas: Kinetic modelling," *Int. J. Heat Mass Transf.*, vol. 50, no. 13–14, pp. 2675–2691, Jul. 2007.

[108] I. N. Shishkova and S. S. Sazhin, "A numerical algorithm for kinetic modelling of evaporation processes," *J. Comput. Phys.*, vol. 218, no. 2, pp. 635–653, Nov. 2006.

[109] I. N. Shishkova, S. S. Sazhin, and J.-F. Xie, "A solution of the Boltzmann equation in the presence of inelastic collisions," *J. Comput. Phys.*, vol. 232, no. 1, pp. 87–99, Jan. 2013.

[110] S. S. Sazhin, J.-F. Xie, I. N. Shishkova, A. E. Elwardany, and M. R. Heikal, "A kinetic model of droplet heating and evaporation: Effects of inelastic collisions and a non-unity evaporation coefficient," *Int. J. Heat Mass Transf.*, vol. 56, no. 1–2, pp. 525–537, Jan. 2013.

[111] V. M. Gun'ko, R. Nasiri, S. S. Sazhin, F. Lemoine, and F. Grisch, "A quantum chemical study of the processes during the evaporation of real-life Diesel fuel droplets," *Fluid Phase Equilibria*, vol. 356, pp. 146–156, Oct. 2013.

[112] C. Ledier, M. Orain, F. Grisch, J. Kashdan, and G. Bruneaux, "Vapour concentration measurements in biofuel sprays using innovative Planar Laser-Induced Fluorescence strategies," in *ILASS 25th*, Estoril, Portugal, 2011.

[113] "ATSDR - Toxicological Profile: Fuel Oils/ Kerosene," Sep-2014. [Online]. Available: http://www.atsdr.cdc.gov/toxprofiles/tp.asp?id=516&tid=91. [Accessed: 01-Sep-2014].

[114] V. M. Gun'ko, R. Nasiri, and S. S. Sazhin, "A study of the evaporation and condensation of n-alkane clusters and nanodroplets using quantum chemical methods," *Fluid Phase Equilibria*, vol. 366, pp. 99–107, Mar. 2014.

[115] I. N. Shishkova and S. S. Sazhin, "A solution of the Boltzmann equations in the presence of three components and inelastic collisions," *Int. J. Heat Mass Transf.*, vol. 71, pp. 26–34, Apr. 2014.

[116] S. S. Sazhin, I. N. Shishkova, and M. Al Qubeissi, "Heating and evaporation of a two-component droplet: hydrodynamic and kinetic models," *Press HMT11178*, 2014.

[117] W. P. Crummett and A. B. Western, *University Physics: Models and Applications*. Dubuque, Iowa: Wm. C. Brown, 1994.

[118] S. S. Sazhin, P. Wild, C. Leys, D. Toebaert, and E. M. Sazhina, "The three temperature model for the fast-axial-flow CO_2 laser," *J. Phys. Appl. Phys.*, vol. 26, no. 11, pp. 1872–1883, Nov. 1993.

[119] S. S. Sazhin and I. N. Shishkova, "Kinetic modelling of Diesel fuel droplet heating and evaporation: effects of inelastic collisions and three components," in *15th International Heat Transfer Conferences*, Kyoto, Japan, 2014, vol. IHTC15–8860.

[120] J.-F. Xie, S. S. Sazhin, and B.-Y. Cao, "Molecular dynamics study of the processes in the vicinity of the n-dodecane vapour/liquid interface," *Phys. Fluids*, vol. 23, no. 11, p. 112104, 2011.

[121] M. Lapuerta, O. Armas, and J. Rodriguezfernandez, "Effect of biodiesel fuels on diesel engine emissions," *Prog. Energy Combust. Sci.*, vol. 34, no. 2, pp. 198–223, Apr. 2008.

[122] Y. Ra, R. D. Reitz, J. McFarlane, and C. S. Daw, "Effects of Fuel Physical Properties on Diesel Engine Combustion using Diesel and Bio-diesel Fuels," SAE International, Warrendale, PA, SAE Technical Paper 2008-01-1379, Apr. 2008.

[123] J. V. Gerpen, "Biodiesel processing and production," *Fuel Process. Technol.*, vol. 86, no. 10, pp. 1097–1107, Jun. 2005.

[124] S. K. Hoekman, A. Broch, C. Robbins, E. Ceniceros, and M. Natarajan, "Review of biodiesel composition, properties, and specifications," *Renew. Sustain. Energy Rev.*, vol. 16, no. 1, pp. 143–169, Jan. 2012.

[125] T. M. Mata, N. Cardoso, M. Ornelas, S. Neves, and N. S. Caetano, "Sustainable production of biodiesel from tallow, lard and poultry fat and its quality evaluation," in *Chemical engineering transactions*, 2010, vol. 19.

[126] L. C. Meher, D. Vidya Sagar, and S. N. Naik, "Technical aspects of biodiesel production by transesterification—a review," *Renew. Sustain. Energy Rev.*, vol. 10, no. 3, pp. 248–268, Jun. 2006.

[127] R. O. Dunn, "Cold-Flow Properties of Soybean Oil Fatty Acid Monoalkyl Ester Admixtures†," *Energy Fuels*, vol. 23, no. 8, pp. 4082–4091, Aug. 2009.

[128] J. Hill, E. Nelson, D. Tilman, S. Polasky, and D. Tiffany, "Environmental, economic, and energetic costs and benefits of biodiesel and ethanol biofuels," *Proc. Natl. Acad. Sci.*, vol. 103, no. 30, pp. 11206–11210, Jul. 2006.

[129] K.-L. Pan, J.-W. Li, C.-P. Chen, and C.-H. Wang, "On droplet combustion of biodiesel fuel mixed with diesel/alkanes in microgravity condition," *Combust. Flame*, vol. 156, no. 10, pp. 1926–1936, Oct. 2009.

[130] J. Tickell and K. Roman, *From the Fryer to the Fuel Tank: the Complete Guide to Using Vegetable Oil as an Alternative Fuel*. New Orleans, LA: Joshua Tickell Media Productions, 2003.

[131] U. EPA, "US Environmental Protection Agency," 15-Nov-2014. [Online]. Available: http://www.epa.gov/. [Accessed: 15-Nov-2014].

[132] W. Yuan, A. C. Hansen, and Q. Zhang, "Predicting the physical properties of biodiesel for combustion modeling," *Trans. ASAE*, vol. 46, no. 6, pp. 1487–1493, 2003.

[133] I. G. Grabar, R. V. Kolodnytska, and V. G. Semenov, *Biofuel Based on Oil for Diesel Engines*. Zhytomyr: ZDTU, 2011.

[134] G. Knothe, "Biodiesel and renewable diesel: A comparison," *Prog. Energy Combust. Sci.*, vol. 36, no. 3, pp. 364–373, Jun. 2010.

[135] G. Knothe, C. A. Sharp, and T. W. Ryan, "Exhaust Emissions of Biodiesel, Petrodiesel, Neat Methyl Esters, and Alkanes in a New Technology Engine †," *Energy Fuels*, vol. 20, no. 1, pp. 403–408, Jan. 2006.

[136] S. Dirbude, V. Eswaran, and A. Kushari, "Droplet vaporization modeling of rapeseed and sunflower methyl esters," *Fuel*, vol. 92, no. 1, pp. 171–179, Feb. 2012.

[137] S. D. Sanford, J. M. White, P. S. Shah, C. Wee, M. A. Valverde, and G. R. Meier, "Feed stock and Biodiesel Characteristics Report," Renewable Energy Group, Ames, Iowa, USA, Nov. 2009.

[138] J. Barata, "Modelling of biofuel droplets dispersion and evaporation," *Renew. Energy*, vol. 33, no. 4, pp. 769–779, Apr. 2008.

[139] A. Schönborn, N. Ladommatos, J. Williams, R. Allan, and J. Rogerson, "The influence of molecular structure of fatty acid monoalkyl esters on diesel combustion," *Combust. Flame*, vol. 156, no. 7, pp. 1396–1412, Jul. 2009.

[140] R. V. Kolodnytska, "Analytical study for atomization of hemp oil biodiesel," *Visnik East-Ukr. Natl. Univ.*, vol. 6, no. 148, pp. 41–46, 2010.

[141] P. Emberger, K. Thuneke, R. Haas, and E. Remmele, "Examination of hemp oil with regard to its suitability as fuel for engines adapted to pure plant oil use." nova-Institut für politische und ökologische Innovation GmbH, 2007.

[142] L. F. Ramírez-Verduzco, J. E. Rodríguez-Rodríguez, and A. R. Jaramillo-Jacob, "Predicting cetane number, kinematic viscosity, density and higher heating value of biodiesel from its fatty acid methyl ester composition," *Fuel*, vol. 91, no. 1, pp. 102–111, Jan. 2012.

[143] H. An, W. M. Yang, A. Maghbouli, S. K. Chou, and K. J. Chua, "Detailed physical properties prediction of pure methyl esters for biodiesel combustion modeling," *Appl. Energy*, vol. 102, pp. 647–656, Feb. 2013.

[144] M. Lapuerta, J. Rodríguez-Fernández, and O. Armas, "Correlation for the estimation of the density of fatty acid esters fuels and its implications. A proposed Biodiesel Cetane Index," *Chem. Phys. Lipids*, vol. 163, no. 7, pp. 720–727, Sep. 2010.

[145] M. Lapuerta, J. Rodríguez-Fernández, and F. Oliva, "Determination of enthalpy of formation of methyl and ethyl esters of fatty acids," *Chem. Phys. Lipids*, vol. 163, no. 2, pp. 172–181, Feb. 2010.

[146] C. L. Yaws, *Thermophysical properties of chemicals and hydrocarbons*. Norwich, NY: William Andrew, 2008.

[147] D. Hopfe, "Thermophysical data of pure substances," Data Compilation of FIZ CHEMIE, Germany, 1, 1990.

[148] E. G. Giakoumis, "A statistical investigation of biodiesel physical and chemical properties, and their correlation with the degree of unsaturation," *Renew. Energy*, vol. 50, pp. 858–878, Feb. 2013.

[149] J.-Y. Park, D.-K. Kim, Z.-M. Wang, P. Lu, S.-C. Park, and J.-S. Lee, "Production and characterization of biodiesel from tung oil," *Appl. Biochem. Biotechnol.*, vol. 148, no. 1–3, pp. 109–117, Mar. 2008.

[150] K. S. Tyson, J. Bozell, R. Wallace, E. Petersen, and L. Moens, "Biomass Oil Analysis: Research Needs and Recommendations," National Renewable Energy Lab., Golden, CO (US), NREL/TP-510-34796, Jun. 2004.

[151] "NIST," *National Institute of Standards and Technology*, 2014. [Online]. Available: http://webbook.nist.gov/chemistry/fluid/. [Accessed: 28-Feb-2014].

[152] P.-C. Chen, W.-C. Wang, W. L. Roberts, and T. Fang, "Spray and atomization of diesel fuel and its alternatives from a single-hole injector using a common rail fuel injection system," *Fuel*, vol. 103, pp. 850–861, Jan. 2013.

[153] S. Som, D. E. Longman, A. I. Ramírez, and S. K. Aggarwal, "A comparison of injector flow and spray characteristics of biodiesel with petrodiesel," *Fuel*, vol. 89, no. 12, pp. 4014–4024, Dec. 2010.

[154] C. Crua, G. de Sercey, M. Gold, and M. R. Heikal, "Image-based analysis of evaporating diesel sprays in the near-nozzle region," in *25th European Conference on Liquid Atomization and Spray Systems*, Chania, Greece, 2013.

[155] S. S. Sazhin and M. R. Heikal, "Droplet heating and evaporation–recent results and unsolved problems," *Comput. Therm. Sci.*, vol. 4, no. 6, pp. 485–496, 2012.

[156] F. Adam, F. Bertoncini, D. Thiébaut, S. Esnault, D. Espinat, and M. C. Hennion, "Towards comprehensive hydrocarbons analysis of middle distillates by LC-GCxGC," *J. Chromatogr. Sci.*, vol. 45, no. 10, pp. 643–649, Dec. 2007.

[157] J. V. Seeley, S. K. Seeley, E. K. Libby, and J. D. McCurry, "Analysis of Biodiesel/Petroleum Diesel Blends with Comprehensive Two-Dimensional Gas Chromatography," *J. Chromatogr. Sci.*, vol. 45, no. 10, pp. 650–656, Nov. 2007.

[158] C. J. Venkatramani and J. B. Phillips, "Comprehensive two-dimensional gas chromatography applied to the analysis of complex mixtures," *J. Microcolumn Sep.*, vol. 5, no. 6, pp. 511–516, 1993.

[159] V. Bykov, I. Goldfarb, V. Gol'dshtein, S. Sazhin, and E. Sazhina, "System decomposition technique for spray modelling in CFD codes," *Comput. Fluids*,

vol. 36, no. 3, pp. 601–610, Mar. 2007.

[160] I. Goldfarb, V. Gol'dshtein, G. Kuzmenko, and S. S. Sazhin, "Thermal radiation effect on thermal explosion in gas containing fuel droplets," *Combust. Theory Model.*, vol. 3, no. 4, pp. 769–787, Dec. 1999.

[161] S. S. Sazhin, G. Feng, M. R. Heikal, I. Goldfarb, V. Gol'dshtein, and G. Kuzmenko, "Thermal ignition analysis of a monodisperse spray with radiation," *Combust. Flame*, vol. 124, no. 4, pp. 684–701, Mar. 2001.

[162] S. M. Sarathy, G. Kukkadapu, M. Mehl, W. Wang, T. Javed, S. Park, M. A. Oehlschlaeger, A. Farooq, W. J. Pitz, and C.-J. Sung, "Ignition of alkane-rich FACE gasoline fuels and their surrogate mixtures," *Proc. Combust. Inst.*, vol. 35, no. 1, pp. 249–257, 2015.

[163] R. F. Sawyer, "Trends in auto emissions and gasoline composition," *Environ. Health Perspect.*, vol. 101, no. Suppl 6, pp. 5–12, Dec. 1993.

[164] S. M. Sarathy, G. Kukkadapu, M. Mehl, W. Wang, T. Javed, S. Park, M. Oehlschlaeger, A. Farooq, W. Pitz, and C.-J. Sung, "Ignition of alkane-rich FACE gasoline fuels and their surrogate mixtures," *Proc. Combust. Inst.*, 2013.

[165] B. Abramzon and S. Sazhin, "Droplet vaporization model in the presence of thermal radiation," *Int. J. Heat Mass Transf.*, vol. 48, no. 9, pp. 1868–1873, Apr. 2005.

[166] X. Ma, C. Jiang, H. Xu, H. Ding, and S. Shuai, "Laminar burning characteristics of 2-methylfuran and isooctane blend fuels," *Fuel*, vol. 116, pp. 281–291, Jan. 2014.

[167] F. L. Paxson, *The last American frontier*. Simon Publications LLC, 2001.

[168] S. S. Sazhin, T. Kristyadi, W. A. Abdelghaffar, S. Begg, M. R. Heikal, S. V. Mikhalovsky, S. T. Meikle, and O. Al-Hanbali, "Approximate Analysis of Thermal Radiation Absorption in Fuel Droplets," *J. Heat Transf.*, vol. 129, no. 9, p. 1246, 2007.

[169] W. J. Pitz, N. P. Cernansky, F. L. Dryer, F. N. Egolfopoulos, J. T. Farrell, D. G. Friend, and H. Pitsch, "Development of an Experimental Database and Chemical Kinetic Models for Surrogate Gasoline Fuels," SAE International, Warrendale, PA, SAE Technical Paper 2007-01-0175, Apr. 2007.

[170] "ChemSpider," 2014. [Online]. Available: http://www.chemspider.com/. [Accessed: 30-Dec-2014].

[171] C. L. Yaws, *Transport properties of chemicals and hydrocarbons: viscosity, thermal conductivity, and diffusivity of C1 to C100 organics and Ac to Zr inorganics*. Norwich, NY: William Andrew, 2009.

[172] F. P. Incropera and D. P. DeWitt, *Fundamentals of Heat and Mass Transfer*. New York: J. Wiley, 2002.

[173] M. Al Qubeissi, *Development of a conjugate heat transfer solver*. Saarbrücken: LAP LAMBERT Academic Publishing, 2013.

[174] K. Krisnangkura, T. Yimsuwan, and R. Pairintra, "An empirical approach in predicting biodiesel viscosity at various temperatures," *Fuel*, vol. 85, no. 1, pp. 107–113, Jan. 2006.

[175] G. Latini, R. Cocci Grifoni, and G. Passerini, Eds., *Transport properties of organic liquids*. Southampton ; Boston: WIT Press, 2006.

[176] R. C. Reid, *The properties of gases and liquids*, 4th ed. New York: McGraw-Hill, 1987.

[177] R. C. Reid, J. M. Prausnitz, and B. E. Poling, *The properties of gases and liquids*, 4th ed. New York: McGraw-Hill, 1987.

[178] K. Anand, R. P. Sharma, and P. S. Mehta, "A comprehensive approach for estimating thermo-physical properties of biodiesel fuels," *Appl. Therm. Eng.*, vol. 31, no. 2–3, pp. 235–242, Feb. 2011.

[179] W. L. H. Hallett and N. A. Clark, "A model for the evaporation of biomass pyrolysis oil droplets," *Fuel*, vol. 85, no. 4, pp. 532–544, Mar. 2006.

[180] Y. L. Wang, Q. Feng, F. N. Egolfopoulos, and T. T. Tsotsis, "Studies of C4 and C10 methyl ester flames," *Combust. Flame*, vol. 158, no. 8, pp. 1507–1519, Aug. 2011.

[181] J. McCrady, A. Hansen, and C.-F. Lee, "Physical Property Measurement of Biodiesel Fuels for Low Temperature Combustion Modeling," 2006.

[182] S. Kerschbaum and G. Rinke, "Measurement of the temperature dependent viscosity of biodiesel fuels," *Fuel*, vol. 83, no. 3, pp. 287–291, Feb. 2004.

[183] F. a. L. Machado, E. B. Zanelato, A. O. Guimarães, E. C. da Silva, and A. M. Mansanares, "Thermal Properties of Biodiesel and Their Corresponding Precursor Vegetable Oils Obtained by Photopyroelectric Methodology," *Int. J. Thermophys.*, vol. 33, no. 10–11, pp. 1848–1855, Nov. 2012.

[184] K. Chakravarthy, J. McFarlane, S. Daw, Y. Ra, R. Reitz, and J. Griffin, "Physical Properties of Bio-Diesel and Implications for Use of Bio-Diesel in Diesel Engines," SAE International, Warrendale, PA, 2007-01-4030, Oct. 2007.

[185] A. A. Vertes, *Biomass to Biofuels Strategies for Global Industries*. Chichester, West Sussex: Wiley, 2010.

[186] O. C. Díaz, F. Schoeggl, H. W. Yarranton, M. A. Satyro, T. M. Lovestead, and T. J. Bruno, "Modelling the vapour pressure of biodiesel fuels," presented at the World Academy of Science Engineering and Technology, 2012, vol. 65, pp. 876–86.

[187] A. K. Mehrotra, "A generalized viscosity equation for pure heavy hydrocarbons," *Ind. Eng. Chem. Res.*, vol. 30, no. 2, pp. 420–427, Feb. 1991.

[188] M. Zábranský and V. Růžička, "Estimation of the Heat Capacities of Organic Liquids as a Function of Temperature Using Group Additivity: An Amendment," *J. Phys. Chem. Ref. Data*, vol. 33, no. 4, pp. 1071–1081, Jan. 2005.

[189] O. P. Bagga, V. K. Rattan, S. Singh, B. P. S. Sethi, and K. S. N. Raju, "Isobaric vapor-liquid equilibria for binary mixtures of ethylbenzene and p-xylene with dimethylformamide," *J. Chem. Eng. Data*, vol. 32, no. 2, pp. 198–201, Apr. 1987.

[190] J. V. Růžička and E. S. Domalski, "Estimation of the Heat Capacities of Organic Liquids as a Function of Temperature using Group Additivity. I. Hydrocarbon Compounds," *J. Phys. Chem. Ref. Data*, vol. 22, no. 3, p. 597, 1993.

[191] A. Osmont, L. Catoire, and I. Gökalp, "Thermochemistry of methyl and ethyl esters from vegetable oils," *Int. J. Chem. Kinet.*, vol. 39, no. 9, pp. 481–491, 2007.

[192] C. L. Yaws, *Handbook of Thermal Conductivity*. Houston: Gulf Pub. Co, 1995.

[193] S. S. Sazhin, M. Al Qubeissi, R. Nasiri, V. M. Gunko, A. E. Elwardany, F. Lemoine, F. Grisch, and M. R. Heikal, "A multi-dimensional quasi-discrete model for the analysis of Diesel fuel droplet heating and evaporation," *Fuel*, vol. Accepted 15/3/2014, 2014.

[194] C. L. Yaws, *Thermophysical properties of chemicals and hydrocarbons*, 2nd ed. Oxford, UK, 2014.

[195] A. K. Mehrotra, "Correlation and prediction of the viscosity of pure hydrocarbons," *Can. J. Chem. Eng.*, vol. 72, no. 3, pp. 554–557, Jun. 1994.

[196] J. C. van Miltenburg, "Fitting the heat capacity of liquid n-alkanes: new measurements of n-heptadecane and n-octadecane," *Thermochim. Acta*, vol. 343, no. 1–2, pp. 57–62, Jan. 2000.

[197] J. Dykyj, J. Svoboda, R. C. Wilhoit, M. Frenkel, and K. R. Hall, *Landolt-Börnstein: Numerical Data and Functional Relationships in Science and Technology: 20: Vapor Pressure of Chemicals. C: Vapor Pressure and Antoine Constants for Hydrocarbons*, vol. 20 C. Springer, 1999.

[198] C. L. Yaws, *The Yaws handbook of vapor pressure: Antoine coefficients*. Houston, Tex.: Gulf Pub., 2007.

[199] J. Daridon, A. Lagrabette, and B. Lagourette, "Speed of sound, density, and compressibilities of heavy synthetic cuts from ultrasonic measurements under pressure," *J. Chem. Thermodyn.*, vol. 30, no. 5, pp. 607–623, May 1998.

[200] G. Liessmann, W. Schmidt, and S. Reiffarth, *Recommended Thermophysical Data; Data Compilation of the Saechsische Olefinwerke*, vol. 1. Germany, 1995.

[201] S. R. S. Sastri and K. K. Rao, "A new temperature–thermal conductivity relationship for predicting saturated liquid thermal conductivity," *Chem. Eng. J.*, vol. 74, no. 3, pp. 161–169, Jul. 1999.

[202] K. R. Hall and K. N. Marsh, *Landolt-Börnstein - Group IV Physical Chemistry: Densities of Polycyclic Hydrocarbons*, vol. 8 F. 1999: Springer, 1999.

[203] D. Ambrose, B. E. Broderick, and R. Townsend, "The vapour pressures above the normal boiling point and the critical pressures of some aromatic hydrocarbons," *J. Chem. Soc. Inorg. Phys. Theor.*, p. 633, 1967.

[204] T. N. Nesterova, I. A. Nesterov, and A. A. Pimerzin, "The thermodynamics of the sorption and evaporation of alkylbenzene," Izvestia Vysshikh Uchebnykh Zavedeniy, 43, 2000.

[205] E. D. Nikitin, A. P. Popov, N. S. Bogatishcheva, and Y. G. Yatluk, "Vapor–Liquid Critical Properties of n-Alkylbenzenes from Toluene to 1-Phenyltridecane," *J. Chem. Eng. Data*, vol. 47, no. 4, pp. 1012–1016, Jul. 2002.

[206] K. H. Simmrock, R. Janowsky, and A. Ohnsorge, *Critical Data of Pure Substances*. Frankfurt/Main, Federal Republic of Germany: DECHEMA, 1986.

[207] K. R. Hall and K. N. Marsh, Eds., *Landolt-Börnstein - Group IV Physical Chemistry. Densities of Aromatic Hydrocarbons*, vol. 8E. Springer Berlin Heidelberg, 1998.

[208] K. G. Joback and R. C. Reid, "Estimation of Pure-Component Properties from Group-Contributions," *Chem. Eng. Commun.*, vol. 57, no. 1–6, pp. 233–243, 1987.

[209] L. Constantinou and R. Gani, "New group contribution method for estimating properties of pure compounds," *AIChE J.*, vol. 40, no. 10, pp. 1697–1710, Oct. 1994.

[210] J. M. N. A. Fareleira, S. F. Y. Li, and W. A. Wakeham, "The thermal conductivity of liquid mixtures at elevated pressures," *Int. J. Thermophys.*, vol. 10, no. 5, pp. 1041–1051, Sep. 1989.

[211] K. N. Marsh, Ed., *Recommended Reference Materials for the Realization of Physicochemical Properties*. Oxford [Oxfordshire]; Boston: Blackwell Scientific Publications, 1987.

[212] R. G. Ross, P. Andersson, B. Sundqvist, and G. Backstrom, "Thermal conductivity of solids and liquids under pressure," *Rep. Prog. Phys.*, vol. 47, no. 10, pp. 1347–1402, Oct. 1984.

[213] N. I. Kolev, *Multiphase Flow Dynamics*. Berlin; New York: Springer, 2007.

[214] A. O. Guimarães, F. A. L. Machado, E. C. da Silva, and A. M. Mansanares, "Investigating thermal properties of biodiesel/diesel mixtures using photopyroelectric technique," *Thermochim. Acta*, Oct. 2011.

[215] J. Bellan, "Supercritical (and subcritical) fluid behavior and modeling: drops, streams, shear and mixing layers, jets and sprays," *Prog. Energy Combust. Sci.*, vol. 26, no. 4–6, pp. 329–366, Aug. 2000.

[216] N. Dadgostar and J. M. Shaw, "A predictive correlation for the constant-pressure specific heat capacity of pure and ill-defined liquid hydrocarbons," *Fluid Phase Equilibria*, vol. 313, pp. 211–226, Jan. 2012.

[217] B. I. Lee and M. G. Kesler, "Private Communication," Mobil Oil Corporation, Princeton, N.J., 1975.

[218] B. I. Lee and M. G. Kesler, "A generalized thermodynamic correlation based on three-parameter corresponding states," *AIChE J.*, vol. 21, no. 3, pp. 510–527, 1975.

[219] F. Gharagheizi and A. Fazeli, "Prediction of the Watson Characterization Factor of Hydrocarbon Components from Molecular Properties," *QSAR Comb. Sci.*, vol. 27, no. 6, pp. 758–767, 2008.

[220] G. Latini, R. Cocci Grifoni, and G. Passerini, Eds., *Transport properties of organic liquids*. Southampton; Boston: WIT Press, 2006.

[221] A. J. Komkoua Mbienda, C. Tchawoua, D. A. Vondou, and F. Mkankam Kamga, "Evaluation of Vapor Pressure Estimation Methods for Use in Simulating the Dynamic of Atmospheric Organic Aerosols," *Int. J. Geophys.*, vol. 2013, p. e612375, Jun. 2013.

Appendix A. THERMODYNAMIC PROPERTIES OF AIR

Thermal conductivity

The following approximation of data for thermal conductivity of air given in [172], valid in the range of temperatures from 250 K to 1200 K, was used:

$$k_{air} = -0.00189\,\tilde{T}^2 + 0.0252\,\tilde{T} + 0.0036, \tag{A.1}$$

where $\tilde{T} = T/300$.

Dynamic viscosity

Air dynamic viscosity (in Pa $\cdot$ s) is approximated as [172]:

$$\mu_{air} = 10^{-7}\,(-0.00028\,T^2 + 0.654\,T + 13.6), \tag{A.2}$$

where $250\text{ K} \leq T \leq 350\text{ K}$. An alternative approximation for the range of temperature where $250\text{ K} \leq T \leq 800\text{ K}$ can be presented as [172]:

$$\mu_{air} = 10^{-7} \begin{pmatrix} -0.00019342657\,T^2 + \\ 0.58086013986\,T + 27.72412587413 \end{pmatrix}. \tag{A.3}$$

Equation (A.3) is used in this analysis.

Specific heat capacity

Specific heat capacity of air in J/kg/K is approximated as [172]:

$$c_{p,air} = 10^{-3}(0.0000002\,T^2 - 0.00009\,T + 1.016), \tag{A.4}$$

where $250\text{ K} \leq T \leq 350\text{ K}$. An alternative approximation for the range of temperature where $250\text{ K} \leq T \leq 800\text{ K}$ can be presented as [172]:

$$c_{p_{air}} = 3.15 \times 10^{-10}\,T^4 - 1.1 \times 10^{-6}\,T^3 + 1.4 \times 10^{-3}\,T^2 - 0.558\,T + 1074.8. \tag{A.5}$$

Equation (A.5) is used in this analysis.

Density

Density of air at atmospheric pressure in kg/m³ is approximated in the range of temperature $250 \text{ K} \leq T \leq 800 \text{ K}$ as [172]:

$$\rho_{air} = -0.00000000685 \, T^3 + 0.00001408584 \, T^2 - 0.01034857135 \, T + 3.19595945166. \tag{A.6}$$

An alternative, direct implementation of density can be found using the equation of state for ideal gas as:

$$\rho_{air} = \frac{P_g}{R \, T_r}, \tag{A.7}$$

where P_g is the ambient pressure (Pa), R is the gas constant for air (287.016 $J \, kg^{-1} \, K^{-1}$), T_r is the reference temperature $(T_r \text{ (in K)} = (2/3)T_s + (1/3)T_g)$. Equation (A.7) is used in this analysis. Most of the above mentioned properties are taken from [172], [173] and shown in Table A.1.

Table A.1 Thermal Properties of dry air at atmospheric pressure.

Temperature - t - (°C)	Density - ρ - (kg/m³)	Specific heat capacity - c_p - (kJ/kg K)	Thermal conductivity - λ - (W/m K)	Kinematic viscosity - ν - (m²/s) × 10⁻⁶	Expansion coefficient - b - (1/K) × 10⁻³	Prandtl's number - P_r -
-150	2.793	1.026	0.0116	3.08	8.21	0.76
-100	1.980	1.009	0.0160	5.95	5.82	0.74
-50	1.534	1.005	0.0204	9.55	4.51	0.725
0	1.293	1.005	0.0243	13.30	3.67	0.715
20	1.205	1.005	0.0257	15.11	3.43	0.713
40	1.127	1.005	0.0271	16.97	3.20	0.711
60	1.067	1.009	0.0285	18.90	3.00	0.709
80	1.000	1.009	0.0299	20.94	2.83	0.708
100	0.946	1.009	0.0314	23.06	2.68	0.703
120	0.898	1.013	0.0328	25.23	2.55	0.70
140	0.854	1.013	0.0343	27.55	2.43	0.695
160	0.815	1.017	0.0358	29.85	2.32	0.69
180	0.779	1.022	0.0372	32.29	2.21	0.69
200	0.746	1.026	0.0386	34.63	2.11	0.685
250	0.675	1.034	0.0421	41.17	1.91	0.68
300	0.616	1.047	0.0454	47.85	1.75	0.68
350	0.566	1.055	0.0485	55.05	1.61	0.68
400	0.524	1.068	0.0515	62.53	1.49	0.68

Appendix B. PROPERTIES OF BIODIESEL FUEL

All values of parameters in this section are given in SI units. For temperatures above the upper limit of the validity of formulae given below it is assumed that the corresponding transport and thermodynamic properties are equal to those at the upper limit temperatures, unless otherwise specified.

B1. Transport and thermodynamic properties of biodiesel fuel components

Liquid density

The density of pure liquid methyl esters shown in Tables 3.1 and 3.2 (Chapter 3) are estimated based on the following general formula [144]:

$$\rho_l = \rho_{l0} - \alpha_T (T - 288.15), \tag{B.1}$$

where $\rho_{l0} = 851.471 + \frac{250.718\,\mathrm{DB} + 280.899}{1.214 + n_\mathrm{acid}}$, $\alpha_T = \frac{7.536}{\ln(n_{acid}) + 3.584} - 0.446$,

n_acid is the number of carbons in fatty acids, and DB is the number of double bonds.

The lower limit of applicability of Equation (B.1) was extended up to 288.15 K (15 °C), while the upper limit of their applicability was not investigated in [144]. However, based on the results presented in [143] we can anticipate that the linear dependence of liquid density on temperature is maintained from room temperature up until the vicinity of the critical temperature with about the same regression rate. This allows us to use this equation from 288.15 K to the critical temperature.

It is anticipated that at temperatures close to the critical temperature, if this range of temperatures is reached, the droplets become close to being completely evaporated and the errors in estimating droplet densities will have negligible effect on the overall droplet evaporation time.

Liquid viscosity

For saturated methyl esters (with zero double bonds, DB = 0) the liquid kinematic viscosity can be estimated based on the following formula, valid in the temperature range $293.15K \leq T \leq 353.15$ K [174]:

$$\ln(10^6 v_l) = -2.177 - 0.202\, n_{acid} + \frac{403.66}{T} + \frac{109.77\, n_{acid}}{T}, \tag{B.2}$$

Formula (B.2) can still be used at temperatures above 353.15 K, although with lower accuracy [174]. Remembering that the final results are not very sensitive to the values of v_l, this formula is used in the temperature range 293.15 K $\leq T \leq \min(700$ K, $T_{cr})$. Note that for the processes considered, the droplet temperatures almost never exceed 700 K.

For unsaturated methyl esters (with non-zero double bonds, DB≥1) the liquid kinematic viscosity is estimated based on the following formula, valid in temperature range $T \leq 0.7 T_{cr}$ [132], [143]:

$$\ln\left(\frac{10^6 v_l \rho_l}{\rho_{l(20)} M}\right) = A_k + \frac{B_k}{T}, \tag{B.3}$$

where $\rho_{l(20)}$ is liquid density at T = 293.15 K, M are molar masses given in Table 3.2 (Chapter 3). Coefficients A_k and B_k are given in Table B1.

Table B.1 Coefficients A_k and B_k used in Formula (B.3).

Coefficient	C16:1 M–C24:1 M	C18:2 M	C18:3 M
A_k	10.83	9.93	9.03
B_k	2099	1721	1343

Liquid thermal conductivity and latent heat of evaporation

The thermal conductivity of pure liquid methyl esters shown in Tables 3.1 and 3.2 (Chapter 3) is estimated based on the following general formula (Latini method) [82], [175]–[177]:

$$k_l = \frac{0.0415\, T_b^{1.2}(1-T_r)^{0.38}}{M\, T_{cr}^{0.167} T_r^{1/6}}, \tag{B.4}$$

where $T_r = T/T_{cr}$. The values of the boiling and critical temperatures (T_b and T_{cr})

for methyl esters used in our study are estimated from the following expressions [23]:

$$T_b = a_b + b_b M, \tag{B.5}$$

$$T_{cr} = a_{cr} + b_{cr} M, \tag{B.6}$$

the values of coefficients in Equations (B.5) and (B.6) for various pure methyl esters are given in Table B.2.

Table B.2 The values of coefficients used in Equations (B.5), (B.6) and (B.8) for various pure methyl esters.

Coefficient	C12:0 M–C24:0 M	C16:1 M–C24:1 M	C18:2 M	C18:3 M
a_b	348.7	350.4	352.1	353.82
b_b	0.8478	0.8463	0.8463	0.8472
a_{cr}	534.3	538.5	542.6	546.8
b_{cr}	0.784	0.777	0.772	0.7711
a_L	1.506×10^7	1.3897×10^7	1.270×10^7	1.154×10^7
b_L	1.814×10^5	1.822×10^5	1.834×10^5	1.843×10^5

The calculation of the thermal conductivity of the mixture of components forming biodiesels, presented in Table 3.1, led to its noticeable (up to 50%) underestimation compared with experimentally observed values. This under-estimation could be attributed to the low accuracy of the estimation of the coefficient 0.0415 for methyl esters. We were able to demonstrate that replacing this coefficient with 0.0713 led to much better agreement with experimental data for the mixtures. This leads to the modification of Equation (B.4) to

$$k_l = \frac{0.0713 \, T_b^{1.2} (1-T_r)^{0.38}}{M \, T_{cr}^{0.167} T_r^{1/6}}. \tag{B.7}$$

The method of estimation of thermal conductivity based on (B.7) is called the modified Latini method. The results predicted by (B.7) were validated based on experimental data presented in [92], [178].

The molar latent heat of evaporation of pure methyl esters shown in Tables 3.1 and 3.2 is estimated based on the following general formula, valid in the temperature range $300 \text{ K} \leq T \leq 700 \text{ K}$ [23], [179]:

$$L = (a_L + b_L M)\emptyset_L, \qquad\qquad (\text{B.8})$$

where

$$\emptyset_L = \left(\frac{T_{cr}-T}{T_{cr}-T_b}\right)^{0.38}, \qquad\qquad (\text{B.9})$$

the values of coefficients in Equations (B.5), (B.6) and (B.8) for various pure methyl esters are given in Table B2.

Note that coefficients for C18:3 M were obtained via the linear extrapolation of the values of the coefficients for C18:1 M and C18:2 M. Although the coefficients in (B.8) were obtained for $300 \ K \leq T \leq 700 \ K$, this formula is used in our analysis for temperatures up to the critical temperature to allow us to capture zero L at the critical temperature. This assumption has no practical importance as droplet surface temperatures in our calculations did not exceed 700 K in almost all cases.

Liquid heat capacity

The specific heat capacities (in J/(kg K)) of pure liquid methyl esters (shown in Tables 3.1 and 3.2 (Chapter 3)) are estimated based on the following general formula, valid in the temperature range $300\text{K} \leq T \leq \min(700 \text{ K}, T_{cr})$ [23], [179]:

$$c_l = \left(a_{pl} + b_{pl}T + c_{pl}T^2\right) \times 10^3, \qquad\qquad (\text{B.10})$$

where the values of coefficients are given in Table B3 [23]. As in the case of Table B2, the coefficients for C18:3 M are obtained via the linear extrapolation of the values of the coefficients for C18:1 M and C18:2 M.

Table B.3 The values of coefficients used in Equation (B.10) for various pure methyl esters.

Coeff.	C12:0 M– C24:0 M	C16:1 M– C24:1 M	C18:2 M	C18:3 M

a_{pl}	1.816	1.915	2.018	2.115
b_{pl}	-1.462×10^{-3}	-2.163×10^{-3}	-2.878×10^{-3}	-3.580×10^{-3}
c_{pl}	7.51×10^{-6}	8.29×10^{-6}	9.09×10^{-6}	9.92×10^{-6}

Liquid diffusion coefficient

In [47], [55], [69] it was suggested that the diffusion coefficient of component j relative to all other components can be estimated based on the simplified versions of the Sanchez and Clifton formula [82]. At the same time it was shown in [85], [86] that a more accurate approximation for D_{jm} is given by Formula (2.34). As mentioned in Chapter 2, the difference between these formulae is not important as the simplified model, based on the assumption that $D^0_{mj} = D^0_{jm}$, is used in this analysis.

As in [43], [45], from amongst various approximations for D^0_{jm} and D^0_{mj} the Wilke-Chang approximation was chosen. Assuming that the associated parameter of solvent in this formula is equal to 1 and D_{jm} is the same for all species, approximation (2.35) in Section 2.6 (Chapter 2) is used.

It is worth mentioning that Expression (2.40), in Section 2.6 (Chapter 2), with M identified as the mixture molar mass, is found to be more convenient for calculations of σ_v, compared with other formulae. Using Expression (2.40), the following values have been obtained: $\sigma_v = 7.86$ Å for PME, $\sigma_v = 7.93$ Å for HME1, HME2 and SME, $\sigma_v = 8.05$ Å for RME. The above values of σ_v for SME and RME were close to the corresponding experimentally observed values reported in [91]. Alternative approaches to the estimation of σ_v are discussed in [90], [92], [93], [96], [180]. These are not used in this study.

B2. Transport and thermodynamic properties of biodiesel fuel mixture

Average values

Data presented in Section B1 are used to calculate average values of liquid density, specific heat capacity, dynamic viscosity and thermal conductivity using the formulae presented in Section 2.8 (Chapter 2).

The values of parameters predicted by Equations (2.46)−(2.52) are compared with the values reported by other authors (measured or calculated) where possible.

Liquid density

The values of liquid density (reported in [181] and calculated from Equations (46) and (27) in the paper) for Palm Methyl Ester (PME), Rapeseed oil Methyl Ester (RME), and Soybean oil Methyl Ester (SME) are compared in Table B.4. The values are presented only for the cases reported in [181]. The same comment applies to Tables B.5 and B.6.

Table B.4 The values of liquid density reported in [181] and calculated from Equations (2.46) and (B.1) for Palm Methyl Ester (PME), Rapeseed oil Methyl Ester (RME), and Soybean oil Methyl Ester (SME).

Temperature (K)	PME measured/calculated	RME measured/calculated	SME measured/calculated
293.15	–	886.4/878.823	891.4/882.303
298.15	876.0/867.303	–	–
313.15	866.4/856.382	871.4/864.634	876.4/867.9
333.15	849.3/843.62	864.3/850.445	869.4/853.497
353.15	841.3/827.260	849.3/836.256	856.3/839.094
360.15	834.3/822.161	841.3/831.290	846.3/834.053

As one can see from Table B.4, the agreement between the values of density obtained by both approaches is reasonably good. In the our calculations the gradients of density inside droplets are ignored. The average density is

calculated based on the average temperature and composition inside the droplets as was done in [55], [69].

Liquid viscosity

The values of liquid dynamic viscosities reported by [147] and obtained from Equations (2.51), (B.2), (B.3) for Palm Methyl Ester (PME), Rapeseed oil Methyl Ester (RME), and Soybean oil Methyl Ester (SME) are compared in Table B.5.

Table B.5 The values of liquid dynamic viscosities (in $kg\,m^{-1}\,s^{-1}$) reported by [147] and calculated from Equations (2.51), (B.2), (B.3) for Palm Methyl Ester (PME), Rapeseed oil Methyl Ester (RME), and Soybean oil Methyl Ester (SME).

Temperature	PME	RME	SME
(K)	Measured/ calculated	Measured/ calculated	Measured/ calculated
293.15	–	0.006777/0.00583394	0.005853/0.00511201
298.15	0.006041/0.00548836	–	–
313.15	0.004256/0.00388956	0.004212/0.0038166	0.003785/0.00342128
333.15	0.002954/0.00257629	0.003052/0.00262691	0.002793/0.00238586
353.15	0.002158/0.00178582	0.002251/0.0018860	0.002099/0.00173252
373.15	0.001654/0.00158557	0.001646/0.0014026	0.001537/0.001561884

As one can see from Table B.5, the agreement between the values of dynamic viscosity obtained by both approaches is reasonably good. They differ by no more than 17% which is acceptable for our analysis remembering that the results are rather weak functions of viscosity in most cases. This is consistent with the results of measurements of biodiesel viscosities reported by various authors. For example, the values of viscosities for two different RMEs at temperature 293.15 K measured by [182] turned out to be 6.09×10^{-3} $kg\,m^{-1}s^{-1}$ and 6.24×10^{-3} $kg\,m^{-1}s^{-1}$. These values are more that 8% smaller than those measured in [181].

As in the case of density, in our calculations the gradients of dynamic viscosity inside droplets are ignored. The average dynamic viscosity is

calculated based on the average temperature and composition inside the droplets as was done in [55], [69] for Diesel and gasoline fuels.

Liquid thermal conductivity and latent heat of evaporation

The values of liquid thermal conductivity estimated in [181]; calculated using Equations (B.7) and (2.52), modified Latini method (see [82], [175] for original Latini approach), (in W m^{-1}K^{-1}) of Palm Methyl Ester (PME), Rapeseed oil Methyl Ester (RME), and Soybean oil Methyl Ester (SME) are compared in Table B.6. The results for temperatures below 300 K, which are not relevant for most automotive applications, are not included in this table.

Table B.6 The values of liquid thermal conductivity (in W m^{-1}K^{-1}) estimated in [181]; calculated from Equations (B.7) and (2.52), modified Latini method; of Palm Methyl Ester (PME), Rapeseed oil Methyl Ester (RME), and Soybean oil Methyl Ester (SME).

Temperature(K)	PME Estimated/ calculated	RME Estimated/ calculated	SME Estimated/ calculated
300	0.16999/0.16950	0.17696/0.16423	0.17887/0.167862
350	0.16158/0.158077	0.16860/0.153490	0.17031/0.156720
400	0.15282/0.14711	0.15991/0.143202	0.16139/0.146016
450	0.14361/0.136234	0.15083/0.13306	0.15204/0.135435
500	0.13384/0.1251531	0.14125/0.12280	0.14216/0.124685
550	0.12333/0.11810	0.13104/0.114150	0.13159/0.116403
600	0.11180/0.1180930	0.11997/0.113173	0.12007/0.116387

As one can see from Table B6, the agreement between the values of thermal conductivity predicted by both approaches is reasonably good. They differ by no more than 14%. The measurements of thermal conductivity of SME and RME reported by [183] gave values 0.154 ± 0.002 W m^{-1}K^{-1} and 0.149 ± 0.001 W m^{-1}K^{-1} respectively, at room temperature. These values are reasonably close to those presented in Table B6. The values predicted by the original Latini method (Equation (B.4)) would lead to the values of thermal conductivity about 50% less than those reported in [181]. Until we are able to understand the root

of the deviation between these results, the modified Latini method will be used to estimate the liquid thermal conductivity.

As in the case of density and dynamic viscosity, in our calculations the gradients of thermal conductivity inside droplets are ignored. The average thermal conductivity is calculated based on the average temperature and composition inside the droplets as was done in [55], [69].

The values of the molar latent heat of evaporation of SME in the temperature range from below 300 K to almost 800 K are presented in [184] in graphical form. This latent heat was shown to be lower than that of Diesel fuel at low temperatures but higher than that of Diesel fuel at high temperatures [185].

Liquid heat capacity

The calculated values of the molar heat capacity of SME in the temperature range from 300 K to 600 K are presented in [184] in graphical form. It was shown to increase almost linearly with temperature. Similar results but for canola and coconut biodiesel fuels and in a narrower temperature range (283–328 K) were reported in [186].

B3. Transport and thermodynamic properties of biodiesel fuel vapour

Saturated vapour pressure

The saturated vapour pressure (in Pa) of pure liquid methyl esters shown in Tables 3.1 and 3.2 (Chapter 3) is approximated by the following general formula, valid in the temperature range $260\,K \leq T \leq 610\,K$ [151]:

$$p_v = 10^3\, a_{CN,0} \left[a_{uc}(\text{DB}+1) + b_{uc} + \frac{c_{uc}}{\text{DB}+1}\right] \exp\left(a_{CN,1} n_{\text{acid}}\right), \qquad (\text{B.11})$$

where

$a_{CN,0} = 1.908\,\exp(0.01715T)$,

$a_{CN,1} = -5.656 + 0.02649\,T - 4.5417 \times 10^{-5}\,T^2 + 2.6571 \times 10^{-8}T^3$,

for DB $= 0$ or $T > 323$ K, $a_{uc} = c_{uc} = 0$, $b_{uc} = 1$, otherwise:

$a_{uc} = 5.05 - 3.06 \times 10^{-2}\,T + 4.62 \times 10^{-5}\,T^2$,

$b_{uc} = -9.93 + 3.39 \times 10^{-2}\,T$,

$c_{uc} = 9.62 - 2.97 \times 10^{-2}\,T$.

Vapour density is calculated using the ideal gas law.

In the case of biodiesel mixture, the following approximation for the saturated vapour pressure of SME (in bars) was suggested in [187], based on data provided by [188]:

$$\log_{10} p_v = 76.08 - 8143\,T^{-1} - 23.011 \log_{10}(T) + 6 \times 10^{-5}\,T + 3.2 \times 10^{-6}\,T^2, \quad (\text{B.12})$$

the temperature range of this equation is (300–700 K).

Similar results but for canola and coconut biodiesel fuels and in a graphical form in the temperature range from about 323 K to 473 K, using experimental data from [189], were reported in [151]. The saturated vapour pressures for biodiesel fuel were shown to be much lower than those for Diesel fuel [190].

Vapour diffusion coefficients

The formulae for binary diffusion coefficients of five dilute gaseous methyl esters in air, valid in the temperature range $300 \text{ K} \leq T \leq min(T_{cr}, 750 \text{ } K)$ and pressure equal to 1 bar are presented in Table B.7 [143].

As follows from Table B.7, the values of all diffusion coefficients are rather close. In this analysis we use only the average values of this coefficient for the mixtures of methyl esters. It is assumed that these values do not depend on the composition of this mixture and can be assumed equal to [74], [87]:

$$D_v = \frac{2 \times 10^{-10} T^{1.75}}{p},$$
(B.13)

where p is pressure in bars. Expression (B.13) is used in our analysis.

Table B.7 The approximations for the binary diffusion coefficients of five dilute gaseous methyl esters in air.

Methyl ester	Binary diffusion coefficient of diluted methyl esters in air
C16:0 M	D_v = 2.048241 X 10^{-10} $T^{1.75}$
C18:0 M	D_v = 1.935023 X 10^{-10} $T^{1.75}$
C18:1 M	D_v = 1.946548 X 10^{-10} $T^{1.75}$
C18:2 M	D_v = 1.958266 X 10^{-10} $T^{1.75}$
C18:3 M	D_v = 1.970184 X 10^{-10} $T^{1.75}$

Vapour heat capacity

Using data provided in [191], [192], the following approximation for the vapour heat capacities of the components of biodiesel fuels in the range of temperatures $300 \text{ K} \leq T \leq 1200 \text{ K}$ was regressed to:

$$c_{pv} = a_{cpv} \tilde{T}^5 + b_{cpv} \tilde{T}^4 + c_{cpv} \tilde{T}^3 + d_{cpv} \tilde{T}^2 + e_{cpv} \tilde{T} + f_{cpv},$$
(B.14)

where $\tilde{T} = T/300$. The values of the coefficients for the components are given in Table B.8. For the component identified as 'Other' the parameters for C18:1 M were used. These provided the required average values for c_{pv} calculated using the remaining components.

The verifications of Equation (B.14) for many different modelcules are shown in Figures B.1 and B.2.

Table B.8 The values of coefficients used in Equation (B.14) for various pure methyl esters.

Comp.	a_{cpv}	b_{cpv}	c_{cpv}	d_{cpv}	e_{cpv}	f_{cpv}
C12:0 M	0.027532	-1.509613	32.489208	-348.51699	1937.2422	-196.0638
C14:0 M	0.028031	-1.537655	33.11172	-355.39110	1975.950	-217.7930
C16:0 M	0.02847	-1.562807	33.666284	2866.5450	2008.022573	-236.281242
C17:0 M	-32.23395	359.06409	-1525.7052	2866.5450	-1140.510	913.0750
C18:0 M	0.029073	-1.592711	34.24248	-366.85710	2035.6890	-252.3560
C20:0 M	-33.507964	372.266358	-1578.271181	2963.634219	-1205.392857	929.231426
C22:0 M	-35.404232	392.035853	-1657.479888	3114.46656	-1334.93298	972.121710
C24:0 M	-38.172408	420.952853	-1773.590013	3337.37856	-1536.64767	1041.9097
C16:1 M	0.028355	-1.5482140	33.1419870	-353.10969	1946.71590	-194.67430
C18:1 M	0.028632	-1.5654230	33.5567610	-358.027218	1976.32596	-210.68717
C20:1 M	-37.732982	415.113425	-1742.582079	3261.99987	-1489.90392	1034.48570
C22:1 M	-43.35771	473.480486	-1975.083156	3702.98628	-1869.74505	1162.5471
C24:1 M	-48.982436	531.847544	-2207.584225	4143.97269	-2249.586144	1290.60857
C18:2 M	0.028537	-1.5528230	33.0974650	-350.761281	1921.716581	-176.117655
C18:3 M	0.028230	-1.5313670	32.5055730	-342.625176	1864.607187	-140.492938
Other	0.028632	-1.565423	33.556761	-358.027218	1976.325960	-210.68717
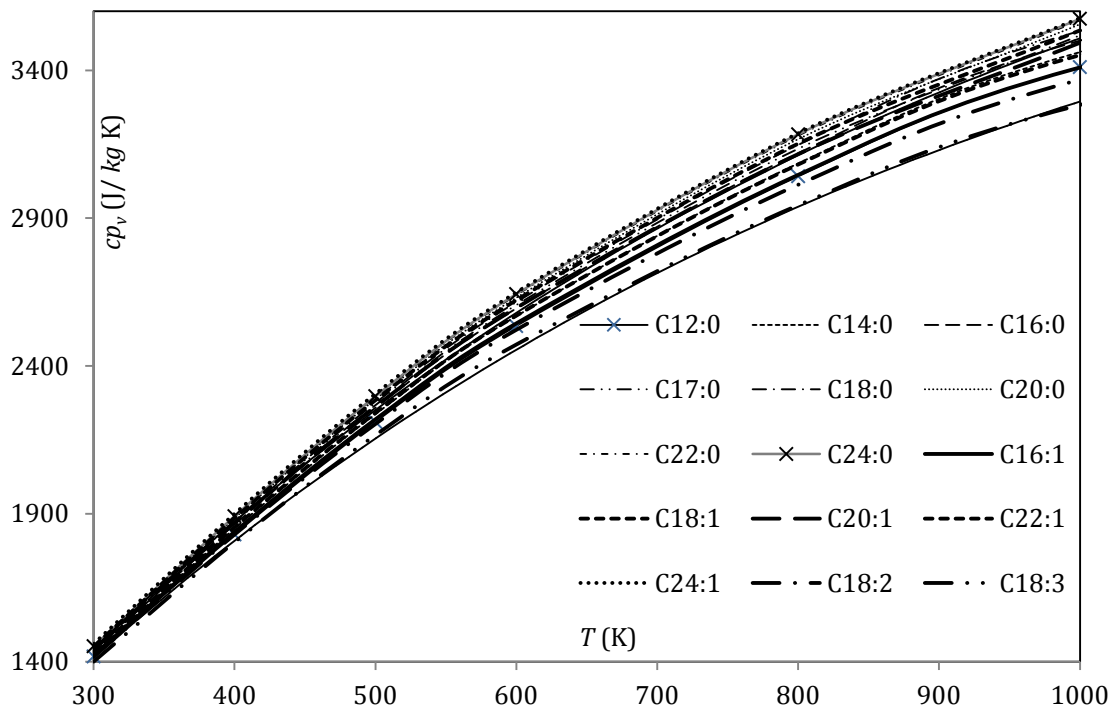
Figure B.1 Specific heat capacities of various methyl esters in biodiesel fuel vapour.
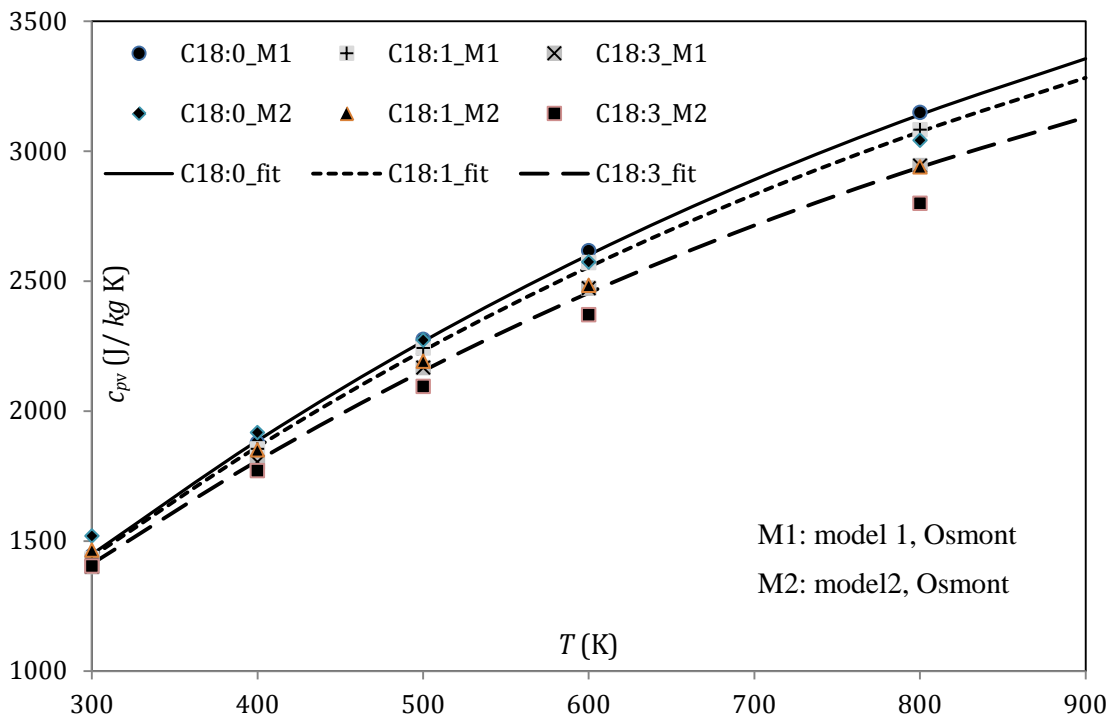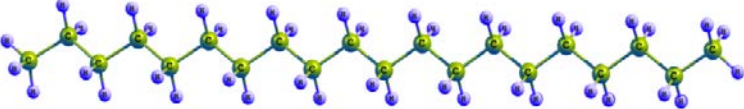
Figure B.2 Regression of experimental data [191] for specific heat capacities of various methyl esters in biodiesel fuel vapour.
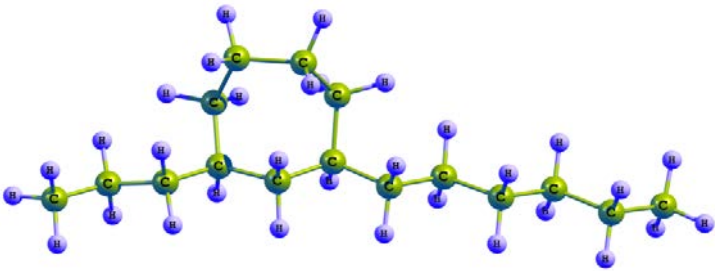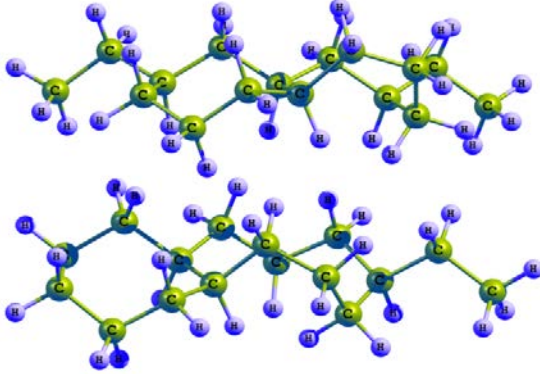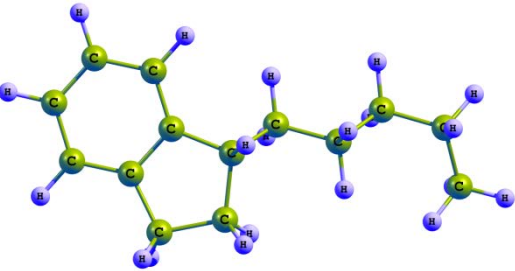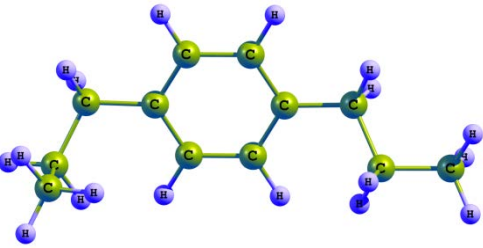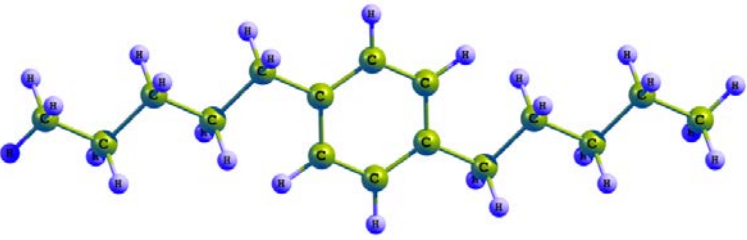
Gas viscosity and thermal conductivity

We assume that fuel vapour is sufficiently diluted to allow us to consider both these transport coefficients for the mixture to be equal to that for air.

Appendix C. PROPERTIES OF DIESEL FUEL

All values of parameters are given in SI units. All approximations for transport and thermodynamic properties are strictly valid only for the limited range of temperatures and carbon numbers stated. Two methods of extrapolating these values beyond this range are commonly used. Firstly, it is assumed that the values at $T < T_{min}$ and $n < n_{min}$ are the same as the values at $T = T_{min}$ and $n = n_{min}$, and the values at $T > T_{max}$ and $n > n_{max}$ are the same as the values at $T = T_{max}$ and $n = T_{max}$. Secondly, the approximations are used beyond the range of temperatures and carbon numbers for which they were originally obtained. In both cases, these extrapolations can lead to errors which are difficult to control, and their choice depends on the physical nature of the properties and the availability of experimental data beyond the range of temperatures for which they were obtained (see [146], [176], [177]). The methods of extrapolation will be specified for specific properties of particular components. The values of properties at $T > T_{cr}$ are assumed to be the same as those at $T = T_{cr}$ (this approximation allows us to avoid rigorous analysis of the case when the droplet temperatures exceed the critical temperatures of the lightest components; the errors imposed by this approximation are expected to be small). In Figure C.1, the structures of some organic components of Diesel fuel are displayed.

Name of molecule	Molecular structure
n-didecyl, $C_{20}H_{42}$	
3,6,9,10-methyl-dodecane, $C_{16}H_{34}$	

1-propyl-3-hexyl-cycloheptan, $C_{16}H_{32}$	
Diethylbicycloheptan, $C_{16}H_{30}$ + ethylcycloheptan-cyclononane, $C_{16}H_{30}$	
pentylindane, $C_{14}H_{20}$	
1,4-dipropylbenzene, $C_{12}H_{18}$	
1,4-dipentylbenzene, $C_{16}H_{26}$	

1-propylnaphthalene, $C_{13}H_{14}$	
di(3-ethyl-phenyl)methane, $C_{19}H_{20}$	
1-propyl-(1,2,3,4-tetrahydronaphthalene), $C_{13}H_{18}$	
ethylphenanthrene, $C_{16}H_{14}$	
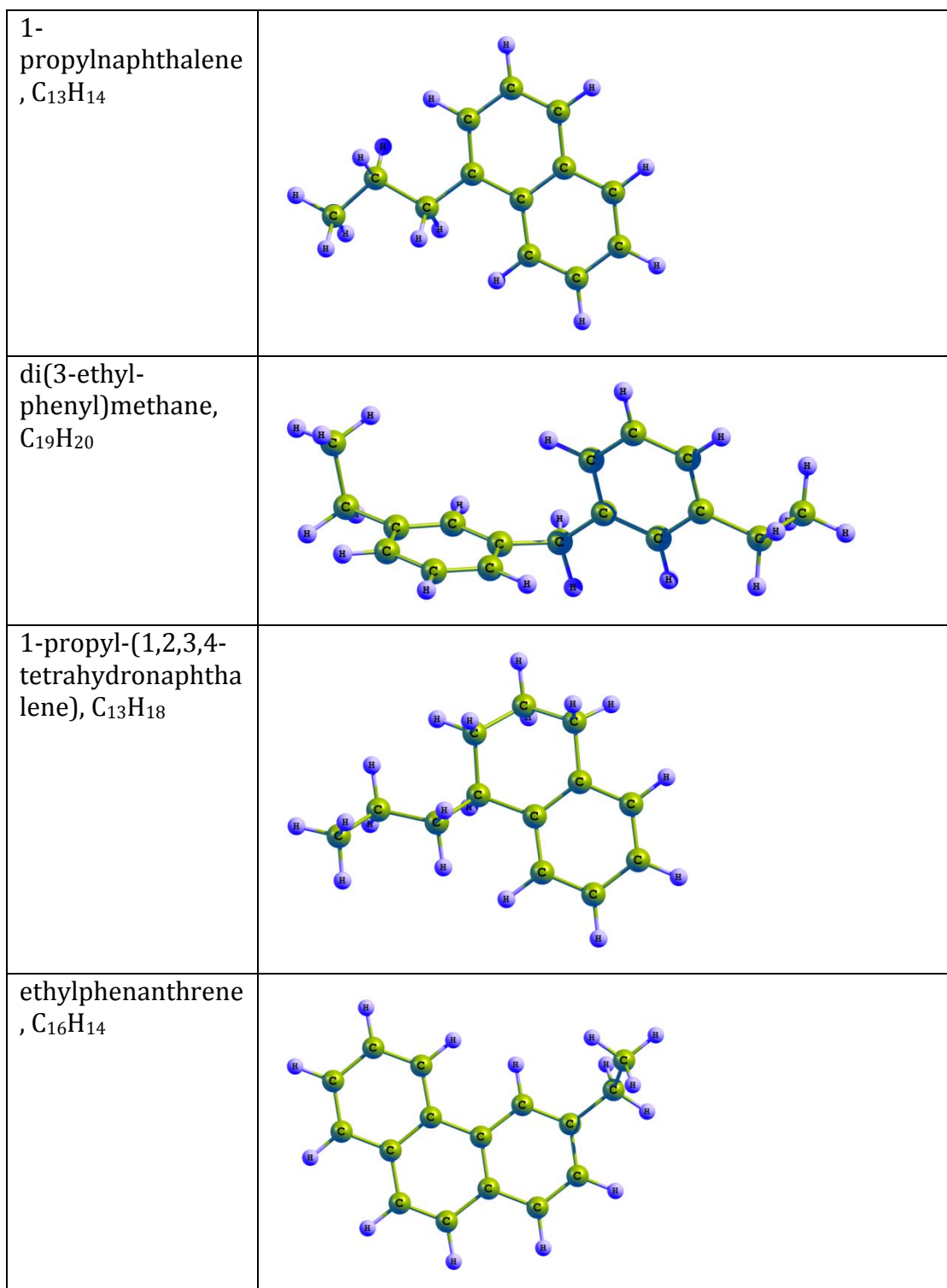
Figure C.1 The structures of some organic components of Diesel fuel [64,108].

C1. Transport and thermodynamic properties of alkanes

Molecular structure, boiling and critical temperatures

The chemical formula of alkanes is C_nH_{2n+2} ($8 \leq n \leq 27$) and they incorporate n-alkanes and iso-alkanes, the chemical structures of which for n = 20 and n = 16 are shown in Figure C.1 (n-icosane and 3,6,9,10-methyl-dodecane). The difference in transport and thermodynamic properties of n-alkanes and iso-alkanes is ignored in our analysis. For example, the difference between the boiling temperatures of alkanes and iso-alkanes for $n = 8 - 20$ does not exceed 4.5 K [146], which is less than about 1% of the value of this boiling temperature.

Using data provided in [146], [194], the dependence of critical and boiling temperatures on n was approximated by the following expressions, valid in the range $5 \leq n \leq 25$ [47]:

$$T_{cr(a)}(n) = a_{ca} + b_{ca}\, n + c_{ca}\, n^2 + d_{ca}\, n^3, \tag{C.1}$$

$$T_{b(a)}(n) = a_{ba} + b_{ba}\, n + c_{ba}\, n^2 + d_{ba}\, n^3, \tag{C.2}$$

where the coefficients are presented in Table C.1, subscript (a) stands for alkanes.

Table C.1 Coefficients used in Equations (C.1) and (C.2).

coefficient	a_{ca}	b_{ca}	c_{ca}	d_{ca}
value	242.3059898052	55.9186659144	−2.1883720897	0.0353374481
coefficient	a_{ba}	b_{ba}	c_{ba}	d_{ba}
value	118.3723701848	44.9138126355	−1.4047483216	0.0201382787

The range of applicability of these coefficients was extended to $26 \leq n \leq 27$, remembering that the molar fractions of alkanes with these n is less than 0.05%. The validity of this approximation was checked via finding new approximations valid in the range $8 \leq n \leq 27$. The predictions of these new

correlations turned out to be almost indistinguishable from those predicted by Correlations (C.1) and (C.2).

Liquid density

The temperature dependence of the density of liquid alkanes for $8 \leq n \leq 27$ was approximated, using data reported in [146], as:

$$\rho_l(T) = 1000 \, A_\rho \, B_\rho^{-\left(1-\frac{T}{T_{cr}}\right)^{C_\rho}},$$

(C.3)

where A_ρ, B_ρ and C_ρ for individual values of n were approximated by the following expressions:

$$\left.\begin{aligned} A_\rho &= 0.00006196104 \, n + 0.234362, \\ B_\rho &= 0.00004715697 \, n^2 - 0.00237693 \, n + 0.2768741, \\ C_\rho &= 0.000597039 \, n + 0.2816916, \end{aligned}\right\}$$

(C.4)

$T_{cr} = T_{cr(a)}$ are critical temperatures (see Equation (C.2)).

Expression (C.3) is identical to the one used in [43], but with different values of the coefficients (these were obtained for $5 \leq n \leq 25$). The maximal difference between the predictions of Expression (C.3) and the corresponding equation given in [43] is less than 0.5%.

Approximation (C.3) is assumed to be valid up to the critical temperatures of all components (T_{cr}). Note that for some components T_{cr} in Expression (C.3) needs to be replaced with a temperature which is slightly less than the critical temperature. This effect is not taken into account in the current analysis.

Liquid viscosity

Following [195], the temperature dependence of the dynamic viscosity of liquid alkanes for $4 \leq n \leq 44$ was approximated as:

$$\mu_l(T) = 10^{-3} \left[10^{\left(100 \, (0.01 \, T)^{b(n)}\right)} - 0.8 \right],$$ (C.5)

where

$$b(n) = -5.745 + 0.616 \, \ln(n) - 40.468 \, n^{-1.5},$$ (C.6)

The temperature range of the applicability of Approximations (C.5) and (C.6) was not explicitly specified in [187], [195], but the author of [43] demonstrated good agreement between the predictions of these approximations and experimental data in the range of temperatures from 283 K to 373 K. Also, it was demonstrated in [43] that the agreement between the values of liquid viscosity predicted by Approximations (C.5) and (C.6) and the results presented on the NIST website [151] is almost ideal.

Note that the values of dynamic viscosity affect droplet heating and evaporation only via the corrections to the values of thermal conductivity and diffusivity in the ETC/ED models. In most practically important cases, the influence of viscosity on the final results is expected to be very weak. In our analysis it was assumed that Approximations (C.5) and (C.6) are valid up to the critical temperatures; no low temperature limits for their validity were imposed.

Liquid heat capacity

Following [196], the temperature dependence of the heat capacity of liquid alkanes for $2 \le n \le 26$ was approximated as:

$$c_l(T) = 1000 \left[\frac{43.9 + 13.99 \, (n-1) + 0.0543 \, (n-1)T}{M(n)} \right],$$ (C.7)

where $M(n) = 14n + 2$ is the molar mass of alkanes.

The temperature range of applicability of Approximation (C.7) was not clearly identified in [196] for all n, except to say that this approximation is not valid at temperatures close to the temperature of fusion. It was shown in [43] that the agreement between the values of the liquid heat capacity predicted by Approximation (C.7) and the experimental results for $T = 300 \, K$ [151] is almost ideal. In our analysis it is assumed that Approximation (C.7) is valid up to the

immediate vicinity of the critical temperatures; no low temperature limit for its validity was imposed remembering that our analysis was focused on liquids. Bearing in mind that molar fractions of alkanes with $n = 27$ were about 0.3%, it was assumed that Equation (C.7) was valid in the whole range $8 \leq n \leq 27$.

Liquid thermal conductivity

Although we were able to show that it is more accurate and reliable to base the estimate of the thermal conductivity of liquid Diesel fuel on experimental data rather than on correlations using the thermal conductivities of individual components, it would be appropriate to present the latter conductivities for all components. This approach opened the way for using more efficient correlations for the estimate of the thermal conductivity of the mixtures, should these correlations be suggested in the future.

Following [192], the temperature dependence of thermal conductivity of liquid alkanes for $5 \leq n \leq 20$ can be approximated as:

$$k_l(T) = 10^{\left[A_k + B_k\left(1 - \frac{T}{T_{cr}}\right)^{2/7}\right]}, \tag{C.8}$$

where T_{cr} are critical temperatures as in Approximation (C.3), the numerical values of A_k and B_k for individual values of n were given in [192]. These values were approximated by the following expressions [43]:

$$\left.\begin{aligned} A_k &= 0.002911\, n2 + 0.071339\, n - 1.319595, \\ B_k &= -0.002498\, n - 2 + 0.058720\, n + 0.710698. \end{aligned}\right\} \tag{C.9}$$

Although Approximations (C.8) and (C.9) were derived for $5 \leq n \leq 20$, they can be used in the whole range $8 \leq n \leq 27$. Possible errors imposed by these approximations in the range $21 \leq n \leq 27$ are expected to have a very small effect on the final results as the molar fractions of alkanes in this range of n are less than 1.5%. The range of applicability of Approximation (C.8) depends on the values of n. For each value of n, this range was determined as [192]:

For $n = 8$, $216 - 540$ K;
for $n = 9$, $243 - 588$ K;

for $n = 10, 248 - 607$ K;

for $n = 11, 230 - 625$ K;

for $n = 12, 264 - 625$ K;

for $n = 13, 268 - 642$ K;

for $n = 14, 279 - 658$ K;

for $n = 15, 283 - 671$ K;

for $n = 16, 291 - 685$ K;

for $n = 17, 327 - 732$ K;

for $n = 18, 301 - 708$ K;

for $n = 19, 305 - 718$ K; and

for $n = 20, 310 - 729$ K.

It is assumed that the temperature range for $n > 20$ is the same as for $n = 20$.

As shown in [43], the values of k_l predicted for $T = 300$ K and $T = 450$ K agreed well with the data reported in [151].

The upper limits of the temperature ranges, shown above, were close to critical temperatures. If they are greater than the corresponding critical temperatures, then these limits can be imposed as the critical temperatures. The values of thermal conductivity at temperatures below the minimal temperatures were assumed to be equal to those at the minimal temperatures.

Saturated vapour pressure and enthalpy of evaporation

The following approximation (Antoine equation) for the dependence of the saturation vapour pressure (in Pa) on n was used in our analysis [197]:

$$\log_{10}[0.001 \times p^{sat}(n)] = A(n) - \frac{B(n)}{T + C(n)}, \tag{C.10}$$

where

$A(n) = 0.022\, n + 5.8474, \quad B(n) = 52.807\, n + 981.92, \quad C(n) = -5.0431\, n - 31.205$, and T is in K.

The above approximations for $A(n)$, $B(n)$, $C(n)$ were derived for $8 < n < 27$. They are valid in the following temperature ranges [197]:

$298 - 423$ K for $n = 8$;

$315 - 449$ K for $n = 9$;

$338 - 468$ K for $n = 10$;

356-499 K for $n = 11$;

367-520 K for $n = 12$;

384-540 K for $n = 13$;

399-559 K for $n = 14$;

413-577 K for $n = 15$;

426-594 K for $n = 16$;

438-610 K for $n = 17$;

449-625 K for $n = 18$;

462-639 K for $n = 19$;

475-652 K for $n = 20$;

393-630 K for $n = 21$;

402-642 K for $n = 22$;

411-653 K for $n = 23$;

419-664 K for $n = 24$;

427-675 K for $n = 25$;

434-685 K for $n = 26$; and

442-695 K for $n = 27$.

In this analysis, Approximation (C.10) was used up to the critical temperature. No low temperature limit for the applicability of this approximation was imposed. At low temperatures (close to the room temperature), the values of pressure are expected to be small and realistic errors in its estimate are not expected to produce noticeable effects on the overall picture of droplet heating and evaporation. By the time the droplet surface temperatures reach values higher than the upper limit in the above-mentioned temperature ranges, their radii have become very small in most cases. In this case the errors in determination of the vapour pressure are also

expected to produce a small effect on the overall picture of droplet heating and evaporation.

This approximation is consistent with the one used earlier in [43], [47]; the approximation used in these papers was valid for $n < 17$.

Following [146] the values of specific enthalpy of evaporation for alkanes were approximated as

$$L = \frac{A(1-T_r)^B}{M(n)} \times 10^6, \tag{C.11}$$

where the values of A for specific values of n provided by [146] were approximated as

$A \equiv A_L = 0.0066\ n^2 + 4.697\ n + 20.258,\ \text{for } n \le 20 \text{ and}$
$A \equiv A_H = -0.1143\ n^2 + 7.853\ n - 8.8344, \text{ for n} > 20.$

The original values of B provided by [146] were used:

$B = 0.439$ for $n = 8$;
$B = 0.377$ for $n = 9$;
$B = 0.451$ for $n = 10$;
$B = 0.413$ for $n = 11$;
$B = 0.407$ for $n = 12$;
$B = 0.416$ for $n = 13$;
$B = 0.418$ for n = 14;
$B = 0.419$ for $n = 15$;
$B = 0.422$ for $n = 16$;
$B = 0.433$ for $n = 17$;
$B = 0.451$ for $n = 18$;
$B = 0.448$ for $n = 19$;
$B = 0.409$ for $n = 20$; and
$B = 0.380$ for $n \ge 21$.

The accuracy of the above-mentioned approximations of A by A_L and A_H is illustrated in Figure C2. As can be seen from this figure, the values provided by [146] are reasonably close to the values of A_L or A_H , which justifies the

application of the latter in our analysis. Similar closeness between approximations and the values of *A* and *B* provided by [146], [194], [198] was observed for other hydrocarbons (the plots are not presented). In all cases, Approximation (C.11) is assumed to be valid up to the critical temperature in all cases [146]. No low temperature limit for the validity of this approximation was imposed.
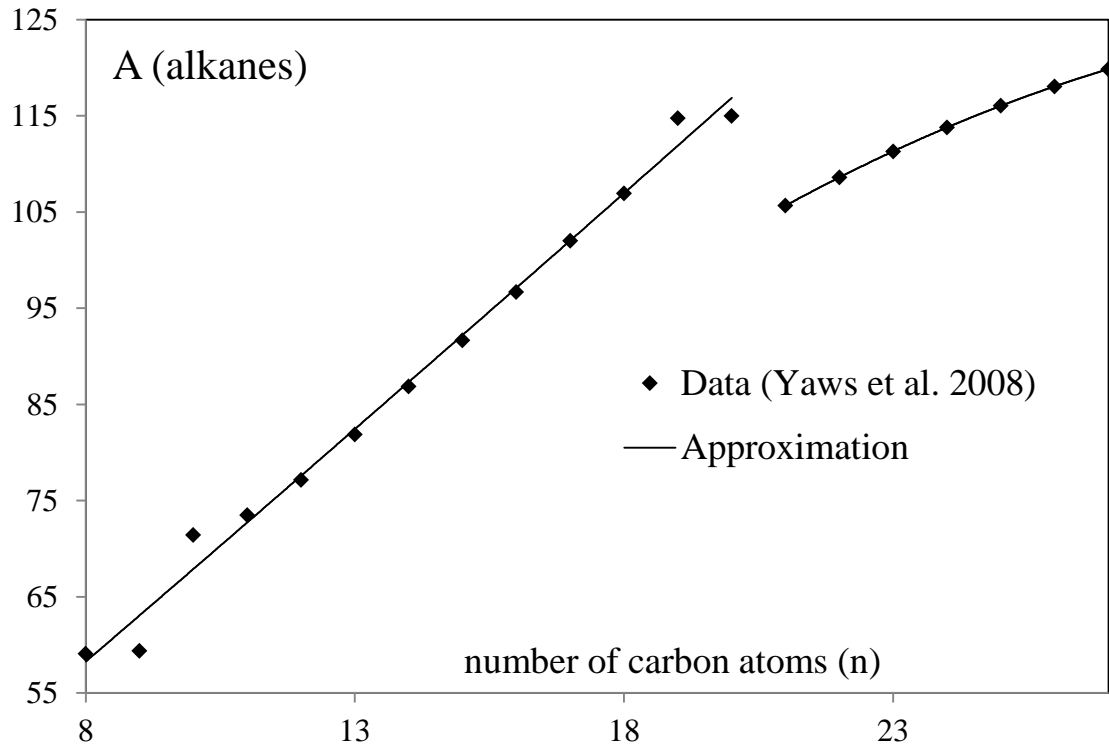
Figure C.2 The values of *A* used in Formula (C.11), as inferred from the data provided by [146], and their approximations by A_L and A_H.

C2. Transport and thermodynamic properties of cycloalkanes

Molecular structure, boiling and critical temperatures

The chemical formula of cycloalkanes is C_nH_{2n} ($10 \leq n \leq 27$) and their typical chemical structure is shown in Figure C1 (1-propyl-3-hexyl-cycloheptan).

Using data provided in [146], the dependence of critical and boiling temperatures on *n* was approximated by the following expressions:

$$T_{cr(c)}(n) = a_{cc} + b_{cc}n + c_{cc}n^2 + d_{cc}n^3 \qquad (C.12)$$

$$T_{b(c)}(n) = a_{bc} + b_{bc}n + c_{bc}n^2, \qquad (C.13)$$

where the coefficients are given in Table C2, subscript (c) stands for cycloalkane.

Expressions similar to those given in (C.12) and (C.13) could be obtained using the analysis presented in [147], [199], [200].

Table C.2 Coefficients in Equations (C.12) and (C.13).

coefficient	a_{cc}	b_{cc}	c_{cc}	d_{cc}
value $n \leq 10$	667	0	0	0
value $n > 10$	425.28	31.442	−0.9002	0.0125
coefficient	a_{bc}	b_{bc}	c_{bc}	
value	176.51	32.312	−0.4776	

Liquid density

The temperature dependence of the density of liquid cycloalkanes for $5 \leq n \leq 25$ was approximated by Expression (C.3) with A_ρ, B_ρ and C_ρ approximated as:

$$\left. \begin{array}{l} A_\rho = 0.00003\ n^2 - 0.0016\ n + 0.278, \\ B_\rho = 0.00003\ n^2 - 0.00237693\ n + 0.2823, \\ C_\rho = 0.28571, \end{array} \right\} \qquad (C.14)$$

$T_{cr} = T_{cr(c)}$ are critical temperatures of cycloalkanes (see Equation (C.12)).

For $11 \leq n \leq 25$ the values of densities predicted by Equation (C.3) with the coefficients defined by Equations (C.14) almost exactly coincide with those given in [146]. For $n \geq 26$ the deviation between these results could be up to 3%. This deviation is not important since the molar fractions of cycloalkanes for these n are expected to be less than 0.03% (see Table 4.2, Chapter 4).

As in the case of alkanes, Approximation (C.3) is valid up to the immediate vicinity of the critical temperatures of all components.

Liquid viscosity

Following [187], the temperature dependence of the dynamic viscosity of liquid cycloalkanes for $10 \leq n \leq 94$ was approximated by (C.5) with $b(n)$ defined as:

$b(n) = -9.001 + 2.350 \log_{10}(14n)$.

As in the case of alkanes, it is assumed that Approximation (C.5) with $b(n)$, defined by the above expression, is valid up to the critical temperatures; no low temperature limits for its validity were imposed.

Liquid heat capacity

Following [188], [190], the temperature dependence of the heat capacity of liquid cycloalkanes for $10 \leq n \leq 27$ was approximated as:

$$c_l(T) = \frac{R_u}{M(n)}\left[a_c + b_c\left(\frac{T}{100}\right) + c_c\left(\frac{T}{100}\right)^2\right], \tag{C.15}$$

where R_u = 8315 J/(K kmole) is the universal gas constant, $M(n)$ is the molar mass in kg/kmole,

a_c= 33.75209+2.7345 $(n-10)$,
b_c= −5.21095283+0.122732 $(n-10)$ K^{-1},

c_c= 2.78089 −0.123482 $(n-10)$ K^{-2}.

The temperature range of applicability of Equation (C.15) is between melting and boiling temperatures.

Liquid thermal conductivity

The temperature dependence of thermal conductivities of liquid cycloalkanes for $10 \leq n \leq 27$ can be estimated from the following expression (derived from the combination of the boiling-point method and Riedel formula) [146], [192], [194], [201]:

$$k_l(T) = \frac{2.64 \times 10^{-3}}{\sqrt{M_n}} \times \frac{3+20(1-T_r)^{2/3}}{3+20(1-T_{br})^{2/3}}, \tag{C.16}$$

where $M_n = 14n$ is the molar mass, $T_r = T/T_{cr}$, $T_{br} = T_b/T_{cr}$. The approximations of T_{cr} and T_b are given by Expressions (C.12) and (C.13).

Expression (C.16) is valid up to the boiling temperatures.

Saturated vapour pressure and enthalpy of evaporation

Following [197], the saturated vapour pressure is approximated by the Antoine equation (C.10) with

$A(n) = 0.0201\,n + 5.8268,\ \ B(n) = 47.34\,n + 1115.2,\ \ C(n) = -5.4145\,n - 23.03.$

Equation (C.10) with the above values of coefficients for cycloalkanes is valid in the ranges:

340-484 K for $n = 10$;
359-508 K for $n = 11$;
376-530 K for $n = 12$;
393-551 K for $n = 13$;
367-399 K for $n = 14$;
423-589 K for $n = 15$;
429-606 K for $n = 16$;
450-622 K for $n = 17$;
458-637 K for $n = 18$;
474-651 K for $n = 19$;
486-665 K for $n = 20$;
496-677 K for $n = 21$;
507-689 K for $n = 22$;
414-664 K for $n = 23$;
422-675 K for $n = 24$; and
430-686 K for $n = 25$.

As in the case of alkanes, the above approximations for $A(n)$, $B(n)$, and $C(n)$ were used outside the range of temperatures for which they were obtained, up to the critical temperatures and below the abovementioned minimal temperatures.

As in the case of alkanes, following [146], the values of *L* for cycloalkanes were estimated by Expression (C.11). The values of *A* for individual *n* provided by [146] were approximated as

$A = -0.0085\ n^3 + 0.4134\ n^2 - 2.556\ n + 56.345,\ \ B = 0.38$

for $n \neq 16$. As in [146], $A = 101.3122$ and $B = 0.49$ for $n = 16$.

As in the case of alkanes, Expression (C.11) for cycloalkanes is assumed to be valid up to the critical temperatures.

C3. Transport and thermodynamic properties of bicycloalkanes

Molecular structure, boiling and critical temperatures

The chemical formula of bicycloalkanes is C_nH_{2n-2} ($10 \leq n \leq 25$) and their typical chemical structures are shown in Figure C1 (diethylbicycloheptan and ethylcycloheptan-cyclononane).

Using data provided in [146] for $10 \leq n \leq 25$, the dependence of critical and boiling temperatures on *n* was approximated by the following equations:

$$T_{cr(b)}(n) = 134.85\ \ln(n) + 395.85, \tag{C.17}$$

for $13 \leq n \leq 24$,

$$T_{b(b)}(n) = 217.41\ \ln(n) - 32.662, \tag{C.18}$$

for $10 \leq n \leq 25$.

$T_{cr(b)}(10) = 703.60$ K, $T_{cr(b)}(11) = 752.51$ K, $T_{cr(b)}(12) = 762.49$ K. The subscript (b) stands for bicycloalkanes.

Following [146], [194], in the approximations shown later in this appendix $T_{cr(b)}(10)$ is replaced with the parameter $T_{cr(b)}(10) = 702.25$ K. Since $T_{cr(b)}(25)$ for bicycloalkanes has not been found in literature, $T_{cr(b)} = 833.34$ K for 1,1

dicyclohexyltridecane was used instead of $T_{cr(b)}(25)$ for bicycloalkanes in these approximations.

Liquid density

Using data supplied in [202], the temperature dependence of the density of liquid bicycloalkanes for $10 \leq n \leq 25$ was approximated by Expression (C.3) with $C_\rho = 0.28571$ and A_ρ and B_ρ approximated by the following expressions.

For $11 \leq n \leq 12$:
$A_\rho = -0.0034\,n + 0.3231$,
$B_\rho = -0.0031\,n + 0.3022$.

For $13 \leq n \leq 18$:
$A_\rho = 0.0002\,n^2 - 0.0072\,n + 0.3529$,
$B_\rho = -0.0003\,n^2 - 0.0278\,n + 0.4966$.

For $19 \leq n \leq 25$:
$A_\rho = 5 \times 10^{-5}\,n^2 - 0.0032\,n + 0.3168$,
$B_\rho = 0.0004\,n^2 - 0.0179\,n + 0.4965$.

Remembering that the molar fraction of bicycloalkanes for $n = 10$ is less than 0.7% we assumed that $\rho_{l(b)}(T)(n = 10) = \rho_{l(b)}(T)(n = 11)$.

As in the case of previously considered components, Approximation (C.3) for bicycloalkanes is assumed to be valid up to the immediate vicinity of the critical temperature, and no low temperature limit was imposed.

Liquid viscosity

Following [187], the temperature dependence of the dynamic viscosity of liquid bicycloalkanes for $10 \leq n \leq 94$ is approximated by Expression (C.5) with $b(n)$ defined as:

$b(n) = -9.513 + 2.248 \log_{10}(14n - 2)$.

As in the case of previously considered components, in our analysis it is assumed that Approximation (C.5) with $b(n)$, defined by the above expression, is valid up to the critical temperatures and no low temperature limits for its validity were imposed.

Liquid heat capacity

Following [188], [190], the temperature dependence of the heat capacity of liquid bicycloalkanes for $10 \leq n \leq 25$ was approximated by Expression (C.15) with the coefficients defined as:

$a_c = 19.2782 + 2.7345 (n - 11)$,
$b_c = 4.722955 + 0.122732(n - 11)$ K^{-1},
$c_c = 0.08912 + 0.123482 (n - 11)$ K^{-2}.

As in the case of previously considered components, the temperature range of applicability of these approximations is between melting and boiling temperatures.

Liquid thermal conductivity

Following [177], the temperature dependence of thermal conductivity of liquid bicycloalkanes for $10 \leq n \leq 25$ was estimated by Expression (C.16) with $M_n = 14n - 2$. As in the case of previously considered components, Expression (C.16) for bicycloalkanes was assumed to be valid up to the boiling temperatures.

Saturated vapour pressure and enthalpy of evaporation

Following [146], [177], the saturated vapour pressure for bicycloalkanes for $10 \leq n \leq 25$ is approximated by the following formula:

$$\ln(p_{vb} / p_{cb}) = f^0 + \omega_b f^1, \tag{C.19}$$

where

$f^0 = 5.92714 - 6.09648/T_r - 1.28862 \ln T_r + 0.169347 T_r^6$,

f^1= 15.2518 −15.6875/T_r−13.4721 ln T_r + 0.43577T_r^6,

T_r = $T/T_{cr(b)}$, $T_{cr(b)}$ is the critical temperature estimated from (C.17), p_{cb} is the critical pressure of bicycloalkanes estimated as

p_{cb} = 10^5 0.0711 n^2 − 3.8116 n + 60.998 Pa,

$\omega \equiv \omega_b$ = −0.001 n^2 + 0.0679 n − 0.3039.

As in the case of previously considered components, Expression (C.19) is assumed to be valid up to the critical temperatures.

As in the case of alkanes and cycloalkanes, the values of L for bicycloalkanes could be estimated by Expression (C.11) with the values of A provided in [146] approximated as

A = −0.1405 n^2 + 8.1341 n − 3.2083,

and B = 0.434 for n = 10 and B = 0.38 otherwise.

In contrast to previously considered hydrocarbons, however, we have found that a more accurate approximation for L for bicycloalkanes is given by the following expression (cf. [82], [177]):

$$L = \begin{cases} -\frac{R_u T_{cr(b)}}{M(n)} \emptyset_1(T_r, \omega_b) & \text{when } T_r < 0.6 \\ \frac{R_u}{M(n)} T_{cr(b)} \emptyset_2(T_r, \omega_b) & \text{when } T_r \geq 0.6 \end{cases}, \tag{C.20}$$

where the units of R_u and $M(n)$ are the same as in Equations (C.15),

Φ_1= (−6.09648 − 15.6875ω_b) + (1.28862 + 13.4721ω_b) T_r −6 (0.169347 + 0.43577ω_b) T_r^7,

Φ_2 = 7.08 (1 − T_r)$^{0.354}$ + 10.95 ω_b (1 − T_r)$^{0.456}$,

T_r = $T/T_{cr\,(b)}$, ω_b was defined earlier.

Approximation (C.20) was compared with the data provided in [146] for $C_{10}H_{18}$, $C_{11}H_{20}$, $C_{12}H_{22}$ and $C_{25}H_{48}$. The maximal deviation between the results predicted by (C.20) and data provided by [146] did not exceed about 5%.

Equation (C.20) was used in our analysis. As in the case of alkanes and cycloalkanes, this expression is valid up to the critical temperatures.

C4. Transport and thermodynamic properties of alkylbenzenes

Molecular structure, boiling and critical temperatures

The chemical formula of alkylbenzenes is C_nH_{2n-6} ($8 \leq n \leq 24$) and their chemical structures are shown in Figure C.1 (1,4-dipropylbenzene and 1,4-dipentylbenzene).

Using data provided in [146], [147], [189], [192], [199], [200], [203]–[206], the dependence of critical and boiling temperatures on n was approximated by the following equations:

$$T_{cr(ab)}(n) = a_{cab} + b_{cab}\, n + c_{cab}\, n^2, \tag{C.21}$$

$$T_{b(ab)}(n) = a_{bab} + b_{bab}\, n + c_{bab}\, n^2, \tag{C.22}$$

where the coefficients are presented in Table C.3, subscripts (ab) stands for alkylbenzenes.

Table C.3 Coefficients used in Equations (C.21) and (C.22).

coefficient	a_{cab}	b_{cab}	c_{cab}
value	427.89	27.408	−0.4388
coefficient	a_{bab}	b_{bab}	c_{bab}
value	171.6	33.426	−0.5252

Liquid density

Using data supplied in [146], the temperature dependence of the density of liquid alkylbenzenes for $5 \leq n \leq 25$ was approximated as:

$$\rho_{l(ab)}(T) = A_{\rho ab} + B_{\rho ab}\, T + C_{\rho ab}\, T^2 + D_{\rho ab}\, T^3, \tag{C.23}$$

where $A_{\rho ab}$, $B_{\rho ab}$, $C_{\rho ab}$ and $D_{\rho ab}$ for individual values of n were approximated by the following expressions.

For $n = 8$ and $n = 9$:

$$
\left.\begin{aligned}
A_{\rho ab} &= -32.04\ n + 1422.6, \\
B_{\rho ab} &=\ \ 0.1831\ n - 2.824, \\
C_{\rho ab} &= -0.0005\ n + 0.0056, \\
D_{\rho ab} &= 6 \times 10^{-7}\ n - 7 \times 10^{-6};
\end{aligned}\right\}
\tag{C.24}
$$

for $n = 11 - 20$:

$$
\left.\begin{aligned}
A_{\rho ab} &= -0.0477\ n^2 - 0.4141\ n + 1082.6, \\
B_{\rho ab} &= 0.0004\ n^2 - 0.0062\ n - 0.7017\ , \\
C_{\rho ab} &= D_{\rho ab} = 0.
\end{aligned}\right\}
\tag{C.25}
$$

It is assumed that $\rho(n= 10) = 0.5\ (\rho(n= 9) + \rho(n= 11))$ and $\rho(n>20) = \rho(n= 20)$. The latter assumption is justified by the fact that molar fractions of components with $n > 20$ is about or less than 0.2%.

Approximations (C.23)–(C.25) are assumed to be valid up to the immediate vicinity of the critical temperatures. Their predictions agree with experimental data provided in [207].

Liquid viscosity

Following [187], the temperature dependence of the dynamic viscosity of liquid alkylbenzenes is approximated by Expression (C.5) with $b(n)$ defined as:

$$b(n) = -9.692 + 2.261\ \log_{10}(14n - 6).$$

As in the case of alkanes, cycloalkanes and bicycloalkanes, in our analysis it is assumed that Approximation (C.5) with $b(n)$, defined by the above expression, is valid up to the critical temperatures; no low temperature limits for its validity were imposed.

Liquid heat capacity

Following [188], [190], the temperature dependence of the heat capacity of liquid alkylbenzenes for $8 \leq n \leq 24$ was approximated by Expression (C.15) with the coefficients defined as:

$a_c = 15.1109 + 2.7345\,(n-7)$,

$b_c = 0.68109 + 0.122732\,(n-7)$ K^{-1},

$c_c = 1.96346 - 0.123482\,(n-7)$ K^{-2}.

The temperature range of applicability of these approximations is between melting and boiling temperatures.

Liquid thermal conductivity

Following [146], [176], [177], the temperature dependence of thermal conductivity of liquid alkylbenzenes for $8 \le n \le 24$ was estimated by Expression (C.16) with $M_n = 14n-6$. As in the case of cycloalkanes and bicycloalkanes, Expression (C.16) for alkylbenzenes is valid up to the boiling temperatures.

Saturated vapour pressure and enthalpy of evaporation

Following [197], the saturated vapour pressure for alkylbenzenes is approximated by the Antoine equation (C.10) with

$A(n) = 0.0007\,n^2 - 0.0064\,n + 6.0715$,

$B(n) = 51.811\,n + 1049.1$,

$C(n) = 0.1215\,n^2 - 9.6892n + 11.161$.

The temperature ranges of applicability of Equation (C.10) for alkylbenzenes are the following:

306-420 K for $n = 8$;

323-455 K for $n = 9$;

343-486 K for $n = 10$;

361-510 K for $n = 11$;

378-531 K for $n = 12$;

394-553 K for $n = 13$;

406-571 K for $n = 14$;

421-590 K for $n = 15$;

438-606 K for $n = 16$;

450-622 K for $n = 17$;

458-636 K for $n = 18$;

473-651 K for $n = 19$;

485-665 K for $n = 20$;

495-677 K for $n = 21$;

505-688 K for $n = 22$;

414-664 K for $n = 23$; and

423-675 K for $n = 24$.

As in the case of alkanes and cycloalkanes, the above approximations for $A(n)$, $B(n)$, $C(n)$ are used up to the critical temperatures. In most cases, the upper limits of applicability of these approximations, as established in [197], are close to the critical temperatures. Temperatures between the abovementioned upper limits of applicability of these expressions and the critical temperatures might be observed only at the very final stage of droplet evaporation and the errors in the estimates of vapour pressure in this case are expected to produce negligibly small effects on the evaporation process.

As in the case of alkanes and cycloalkanes, values of L for alkylbenzenes were estimated by Expression (C.11) [146]. The values of A and B provided in [146] are approximated as:

$A = 0.0007124\, n^5 - 0.05315\, n^4 + 1.4963\, n^3 - 19.83\, n^2 + 128.65\, n - 276.8$,

$B = -0.007\, n^2 + 0.1172\, n - 0.0989$ when $8 \le n \le 10$,

$B = -0.0062\, n2 + 0.1829\, n - 0.9093$ when $11 \le n \le 14$,

$B = -0.0013315\, n^2 + 0.0634\, n^2 - 0.9842\, n + 5.3794$ when $15 \le n \le 19$,

$B = 0.38$ when $n \ge 20$.

As in the case of alkanes and cycloalkanes, Expression (C.11) for alkylbenzenes is assumed to be valid up to the critical temperatures.

C5. Transport and thermodynamic properties of indanes and tetralines

Molecular structure, boiling and critical temperatures

The chemical formula of indanes and tetralines is C_nH_{2n-8} ($10 \leq n \leq 22$) and their chemical structures are shown in Figure C1 (pentylindane, as an example of indanes, and 1-propyl-(1,2,3,4-tetrahydronaphthalene), as an example of tetralines). Indanes and tetralines differ by the numbers of carbon atoms in the second ring. When this number is equal to 5 it is classified within indanes; when this number is equal to 6 it is classified within tetralines. Their properties are very close and will not be distinguished in this appendix.

Using data provided in [146], the dependence of critical and boiling temperatures on n was approximated by the following equations:

$$T_{cr(i)}(n) = a_{ci} + b_{ci}n + c_{ci}n^2, \qquad\qquad (C.26)$$

$$T_{b(i)}(n) = a_{bi} + b_{bi}n + c_{bi}n^2, \qquad\qquad (C.27)$$

where the coefficients are presented in Table C4, subscripts (i) stand for indanes & tetralines.

Table C.4 Coefficients used in Equations (C.26) and (C.27).

coefficient	a_{ci}	b_{ci}	c_{ci}
Value ($n = 10$)	720.15	0	0
Value ($n > 10$)	555.59	17.898	−0.2486
coefficient	a_{bi}	$\underline{b}_{bi}$	c_{bi}
value	249.21	25.894	−0.3319

Liquid density

Following (Yaws, 2008), the temperature dependence of the density of liquid indanes and tetralines for $10 \leq n \leq 22$ was approximated by Expression (C.3) with A_ρ, B_ρ and C_ρ approximated by the following expressions.

For $10 \leq n \leq 16$:

$$A_{\rho i} = 0.0002 \, n^2 - 0.0079 \, n + 0.3622,$$
$$B_{\rho i} = -7 \cdot 10^{-5} \, n^{3-} + 0.0031 \, n^2 - 0.0438 \, n + 0.4608, \qquad (C.28)$$
$$C_{\rho i} = 0.2677 \text{ for } n = 10; \; C_{\rho i} = 0.28571 \text{ for } 11 \leq n \leq 16;$$

for $17 \leq n \leq 20$:

$$A_{\rho i} = 0.0002 \, n^2 - 0.0079 \, n + 0.3622,$$
$$B_{\rho i} = 6 \times 10^{-5} \, n^{-2} - 0.0025 \, n + 0.2908, \qquad (C.28)$$
$$C_{\rho i} = 0.28571.$$

It is assumed that $\rho(n > 20) = \rho(n = 20)$. This is justified by the fact that molar fractions of these components are less than 0.2%.

Equations (C.27) and (C.28) are valid in the following ranges of temperatures:

237.4 – 720.15 K for $n = 10$;

232.3 – 722 K for $n = 11$;

243.6 – 735 K for $n = 12$;

254.8 – 745 K for $n = 13$;

266.1 – 756 K for $n = 14$;

277.4 – 767 K for $n = 15$;

288.6 – 777 K for $n = 16$;

299.9 – 788 K for $n = 17$;

311.2 – 797 K for $n = 18$;

322.5 – 805 K for $n = 19$; and

333.7 – 814 K for $n \geq 20$.

As in the case of previously considered components, Approximations (C.27)–(C.28) are assumed to be valid up to the immediate vicinity of the critical temperatures.

Liquid viscosity

Following [187], the temperature dependence of the dynamic viscosity of liquid indanes & tetralines for $10 \leq n \leq 94$ is approximated by Expression (C.5) with $b(n)$ defined as:

$b(n) = -9.411 + 2.217 \log_{10}(14n - 8).$

As in the case of previously considered components, in our analysis it is assumed that Approximation (C.5) with $b(n)$, defined by the above expression, is valid up to the critical temperatures; no low temperature limits for its validity were imposed.

Liquid heat capacity

Following [188], [190], the temperature dependence of the heat capacity of liquid indanes & tetralines for $10 \leq n \leq 22$ was approximated by Expression (C.15) with the coefficients defined as:

$a_c = 14.136 + 2.7345 \, (n - 11),$
$b_c = 6.43698 + 0.122732 \, (n - 11) \, K^{-1},$
$c_c = 14.136 - 0.123482 \, (n - 11) \, K^{-2}.$

As in the case of previously considered components, the temperature range of applicability of these approximations is between melting and boiling temperatures.

Liquid thermal conductivity

Following [146], [176], [177], the temperature dependence of thermal conductivity of liquid indanes & tetralines for $10 \leq n \leq 22$ was approximated by Expression (C.16) with $M_n = 14n - 8$. As in the case of previously considered

components, Expression (C.16) for indanes & tetralines is valid up to the boiling temperatures.

Saturated vapour pressure and enthalpy of evaporation

Following [146], [176], [177], the saturated vapour pressure for indanes & tetralines is approximated by Expression (C.19) in which f^0 and f^1 were defined earlier, $T_r = T/T_{cr(i)}, T_{cr(i)}$ is the critical temperature estimated from (C.26) (cf. Expression (C.19) for bicycloalkanes), p_{ci} is the critical pressure estimated as

$p_{ci} = 10^5 \ (0.0693 \ n^2 - 3.8821 \ n + 63.771) \ $ Pa,

ω_i (the acentric factor) is estimated as

$\omega_i = 0.617 \ln(n) - 1.11$.

As in the case of previously considered components, Expression (C.19) for indanes & tetralines is assumed to be valid up to the critical temperatures.

As in the case of alkanes, cycloalkanes and alkylbenzenes, the values of L for indanes & tetralines were estimated by Expression (C.11). The values of A provided in [146] are approximated as:

$A = -0.0793 \ n^2 + 6.3293 \ n + 5.7796$.

The following values of B provided in [146] were used: $B = 0.303$ when $n \leq 10$ and $B = 0.38$ when $n > 10$.

As in the case of alkanes, cycloalkanes and alkylbenzenes, Expression (C.11) for indanes & tetralines is assumed to be valid up to the critical temperature.

C6. Transport and thermodynamic properties of naphthalenes

Molecular structure, boiling and critical temperatures

The chemical formula of naphthalenes is C_nH_{2n-12} ($10 \leq n \leq 20$) and their typical chemical structure is shown in Figure C.1 (1-propylnaphthalene).

Using data provided in [146], the dependence of critical and boiling temperatures on n was approximated by the following equations:

$$T_{cr(n)}(n) = a_{cn} + b_{cn}n, \tag{C.29}$$
$$T_{b(n)}(n) = a_{bn} + b_{bn}n, \tag{C.30}$$

where the coefficients are presented in Table C5, subscript (n) stands for naphthalenes.

Table C.5 Coefficients used in Equations (C.29) and (C.30).

coefficient	a_{cn}	b_{cn}
value	655.14	9.7878
coefficient	a_{bn}	b_{bn}
value	350.37	15.218

Liquid density

Using data supplied in [202], [207], the temperature dependence of the density of liquid naphthalenes for $10 \leq n \leq 20$ was approximated as:

$$\rho_{l(n)}(T) = A_{\rho n} + B_{\rho n}T, \tag{C.31}$$

where $A_{\rho n}$ and $B_{\rho n}$ for individual values of n were approximated by the following expressions:

$$A_{\rho n} = 1.45\,n^2 - 55.715\,n + 1671.9 \tag{C.32}$$
$$B_{\rho n} = 0.0087\,n - 0.8084.$$

As in the case of previously considered components, Approximation (C.31) is assumed to be valid up to the immediate vicinity of the critical temperature, and no low temperature limit was imposed.

Liquid viscosity

Following [187], the temperature dependence of the dynamic viscosity of liquid naphthalenes for $10 \le n \le 94$ is approximated by Expression (C.5) with $b(n)$ defined as:

$b(n) = -9.309 + 2.185 \log_{10}(14n - 12)$.

As in the case of previously considered components, in our analysis it is assumed that Approximation (C.5) with $b(n)$, defined by the above expression, is valid up to the critical temperatures; no low temperature limits for its validity were imposed.

Liquid heat capacity

Following [188], [190], the temperature dependence of the heat capacity of liquid naphthalenes for $10 \le n \le 20$ was approximated by Expression (C.15) with the coefficients defined as:

$a_c = 9.67805 + 2.7345\,(n - 11)$,
$b_c = 5.982952 + 0.122732\,(n - 11)\ \text{K}^{-1}$,
$c_c = 0.2688 + 0.123482\,(n - 11)\ \text{K}^{-2}$.

As in the case of previously considered components, the temperature range of applicability of these approximations is between melting and boiling temperatures.

Liquid thermal conductivity

Following [146], [176], [177], the temperature dependence of thermal conductivity of liquid naphthalenes for $10 \le n \le 20$ was approximated by Expression (C.16) with $M_n = 14n - 12$. As in the case of previously considered

components, Expression (C.16) for naphthalenes is valid up to the boiling temperatures.

Saturated vapour pressure and enthalpy of evaporation

Following [146], [176], [177], the saturated vapour pressure for naphthalenes for $10 \leq n \leq 20$ is approximated by the same Equation (C.19) as for bicycloalkanes and indanes & tetralines, but for

$p_c \equiv p_{cn} = 10^5 \ (0.2009 \ n^2 - 8.443 \ n + 104.09)$ Pa,

$\omega \equiv \omega_n = -0.0018 \ n^2 + 0.0997 \ n - 0.5082$,

$A = 0.2607 \ n^2 - 2.1791 \ n + 66.218$ for $10 \leq n \leq 16$, and

$A = -0.1929 \ n^2 + 10.926 \ n - 37.384$ for $n \geq 17$.

As in the case of previously considered components, Expression (C.19) is assumed to be valid up to the critical temperatures.

As in the case of alkanes, cycloalkanes, alkylbenzenes and indanes & tetralines, the values of L for naphthalenes were estimated by Expression (C.11). The values of B provided in [146] are approximated as:

$B = -0.0003165 \ n^3 + 0.01545 \ n^2 - 0.2495 \ n + 1.722$ for all n.

As in the case of alkanes, cycloalkanes, alkylbenzenes, and indanes & tetralines, Expression (C.11) for naphthalenes is assumed to be valid up to the critical temperatures.

C7. Transport and thermodynamic properties of tricycloalkane, diaromatic and phenanthrene

The molar fractions of the three characteristic components, tricycloalkane, diaromatic and phenanthrene, are 1.5647%, 1.2240% and 0.6577% respectively. Their range of n is rather narrow: $14 \leq n \leq 20$ for tricycloalkanes, $13 \leq n \leq 16$ for diaromatics and $14 \leq n \leq 18$ for phenanthrenes. This allows us to ignore the dependence of the properties of these substances on n and consider the properties for just one n for which the properties are available. Thus, the analysis of these three groups will be reduced to the analysis of three representative components referred to as tricycloalkane, diaromatic and phenanthrene.

Molecular structure, boiling and critical temperatures

The chemical formula of tricycloalkanes is C_nH_{2n-4}. The properties presented in this appendix refer to $n = 19$ ($C_{19}H_{34}$). The chemical formula of diaromatics is C_nH_{2n-14}. The properties presented in this appendix refer to $n = 13$ ($C_{13}H_{12}$). The chemical formula of phenanthrenes is C_nH_{2n-18}. The properties presented in this appendix refer to $n = 14$ ($C_{14}H_{10}$). Typical chemical structures of diaromatics and phenanthrenes are shown in Figure C.1 (di(3-ethyl-phenyl)methane and ethylphenanthrene, respectively).

Using data provided in [208], the boiling and critical temperatures for tricycloalkane were estimated as:

$T_{b(t)} = 692.33$ K, $T_{cr(t)} = 0.738686^{-1} \times T_{b(t)} = 937.25$ K.

Using data provided in [146], these temperatures for the remaining two substances were estimated as:

$T_{b(d)} = 537.42$ K, $T_{cr(d)} = 760.00$ K
for diaromatics, and

$T_{b(p)} = 610.00$ K, $T_{cr(p)} = 869.00$ K
for phenanthrenes. Subscript (t) stands for tricycloalkanes, (d) stands for

diaromatics, and (p) stands for phenanthrenes.

Liquid density

Using data supplied in [197], the temperature dependence of the density of liquid tricycloalkane and phenanthrene was approximated as:

$$\rho_{l(t)}(T) = A_{\rho t} + B_{\rho t}T, \qquad (C.33)$$

where

$A_{\rho t} = 1151.17, \ B_{\rho t} = -0.69469$, for tricycloalkanes, and
$A_{\rho t} = 1374.16, \ B_{\rho t} = -0.819355$, for phenanthrenes.

The approximation for tricycloalkane is valid in the range of temperatures (273.15 – 372.05) K, while the approximation for phenanthrenes is valid in the range of temperatures (490.70 – 557.80) K.

Using data supplied in [202], the temperature dependence of the density of liquid diaromatic was approximated as:

$$\rho_{l(t)}(T) = A_{\rho d} + B_{\rho d}\,T + C_{\rho d}\,T^2 + D_{\rho d}\,T^3, \qquad (C.34)$$

where
$A_{\rho d} = 1.22498 \times 10^3$,
$B_{\rho d} = -7.21739 \times 10^{-1}$,
$C_{\rho d} = -8.65342 \times 10^{-5}$,
$D_{\rho d} = 1.63332 \times 10^{-9}$.

This approximation is valid in the range of temperatures (284.15 – 523.15) K.

In contrast to the previously considered components, it was assumed that the values at $T < T_{min}$ are the same as the values at $T = T_{min}$, and the values at $T > T_{max}$ are the same as the values at $T = T_{max}$. This 'cautious' approach can be justified by the very small contribution of these components to the process of Diesel fuel droplet heating and evaporation.

Liquid viscosity

Following [208], [209], the temperature dependence of the liquid dynamic viscosity is approximated as:

$$\mu_l = M \, \exp\left\{\frac{\eta_a - 597.82}{T} + \eta_b - 11.202\right\}, \tag{C.35}$$

where M is molar mass,

$M = 262.4733$ kg/kmole, $\eta_a = 3107.93$, $\eta_b = -9.936$
for tricycloalkanes,

$M = 168.23$ kg/kmole, $\eta_a = 2199.18$, $\eta_b = -5.395$
for diaromatics, and

$M = 178.23$ kg/kmole, $\eta_a = 1613.54$, $\eta_b = -3.372$
for phenanthrenes.

Equation (C.35) is valid up to 0.7 T_{cr}.

Liquid heat capacity

Following [188], [190], the temperature dependence of the heat capacity of liquid tricycloalkanes and polycyclic aromatics (diaromatics and phenanthrenes) was approximated by Expression (C.15) with the coefficients defined as:

$a_c = 32.9773$, $b_c = 8.243707$ K^{-1}, $c_c = 0.93225$ K^{-2}
for tricycloalkanes,

$a_c = 17.9997$, $b_c = 3.230018$ K^{-1}, $c_c = 0.5203$ K^{-2}
for diaromatics, and

$a_c = 2.43092$, $b_c = 12.11225$ K^{-1}, $c_c = 0.80569$ K^{-2}
for phenanthrenes.

As in the case of previously considered components, the temperature range of applicability of these approximations is between melting and boiling points.

Liquid thermal conductivity

Following [177], the temperature dependence of thermal conductivity of liquid tricycloalkanes and polycyclic aromatics can be estimated based on Expression (C.16) with $M_n = 14n - 4$ for tricycloalkanes, $M_n = 14n - 14$ for diaromatics and $M_n = 14n - 18$ for phenanthrenes. As in the case of previously considered components, Expression (C.16) for tricycloalkanes, diaromatics and phenanthrenes is assumed to be valid up to the critical temperatures.

Saturated vapour pressure and enthalpy of evaporation

Following [197], the saturated vapour pressures for tricycloalkane, diaromatic and phenanthrene are approximated by the Antoine equation (C.10) with

$A(n) = 15.14702$, $B(n) = 6103.355$, $C(n) = 0$

for tricycloalkane in the range of temperatures 301-321 K,

$A(n) = 6.38684$, $B(n) = 2334.129$, $C(n) = -92.028$

for tricycloalkane in the range of temperatures 333-464 K,

$A(n) = 9.79557$, $B(n) = 3740.286$, $C(n) = 0$

for diaromatic in the range of temperatures 273-298 K,

$A(n) = 6.19796$, $B(n) = 1885.888$, $C(n) = -88.292$

for diaromatic in the range of temperatures 333-647 K,

$A(n) = 11.631$, $B(n) = 4873.4$, $C(n) = 0.05$

for phenanthrene in the range of temperatures 306-321 K, and

$A(n) = 6.37081$, $B(n) = 2329.54$, $C(n) = -77.87$

for phenanthrene in the range of temperatures 356-650 K.

The upper bounds of the temperatures mentioned above are very close to the critical temperatures of the components. In our analysis these bounds are identified with critical temperatures. At temperatures below T_{min} and above T_{max} it is assumed that $p_v(T < T_{min}) = p_v(T = T_{min})$ and $p_v(T > T_{max}) = p_v(T = T_{max})$. At intermediate temperatures when $p_v(T \leq T_1)$ and $p_v(T \geq T_2)$ are known but

$p_v(T_1 < T < T_2)$ are not known, it is assumed that in the latter range of temperatures p_v can be approximated by interpolation as:

$$p_v(T) = p_v(T_1) + \frac{p_v(T_2) - p_v(T_1)}{T_2 - T_1}(T - T_1),$$

As in the case of density, this 'cautious' approach can be justified by the very small contribution of these components to the process of Diesel fuel droplet heating and evaporation.

Following [82], [177], L for tricycloalkane, diaromatic and phenanthrene was estimated by the equation, inferred from the Clausius-Clapeyron equation [35]:

$$L = -\frac{R_u}{M(n)} \frac{d \ln p^{sat}(n)}{d(1/T)},$$ (C.36)

where R_u is the universal gas constant. Remembering Equation (C.19), it can be shown that:

$$p^{sat} = p_{ci} \, exp(f^0 + \omega_i \, f^1),$$ (C.37)

where f^0 and f^1 are represented as:

$$f^0 = a_0 + \frac{b_0}{T_r} + c_0 \ln T_r + d_0 \, T_r^6,$$

$$f^1 = a_1 + \frac{b_1}{T_r} + c_1 \ln T_r + d_1 \, T_r^6,$$

a, b, c and d are fixed values given for each group of components, p_{ci} is the critical pressure, which is a function of carbon numbers only, ω_i is the acentric factor, which is the function of carbon numbers as well, and T_r is the ratio $(\frac{T}{T_{cr}})$.

Assuming that $z = \ln p^{sat}$ and $= \frac{1}{T}$, and substituting these variables into Equation (C.36) we can rewrite the latter equationas:

$$L = -\frac{R_u}{M(n)} \frac{dz}{dy}, \text{ where, } z = \ln p_{ci} + f^0 + \omega_i f^1.$$

Note that $\frac{dz}{dy} = (b_0 + b_1 \omega_i) T_{cr} - (c_0 + c_1 \omega_i) T - 6(d_0 + d_1 \omega_i) T \cdot T_r^6,$

where,

a_0= 5.92714, b_0= -6.09648, c_0= -1.28862, d_0 = 0.169347, a_1= 15.2518, b_1= -15.6875, c_1= -13.4721, and d_1= 0.43577.

The substitution of $\frac{dz}{dy}$ into the equation of L gives:

$$L = -\frac{R_u\, B(n)\, T^2}{M(n)(T+C(n))^2},$$
(C.38)

where $B(n)$ and $C(n)$ are given earlier in this appendix.

Expression (C.38) is assumed to be valid up to the critical temperature. Expression (C.38) was verified against the numerical solution of (C.36) using the finite difference approach. The results are shown in Figure C.3.
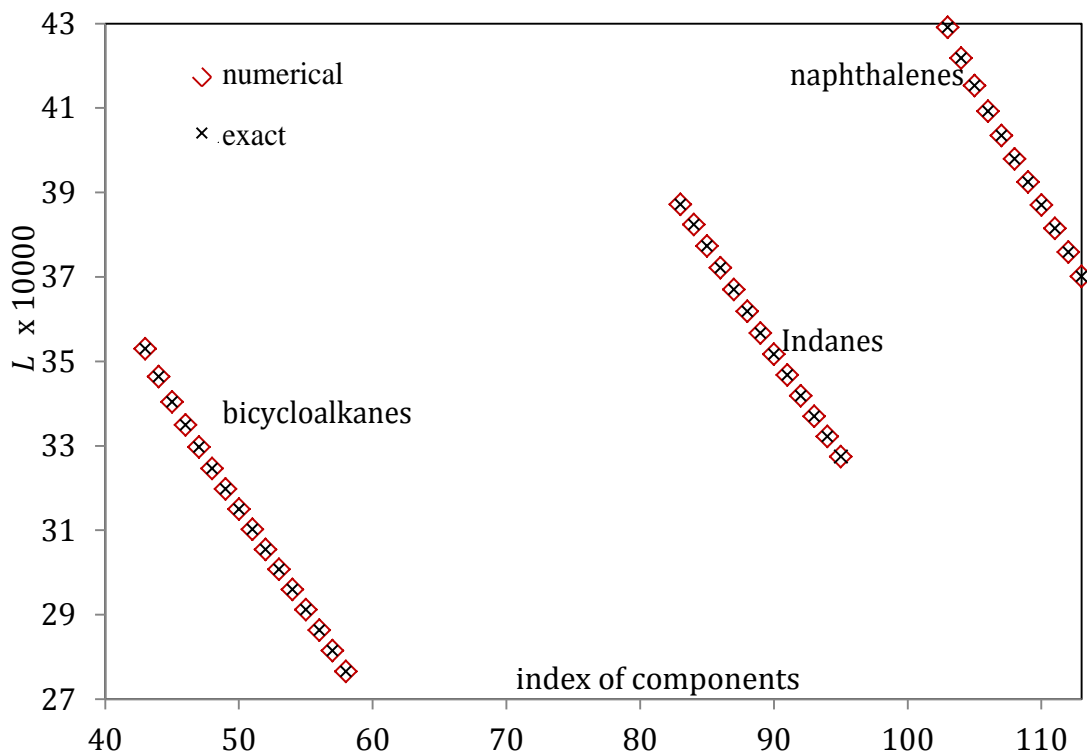
Figure C.3 The comparison between the exact and approximated values of the latent heat of evaporation (Equation (C.37)) for three groups of Diesel components as indicated near the symbols.

C8. Thermal conductivity of liquid Diesel fuel

As mentioned in Section 2.8, Expression (2.52), widely used for the estimation of the thermal conductivity of mixtures (e.g. [46]), is not applicable for the estimation of the thermal conductivity of realistic Diesel fuels, including the one considered in this thesis, as the maximal ratio of thermal conductivities of components for these is well above two. On the other hand, no experimental measurements of Diesel fuel, considered in this thesis, are available to the best of our knowledge. In these circumstances, the most sensible action would be to base the analysis on published experimental data referring to other types of Diesel fuel assuming that the difference between the values of thermal conductivities of various types of Diesel fuels is not large. This assumption is implicitly supported by the results of our analysis. Note that liquid thermal conductivity depends both on temperature and ambient pressure in the general case (e.g. [210]–[212]). This is taken into account in our analysis.

In [213] selective measurements of Diesel fuel thermal conductivities were reported for a typical summer Diesel fuel at various ambient pressures, up to 240 MPa. The results of these measurements were approximated by the following formula [98]:

$$k_D(T, p) = \sum_{i=1}^{3} \left(\sum_{j=1}^{3} a_{ij} T^{j-1} \right) p^{i-1}, \tag{C.39}$$

where a_{ij} are the elements of the matrix

$$a = \begin{pmatrix} 0.13924 & 3.78253 \times 10^{-5} & -2.89732 \times 10^{-7} \\ -6.27425 \times 10^{-11} & 6.08052 \times 10^{-13} & 3.64777 \times 10^{-16} \\ -1.38756 \times 10^{-19} & -2.57608 \times 10^{-22} & -2.70893 \times 10^{-24} \end{pmatrix}, \tag{C.40}$$

T is in K, p is in Pa and k_D is in SI units.

The plots of k_D versus T for $p = 10^5$ Pa (1 bar) and $p = 3 \times 10^6$ Pa (30 bars) are shown in Figure C.4. As can be seen from this figure, thermal conductivities predicted by Expression (C.39) for p =1 bar and p =30 bars almost coincide, which indicates that the dependence of Diesel fuel thermal conductivity on ambient pressure is weak.

Also, the result of the measurements of thermal conductivity at atmospheric pressure and temperature 24° C were shown in Figure C.4 based on [214] (the value of temperatures at which the measurements were performed were communicated with the lead author of [211] (Guimarães); this is not mentioned in the original paper). As one can see from Figure C4, the difference between the results reported in [214] and predicted by Expression (C.39) is less than 10%. This indirectly supports our choice of Expression (C.39) for the estimation of the thermal conductivity of Diesel fuel. To be consistent with the choice of other parameters used for calculations, this thermal conductivity was estimated for *p* =30 bars.

In the same figure, the plots for thermal conductivity of n-dodecane, recommended by [74]:

$$k_D(T) = 0.1405 - 0.00022 (T - 300). \tag{C.41}$$
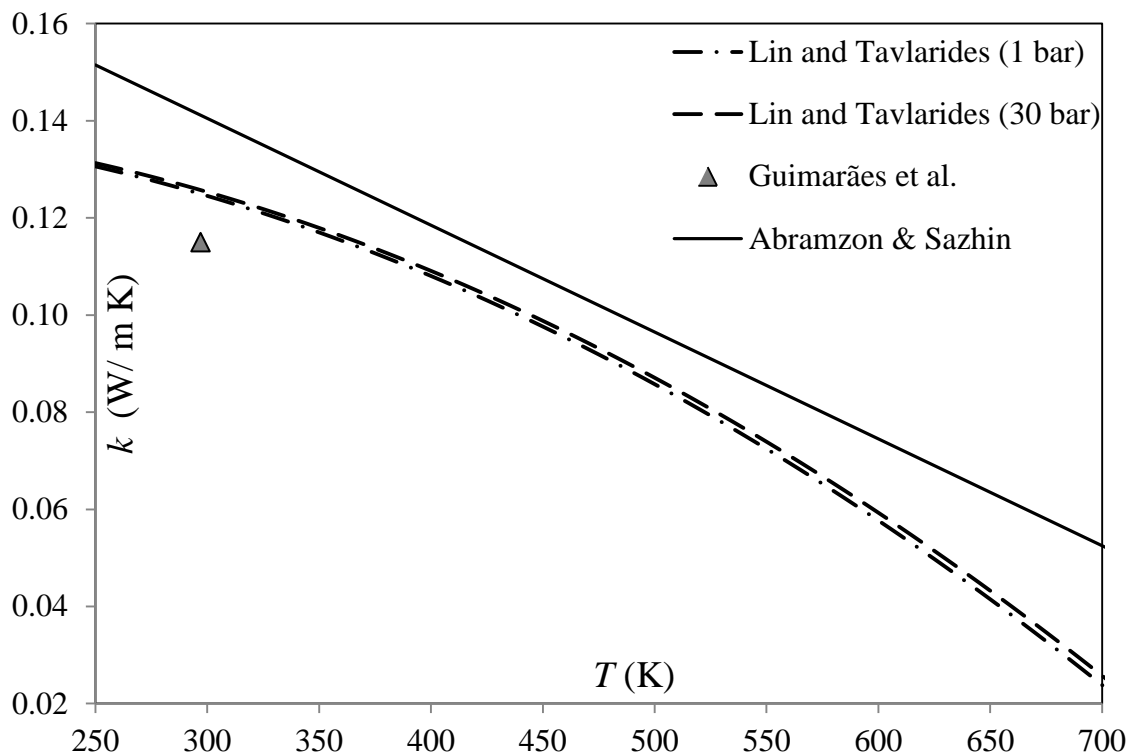
Figure C.4 The plots of thermal conductivity of Diesel fuel as predicted by Formula (C.39), recommended by Lin and Tavlarides [98], for 1 and 30 bars, the result of the measurements of the fuel thermal conductivity at atmospheric pressure and temperature 24 ℃ as reported by Guimarães et al. [214], and the values of thermal conductivity of n-dodecane estimated based on Formula (C.41) taken from [74].

As can be seen from Figure C.4, the values of thermal conductivity of n-dodecane are higher than those of Diesel fuel, and the difference between them is particularly noticeable at high temperatures. It is recommended that the thermal conductivity of Diesel fuel is estimated based on Formula (C.39) rather than Formula (C.41). As mentioned earlier, the approximation of Diesel fuel by n-dodecane is widely used in the literature.

Note that in all cases shown in Figure C.4 the thermal conductivity of Diesel fuel decreases with temperature. This trend does not capture the expected infinitely large values of thermal conductivity of components when the temperatures of these components reach critical temperatures [215]. The critical temperatures of Diesel fuel varies from one sample to another, but in all cases they were above 700 K [98]. Since no direct comparison of the predictions of Expression (C.39) with experimental data for high temperatures was presented in [98], it was assumed that $k_D(T > 700 \text{ K}) = k_D(T = 700 \text{ K})$.

C9. Diesel fuel vapour molar heat capacity

In contrast to most transport and thermodynamic properties of the components of Diesel fuel, considered in Appendices C1-C8, vapour molar heat capacities (in J/(mole K)) of all these components can be estimated by a single formula, derived from group-contributions [208]:

$$c_{pv} = a_{cpv} - 37.93 + \left[b_{cpv} + 0.21\right] T + \left[c_{cpv} - 3.9 \times 10^{-4}\right] T^2 + \left[d_{cpv} + 2.06 \times 10^{-7}\right] T^3, \tag{C.42}$$

where the values of coefficients for Diesel fuel components were calculated using the methodology described in [208]; they are shown in Table C.6.

Table C.6 Coefficients in Equation (C.42) for Diesel fuel components.

Alkanes

(number of carbon atoms)	a_{cpv}	b_{cpv}	c_{cpv}	d_{cpv}
8	33.546	0.55384	-2×10^{-5}	-1.2×10^{-7}
9	32.637	0.64884	-7.5×10^{-5}	-1.1×10^{-7}
10	31.728	0.74384	-0.00013	-9.8×10^{-8}
11	30.819	0.83884	-0.00018	-8.6×10^{-8}
12	29.91	0.93384	-0.00024	-7.4×10^{-8}
13	29.001	1.02884	-0.00029	-6.3×10^{-8}
14	28.092	1.12384	-0.00035	-5.1×10^{-8}
15	27.183	1.21884	-0.0004	-3.9×10^{-8}
16	26.274	1.31384	-0.00046	-2.7×10^{-8}
17	25.365	1.40884	-0.00051	-1.5×10^{-8}
18	24.456	1.50384	-0.00056	-3×10^{-9}
19	23.547	1.59884	-0.00062	8.9×10^{-9}
20	22.638	1.69384	-0.00067	2.08×10^{-8}
21	21.729	1.78884	-0.00073	3.27×10^{-8}
22	20.82	1.88384	-0.00078	4.46×10^{-8}
23	19.911	1.97884	-0.00084	5.65×10^{-8}
24	19.002	2.07384	-0.00089	6.84×10^{-8}
25	18.093	2.16884	-0.00095	8.03×10^{-8}
26	17.184	2.26384	-0.0010	9.22×10^{-8}
27	16.275	2.35884	-0.00105	1.04×10^{-7}

Cycloalkanes

(number of carbon atoms)	a_{cpv}	b_{cpv}	c_{cpv}	d_{cpv}
10	-33.877	0.86592	-0.00021	-8.9×10^{-8}
11	-34.786	0.96092	-0.00026	-7.7×10^{-8}
12	-35.695	1.05592	-0.00032	-6.5×10^{-8}
13	-36.604	1.15092	-0.00037	-5.3×10^{-8}
14	-37.513	1.24592	-0.00043	-4.1×10^{-8}
15	-38.422	1.34092	-0.00048	-2.9×10^{-8}
16	-39.331	1.43592	-0.00054	-1.7×10^{-8}
17	-40.24	1.53092	-0.00059	-5.3×10^{-9}
18	-41.149	1.62592	-0.00065	6.6×10^{-9}
19	-42.058	1.72092	-0.0007	1.85×10^{-8}
20	-42.967	1.81592	-0.00075	3.04×10^{-8}
21	-43.876	1.91092	-0.00081	4.23×10^{-8}
22	-44.785	2.00592	-0.00086	5.42×10^{-8}
23	-45.694	2.10092	-0.00092	6.61×10^{-8}
24	-46.603	2.19592	-0.00097	7.8×10^{-8}
25	-47.512	2.29092	-0.00103	8.99×10^{-8}
26	-48.421	2.38592	-0.00108	1.02×10^{-7}
27	-49.33	2.48092	-0.00114	1.14×10^{-7}

Bicycloalkanes

(number of carbon atoms)	a_{cpv}	b_{cpv}	c_{cpv}	d_{cpv}
10	-84.21	1.07572	-0.00038	-3.6×10^{-8}
11	-85.119	1.17072	-0.00044	-2.4×10^{-8}
12	-86.028	1.26572	-0.00049	-1.2×10^{-8}
13	-86.937	1.36072	-0.00055	2×10^{-10}

14	−87.846	1.45572	−0.0006	1.21×10^{-8}
15	−88.755	1.55072	−0.00066	2.4×10^{-8}
16	−89.664	1.64572	−0.00071	3.59×10^{-8}
17	−90.573	1.74072	−0.00076	4.78×10^{-8}
18	−91.482	1.83572	−0.00082	5.97×10^{-8}
19	−92.391	1.93072	−0.00087	7.16×10^{-8}
20	−93.3	2.02572	−0.00093	8.35×10^{-8}
21	−94.209	2.12072	−0.00098	9.54×10^{-8}
22	−95.118	2.21572	−0.00104	1.07×10^{-7}
23	−96.027	2.31072	−0.00109	1.19×10^{-7}
24	−96.936	2.40572	−0.00114	1.31×10^{-7}
25	−97.845	2.50072	−0.0012	1.43×10^{-7}

Alkylbenzene

(number of carbon atoms)	a_{cpv}	b_{cpv}	c_{cpv}	d_{cpv}
8	−0.359	0.47492	-5.2×10^{-5}	-9.7×10^{-8}
9	−1.268	0.56992	−0.00011	-8.5×10^{-8}
10	−2.177	0.66492	−0.00016	-7.3×10^{-8}
11	−3.086	0.75992	−0.00021	-6.1×10^{-8}
12	−3.995	0.85492	−0.00027	-4.9×10^{-8}
13	−4.904	0.94992	−0.00032	-3.7×10^{-8}
14	−5.813	1.04492	−0.00038	-2.5×10^{-8}
15	−6.722	1.13992	−0.00043	-1.3×10^{-8}
16	−7.631	1.23492	−0.00049	-1.3×10^{-9}
17	−8.54	1.32992	−0.00054	1.06×10^{-8}
18	−9.449	1.42492	−0.0006	2.25×10^{-8}
19	−10.358	1.51992	−0.00065	3.44×10^{-8}
20	−11.267	1.61492	−0.0007	4.63×10^{-8}
21	−12.176	1.70992	−0.00076	5.82×10^{-8}
22	−13.085	1.80492	−0.00081	7.01×10^{-8}
23	−13.994	1.89992	−0.00087	8.2×10^{-8}
24	−14.903	1.99492	−0.00092	9.39×10^{-8}

Indanes & tetraline

(number of carbon atoms)	a_{cpv}	b_{cpv}	c_{cpv}	d_{cpv}
10	−38.12	0.75632	−0.00031	1.7×10^{-9}
11	−39.029	0.85132	−0.00037	1.36×10^{-8}
12	−39.938	0.94632	−0.00042	2.55×10^{-8}
13	−40.847	1.04132	−0.00048	3.74×10^{-8}
14	−41.756	1.13632	−0.00053	4.93×10^{-8}
15	−42.665	1.23132	−0.00059	6.12×10^{-8}
16	−43.574	1.32632	−0.00064	7.31×10^{-8}
17	−44.483	1.42132	−0.00069	8.5×10^{-8}
18	−45.392	1.51632	−0.00075	9.69×10^{-8}

19	−46.301	1.61132	−0.0008	1.09×10^{-7}
20	−47.21	1.70632	−0.00086	1.21×10^{-7}
21	−48.119	1.80132	−0.00091	1.33×10^{-7}
22	−49.028	1.89632	−0.00097	1.45×10^{-7}

Naphthalenes

(number of carbon atoms)	a_{cpv}	b_{cpv}	c_{cpv}	d_{cpv}
10	−39.73	0.7048	−0.00044	9.21×10^{-8}
11	−20.23	0.69672	−0.00028	-4.6×10^{-9}
12	−21.139	0.79172	−0.00034	7.3×10^{-9}
13	−22.048	0.88672	−0.00039	1.92×10^{-8}
14	−22.957	0.98172	−0.00045	3.11×10^{-8}
15	−23.866	1.07672	−0.0005	4.3×10^{-8}
16	−24.775	1.17172	−0.00056	5.49×10^{-8}
17	−25.684	1.26672	−0.00061	6.68×10^{-8}
18	−26.593	1.36172	−0.00067	7.87×10^{-8}
19	−27.502	1.45672	−0.00072	9.06×10^{-8}
20	−28.411	1.55172	−0.00077	1.03×10^{-7}

Tricycloalkanes, diaromatics and phenanthrenes

Component	a_{cpv}	b_{cpv}	c_{cpv}	d_{cpv}
Tricycloalkanes	−140.906	1.95052	−0.00094	1.009×10^{-7}
Diaromatics	−25.419	0.90652	−0.00034	-2.45×10^{-8}
Phenanthrenes	−54.4	0.978	−0.00058	1.122×10^{-7}

For the remaining transport and thermodynamic properties of Diesel vapour, we assume that Diesel fuel vapour is sufficiently diluted to allow us to consider transport properties for the mixture to be equal to that for air as in the case of biodiesel fuel vapour (in Appendix B3).

Appendix D. PROPERTIES OF GASOLINE FUEL

D1. Transport and thermodynamic properties of n-alkanes

As mentioned earlier, in the analysis of gasoline fuel, the the difference in properties of n-alkanes and iso-alkanes is taken into account in contrast to to the case of Diesel fuel.

Boiling and critical temperatures

The chemical formula for n-alkanes is C_nH_{2n+2}. Using data from [82], [146], [194], the dependences of boiling temperature at atmospheric pressure, critical temperature and pressures on n were approximated by the following equations, valid for the range $4 \leq n \leq 12$:

$$T_b = -1.1328\,n^2 + 45.02\,n + 111.68 \;\; (K), \tag{D.1}$$

$$T_{cr} = -1.7679\,n^2 + 56.967\,n + 227.57 \quad (K), \tag{D.2}$$

$$P_{cr} = -0.0404\,n^3 + 1.2475\,n^2 - 14.239\,n + 79.185 \quad (bar). \tag{D.3}$$

Regressions in Equations (D.1)-(D.3) were found to lead to errors of up to 0.4%, 0.5% and 1.3% respectively.

Liquid density

Liquid density was approximated as [146], [194]:

$$\rho(T) = 1000\,A\,B^{-(1-T_r)^C} \;\; (kg\,m^{-3}), \tag{D.4}$$

where coefficients A, B and C, as functions of the carbon number n, were approximated as (leading to maximum errors of 0.24%, 0.22% and 2.2% respectively):

$A = -0.000248142613151153\,n^2 + 0.00470185738684884\,n + 0.213705550811272,$

$B = \;\;0.0000384180187873567\,n^2 - 0.00298658198121256\,n + 0.282644927412468,$

$C = 0.0000635183603757482\,n^2 - 0.000196481639624268\,n + 0.279692698548249.$

Liquid viscosity

Liquid viscosity was approximated as [146, p. 200], [194]:

$$\mu = 10^{\left(a + \frac{b}{T} + c\,T + d\,T^2\right) - 3} \quad (\text{Pa }s^{-1}), \tag{D.5}$$

where the values of coefficients are presented in Table D.1.

Table D.1 The coefficients used in Equation (D.5) for estimating the liquid viscosity of n-alkanes.

component	n	a	b	c	d
n-butane	4	-4.6402	4.850E2	1.340E-2	-1.970E-5
n-pentane	5	-7.1711	7.470E2	2.170E-2	-2.720E-5
n-hexane	6	-5.0715	6.550E2	1.230E-2	-1.50E-5
n-decane	10	-6.0716	1.020E3	1.220E-2	-1.190E-5
n-dodecane	12	-7.0687	1.263E3	1.3735E-2	-1.2215E-5

Liquid heat capacity

The temperature dependence of heat capacity, applicable to all groups, is approximated as [216]–[218]:

$$c_p = A_1 + A_2\,T + A_3\,T^2 \quad (\text{J. kg}^{-1}\text{K}^{-1}), \tag{D.6}$$

where

$$A_1 = 4184\left(-1.17126 + (0.023722 + 0.024907\,\tilde{\rho})K_W + \frac{1.14982 - 0.046535\,K_W}{\tilde{\rho}}\right),$$

$$A_2 = 7531.2\left((10^{-4})(1 + 0.82463\,K_W) + (1.12172 - \frac{0.27634}{\tilde{\rho}})\right),$$

$$A_3 = 13556.16\left((-10^{-8})(1.0 + 0.82463\,K_W) + (2.9027 - \frac{0.70958}{\tilde{\rho}})\right),$$

K_W is the Watson characterisation factor, defined as $K_W = (1.8\,T_b)^{\frac{1}{3}}/\tilde{\rho}$ (see [219]), and $\tilde{\rho}$ is the relative density at 288.706 K, as shown in Table D.2. Approximation (D.6) is valid for $0.4 < T_r < 0.85$.

Table D.2 The carbon numbers and relative densities of components at 288.706 K.

group	carbon number	relative density
n-alkanes	4	0.592
	5	0.631
	6	0.662
	10	0.737
	12	0.753
iso-alkanes	4	0.566
	5	0.620
	6	0.661
	7	0.691
	8	0.713
	9	0.729
	10	0.739
	11	0.743
aromatics	8	0.884
	9	0.875
	10	0.872
	11	0.862
indanes/naphthalenes	9	0.969
cycloalkanes	8	0.771
olefins	9	0.733

Liquid thermal conductivity

Following [82], [163], [220], the liquid thermal conductivity of *n*-alkanes was estimated, using the Latini formula, as:

$$\lambda_L = \frac{A\,(1-T_r)^{0.38}}{(T_r)^{\frac{1}{6}}}\ (\text{W}\ m^{-1}\ \text{K}^{-1}), \tag{D.7}$$

where λ_L is thermal conductivity of liquid, A is given in the following expression [175]:

$$A = \frac{A^*\,T_b^{\,\alpha}}{M_w^{\,\beta}\,T_c^{\,\gamma}}, \tag{D.8}$$

M_w is molar mass (in g mol^{-1}); the values of other coefficients are shown in Table D.3.

Table D.3 The coefficients used in Equation (D.7) for six groups of components.

group	A^*	a	β	γ
n-/iso- alkanes	0.0035	1.2	0.5	0.167
aromatics	0.0346	1.2	1	0.167
indanes/naphthalenes	0.035	1.2	0.5	0.167
cycloalkanes	0.031	1.2	1	0.167
olefins	0.0361	1.2	1	0.167

Saturated vapour pressure

Following [82], [221], saturated vapour pressure of n-alkanes (in Pa) was calculated from the following equation:

$$\ln P_r{}^{\text{vap}} = f^0(T_r) + \omega f^1(T_r), \tag{D.9}$$

where f^0 and f^1 are the Pitzer's functions of T_r:

$$f^0(T_r) = 5.92714 - \frac{6.09648}{T_r} - 1.28862 \ln T_r + 0.169347 \ln T_r{}^6, \tag{D.10}$$

$$f^1(T_r) = 15.2518 - \frac{15.6875}{T_r} - 13.4721 \ln T_r + 0.43577 \ln T_r{}^6 . \tag{D.11}$$

$$\omega = \frac{-\ln P_{cr} - f^0(\theta)}{f^1(\theta)}, \tag{D.12}$$

$$\theta = \frac{T_b}{T_{cr}},$$

Equation (D.9) is applied to all other groups of components in gasoline fuels.

Enthalpy of evaporation

Enthalpy of evaporation was estimated using the following expression [1]:

$$L = A(1 - T_r)^B \times 10^6 / M_w \ (\text{J kg}^{-1}), \tag{D.13}$$

where coefficients A and B are given in Table D.4.

Table D.4 The coefficients used in Equation (16) for estimation of the enthalpy of evaporation of n-alkanes.

component	n	A	B
n-butane	4	33.0198	0.377
n-pentane	5	39.8543	0.398
n-hexane	6	45.610	0.401
n-decane	10	71.4282	0.451
n-dodecane	12	77.1658	0.407

D2. Transport and thermodynamic properties of iso-alkanes

Boiling and critical temperatures

Using data from [146] the dependence of the boiling temperature at atmospheric pressure, critical temperature and pressure were approximated by the following expressions, valid for the range $4 \leq n \leq 11$:

$$T_b = -1.1597\, n^2 + 44.011\, n + 107.75\,\text{(K)}, \tag{D.14}$$

$$T_{cr} = -2.4511\, n^2 + 66.891\, n + 183.88 \quad \text{(K)}, \tag{D.15}$$

$$P_{cr} = -0.0186\, n^3 + 0.459\, n^2 - 5.924\, n + 54.071\,\text{(bar)}. \tag{D.16}$$

Errors of Approximations (D.14)-(D.16) were estimated to be 1.45%, 1.61% and 1.17%, respectively.

Liquid density

The temperature dependence of the liquid density of iso-alkanes was approximated by Expression (D.4) with coefficients A, B and C estimated as [146]:

$$A = -0.0009814116\, n^2 + 0.01674035534\, n + 0.175683061,$$

$$B = -0.00070608196\, n^2 + 0.0087362911\, n + 0.249117017,$$

$$C = 0.0011445699\, n^2 - 0.01744247312\, n + 0.343958172.$$

Liquid viscosity

The liquid viscosity of iso-alkanes was estimated based on Expression (D.5) with coefficients given in Table D.5 [146], [194].

Table D.5 The coefficients used in Equation (D.5) for estimating the liquid viscosity of iso-alkanes.

component	n	a	b	c	d
i-butane	4	-1.80770	258.930	0.003021	-8.64410E-06
C_5H_{12}	5	-5.80889	706.6875	0.014813	-1.85303E-05
C_6H_{14}	6	-10.2364	1387.157	0.024213	-2.40762E-05
C_7H_{16}	7	-4.84309	641.4304	0.011545	-1.37435E-05
C_8H_{18}	8	-10.2217	1423.586	0.024242	-2.33636E-05
C_9H_{20}	9	-4.25773	652.8668	0.008355	-8.98181E-06
$C_{10}H_{22}$	10	-4.8378	782.6433	0.009299	-9.37893E-06
$C_{11}H_{24}$	11	-4.23052	709.6763	0.007402	-7.41622E-06

Liquid heat capacity and thermal conductivity

Following [216]–[218], The liquid heat capacity of iso-alkanes is calculated using Equation (D.6) and coefficients are taken from Table D.2.

Following [82], [163], [220], the liquid thermal conductivity of iso-alkanes was estimated using the Latini formula (Equations (D.7) and (D.8)).

Enthalpy of evaporation and saturated vapour pressure

The enthalpy of evaporation was estimated using Equation (D.13) with coefficients A and B given in Table D.6.

Following [82], [221], the saturated vapour pressure of iso-alkanes was calculated from Equations (D.9)-(D.12) as in the case on n-alkanes.

Table D.6 The coefficients used in Equation (16) for estimating the enthalpy of evaporation of iso-alkanes.

component	n	A	B
i-butane	4	31.95380	0.392
C_5H_{12}	5	37.68615	0.394981
C_6H_{14}	6	42.32119	0.389105
C_7H_{16}	7	46.95571	0.388222
C_8H_{18}	8	49.32456	0.382229
C_9H_{20}	9	56.10624	0.38
$C_{10}H_{22}$	10	59.25229	0.38
$C_{11}H_{24}$	11	65.11180	0.38

D3. Transport and thermodynamic properties of aromatics

Boiling and critical temperatures

Using data from [146], [194], the dependence of boiling temperature of aromatics at atmospheric pressure, critical temperature and pressures on n in the range $8 \le n \le 11$ were approximated as:

$$T_b = -1.4662 \, n^2 + 46.596 \, n + 136.63 \quad (K), \tag{D.17}$$

$$T_{cr} = 0.0257 \, n^2 + 15.718 \, n + 499.56 \quad (K), \tag{D.18}$$

$$P_{cr} = 0.7329 \, n^2 - 17.615 \, n + 131.36 \quad (bar). \tag{D.19}$$

Errors of these regressions were found to be 2.77%, 3.22% and 0.26% respectively.

Liquid density, viscosity, heat capacity and thermal conductivity

The liquid density of arpomatics was estimated using Equation (D.4) with the values of coefficients given in Table D.7.

Table D.7 The coefficients used in Equation (D.4) for the estimation of the liquid density of aromatics.

component	n	A	B	C
o-xylene	8	0.28760	0.265130	0.27410
C_9H_{12}	9	0.269256	0.249881	0.274542
$C_{10}H_{14}$	10	0.276930	0.258413	0.288381
$C_{11}H_{16}$	11	0.275810	0.262610	0.285710

The liquid viscosity was estimated using Equation (D.5) with the coefficients given in Table D.8.

Table D.8 The coefficients used in Equation (D.5) for estimating the liquid viscosity of aromatics.

component	n	a	b	c	d
o-xylene	8	-7.8805	1250.0	0.016116	-1.39930E-05
C_9H_{12}	9	-5.30135209	897.6554	0.009761	-8.86622E-06
$C_{10}H_{14}$	10	-4.346850	781.4415	0.007281	-6.73705E-06
$C_{11}H_{16}$	11	-4.6410	853.230	0.007850	-7.10120E-06

Following [216]–[218], the liquid heat capacity was calculated based on Equation (D.6) using the coefficients presented in Table D.2. Following [82], [163], [220], the liquid thermal conductivity was estimated using the Latini formula with the coefficients given in Table D.3.

Enthalpy of evaporation and saturated vapour pressure

The latent heat of evaporation was estimated from Equation (D.13), using the coefficients given in Table D.9.

Table D.9 The coefficients used in Equation (D.13) for estimation of the enthalpy of evaporation of aromatics.

Component	n	A	B
o-xylene	8	55.6060	0.3750
C_9H_{12}	9	59.97485694	0.38526
$C_{10}H_{14}$	10	63.32651773	0.379614
$C_{11}H_{16}$	11	65.20160	0.380

Following [82], [221], the saturated vapour pressure of aromatics was calculated from Equations (D.9)-(D.12) with the critical pressures given by Equation (D.16).

D4. Transport and thermodynamic properties of indanes/ naphthalenes, cycloalkanes and olefins

Boiling and critical temperatures

The boiling temperature at atmospheric pressure, critical temperature and pressure of characteristic components of indanes/naphthalenes (C_9H_{10}), cycloalkanes (cis-1-ethyl-3-methylcyclopentane; C_8H_{16}), and olefins (1-nonene; C_9H_{18}) are the following [82], [146], [194], [198]:

$T_b = 451.12$ K, $T_{cr} = 684.9$ K and $P_{cr} = 39.50$ bar, for indane (C_9H_{10});

$T_b = 394.25$ K, $T_{cr} = 586.99$ K and $P_{cr} = 29.57$ bar, for cis-1-ethyl-3-methylcyclopentane;

$T_b = 420.02$ K, $T_{cr} = 594$ K and $P_{cr} = 23.30$ bar, for 1-nonene.

Liquid density, viscosity, heat capacity and thermal conductivity

The liquid densities of the characteristic components for indanes/naphthalenes, cycloalkanes and olefins are calculated using Equation (D.4) with the coefficients A, B and C given in Table D.10.

Table D.10 The coefficients used in Equation (D.4) for the estimation of the liquid density of three characteristic components for indanes/naphthalenes, cycloalkanes and olefins.

group	A	B	C
indanes/naphthalenes	310.20	0.26114	0.30223
cycloalkanes	264.97	0.27385	0.28571
olefins	239.10	0.25815	0.28571

The liquid viscosities of the characteristic components for indanes/naphthalenes, cycloalkanes and olefins were estimated using Equation (D.5) with the coefficients given in Table D.11.

Following [216]–[218], the liquid heat capacity of the characteristic components for indanes/naphthalenes, cycloalkanes and olefins were calculated using Equation (D.6) with the coefficients given in Table D.2.

Following [82], [163], [220], the liquid thermal conductivities of the characteristic components for indanes/naphthalenes, cycloalkanes and olefins were estimated using the Latini formula (Equations (D.7) and (D.8)) with the coefficients given in Table D.3.

Table D.11 The coefficients used is Equation (D.5) for estimating the liquid viscosity of the characteristic components for indanes/naphthalenes, cycloalkanes and olefins.

group	a	b	c	d
Indanes/naphthalenes	-7.3304	1330.6	0.0126170	-8.6008E-6
cycloalkanes	-4.2467	654.41	0.0085394	-9.3374E-6
olefins	-6.5557	993.50	0.0142320	-1.4097E-5

Saturated vapour pressure and enthalpy of evaporation

Following [82], [221], the saturated vapour pressures of the characteristic components for indanes/naphthalenes, cycloalkanes and olefins were calculated from Equations (D.9)-(D.12).

The latent heats of evaporation of the characteristic components for indanes/naphthalenes, cycloalkanes and olefins were calculated using Equation (D.13) with coefficients A and B given in Table D.12.

Table D.12 The coefficients used in Equation (D.13) for estimation of the enthalpy of evaporation of three characteristic components for indanes/naphthalenes, cycloalkanes and olefins.

group	A	B
indanes/naphthalenes	62.1067	0.42
cycloalkanes	50.9505	0.38
olefins	61.7073	0.38

Appendix E. IMPLEMENTATION OF THE NEW MODELS INTO THE ANSYS-FLUENT

The new model described in the thesis is in process of being implementated into the commercial CFD code ANSYS FLUENT. This appendix shows some preliminary results of this implementation and testing. This implementation was performed via User Defined Functions (UDF) and User defined Subroutines (UDS) available in FLUENT. The presented figures have been produced in collaboration with Dr Oyuna Rybdylova and Dr Elena Sazhina, from Sir Harry Ricardo Laboratories at the University of Brighton, and in consultation with Dr Markus Braun (Principle software developer, fluids product development at ANSYS Inc.).

E.1. Preliminary results

A simplified case study has been studied. The thermodynamic and transport properties have been inferred from Abramzon and Sazhin [74] for n-decane. The properties of air used in our analysis are shown in Table E.1.

Table E.1 The properties of air used in the analysis.

Property	Value	Units
thermal conductivity	0.0454	$W\,m^{-1}\,K^{-1}$
viscosity	$1.72 \cdot 10^{-5}$	$Pa \cdot s$
specific heat capacity	1013	$J\,kg^{-1}\,K^{-1}$
Molecular mass	28.967	$g\,mol^{-1}$

Two tests have been performed, based on incompressible and compressible injections. In the case of incompressible injection, the density is assumed constant and thermal swelling is ignored; while in the case of compressible injection, the density of n-dodecane is temperature dependent (see [74]) and the effects of thermal swelling are taken into account.

The plots referring to the incompressible injection, where the predictions of our in-house code Fluent-ANSYS software are compared for the evolutions of mono-componenst droplet radii and surface temperatures, are shown in Figures E.1 and E.2.
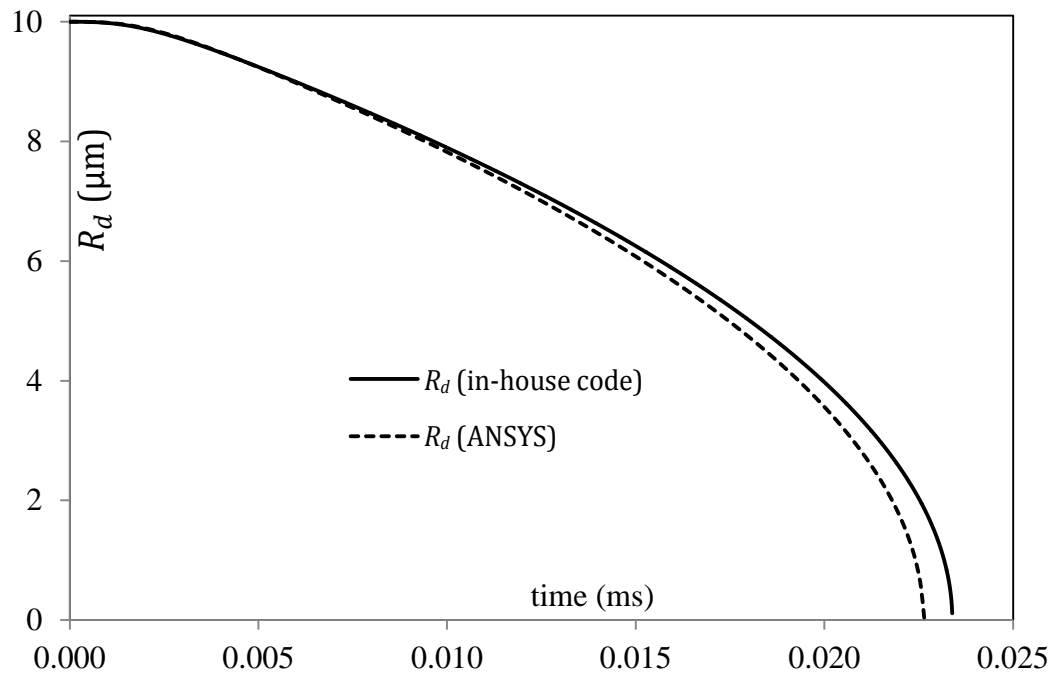

Figure E.1 Evolution of droplet radii predicted by the in-house code and ANSYS-Fluent. A stationary n-dodecane droplet with initial radius 10 μm and temperature 300 K is immersed in still air of 400 K and 1 bar. The density of liquid is assumed constant $\rho = 675$ kg m^3; and thermal swelling is ignored.
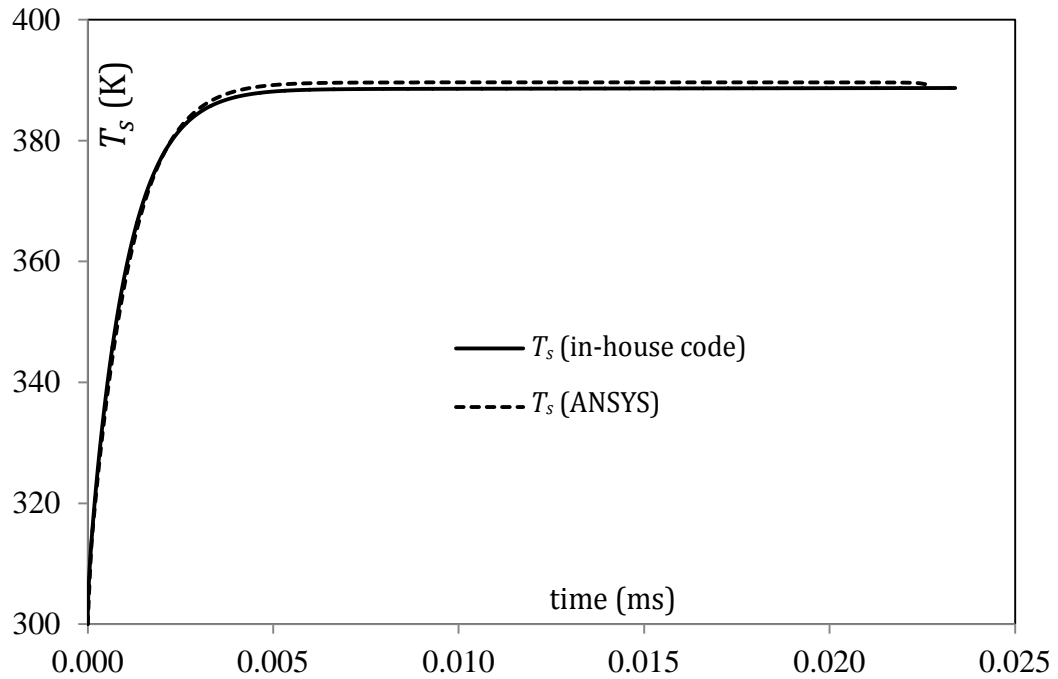
Figure E.2 Evolution of droplet surface temperatures using the same conditions as in Figure E.1.

The discrepancy between the results shown in both Figures E.1 and E.2 is reasonable, which supports the reliability of both approaches. The calculations by ANSYS Fluent show marginally smaller evaporation time.

The same plots as the ones shown in Figures E.1 and E.2, but taking into account the thermal swelling effects, are shown in Figures E.3 and E.4.
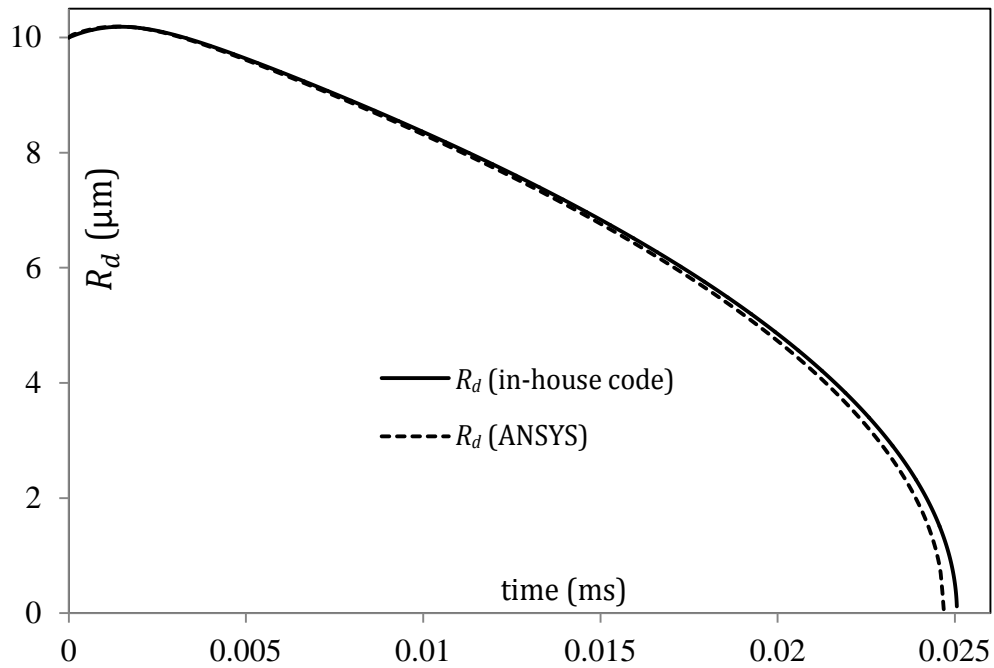
Figure E.3 The same as Figure E.1, but for compressible injection, using the same conditions as in Figures E.1-E.2, except that the dependence of the liquid density on temperature is taken into account following [74].
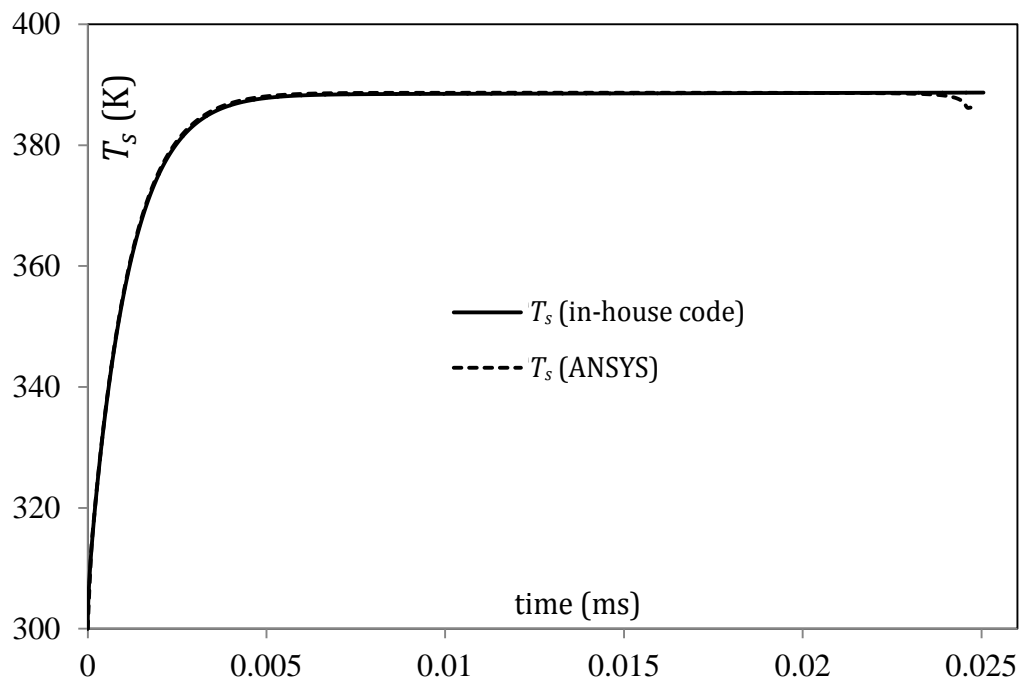

Figure E.4 The same as Figure E.3, but for droplet surface temperatures.

In Figures E.3 and E.4, the evolutions of droplet radii and surface temperatures, for the case when liquid density is temperature dependent and the effects of thermal swelling are taken into account, as predicted by the in-

house code and FLUENT, are presented. The agreement between the results is believed to be satisfactory. As in the case shown in Figures E.1 and E.2, calculations by ANSYS-Fluent show marginally smaller evaporation time.

Overall, the deviations between the two codes in predicting the evaporation times were up to 3.2% in the case of constant liquid density and up to 1.4% in the case of temperature dependent liquid density taking into account the effect of thermal swelling.

E.2. In progress

At the next step, we plan to implement the multi-component fuel droplet into ANSYS-FLUENT. The results will be tested for realistic IC engine conditions and geometries of the combustion chamber as shown in Figures E.5-E.7.

Mesh (Time=2.0000e-04)   Jan 21, 2015
Crank Angle=3.96(deg)   ANSYS Fluent 15.0 (3d, dp, pbns, spe, skw, transient)
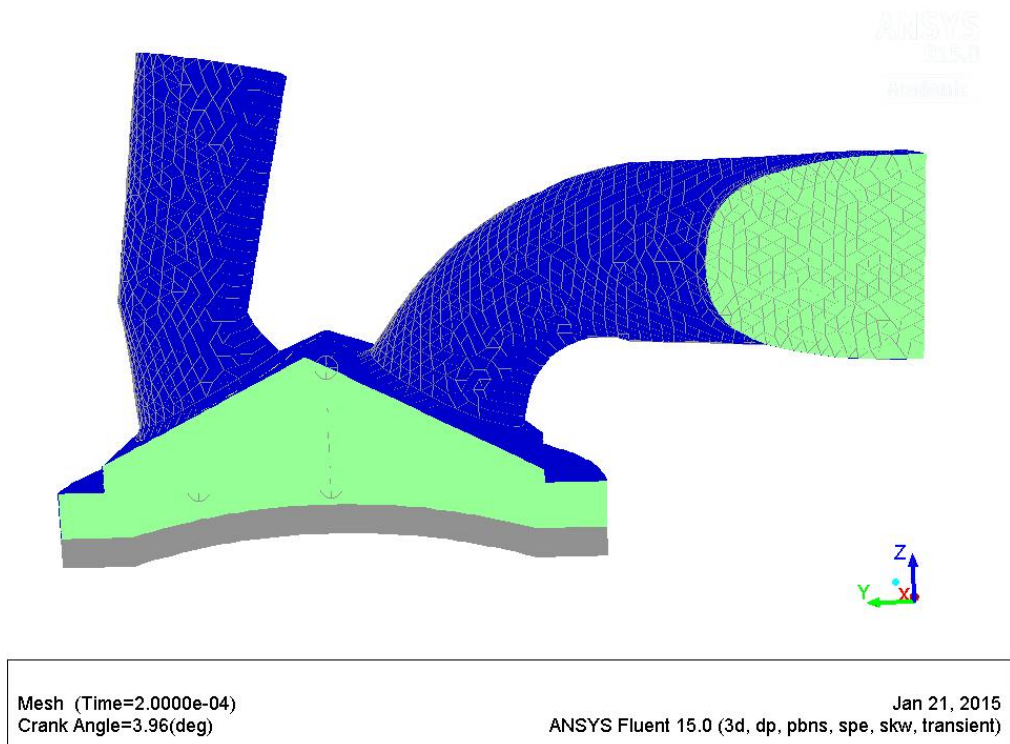
Figure E.5 Cross section of the combustion chamber geometry used in our simulations with inlet and outlet valves shown.
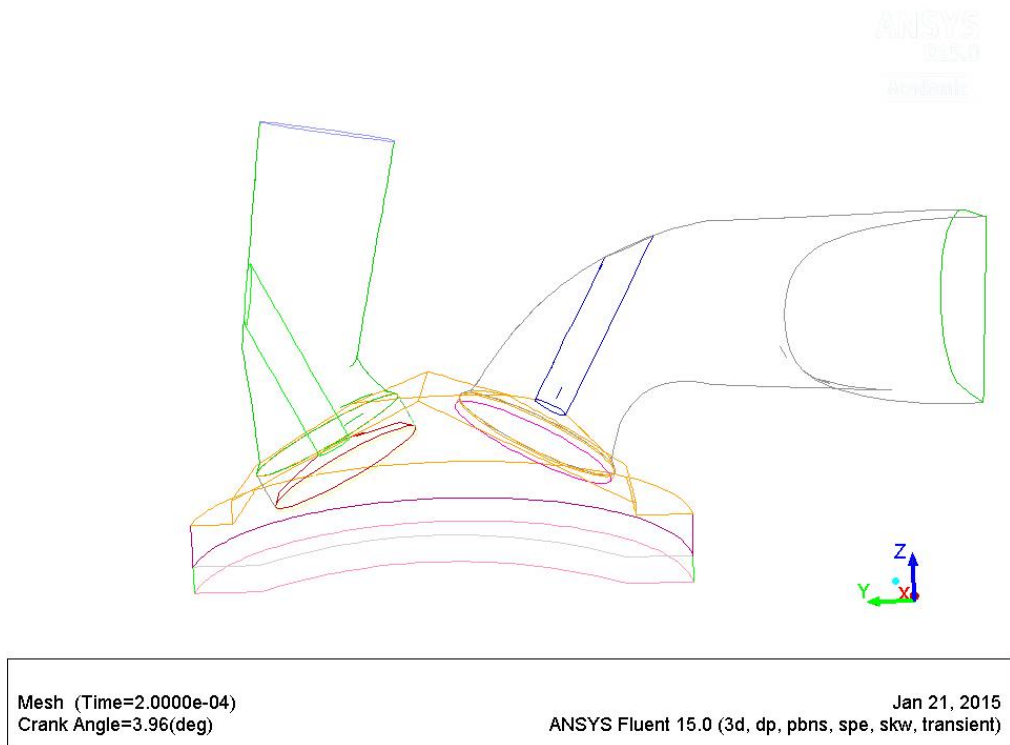

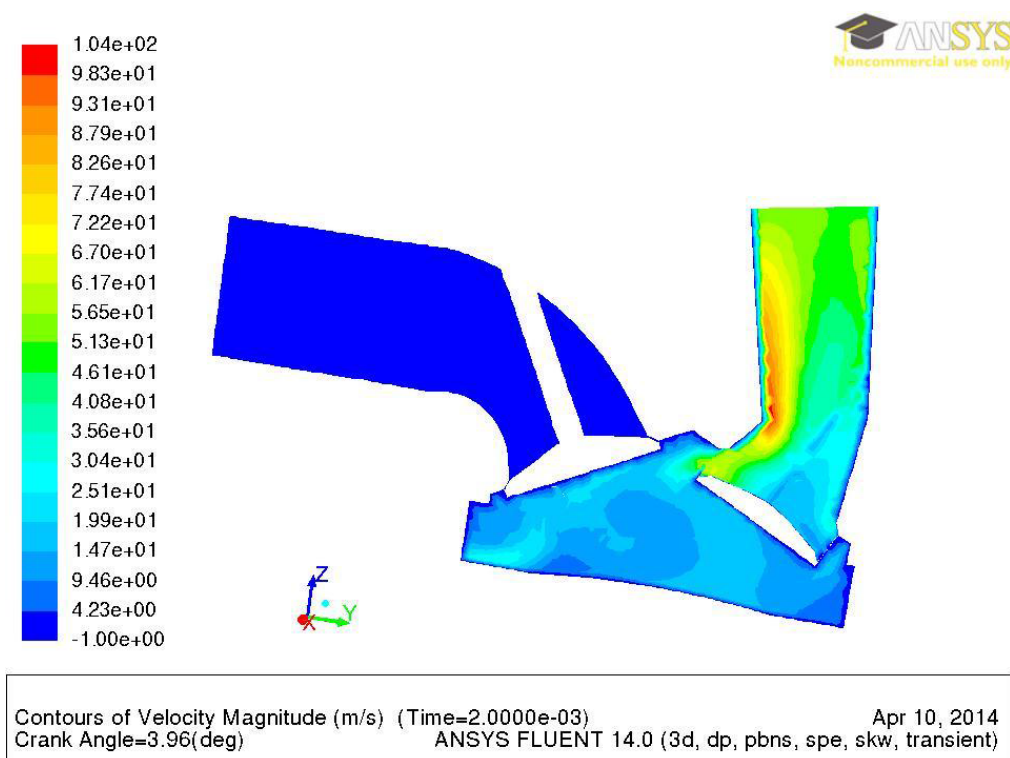Figure E.6 Wireframe of the schematic in Figure E.5.

Figure E.7 Two-dimensional view of velocity contours at 2 ms time instant from start of injection before implementation of our new models.